MECHANISMS OF GLYCEROL ELECTROREDUCTION ON ACTIVATED CARBON-BASED ELECTRODES

SITI AQILAH NADHIRAH BINTI MD. RAHIM

FACULTY OF ENGINEERING
UNIVERSITY OF MALAYA
KUALA LUMPUR

2022

MECHANISMS OF GLYCEROL ELECTROREDUCTION ON ACTIVATED CARBON-BASED ELECTRODES

SITI AQILAH NADHIRAH BINTI MD. RAHIM

DISSERTATION SUBMITTED IN FULFILMENT OF THE REQUIREMENTS FOR THE DEGREE OF MASTER OF ENGINEERING SCIENCE

FACULTY OF ENGINEERING
UNIVERSITY OF MALAYA
KUALA LUMPUR

2022

UNIVERSITI MALAYA

ORIGINAL LITERARY WORK DECLARATION FORM

Name of Candidate: Siti Aqilah Nadhirah Binti Md. Rahim

Registration/Matric No: KGA180027 (17198017/1)

Name of Degree: Master of Engineering Science

Title of ~~Project Paper/ Research Report/~~ Dissertation/ ~~Thesis~~ ("this Work"):

Mechanisms of Glycerol Electroreduction on Activated Carbon-Based Electrodes

Field of Study:

Reaction engineering (chemical and process)

I do solemnly and sincerely declare that:

(1) I am the sole author/writer of this Work;
(2) This Work is original;
(3) Any use of any work in which copyright exists was done by way of fair dealing and for permitted purposes and any excerpt or extract from, or reference to or reproduction of any copyright work has been disclosed expressly and sufficiently and the title of the Work and its authorship have been acknowledged in this Work;
(4) I do not have any actual knowledge nor do I ought reasonably to know that the making of this work constitutes an infringement of any copyright work;
(5) I hereby assign all and every rights in the copyright to this Work to the University of Malaya ("UM"), who henceforth shall be owner of the copyright in this Work and that any reproduction or use in any form or by any means whatsoever is prohibited without the written consent of UM having been first had and obtained;
(6) I am fully aware that if in the course of making this Work I have infringed any copyright whether intentionally or otherwise, I may be subject to legal action or any other action as may be determined by UM.

Candidate's Signature Date: 12/8/2022

Subscribed and solemnly declared before,

Witness's Signature Date: 20/8/2022

Name:
Designation:

MECHANISMS OF GLYCEROL ELECTROREDUCTION ON ACTIVATED CARBON-BASED ELECTRODES

ABSTRACT

Glycerol generated from biodiesel manufacture is a beneficial waste that can be potentially used to synthesize valuable products *via* the low-cost and simple setup method, namely electrolysis. This waste can produce oxygenated and reduced compounds through electrooxidation and reduction reactions, respectively. This work aims to study the reaction mechanisms of glycerol electroreduction in the cathode region using inexpensive activated carbon-based electrodes. The experiments were divided into three sections. The first part is to synthesize the activated carbon composite (ACC) electrodes with various activated carbon compositions. The influence of different activated carbon percentages (60%, 70%, 80%, and 90%) of the total weight in the ACC electrodes on the physicochemical and electrochemical properties was explored by field emission scanning electron microscopy and energy-dispersive X-ray spectroscopy (FESEM-EDX), cyclic voltammetry (CV), and chronoamperometry (CA) analyses. Results indicated that high activated carbon content portrayed a dominant role in controlling an electroactive surface area (EASA), and the electrons transfer process which eventually improved the electrocatalytic activity. 80ACC outperformed other ACC electrodes by generating Amberlyst-15 anionic radicals (A-15•$^-$) with the highest EASA (36.7 cm^2) and current density (-0.2018 A/cm^2) at low potential. A-15•$^-$ served as the electron-donor for the homogeneous redox reaction with glycerol in delivering highly reactive glycerol radical for further intermediates development and generated 1,2-propanediol. Meanwhile, the low activated carbon percentage preferred diethylene glycol formation. Acetol and ethylene glycol were subsequently suggested as the intermediates for 1,2-propanediol and diethylene glycol formation, which were produced from the dissociation of glycerol either through the C-C bond or C-O bond cleavage, respectively. Hence, in the second part, the proposed intermediates were employed as the glycerol substitutes to elucidate the overall reaction mechanisms of glycerol electroreduction on the 80ACC electrode. Data proved 80ACC in Amberlyst-15 redox mediator solution demonstrated a superior activity for acetol electro-hydrogenation into 1,2-propanediol. At 80 °C, 1,2-propanediol selectivity (with 59.8 C mol% yield) reached 77.3% at the 7th hour using 3.0 M of acetol and 0.28 A/cm^2 current density. Whereas diethylene glycol was acquired through intermolecular dehydration of ethylene glycol in the Amberlyst-15 solution without electricity. Besides, H^+ ions from Amberlyst-15 are advantageous in facilitating glycerol conversion to a selective acetol. Lastly, the preliminary experiments for glycerol electroreduction to study the effects of reaction temperature (27-106.5 °C), initial glycerol concentration (0.3-4.35 M), and current density (0.07-0.28 A/cm^2) on the reaction were carried out. Findings revealed the generation of acetol, and ethylene glycol intermediates was profoundly controlled by the temperature where a mild value is needed to maintain a selective acetol-1,2-propanediol route. Additionally, a moderate glycerol initial concentration reduced the hydrogen formation and indirectly improved 1,2-propanediol yield. A medium current density raised the conversion rate and minimized the intermediates growth. At 80.0 °C and 0.21 A/cm^2, glycerol (3.0 M) electroreduction to 1,2-propanediol reached the maximum yield of 42.3 C mol%. The experimental value obtained was close to the predicted yield (41.8 C mol%) from the polynomial model developed using response surface methodology (RSM) and analysis of variance (ANOVA).

Keywords: Glycerol, Activated carbon-based electrodes, Indirect electrolysis, Amberlyst-15, 1,2-propanediol.

MEKANISME ELEKTROREDUKSI GLISEROL DI ATAS ELEKTROD BERASASKAN KARBON AKTIF

ABSTRAK

Gliserol yang dihasilkan daripada pembuatan biodiesel adalah sisa yang berpotensi digunakan untuk mensintesis produk berharga melalui kaedah persediaan kos rendah dan mudah, iaitu elektrolisis. Sisa ini boleh menghasilkan molekul beroksigen dan terkurang melalui elektrooksida dan reduksi, masing-masing. Kerja ini bertujuan untuk mengkaji mekanisme tindak balas elektroreduksi gliserol di katod menggunakan elektrod berasaskan karbon teraktif yang murah. Eksperimen dibahagikan kepada tiga bahagian. Bahagian pertama adalah untuk mensintesis elektrod komposit karbon teraktif (ACC) dengan pelbagai komposisi karbon teraktif. Pengaruh komposisi karbon teraktif yang berbeza (60%, 70%, 80%, dan 90%) daripada jumlah berat dalam elektrod ACC terhadap sifat fizikokimia dan elektrokimia telah diterokai oleh mikroskop elektron pengimbasan pelepasan medan dan spektroskopi sinar-X penyebaran tenaga (FESEM-EDX), voltammetri kitaran (CV) dan kronoamperometri (CA). Keputusan menunjukkan kandungan karbon teraktif yang tinggi memainkan peranan yang dominan dalam mengawal kawasan permukaan elektroaktif (EASA), dan proses pemindahan elektron yang akhirnya meningkatkan aktiviti elektrokatalitik. 80ACC mengatasi elektrod ACC yang lain dengan menghasilkan radikal Amberlyst-15 (A-15$\bullet^-$) dengan EASA tertinggi (36.7 cm^2) dan ketumpatan arus (-0.2018 A/cm^2) pada voltan rendah. A-15$\bullet^-$ berfungsi sebagai penderma elektron untuk tindak balas redoks homogen dengan gliserol dalam menyampaikan radikal gliserol yang sangat reaktif untuk pembangunan perantara selanjutnya dan menghasilkan 1,2-propanediol. Sementara itu, peratusan karbon teraktif yang rendah mengutamakan pembentukan dietilena glikol. Asetol dan etilena glikol kemudiannya dicadangkan sebagai perantara pembentukan 1,2-propanediol dan dietilena glikol, yang dihasilkan daripada penceraian gliserol melalui belahan ikatan C-C atau ikatan C-O, masing-masing. Oleh itu, dalam bahagian kedua, perantara yang dicadangkan digunakan sebagai pengganti gliserol untuk menjelaskan mekanisme tindak balas keseluruhan elektroreduksi gliserol pada elektrod 80ACC. Data membuktikan bahawa 80ACC dalam larutan pengantara redoks Amberlyst-15 menunjukkan aktiviti unggul untuk elektro-hidrogenasi asetol kepada 1,2-propanediol. Pada 80 °C, selektiviti 1,2-propanediol (dengan 59.8 C mol% hasil) mencapai 77.3% pada jam ke-7 menggunakan 3.0 M asetol dan ketumpatan arus 0.28 A/cm^2. Manakala dietilena glikol diperoleh melalui intermolekul dehidrasi etilena glikol dalam larutan Amberlyst-15 tanpa elektrik. Selain itu, ion H^+ daripada Amberlyst-15 juga berfaedah dalam memudahkan penukaran gliserol kepada asetol secara terpilih. Akhir sekali, eksperimen awal untuk elektroreduksi gliserol bagi mengkaji kesan suhu (27-106.5 °C), kepekatan awal gliserol (0.3-4.35 M), dan ketumpatan arus (0.07-0.28 A/cm^2) ke atas tindak balas adalah dijalankan. Penemuan mendedahkan penjanaan molekul perantara, asetol dan etilena glikol dikawal dengan mendalam oleh suhu, di mana nilai sederhana diperlukan untuk mengekalkan laluan asetol-1,2-propanediol terpilih. Di samping itu, kepekatan sederhana mengurangkan pembentukan hidrogen dan secara tidak langsung meningkatkan hasil 1,2-propanediol. Ketumpatan arus yang sederhana meningkatkan kadar penukaran dan meminimumkan pertumbuhan molekul perantaraan. Pada 80.0 °C dan 0.21 A/cm^2, elektroreduksi gliserol (3.0 M) kepada 1,2-propanediol mencapai hasil maksimum 42.3 C mol%. Nilai eksperimen yang diperoleh adalah hampir dengan hasil yang diramalkan (41.8 C mol%) daripada model polinomial yang dibangunkan menggunakan kaedah permukaan tindak balas (RSM) dan analisis varians (ANOVA).

Kata kunci: Gliserol, Elektrod berasaskan karbon teraktif, Elektrolisis tidak langsung, Amberlyst-15, 1,2-propanediol.

ACKNOWLEDGEMENTS

Firstly, all praise and thanks to Allah for providing me with unbelievable strength, patience, and perseverance to complete this research project and blessing me with numerous opportunities.

I would like to express my utmost gratitude and appreciation to my supervisors, Professor Dr. Wan Mohd Ashri Wan Daud and Professor Dr. Mohamed Kheireddine Aroua. Thank you for the guidance and encouragement throughout the entire process in achieving the success of this research. My deepest appreciation is also given to my research project advisors, Dr. Lee Ching Shya, and Dr. Faisal Abnisa. They have been great mentors for me and without their motivation, I would not have surpassed all the obstacles during my study period. Their advice has been priceless and helped me to grow as a research scientist. I am also grateful and indebted to the University of Malaya and the Ministry of Education, Malaysia for providing financial support through the Fundamental Research Grant Scheme (FRGS) (Project No.: FP046-2017A).

Besides, it is a pleasure to thank the lab staff in the Department of Chemical Engineering, namely, Mr. Kamaruddin, Mr. Azaruddin, Mr. Hadi, Ms. Fazizah, Ms. Azira, Mr. Rizman, and Mr. Rustam for the opportunity they provided to use the research laboratories and equipment there. Special thanks to all my friends who are always willing to share their knowledge and experiences with me. Lastly, I would like to cherish my parents, Md. Rahim Bachik and Rasidah Abd. Latif, and siblings for the unconditional support and understanding since the first day I started as a postgraduate candidate. It is a blessing to have you in my life.

TABLE OF CONTENTS

ORIGINAL LITERARY WORK DECLARATION FORM ii

ABSTRACT iii

ABSTRAK v

ACKNOWLEDGEMENTS vii

TABLE OF CONTENTS viii

LIST OF FIGURES xii

LIST OF TABLES xv

LIST OF SCHEMES xvi

LIST OF SYMBOLS AND ABBREVIATIONS xvii

LIST OF APPENDICES xx

CHAPTER 1: INTRODUCTION 1

1.1 Background 1

1.2 Problem statement 4

1.3 Objectives of research 5

1.4 Scope of work 5

1.5 Dissertation structure 6

CHAPTER 2: LITERATURE REVIEW 8

2.1 Introduction 8

2.2 Glycerol and value-added chemicals in the market prospects 8

2.3 Fundamental reactions in electrochemical conversion 13

2.4 Effects of parameters on mechanism pathways and reaction performances 16

  2.4.1 Effect of electrodes 21

  2.4.2 Effect of electrolyte pH 29

2.4.3 Effect of applied potential and current density..38

2.4.4 Effect of reaction temperature 43

2.4.5 Effect of additives...46

2.5 Activated carbon-based electrodes and modification techniques 55

2.6 Optimization study..59

2.7 Outlook and conclusion 60

CHAPTER 3: METHODOLOGY 63

3.1 Introduction...63

3.2 Chemicals and reagents list..65

3.3 Activated carbon composite (ACC) electrodes preparation 65

3.4 Electrochemical and physicochemical characterization 66

3.4.1 Field emission scanning electron microscopy with energy dispersive x-ray spectroscopy (FESEM-EDX) 66

3.4.2 Electroactive surface areas measurement 66

3.4.3 Electrochemical responses on ACC electrodes by cyclic voltammetry (CV) and chronoamperometry (CA) analyses 68

3.5 Glycerol electroreduction reaction under galvanostatic mode 69

3.6 Reaction mechanisms elucidation for glycerol electroreduction 70

3.7 Preliminary experiments: Glycerol electroreduction on 80ACC...........................71

3.8 Optimization study of glycerol electroreduction 72

3.9 Standards calibration and samples preparation...75

3.10 Products characterization and quantification (GC-MS and GC-FID) 77

CHAPTER 4: RESULTS AND DISCUSSION 80

4.1 Introduction...80

4.2 Characterization and evaluation of ACC electrodes 81

4.2.1 Field emission scanning electron microscopy and energy-dispersive X-ray spectroscopy (FESEM-EDX) of the ACC electrodes.......81
4.2.2 Electroactive surface areas (EASA) of ACC electrodes 85
4.2.3 Electrochemical behaviour on ACC electrodes using cyclic voltammetry (CV).......87
4.2.4 Electrochemical performance by chronoamperometry (CA) 90
4.2.5 Bulk electrolysis: Glycerol electroreduction on ACC electrodes.......92
4.2.5.1 Products distribution and the proposed reaction mechanisms...95
4.3 Reaction mechanisms investigation on the selected ACC electrode 103
4.3.1 Acetol as a reactant in the presence of electricity 103
4.3.1.1 Effect of reaction temperature.......106
4.3.1.2 Effect of acetol initial concentration 108
4.3.1.3 Effect of current density 110
4.3.2 Ethylene glycol and glycerol as the reactants without electricity 113
4.3.3 Identified reaction mechanisms.......116
4.4 Preliminary experiments for glycerol electroreduction on 80ACC electrode 124
4.4.1 Effect of reaction temperature 124
4.4.2 Effect of glycerol initial concentration.......129
4.4.3 Effect of current density 133
4.4.4 Optimization of glycerol electroreduction using RSM method 136
4.5 Energy consumptions for acetol and glycerol electrochemical conversion.......141

CHAPTER 5: CONCLUSION.......144

5.1 Conclusion 144
5.2 Recommendations.......146
REFERENCES.......147
LIST OF PUBLICATIONS AND PAPERS PRESENTED 166

APPENDICES 167

LIST OF FIGURES

Figure 1.1: Workflow of the thesis......6

Figure 2.1 Working principles of a) AEM-fuel cell, b) AEM-electrolysis, c) PEM-fuel cell and d) PEM-electrolysis (Marshall & Haverkamp, 2008; Pan et al., 2017; Simões et al., 2012)......15

Figure 2.2: *In situ* FTIR spectra for a Pt electrode in 0.1 M $HClO_4$ and different concentrations of glycerol (Gomes et al. 2013). 36

Figure 2.3: a) Cyclic voltammogram of glycerol electrooxidation at different temperatures (235-260 °C), b) Arrhenius plots for current densities of glycerol electrooxidation at different applied potentials (150-500 mV) and c) Apparent activation energies of glycerol and ethylene glycol electrooxidation *vs.* electrode potentials. 46

Figure 2.4: Basic principles of a) direct electrolysis and b) indirect electrolysis (Francke and Little, 2014; Pauwels, 2018)......47

Figure 3.1: Flowchart of complete research methodology......64

Figure 3.2: CV and CA analyses setup. 69

Figure 3.3: Experimental setup in a two-compartment reactor. 70

Figure 3.4: Experimental setup in a one-compartment reactor without electricity. 71

Figure 3.5: Calibration curve of glycerol. 76

Figure 4.1: FESEM images of a) 60ACC, b) 70ACC, c) 80ACC and d) 90ACC cathode electrodes......82

Figure 4.2: EDX maps of a) 60ACC, b) 70ACC, c) 80ACC, and d) 90ACC cathode electrodes with their EDX spectra e), f), g) and h), respectively. 84

Figure 4.3: Cottrell plots of a) 60ACC, b) 70ACC, c) 80ACC, and d) 90ACC electrodes in the ferrocyanide solution......86

Figure 4.4: Electrochemical responses in acidic Amberlyst-15 electrolyte a) without and b) with 0.3 M of glycerol. 89

Figure 4.5: Chronoamperometric measurements of the ACC electrodes at -2.5 V versus Ag/AgCl in 0.3 M glycerol + 9.6% (w/v) Amberlyst-15 in 0.3 M Na_2SO_4 solution. 91

Figure 4.6: a) Glycerol conversion and b) first-order kinetics model for glycerol electroreduction on Pt, 60ACC, 70ACC, 80ACC, and 90ACC electrodes in Amberlyst-15 solution after 8 hours of electrolysis. 94

Figure 4.7: GC-MS chromatogram after 8 hours of reaction on the 80ACC electrode. .95

Figure 4.8: Products distribution from 8 hours of glycerol electroreduction on a) Pt, b) 60ACC, c) 70ACC, d) 80ACC and e) 90ACC cathode electrodes. 96

Figure 4.9: Products selectivity (%) on a) Pt, b) 60ACC, c) 70ACC, d) 80ACC and e) 90ACC cathode electrodes. 102

Figure 4.10: GC-MS chromatogram of acetol electrolysis. 104

Figure 4.11: a) Conversion and b) first-order kinetics model of acetol electrolysis at different reaction temperatures. 107

Figure 4.12: a) Conversion and first-order kinetics model of acetol electrolysis with different initial concentrations. 109

Figure 4.13: a) Conversion and b) first-order kinetics model of acetol electrolysis at different current densities. 111

Figure 4.14: a) Products distribution (C mol%) and b) selectivity (C mol%) of acetol electrolysis at the optimum conditions. 112

Figure 4.15: a) Glycerol and ethylene glycol conversion and b) their kinetics rate constants in the absence of electrical current. 114

Figure 4.16: Products distributions from the reactions with a) ethylene glycol and c) glycerol as the feedstocks. 115

Figure 4.17: Overall identified reaction mechanisms of glycerol electroreduction 118

Figure 4.18: GC-FID result at the optimum conditions. 124

Figure 4.19: a) Glycerol conversion and b) first-order kinetics model for 0.3 M of glycerol electroreduction at different reaction temperatures. 125

Figure 4.20: Products distribution for 0.3 M of glycerol electroreduction at a) 27.0 °C, b) 53.5 °C, c) 80.0 °C and d) 106.5 °C with 0.14 A/cm^2 of current density. 128

Figure 4.21: a) Glycerol conversion and b) first-order kinetics model for electroreduction of glycerol with different initial concentrations. 130

Figure 4.22: Products distribution with glycerol initial concentration of a) 0.30 M, b) 1.65 M, c) 3.00 M and d) 4.35 M during the electroreduction reaction at 80.0 °C and 0.14 A/cm^2. 132

Figure 4.23: a) Glycerol conversion (%) and b) first-order kinetics model for glycerol electroreduction at different current densities. 133

Figure 4.24: Products distribution at a) 0.07 A/cm^2, b) 0.14 A/cm^2, c) 0.21 A/cm^2, and d) 0.28 A/cm^2 of current densities with 3.0 M of glycerol at 80.0 °C. 135

Figure 4.25: Optimization of 1,2-propanediol (12PDO) yield as a function of operating conditions: The combined of a) temperature and initial concentration, b) temperature and current density, and c) current density and initial concentration. 140

LIST OF TABLES

Table 2.1: Products available from glycerol electrooxidation and electroreduction reactions with their applications. 9

Table 2.2: Electrodes used in glycerol electrochemical conversion, reaction conditions, glycerol conversion, products selectivity, and yield. 17

Table 2.3: Advantages and disadvantages of some of the recent mono-metallic electrocatalysts/ electrodes. 31

Table 2.4: Additives used in the glycerol electroreduction and catalytic conversion. 50

Table 3.1: List of chemicals and reagents used. 65

Table 3.2: Range of independent variables with their coded experimental domains. 73

Table 3.3: The central composite design (CCD) matrix for 20 experiments of glycerol electroreduction. 73

Table 3.4: Glycerol standards solutions prepared for the calibration curve. 75

Table 3.5: List of chemical standards, their physical properties, and retention time generated in GC-MS and GC-FID analyses. 77

Table 4.1: Electrochemical properties from cyclic voltammetry and chronoamperometric measurements. 91

Table 4.2: 1,2-propanediol and minor products selectivity and yield under different operating conditions using Pt anode and 80ACC cathode electrodes for 8 hours of electrolysis. 105

Table 4.3: The central composite design (CCD) matrix for 20 experiments of glycerol electroreduction with the response (*Y*). 137

Table 4.4: ANOVA for response surface quadratic model. 138

Table 4.5: Elementary steps for the overall glycerol electroreduction reaction. 143

LIST OF SCHEMES

Scheme 2.1: General reaction pathway of glycerol electrooxidation on Pt-based electrodes incorporated with d-group metals in alkaline medium...28

Scheme 2.2: General reaction pathway of glycerol electrooxidation on Pt-based electrodes incorporated with p-group metals in acidic medium..29

Scheme 2.3: Proposed reaction mechanism of glycerol electroreduction on Pt cathode electrode in different pH of reaction media. 32

Scheme 2.4: Glycerol electrooxidation pathway on the platinum electrode in an acidic medium at 0.75 V and 1.30 V *vs.* RHE (Roquet et al., 1994). 40

Scheme 2.5: Proposed reaction mechanisms for electrooxidation of glycerol (Zhang et al., 2012; Zhang et al., 2014) 41

Scheme 2.6: Reaction mechanisms for 1,2-propanediol and 1,3-propanediol production from glycerol a) Two-step mechanism (Dehydration and hydrogenation) and b) Three-step mechanism (Dehydrogenation, dehydration, and hydrogenation)..........................55

Scheme 4.1: Schematic diagrams of a) general two-steps catalytic/electroreduction mediated by Amberlyst-15 and b) the proposed reactions mechanism for glycerol electroreduction...98

Scheme 4.2: Formation of 1,2-propanediol and by-products from acetol reaction.......104

Scheme 4.3: a) Dehydration of protonated glycerol *via* pinacol rearrangement and b) reductive reaction mediated by Amberlyst-15 mechanism pathways..........................121

Scheme 4.4: Electro-hydrogenation of acetol. 122

Scheme 4.5: a) Electrocatalytic cleavage of glycerol radical and b) intermolecular dehydration of ethylene glycol...123

LIST OF SYMBOLS AND ABBREVIATIONS

ABBREVIATIONS

12PDO	:	1,2-propanediol
ACC	:	Activated carbon composite
ACTL	:	Acetol
BP	:	Boiling point
CA	:	Chronoamperometry
CE	:	Counter electrode
CV	:	Cyclic voltammetry
DEG	:	Diethylene glycol
EDX	:	Energy-dispersive X-ray spectroscopy
e. g	:	*Exempli gratia* means for example
EG	:	Ethylene glycol
df	:	Degree of freedom
FESEM	:	Field emission scanning electron microscopy
GC-FID	:	Gas chromatography - Flame ionization detector
GC-MS	:	Gas chromatography - Mass spectroscopy
h	:	Hour
MW	:	Molecular weight
min	:	Minute
PEM	:	Proton exchange membrane
PTFE	:	Polytetrafluoroethylene
Q^2	:	Predictive relevance
R^2	:	Determination coefficient
RE	:	Reference electrode

RT : Room temperature

TEG : Tetraethylene glycol

TEMPO : 2,2,6,6-tetramethylpiperidinyl-N-oxyl

s : Second

WE : Working electrode

SYMBOLS

Symbol		Meaning	Unit
E	:	Voltage	V
EASA	:	Electroactive surface area	cm^2
C_o	:	Initial concentration of the reducible reactant	M
D	:	Diffusion coefficient	cm^2/s
F	:	Faraday constant	C/mol
I	:	Current	A
j	:	Current density	A/cm^2
k	:	Rate constant	s^{-1}
n	:	Number of electrons	-
t		Time	s, min, or h
T	:	Temperature	°C
R_t	:	Retention time	min
W	:	Energy consumptions	kWh/ kg

NOMENCLATURE

$ACC\text{-}H_{ads}$: Hydrogen adsorbed on ACC electrode
$C_3H_8O_3$: Glycerol
$(C_3H_9O_3)^+$: Protonated glycerol
$C_3H_6O_2$: Acetol
$(C_3H_9O_3)\bullet^-$: Anionic radical glycerol
$C_2H_5O_2\bullet$: Ethylene glycol free-radical
CH_2O^- : Methanol free-anion
$C_2H_6O_2$: Ethylene glycol
CH_3O : Methanol
$C_3H_8O_2$: 1,2-propanediol
$(C_2H_7O_2)^+$: Protonated ethylene glycol
$C_4H_{10}O_3$: Diethylene glycol
e^- Electron
H^+ : Hydrogen ion
$H\bullet$: Hydrogen radical
H_2 : Hydrogen
H_2O : Water
OH^- : Hydroxide ion

LIST OF APPENDICES

APPENDIX A: Electroactive surface areas (EASA) calculation for each electrode using chronoamperometry analysis... 167

APPENDIX B: GC mass spectra for compounds obtained from electrolysis............... 172

APPENDIX C: GC chromatograms for the standards 176

APPENDIX D: Standards calibration curves.. 179

APPENDIX E: The calculation of glycerol conversion, products yield and selectivity 188

CHAPTER 1: INTRODUCTION

1.1 Background

Glycerol is an attractive biomass resource that is presently produced as waste from biodiesel manufacture. Biodiesel production was more than 30.8 million m^3 in 2016, 7.5% than in 2015 (Monteiro et al., 2018). Future evaluations also proposed this green energy will increase about 4.5% yearly and reach 41 million m^3 in 2022, showing that more crude glycerol will be unavoidably produced. Attributable to the impurities including alcohol, unreacted glycerides, fatty acids, water, and catalysts in crude glycerol, this waste cannot be exploited directly in most applications (Qadariyah et al., 2011). Crude glycerol purification using the distillation technique is costly and economically impractical, particularly for a small-scale biodiesel plant (Bruno et al., 2018; Pitt et al., 2019). Because of these problems, glycerol value has declined year by year with a recent cost of \$180 to \$540 per metric ton for low-grade glycerol and \$1100 per metric ton for high-quality glycerol (Biddy et al., 2016). As an urgent new usage is essential, many researchers have taken initiative to convert this low-cost biomass into value-added compounds such as synthesis gas, acrylonitrile or liquid fuels, and organic compounds, *e. g*., glycolic acid, glyceric acid, tartronic acid, mesoxalic acid, lactic acid, 1,2-propanediol, and 1,3-propanediol. This innovation can concurrently reduce glycerol surplus and open new opportunities for biodiesel producers.

The glycerol conversion can be achieved *via* selective oxidation, hydrogenolysis, hydrodeoxygenation, catalytic reforming, dehydration, fermentation, and electrochemical conversion (Anitha et al., 2016; Dai et al., 2017; James et al., 2018; Lee et al., 2018; Rukowicz & Alejski, 2018; Valter et al., 2018). However, the electrochemical method is recommended for this conversion due to its simple operation. It can be considered as green technology since it uses electrons as the redox reagent rather than relying on potentially hazardous chemical oxidants and reductants. This method can be completely eco-friendly when the electricity employed in it is obtained from sustainable sources such as wind and solar energies (Orella et al., 2018). Unlike the catalytic hydrogenolysis and hydrodeoxygenation practices which normally involve high temperature and high hydrogen pressure (Sharma et al., 2014; Torres et al., 2010; Yfanti & Lemonidou, 2018; Zhou et al., 2010), the electrolysis can be done at low temperature and ambient pressure. Besides, unaccompanied by the heating and pressuring equipment, the electrochemical performance can still be improved by altering the kinetics parameters (Dai et al., 2017; Orella et al., 2018). Indeed, each product formed through this technique has different optimal conditions of electrode material, electrolyte pH, applied voltage or current density, and electrolysis time.

Nonetheless, recently, the expensive metal-based electrodes such as platinum, palladium, and gold which are inconvenient for large scale are still used in the electrochemical technique (Araujo et al., 2019; Carrettin et al., 2003; Inoue et al., 2018; Sarno & Iuliano, 2018). Research efforts are then focused on multi-metallic electrodes by alloying them with foreign metals (such as Bi, Sb, Sn, In, and Ag) or other polymers (like PANI) to resolve the issues. Their modification is not only reducing the onset potential and electrodes production cost but also improves the catalytic activity and alters the mechanism pathways to more selective reactions. Even so, these metal-based electrodes only focused on electrooxidation reaction, and the studies were mostly conducted using pure glycerol instead of crude glycerol. The electrooxidation of glycerol is usually coupled with numerous cathodic reactions, such as, carbon dioxide reduction reaction (CO_2RR), hydrogen evolution reaction (HER), oxygen reduction reaction (ORR), and glycerol electroreduction. The combination of glycerol electrooxidation with these cathodic reactions can benefit in terms of energy effectiveness or additional valuable compounds be achieved differing on the cathode reduction reaction chosen in the process (Fan et al., 2021). Thus far, the information of glycerol electroreduction reaction is very limited. Although some researchers reported the success of this approach, the cathode electrodes used yet need to be enhanced. The mechanistic investigation for this reaction also remained difficult because of the complexity arising from hydroxyl groups in glycerol molecule and the complex behaviour of its reaction in the catalyst presence (Nimlos et al., 2006; Tavakol et al., 2019). The knowledge and indication on how the addition and removal of hydroxyl groups or oxygen species are constrained due to various intermediary steps and potential products (Nimlos et al., 2006). These reasons make the mechanistic and kinetics studies of glycerol electroreduction more crucial in industrial processes. The estimation of the accurate mechanisms is able to help the optimization or standardization in the glycerol electrochemical conversion (Kongjao et al., 2011). Therefore, to unravel this crisis, the activated carbon-based electrodes in the Amberlyst-15 solution were employed for the electroreduction of glycerol. Amberlyst-15 as a redox mediator which can provide an effective way to stimulate electrons transport between the inexpensive electrode and glycerol was also used in this work. To investigate the reaction mechanisms of glycerol electroreduction, the proposed intermediates were used as the reactants. Apart from that, the effects of kinetics parameters like reaction temperature, glycerol initial concentration, and current density were adjusted to obtain the best conditions for glycerol electroreduction on the activated carbon-based electrodes. Response surface methodology (RSM) was employed to get the optimum conditions for high yield of major product.

1.2 Problem statement

As mentioned earlier, aside from achieving proper operating conditions, an efficient and affordable cathode electrode is also significant. The investigation on this problem is essential because the current research findings showed that the valuable products, for instance, 1,2-propanediol, 1,3-propanediol, ethylene glycol, and acrolein were mostly acquired on Pt electrodes (Hunsom & Saila, 2015). Other than its expensive price, Pt electrode is easily poisoned by CO molecules or intermediates, hence, Pt loading should be lowered or substituted with better materials and its durability must be increased. The low-cost carbon-black activated carbon (CBAC) and carbon-black diamond (CBD) electrodes have then successfully obtained 1,2-propanediol (with 86% and 68% selectivity, respectively) but, with the minimum yield (Lee et al., 2018). Moreover, the reaction mechanisms are still uncertain, and no works have paid particular attention to the role of activated carbon composition in the electrodes towards the electrochemical properties, products distribution, and overall reaction mechanisms.

Despite the fact that the carbon-based electrodes have started to develop for the past few years, owing to the mechanistic complexity of reactions, the detailed understanding of these kinetics parameters is also inadequate. Hunsom and Saila's research team has so far obtained the highest yield for 1,2-propanediol (only approximately 15%) on the Pt electrode (Hunsom & Saila, 2013, 2015; Saila & Hunsom, 2015). It was proposed that glycerol was selectively oxidized in the early step, followed by the reduction reaction. The yield and selectivity were relatively minimal due to a wide distribution of products in an undivided reactor. Additionally, the kinetics model discussed in their works did not clearly explain each intermediate reaction step that occurred in the process, thus, could not deliver sufficient mechanistic insights. Therefore, the authentication of glycerol electroreduction mechanism pathways especially, into 1,2-propanediol and its kinetics study is necessary to improve the major product yield and selectivity.

1.3 Objectives of research

The objectives of this work are:

1. To study the influence of activated carbon on the physicochemical and electrochemical properties of activated carbon composite (ACC) electrodes for glycerol electroreduction.
2. To verify the suggested reaction mechanisms of glycerol electroreduction on the selected ACC electrode using the proposed intermediates (acetol and ethylene glycol) as the glycerol substitutes.
3. To investigate the effects of kinetics parameters such as reaction temperature, glycerol initial concentration, and current density on the reaction mechanisms and products distribution from glycerol electroreduction reaction.

1.4 Scope of work

Figure 1.1 shows the procedures that were described in this dissertation. This work has three stages. In part I, the first investigation is to synthesize activated carbon composite (ACC) cathode electrodes with different activated carbon loading percentages, which later the performance of the electrodes is compared to platinum. The reaction mechanisms of glycerol electroreduction on the selected ACC electrode are elucidated and verified using the suggested intermediates (acetol and ethylene glycol) as the feedstocks in part II. The effects of reaction temperature, glycerol initial concentration, and electric current density are explored in part III.

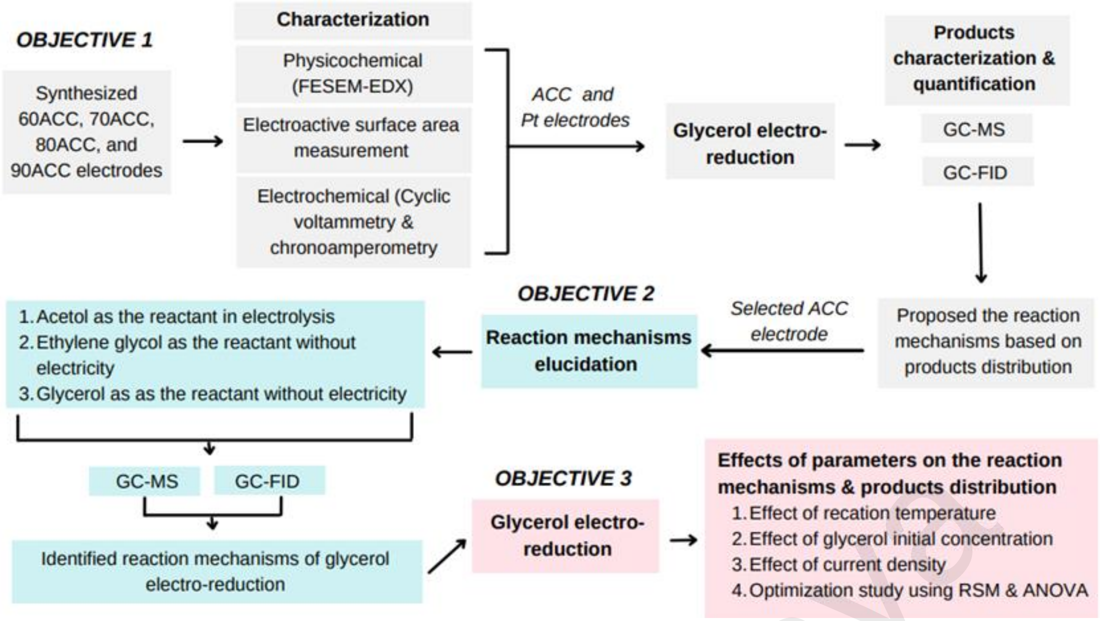

Figure 1.1: Workflow of the thesis.

1.5 Dissertation structure

Overall, this dissertation consists of five main chapters in sequences of introduction, literature review, research methodology, results and discussion, and conclusion.

The introductory chapter briefly discusses the recent problems encountered for techniques used in the conversion of glycerol, research objectives, the work scope, and the structure of this thesis.

In the literature review chapter, the current scenario in the electrochemical method for glycerol conversion with its factors affecting reaction mechanisms, reaction rates, product selectivity, and yield are evaluated. The modification techniques of activated carbon-based electrodes are also reviewed. Moreover, future prospects such as solid acid catalysts as additives, and activated carbon-based electrodes are covered in this part.

The research methodology chapter explains the synthesis of activated carbon composite (ACC) electrodes and their physicochemical and electrochemical characterization techniques. Besides, the detailed approach for reaction mechanisms elucidation on the selected ACC electrode is confirmed. The variation range of operating kinetics parameters is demonstrated in the preliminary studies and response surface methodology (RSM). The characterization and quantification of the liquid products that were done using the analytical techniques are also illustrated in this section.

Chapter 4 includes the discussion on the physicochemical and electrochemical properties of different ACC electrodes. The products formed with different values of selectivity and yield on the ACC electrodes after the bulk electrolysis are also debated. Furthermore, the elucidated reaction mechanisms are assessed in detail. Additionally, the effects of kinetics parameters such as reaction temperature, initial glycerol concentration, and current density on the reaction mechanisms, products selectivity, and yield are also reviewed in this section.

Lastly, the conclusion chapter summarizes all research outputs and recommends further works for future research.

CHAPTER 2: LITERATURE REVIEW

2.1 Introduction

This part presents an overview of the current scenario in the glycerol electrochemical conversion, the factors affecting the reaction mechanisms, reaction rates, product selectivity, and yield. Possible products obtained from the process, their market price, and benefits to the industries are also discussed. In addition, the utilization of solid acid catalysts as additives and activated carbon-based electrodes for future studies are suggested.

2.2 Glycerol and value-added chemicals in the market prospects

Glycerol is a multi-functional compound that could be transformed to more than 2000 fine chemicals from its crude form (Okoye et al., 2017; Tan et al., 2013). The most common oxidation products are glyceraldehyde, dihydroxyacetone, glyceric acid, hydroxypyruvic acid, tartronic acid, mesoxalic acid, glycolic acid, lactic acid, and glyoxylic acid. Although some of these products like glycolic acid, glyceric acid and lactic acid are vastly valuable compounds, others like dihydroxyacetone have a lower price in the market. The valuable compounds like 1,2-propanediol and 1,3-propanediol are the new potential products that have been achieved recently *via* glycerol electroreduction reaction, where 1,3-propanediol has higher market price than 1,2-propanediol (James et al., 2018; Lee et al., 2018). Some products available from both glycerol electrooxidation and electroreduction reactions with their applications are listed in Table 2.1.

Table 2.1: Products available from glycerol electrooxidation and electroreduction reactions with their applications.

Products	Description	Application	Selling price in USD (% Purity) *	Ref.
Glyceraldehyde 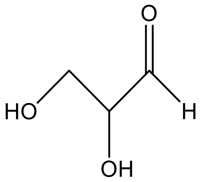	• It is a triose monosaccharide, which is the simplest of all common aldoses and it is known as glyceral. • It is a colorless and sweet crystalline solid, which could be obtained as an intermediate species during glycerol oxidation.	▪ Anti-ageing agent in production of advanced glycation end-products (AGEs). ▪ A fundamental metabolite, modification, and crosslinking of proteins.	105-199/g (98%)[a]	(Bijvoet et al., 1951; Clough, 2014; Pinter et al., 1967)
Dihydroxyacetone 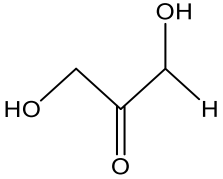	• Dihydroxyacetone, also called glycerone, is a simple saccharide (a triose). • It is a ketotriose comprising acetone with hydroxyl substituents at 1 and 3 positions. • It is the parent of the class of glycerones and the simplest member of the class of ketoses.	▪ A versatile intermediate to produce other organic compounds and as tanning agent in cosmetics. ▪ Antifungal agent and raw material for D, L-serin production, monomer for polymeric biomaterials. ▪ As a metabolite for human, Escherichia coli and Saccharomyces cerevisiae metabolite	69-83.5/g (97%)[a]	(Bagheri et al., 2015; Pagliaro et al., 2007; Petersen et al., 2003)
Glycolic acid 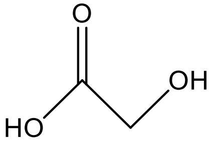	• It is a conjugate acid of glycolate and the smallest α-hydroxy acid (AHA) that is known as hydroxyacetic acid or hydroacetic acid. • It is an odorless, hygroscopic, and colorless crystalline solid, which is extremely water-soluble.	▪ As an anti-oxidizing agent or chemical peeling product in the cosmetic industries. ▪ A precursor for drug synthesis material and biopolymer material production. ▪ It is used broadly in the production of biodegradable poly(glycolic acid) (PGA) for ideal packaging material and poly(lactic-co-glycolic acid) (PLGA) for medical applications.	464/kg (99%)[b]	(Hua et al., 2018)

Table 2.1 continued.

Glyceric acid 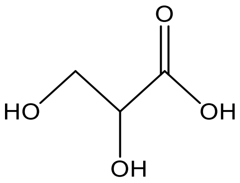	• It is a conjugate acid of glycerate, and a natural a natural three-carbon sugar acid. • It is a trionic acid, comprising propionic acid substituted at the second and third positions by hydroxy groups.	▪ As an intermediate for further oxidation to tartronic acid or mesoxalic acid. ▪ It possesses anticholesterol activity and esters of glyceric acid that have antitrypsin activity.	563/g (99%)[c]	(Coelho et al., 2018; Hirasawa et al., 2013; Katryniok et al., 2011)
Lactic acid 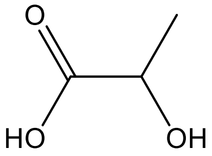	• It is the conjugate acid of lactate, and an alphahydroxy acid (AHA) because of the existence of carboxyl group, which is adjacent to the OH group. • Lactic acid is synthesized conventionally by chemical synthesis or by fermentation of carbohydrates like glucose, lactose, or sucrose.	▪ As the main ingredient in the food industry as a preservative, ascidulant and inhibitor of bacterial spoilage. ▪ A raw material in cosmetics, pharmaceuticals, textiles and leather and bioplastic (PLA) manufactures ▪ As an intermediate compound to generate acrylic acid, 1,2-propanediol, pyruvic acid, acetaldehyde and 2,3-pentanedione	123/kg (85%)[d]	(Arcanjo et al., 2017; Oberhauser et al., 2018; Zhang et al., 2016)
Tartronic acid 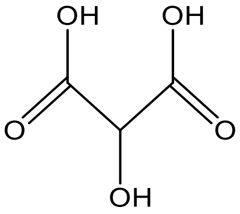	• It is a conjugate acid of tartronate and a dicarboxylic acid that is known as 2-hydroxymalonic acid. • It is a malonic acid substituted by a hydroxy group at the second position and its derivative, 2-methyltartronic acid is an isomalic acid.	▪ As a drug-delivery agent in the treatment of diabetes and osteoporosis diseases. ▪ As an anti-corrosive and protective agent which its role as an oxygen scavenger helps to prevent the oxidative decomposition in the food industry and corrosion in boilers or other high temperature applications. ▪ As an intermediate compound to generate mesoxalic acid via catalytic oxidation technique.	9.93/g (97%)[c]	(Caselli et al., 1997; Coelho et al., 2018; Tian et al., 2016)

Table 2.1 continued.

Mesoxalic acid 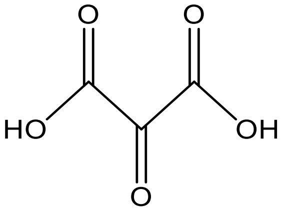	• It is a conjugate acid of mesoxalate that is known as ketomalonic acid or oxomalonic acid. • Mesoxalic acid is both a ketonic acid and a dicarboxylic acid, which voluntarily loses two protons to produce mesoxalate, a divalent anion $C_3O_5^{2-}$.	▪ As a precursor in the synthesis of 4-chlorophenylhydrazone mesoxalic acid which is known to be an anti-HIV agent.	140/g (98%)^c	(Ciriminna & Pagliaro, 2004; Davis et al., 2000)
Acetol 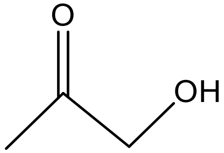	• It is known as hydroxyacetone that consists of a primary alcohol (-OH) on acetone. • Acetol is an α-hydroxyketone (called as ketol) that is colorless, hygroscopic and miscible with ethanol and ethyl ether. • It is extremely reactive due to the hydroxyl and carbonyl functional groups in its structure.	▪ As an intermediate molecule to synthesize propylene glycol, acrolein, propionaldehyde, acetone and furan derivatives ▪ It gives aroma to the bread and induce flavor compounds in the food industry. ▪ As a precursor to reduce dye to a water-soluble compound in the textile industry. ▪ As a skin tanning agent in the cosmetics.	250/kg (90%)^f	(Chiu et al., 2006b; Mohd Hanif et al., 2011)
Ethylene glycol 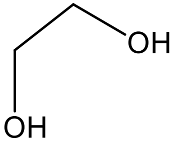	• It is known as ethane-1,2-diol that is sweet-tasting, odorless, colorless, hygroscopic liquid and toxic. • It is completely soluble in the polar solvents and only slightly soluble in non-polar solvents.	▪ As a desiccant in the production of natural rubber. ▪ As an antifreeze and coolant in automobiles, and a de-icing fluid for aircraft and windshields. ▪ As a precursor for polyester fibres and resins manufacturing.	97.50/L (99%)^b	(Caldeira et al., 2021; Yue et al., 2012)

Table 2.1 continued.

3-methoxy-1,2-propanediol 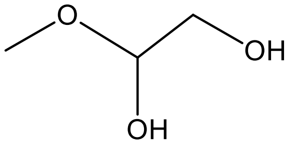	• It is known as glycerol ether that has two hydroxyl functional groups on its structure.	▪ Used as the solvents and precursor in polymers, lubricants, inks, and liquid detergents. ▪ As the fuel additives.	20.4/g (98%) ^{c}	(Bruniaux et al., 2019; Sutter et al., 2015)
Diethylene glycol 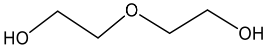	• It is clear, odorless, colorless chemical with sweet taste.	▪ As a precursor in the preparation of anti-freeze, cosmetics, brake fluids, lubricants, and heating or cooling fuel.	42.80/kg (99%)^{b}	(Vale, 2007)
1,2-Propanediol 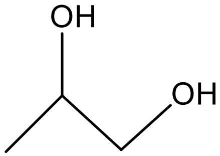	• It is known as propylene glycol, is a colorless, odorless, clear, and viscous liquid with slightly sweet taste.	▪ Used in unsaturated polyester resins, pharmaceutical products, food, cosmetics, liquid detergents, tobacco, flavourings and scents, personal hygienic products, and paints preparation. ▪ As the anti-freezing and de-icing agents.	298/kg (99%)^{b}	(Ardila et al., 2017; Dieuzeide et al., 2017)
1,3-propanediol 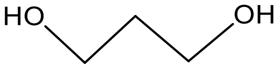	• It is a diol compound that similar with 1,2-propanediol properties. • It is also a colorless and viscous liquid miscible with water.	▪ Used in cosmetics, lubricants, and medicines. ▪ As an intermediate compound in the polymers production (polyesters, polyethers, polyurethanes and polytrimethylene terephthalate (PTT)).	263/L (98%) ^{c}	(Rukowicz & Alejski, 2018; Vivek et al., 2018; Waszak et al., 2016)

^{a}HPLC grade, ^{b}ReagentPlus® grade, ^{c}Aldrich grade, ^{d}Natural grade, ^{e}ACS reagent grade and ^{f}technical grade, and *: selling price adopted from SigmaAldrich.

2.3 Fundamental reactions in electrochemical conversion

An understanding of the basic chemistry in the electrochemical reaction and its engineering aspect is very important since most of these compounds serve great opportunities in many industries. Fuel cells and electrolysis cells are recently employed for glycerol conversion. A fuel cell generates both valuable compounds and electrical energy by glycerol electrooxidation at the anode and oxygen reduction at the cathode (Figure 2.1a), whereas, electrolysis leads to the co-generation of valuable compounds and hydrogen through glycerol oxidation at the anode and water reduction at the cathode (Figure 2.1b) (Simões et al., 2012; Talebian-Kiakalaieh et al., 2018). Compared with other conventional heterogeneous catalytic reactors, the operating cost of glycerol electrochemical conversion is cheaper due to the simplicity of the reaction process and the reactor design (Kim et al., 2017). It also saved approximately 2.1 kWhm^{-3} H_2 of electrical energy, and the energy efficiency of glycerol conversion to hydrogen was around 44%. Although 82% of electricity generated from hydrogen is supplied by glycerol and 18% of the energy came from electrical energy, the electricity consumption was reduced from 82% to 66% (Marshall & Haverkamp, 2008). Therefore, in terms of economic feasibility, this process has achieved this benchmark and could bring forth upscale study in the future.

Other than a single cell, a two-compartment cell is frequently performed through an anion-exchange membrane (AEM) that is known as a reversed ionic diffusion migration process or a proton-exchange membrane (PEM) which is a direct proton diffusion migration process. Ideally, these membranes must easily transport ions to maintain a high conductivity and a low applied potential between the electrodes when using high currents. They should be low permeability which means a minimal exchange of solvent and neutral molecules (Frontana-Uribe et al., 2010). The difference between these membranes is the charge carrier where hydroxide ions (OH^-) will migrate through AEM from the cathode to anode whilst the hydrogen ions (H^+) travel through PEM from the anode to cathode in order to allow the completion of redox catalysis (Figure 2.1). The electrons that are released from the electrooxidation reactions will migrate through the external circuit to complete the loop (Pan et al., 2017). These electrons have been successfully used to convert glycerol into oxidized (*e.g.,* glyceraldehyde and glyceric acid) and reduced (*e.g.*; 1,2-propanediol and 1,3-propanediol) compounds instead of using a stoichiometric chemical oxidant (like H_2O_2 and O_2) or reductant (like H_2) (Kim et al., 2014; Nakagawa et al., 2018). The basic products formation through this redox catalysis with both reactors has been discussed in the literature (Simões et al., 2012).

However, the glycerol mechanistic studies remained difficult because of the complexity arising from hydroxyl groups and the presence of different electrocatalysts (Nimlos et al., 2006). By understanding the precise reaction mechanisms and kinetics, process optimization and design will become easier. At this point, the reaction mechanisms, and the rates at which glycerol electrochemical conversion proceed are dependent on various kinetics and thermodynamic parameters such as electrodes characteristics, pH of the solution, current density, applied potential, temperature, and additives, which must be optimized to achieve high selectivity and yield of desired products.

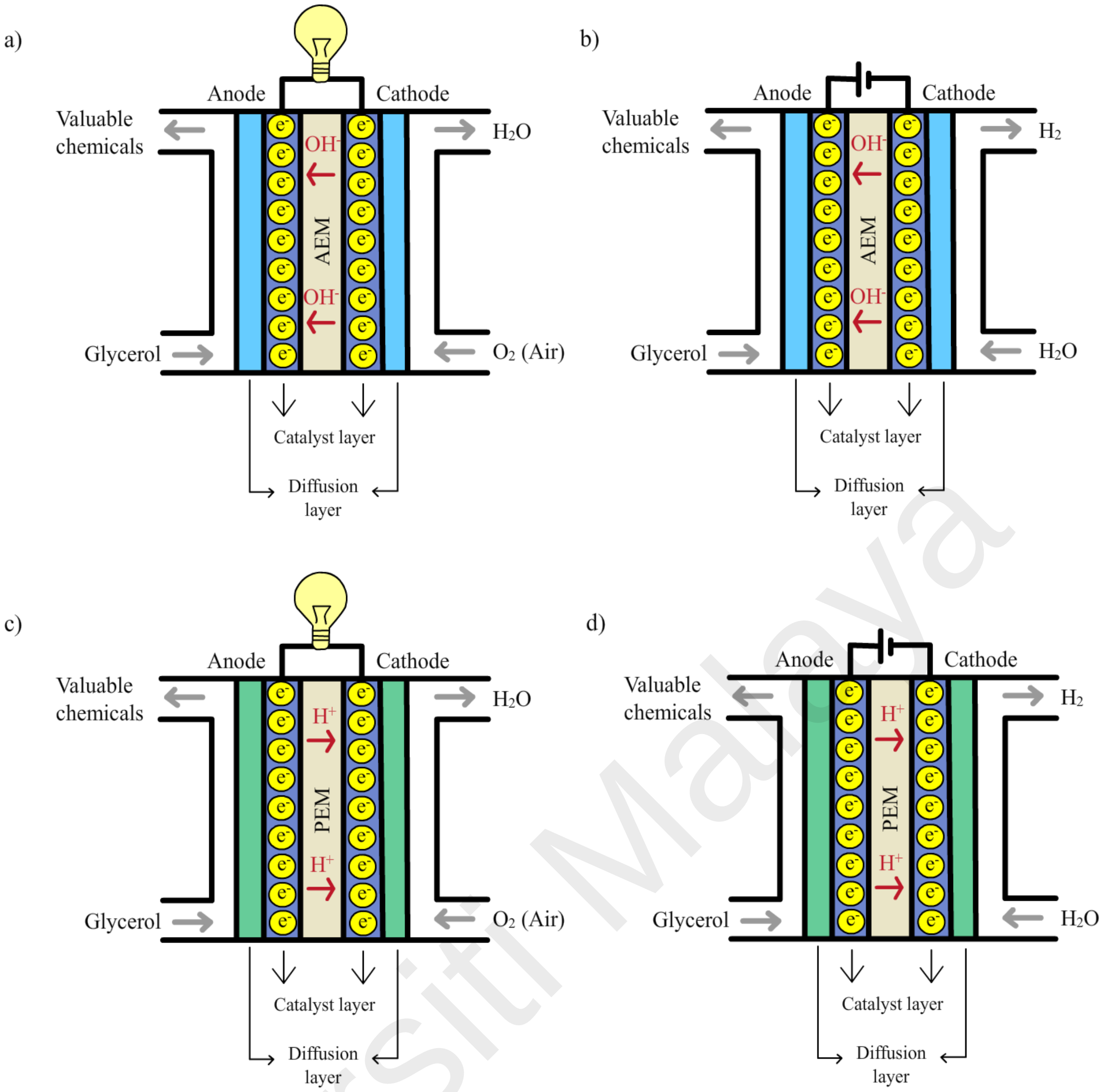

Figure 2.1 Working principles of a) AEM-fuel cell, b) AEM-electrolysis, c) PEM-fuel cell and d) PEM-electrolysis (Marshall & Haverkamp, 2008; Pan et al., 2017; Simões et al., 2012).

2.4 Effects of parameters on mechanism pathways and reaction performances

The mechanism pathways and reaction kinetics can be influenced by overpotential, glycerol conversion, selectivity, and yield of desired products, which could alter reaction parameters like activation energy barrier to stimulate fast molecular collision and surmount the binding energies of the reactants. Figure 2.4 presents various types of electrodes used in their corresponding reaction conditions, glycerol conversion, selectivity, and yield of products. Depending on the properties of electrodes and reaction conditions (pH of electrolyte, temperature, applied potential and current density), primary or secondary hydroxyl group of glycerol can be oxidized to glyceraldehyde and dihydroxyacetone, respectively. Normally, the effect of each parameter on the reaction is determined when all the parameters are kept constant while varying the parameter under investigation. The glycerol electrochemical conversion performance can be explained by many parameters including the electroactive surface area (EASA), onset applied potential (E_{onset}), current density (j), overpotential (η), Tafel slope, electrode stability, charge transfer resistance (R_{ct}), double-layer capacitances (C_{dl}), production rate, yield, Faraday efficiency (FE), and products selectivity (Fan et al., 2021). These parameters are then validated using kinetics rate laws or other electrochemical (*e.g.*, voltammetry and chronoamperometry), instrumentation (*e.g.*, *ex-situ* or *in-situ* spectroscopic, and online chromatography), and computational techniques.

Table 2.2: Electrodes used in glycerol electrochemical conversion, reaction conditions, glycerol conversion, products selectivity, and yield.

Electrode		Reaction parameters							Results			Ref.
WE (A)	CE (C)	Electrolyte	Additives	Current onset (A)	Voltage onset (V)	Temp. (˚C)	Stirring speed (rpm)	Reaction time (h)	Selectivity (%)	Yield (%)	Glycerol conversion (%)	
Major product: Glyceraldehyde												
Pt/C	Pt wire	0.1 M glycerol + 0.5 M H_2SO_4	-	-	0.697 *vs.* SHE	60	-	70	48.8	-	34.2[a]	(Kim et al., 2014)
Pt	Pt	0.1 M glycerol + 0.1 M NaOH	-	-	0.4 *vs.* RHE	-	-	-	100	-	-	(Kwon et al., 2011)
Pt	Pt	0.1 M glycerol + 0.5 H_2SO_4	-	-	0.4 *vs.* RHE	-	-	-	100	-	-	(Kwon et al., 2011)
Pt	Pt	0.1 M glycerol + 0.1 M NaOH	-	-	0.79 *vs.* RHE	25	-	28	88	-	49	(Roquet et al., 1994)
Pt	Pt	0.1 M glycerol + 0.1 M $HClO_4$	-	-	0.75 *vs.* RHE	25	-	28	97	-	49	(Roquet et al., 1994)
Pt	Pt	0.1 M glycerol + 0.1 M $HClO_4$	-	-	1.30 *vs.* RHE	25	-	28	56	-	49	(Roquet et al., 1994)
Pd NCs	Pt	0.5 M glycerol + 0.5 M KOH	-	-	-0.4 *vs.* SCE	-	-	-	61.2	-	-	(Zhou & Shen, 2018)
Ti-RuO_2	Pt	0.25 M glycerol + 0.5 M NaCl	-	-	2.5 *vs.* AgCl/Cl	25	-	2	85	-	>10	(James et al., 2018)
Ti-RuO_2	Pt	0.25 M glycerol + 0.5 M HCl	-	-	2.5 *vs.* AgCl/Cl	25	-	2	60	-	30	(James et al., 2018)
Pb	Ti-RuO_2	0.25 M glycerol + 0.5 M KCl	-	-	-1.8 *vs.* AgCl/Cl	25	-	4	55	-	>10	(James et al., 2018)
Pb	Ti-RuO_2	0.25 M glycerol + 0.5 M HCl	-	-	-1.8 *vs.* AgCl/Cl	25	-	4	75	-	30	(James et al., 2018)
Zn	Ti-RuO_2	0.25 M glycerol + 0.5 M NaCl	-	-	2.5 *vs.* AgCl/Cl	25	-	2	75	-	>10	(James et al., 2018)

Note: Temp. (Temperature), [a](batch reactor), [b](continuous reactor), SHE: Standard hydrogen electrode, RHE: Reversible hydrogen electrode and SCE: Saturated calomel electrode.

Table 2.2 continued.

Major product: Dihydroxyacetone												
Pt	Pt	0.3M glycerol + pH 1.0	1mM TEMPO	0.14 A/cm^2	-	25	-	24	-	57.2	100	(Saila and Hunsom, 2015)
Pt	Pt	0.3M glycerol + pH 1.0	3mM TEMPO	0.14 A/cm^2	-	25	-	24	-	65.0	100	(Saila and Hunsom, 2015)
Pt	Pt	0.3M glycerol + pH 1.0	5mM TEMPO	0.14A/cm^2	-	25	-	24	-	69.2	100	(Saila and Hunsom, 2015)
$Pt_4Au_6@Ag$	Pt	0.5 M glycerol + 0.5 M KOH	-	-	1.1 *vs.* Hg/HgO	-	-	-	77.1	-	-	(Zhou et al., 2019)
3D nanoporous PtAg skeleton	Pt	0.5 M glycerol + 0.5 M KOH	-	-	0.7 *vs.* RHE	-	-	1	82.6	-	-	(Zhou et al., 2019)
3D nanoporous PtAg skeleton	Pt	0.5 M glycerol + 0.5 M KOH	-	-	0.9 *vs.* RHE	-	-	1	61.5	-	-	(Zhou et al., 2019)
3D nanoporous PtAg skeleton	Pt	0.5 M glycerol + 0.5 M KOH	-	-	1.0 *vs.* RHE	-	-	1	79.2	-	-	(Zhou et al., 2019)
3D nanoporos PtAg skeleton	Pt	0.5 M glycerol + 0.5 M KOH	-	-	1.3 *vs.* RHE	-	-	1	79.8	-	-	(Zhou et al., 2019)
PtSb/C	Pt wire	0.1 M glycerol + 0.5 M H_2SO_4	-	-	0.797 *vs.* SHE	60	400	10	68.1	61.4	90.3	(Lee et al., 2016)
PtSb/C	Pt/C	0.1 M glycerol + 0.5 M H_2SO_4	-	-	0.35-0.55 *vs.* RHE	Room T	-	-	80	-	-	(Kwon, et al., 2014)
PtBi/C	Pt/C	0.1 M glycerol + 0.5 M H_2SO_4	-	-	0.4 vs. RHE	Room T			100	0.2 mM	-	(Kwon et al., 2012)
Glassy carbon	Pt	0.05 M glycerol + 0.2 M bicarbonate (pH 9.1)	15% mol TEMPO (0.0075 M)	-	1.1 *vs.* Ag/AgCl	25	-	200	35	25	-	(Ciriminna et al., 2006)

Note: ^{a}(batch reactor), ^{b}(continuous reactor), SHE: Standard hydrogen electrode, RHE: Reversible hydrogen electrode and SCE: Saturated calomel electrode.

Table 2.2 continued.

Major product: Glycolic acid												
Pt	CBAC	0.3 M glycerol + Acidic medium	9.6% (w/v) Amberlyst-15	2.0	-	80	-	6	70	66.1	90	(Lee et al., 2019)
Pt/GNS	Pt	0.5 M glycerol + 0.5 M KOH	-	-	0.2 *vs.* SCE	60	-	2	65.4	-	-	(Zhou et al., 2018)
Au	Pt	0.1 M glycerol + 0.1 M NaOH	-	-	1.6 *vs.* RHE	-	-	-	50	-	-	(Kwon et al., 2011)
Au/C	Pt	0.5 M glycerol + 0.5 M NaOH	-	-	0.1 *vs.* Ag/AgCl	Room T	-	2	43.98	-	-	(Thia et al., 2016)
Au/CNT	Pt	1.0 M glycerol + 4.0 M KOH	-	-	1.6 *vs.* RHE	Room T	-	3	80	-	43	(Zhang et al., 2012)
Au/CNT	Pt	1.0 M glycerol + 2.0 M KOH	-	-	1.6 *vs.* RHE	Room T	-	3	85	-	34	(Zhang et al., 2012)
Au/CNT	Pt	1.0 M glycerol + 1.0 M KOH	-	-	1.6 *vs.* RHE	Room T	-	3	81	-	26	(Zhang et al., 2012)
Au/CNT	Pt	1.0 M glycerol + 0.5 M KOH	-	-	1.6 *vs.* RHE	Room T	-	3	79	-	16	(Zhang et al., 2012)
Au/CNT	Pt	2.0 M glycerol + 2.0 M KOH	-	-	1.6 *vs.* RHE	Room T	-	3	78	-	19	(Zhang et al., 2012)
Au/CNT	Pt	0.5 M glycerol + 2.0 M KOH	-	-	1.6 *vs.* RHE	Room T	-	3	87	-	29	(Zhang et al., 2012)
Pd (Ag/Pd)	Pt	0.1 M glycerol + 1 M KOH	-	-	-0.1 *vs.* Hg/HgO	Room T	-	6	-	70	-	(Inoue et al., 2018)
Major product: Glyceric acid												
Pt/C	Pt wire	0.1 M glycerol + 0.5 H_2SO_4	-	-	1.097 *vs.* SHE	60	-	70	79.9	87	91.8[a]	(Kim et al., 2014)
Pt/C	Pt wire	0.1 M glycerol + 0.5 M H_2SO_4	-	-	0.897 *vs.* SHE	60	-	70	47.4	69	68.6[a]	(Kim et al., 2014)
Pt/C	Pt wire	0.1 M glycerol + 0.5 M H_2SO_4	-	-	1.0 *vs.* SHE	60	-	70	-	80	10[b]	(Kim et al., 2014)
Pt	Pt	0.1 M glycerol + 0.1 M NaOH	-	-	1.6 *vs.* RHE	-	-	-	100	-	-	(Kwon et al., 2011)

Note: [a](batch reactor), [b](continuous reactor), SHE: Standard hydrogen electrode, RHE: Reversible hydrogen electrode and SCE: Saturated calomel electrode.

Table 2.2 continued.

PtNi/GNS	Pt	0.5 M glycerol + 1.0 M KOH	-	-	0.1 *vs.* SCE	60	-	2	47.7	-	-	(Zhou et al., 2018)
PtRhNi/GNS	Pt	0.5 M glycerol + 1.0 M KOH	-	-	-0.4 *vs.* SCE	60	-	2	55	-	-	(Zhou et al., 2018)
Pt_5Ru_5/C	Pt	0.1 M glycerol + 0.5 M H_2SO_4	-	-	1.1 *vs.* SHE	60	-	7	58.7	-	-	(Kim et al., 2017)
Au	Pt	0.1 M glycerol + 0.1 M NaOH	-	-	0.8 *vs.* RHE	-	-	-	100	-	-	(Kwon et al., 2011)
Au-P4P/G	Pt	0. 5 M glycerol + 0.5 M NaOH	-	-	0.2 *vs.* Hg/HgO	Room T	-	10	68.6	-	52.5	(Wang et al., 2015)
Au-P4P/rGO	Pt	0. 5 M glycerol + 0.5 M NaOH	-	-	0.2 *vs.* Hg/HgO	Room T	-	10	57.4	-	52.5	(Wang et al., 2015)
Au-PmAP	Pt	0.5 M glycerol + 0.5 M NaOH	-	-	0.2 *vs.* Hg/HgO	Room T	-	10	42.2	-	52.5	(Wang et al., 2015)
Pd	Pt	0.1 M glycerol + 1.0 M KOH	-	-	-0.1 *vs.* Hg/HgO	Room T	-	6	-	56	-	(Inoue et al., 2018)
Major product: Lactic acid												
$AuPt_{0.15}$	Graphite	0.5 M glycerol + 1.0 M KOH	-	-	0.45 *vs.* Hg/HgO	Room T	-	12	73	-	29.50	(Dai et al., 2017)
$AuPt_{0.29}$	Graphite	0.5 M glycerol + 1.0 M KOH	-	-	0.45 *vs.* Hg/HgO	Room T	-	12	61	-	28.80	(Dai et al., 2017)
$AuPt_{0.64}$	Graphite	0.5 M glycerol + 1.0 M KOH	-	-	0.45 *vs.* Hg/HgO	Room T	-	12	60	-	27.10	(Dai et al., 2017)
$AuPt_{0.90}$	Graphite	0.5 M glycerol + 1.0 M KOH	-	-	0.45 *vs.* Hg/HgO	Room T	-	12	69	-	16.08	(Dai et al., 2017)
Pt	Graphite	0.5 M glycerol + 1.0 M KOH	-	-	0.45 *vs..* Hg/HgO	Room T	-	12	50	-	10.70	(Dai et al., 2017)
Co-DPPE	Ni	250 mM glycerol + 1.0 M NaOH	-	1.8 mA/cm^2	-	60	400	48	45	-	85	(Lam et al., 2017)
Diamond coated	Pt	0.3% (w/w) glycerol + 3.6% (w/w) $Al_2(SO_4)_3$	-	60 A/cm^2	-	55	-	18	-	90	5-10	(Lux et al., 2010)

Note: SHE: Standard hydrogen electrode and RHE: Reversible hydrogen electrode.

2.4.1 Effect of electrodes

Up to now, noble metals such as platinum (Pt), gold (Au), and palladium (Pd) monometallic catalysts are the most efficient in the electrochemical conversion of glycerol (Carrettin et al., 2002). These materials are typically used in this conversion as tabulated in Table 2.2. Pt is known as the only material that is active for the glycerol conversion in acidic and alkaline media while Pd and Au are more active in alkaline than in acidic medium. Despite its excellent performance, Pt can be easily contaminated and is expensive (Sankar et al., 2009). The adsorbed species such as carbon monoxide (CO) and aldehydes on Pt catalyst will block the surface, and further oxidation is only allowed with the presence of adsorbed OH species (Petukhov et al., 1998). It was reported Pt (111) facets had better resistance to these poisoning species compared to those of Pt (100) and Pt (110) facets owing to the weaker binding strength with the intermediates (Gomes & Tremiliosi-Filho, 2011). In this regard, many efforts have been taken to implement the idea of cost-effective materials or reduce Pt catalyst. The combination of noble metals with earth-abundant metals from d-group (such as Au, Ag, Ni, Ru) and p-group (like In, Bi, Sn, Pb, Sb) does not only reduce the onset potential and production cost, but it also improves the catalytic activity and alters the mechanism pathways to more selective reactions. The electrodes particle size also makes significant impacts on the glycerol electrochemical reactions. As such, the small gold particles of Au/C catalyst exhibited the highest mass activities and were at least twice active than the large gold particles in the alkaline medium. It also resulted in lower glycerol oxidation onset potentials which are at least 100 mV *vs.* Hg/HgO earlier than the large gold particles of Au/C catalyst. (Padayachee et al., 2014). But, when the gold particles of the Au/C catalyst were too small, they became unstable and have grown by at least 2 nm with repetitive cycling in an alkaline medium.

The catalytic activity of the electrodes could also be enhanced by modifying their surface with different surface compositions, shapes, catalysts supports, geometries, and morphologies or applications of bi- or multi-metallic electrocatalysts since they are more active, more selective, and less prone to deactivation than monometallic electrocatalysts (Beltrán-Prieto et al., 2013; Rousseau et al., 2006). The deactivation of electrocatalysts can be avoided by the bifunctional mechanisms provided from bi- or multi-metallic catalysts (Iwasita, 2002). For instance, when two noble-metal electrodes were combined, high selectivity (73%) of lactic acid was obtained on $AuPt_{0.15}$ electrode in 1 M KOH medium instead of glyceric acid and glycolic acid. It was proposed that glycerol is oxidized to glyceraldehyde and dihydroxyacetone (DHA) through deprotonation of glycerol. The deprotonation of glycerol or the abstraction of hydroxide ions can occur with two steps which are (i) base-catalyzed oxidation to dihydroxyacetone and (ii) metal-catalyzed oxidation (Kwon et al., 2011; Zope et al., 2010). However, lactic acid was only formed when dihydroxyacetone went through base-catalyzed dehydrogenation to 2-hydroxypropenal or pyruvaldehyde followed by Cannizzaro rearrangement. The enrichment of Au on $AuPt_{0.15}$ electrode has led to the oxidation of secondary alcohol, formed DHA, and subsequently produced lactic acid with 73% selectivity (Dai et al., 2017). Formation of this DHA intermediate could be achieved either on bi-metallic (AuPt electrode) or tri-metallic electrocatalysts (Pt_4Au_6@Ag electrode) as long as the Au catalyst is slightly higher than Pt catalyst (Zhou et al., 2019).

In Zhou et al. (2019) work, Pt_4Au_6@Ag exhibited higher DHA selectivity (77.1%) compared to the Pt_6Au_4@Ag at 1.1 V *vs.* Hg/HgO using a similar basic medium (0.5 M KOH). While Zhou and Shen (2018) reported Pd@Pt NCs electrode selectively produced glyceraldehyde in 0.5 M KOH and subsequently electro-oxidized into glyceric acid which differs from Dai et al., (2017) and Zhou et al., (2019) results. From cyclic voltammetry

(CV) result, Pd@Pt NCs electrode has the highest current density (3.22 $mAcm^{-2}$) which was 3.5, 4.8, and 1.5 times from the conventional Pd/C, Pt/C, and Pd NCs catalysts (Zhou & Shen, 2018).

Gomes et al. (2014) and Inoue et al. (2018) have also replaced Pt with Au and Pd catalysts, respectively, to encounter the poisoning issue, and silver (Ag) was introduced on their catalysts. Ag has no activity toward glycerol electrochemical reactions but, the introduction of Ag on both Au and Pd catalysts has greatly enhanced the activity and selectivity of desired products at relatively low potentials (Gomes et al., 2014; Inoue et al., 2018). Based on *in situ* infrared reflectance-absorption spectra (IRAS) and high-performance liquid chromatography (HPLC) results, glycerate and glycolate were obtained as major products on both Pd and Pd (Ag/Pd) electrode at -0.1 V *vs.* Hg/HgO. On the Pd electrode, glycerate (56%) has a higher yield than glycolate (35%) while the formation of glycolate (70%) was favoured than glycerate (25%) only on Pd (Ag/Pd) electrode (Inoue et al., 2018). This result revealed the modification of Ag on the Pd electrode facilitated the C-C bond cleavage to glycolic acid similar to the presence of Ag on the Au electrode which favoured the C-C-C bond breaking, as evidenced by the selective formation of formic acid (Gomes et al., 2014; Inoue et al., 2018). It happened because of the electronic modification that changed the adsorption strength of adsorbates on the Au and Pd surfaces and eventually lead to lower onset potential. However, the excessive addition of Ag content caused the active sites of Pd to be more covered by Ag catalyst and reduced the glycerol conversion and power density as investigated by Benipal et al. (2017). Unlike these studies (PdAg and AuAg electrodes), three-dimensional (3D) nanoporous PtAg electrode favoured DHA formation of mechanism pathway with the highest current density (7.5 $mAcm^{-2}$) and 15.4 times higher than the commercial Pt/C catalyst. The remarkable DHA selectivity of 82.6%, 61.5%, 79.2%, and 79.8% were obtained at applied potentials of 0.7, 0.9, 1.0 and 1.3 V *vs.* RHE, which are 1.64, 1.46, 2.10 and 2.12 times those of the Pt/C electrocatalysts, respectively (Zhou et al., 2019). Its interconnected porous structure is advantageous for the glycerol, intermediates, and products diffusion (Fu et al., 2016) and to prevent their accumulation on catalysts surface, hence, enhancing its stability (Zhang et al., 2015).

Pt catalysts can also be fortified by incorporating carbon-based supports like graphene, carbon black, carbon nanocubes, and multi-walled carbon nanotube (MWCNT). The morphology of the graphene nanosheets could be created as wrinkles surface, thus, it will generate a large surface area with powerful adsorptive sites for glycerol electrooxidation reaction (Wang et al., 2016). This fortification will benefit in reducing the amounts of metal loading as well as enhancing their stability, electrocatalytic activity, and utilization efficiency. As such, Lee et al. (2019) attained a 1.6-fold higher peak current density of highly-dispersed Pt nanoclusters supported on microporous three-dimensional (3D) graphene-like carbon (Pt/3D-GLC) than conventional Pt/C which is relatively less poisoned by accretion of intermediates on its surface compared to Pt/C. Their reaction kinetics study using Tafel slopes revealed a value of 171.28 mV/dec was obtained on Pt/3D-GLC while Pt/C has 201.83 mV/dec value. It indicates faster electrocatalytic reaction kinetics was achieved at lower Tafel slope value that shows Pt/3D-GLC leads to enhanced glycerol electrooxidation reaction (Lee et al., 2019). Zhou et al. (2018) developed a few hybrid catalysts comprising Pt particles incorporated on graphene nanosheet (GNS) and fortified with ruthenium (Ru), nickel (Ni) and rhodium (Rh). Among the catalysts, they found PtRhNi/GNS and PtRh/GNS catalysts unveiled the superior activity in terms of the largest current density (5.58 and 4.47 $\mathrm{mAcm^{-2}}$, respectively) and lowest onset potential (-0.71 and -0.719 V *vs.* SCE, respectively) towards glycerol electrooxidation, which due to their synergistic effects. It is worth mentioning that the introduction of Ru on PtRuNi/GNS catalyst accelerated the C-C bond breakage of glycerol to glyceraldehyde better as the selectivity of this intermediate was higher (39.2%) than the bi-metallic PtNi/GNS catalyst (29.8%) at 0.2 V *vs.* SCE. After 500 cycles of CV analysis, Kim et al. (2017) found Pt_5Ru_5/C catalyst has higher stability with a normalized current density ratio of 0.635 than the conventional Pt/C catalyst (0.465). The remarkable performance of this catalyst is traceable to the DHA formation on Pt_5Ru_5/C catalyst with 35% selectivity in 0.5 M H_2SO_4 medium.

As nickel can provide different oxygen-containing species such as NiOOH and $Ni(OH)_2$ through electrodeposition, predominantly in alkaline electrolyte, Han et al. (2017) and Moraes et al. (2019) have also prepared ALD(TiO_2)-Ni/C and Pt-NiO/Ti electrocatalysts by atomic layer deposition (ALD) and thermal decomposition of polymeric precursors, respectively. The addition of nickel element on electrocatalysts would yield DHA intermediate. They revealed ALD(TiO_2)-Ni/C electrocatalyst displayed high activity with 2.4 times of current density higher than the uncoated Ni/C. The onset potential of glycerol oxidation with ALD(TiO2)-Ni/C occurred at a more negative value compared with the Ni/C catalyst, indicating an improvement in oxidation kinetics. As studied by Moraes et al. (2019), a high catalytic activity of Pt-based incorporated with nickel could also be observed on $Pt_{0.8}Ni_{0.2}O_y/Ti$ and $Pt_{0.9}Ni_{0.1}O_y/Ti$ electrocatalysts. They have better electrical conductivity compared to NiO/Ti and PtO_y/Ti catalysts due to proton transfer redox processes with O/OH ligands on the Ni atoms in alkaline medium and hence, it will increase the kinetics of glycerol electrooxidation. Also, the voltammetric charge was increased because of their synergistic effects with a porous and high active surface area. The surface area was increased as the Pt content increased, but, only up to $Pt_{0.8}Ni_{0.2}O_y/Ti$ (706.2 cm^2). Higher Pt content ($Pt_{0.9}Ni_{0.1}O_y/Ti$) reduced its surface area

(307.1 cm^2) because the layer became more compact and dense, leading to reducing the porous grains and hence, decreasing the voltammetric charge (Moraes et al., 2019).

Several authors have also reported the significant performance of Pt catalysts combined with the p-group elements. Simões et al. (2011) modified carbon-supported Pd and Pt-based nanoparticles by depositing the low amount of bismuth (Bi) on their surfaces. $Pd_{0.45}Pt_{0.45}Bi_{0.1}/C$ successfully traded the expensive Pt into half and performed better than monometallic metals like Pt/C and Pd/C electrodes. There seems to be the same general agreement by Coutanceau et al. (2014) on this issue when glycerol electrooxidation on Pt_9Bi_1/C and $Pd_{0.45}$ $Pt_{0.45}Bi_1/C$ electrodes were started at lower onset potential 0.2 V *vs.* RHE. The modification of Pd electrode by bismuth did not affect the products selectivity. Carboxylate compounds were only formed on Pd_xBi_{10-x}/C electrode at too high applied potential. But aldehydic and ketonic compounds with high selectivity were obtained on Pt electrode containing bismuth at very low potentials. This is because the glycerol oxidation occurred without activation of OH species at potentials and thus, led to the formation of aldehyde (absorption band at ca. 1335cm^{-1}) and ketone (absorption band at ca. 1225cm^{-1}) groups instead of carboxylate group (Coutanceau et al., 2014).

In a similar study by Kwon et al (2014), the enhanced catalytic activity and selectivity towards dihydroxyacetone (DHA) using carbon-supported Pt/C with adatoms (Sb, Bi, Pb, Sn, and In) were also recognized. Both Bi and Sb promoted the secondary hydroxyl oxidation to DHA while primary hydroxyl oxidation was favoured by Pb, In, and Sn elements. From the CV scan that has been conducted in 0.1 M glycerol with 0.5 M H_2SO_4, it was shown that the presence of irreversibly modified Sb on Pt/C has improved the glycerol electrooxidation and selectively oxidized the secondary hydroxyl group to DHA with the highest selectivity of DHA (80%) at 0.35 V *vs.* RHE (Kwon et al., 2014), which is in agreement with recent results using PtSb/C by Lee et al. (2016). PtSb nanoparticles can enhance the oxidative dehydrogenation of glycerol and hinder further oxidation of intermediate. DHA intermediate was formed with 61.4% yield and 90.3% glycerol conversion at 0.797 *vs.* SHE (Lee et al., 2016). The selectivity of nearly 100% DHA from glycerol also could be achieved successfully when Pt/C with Bi was used as the electrode (Kwon et al., 2012). The presence of Bi in the electrode is capable to block primary hydroxyl oxidation, avoiding CO formation, and offering a specific Pt-Bi surface site for secondary hydroxyl oxidation and led to DHA formation. The glycerol electrooxidation on the PtBi electrode predominantly generated DHA intermediate which is contradicting to pure Pt catalyst that formed glyceraldehyde as the main intermediate. However, the improvement of activity and selectivity towards DHA which is due to the bismuth addition is only applicable for Pt(111) electrode but not on Pt(100) electrode (Garcia et al., 2017). With a combination of detailed electrochemical experiments, online spectroscopy, and density functional theory (DFT) calculations, Garcia et al. (2016) proved that the surface crystallographic structure of Pt(111) and Pt(100) catalysts will affect the activity and selectivity of desired products in acidic medium. This is due to the different binding modes of dehydrogenated glycerol to their surfaces at the initial oxidation reaction. Based on the DFT study, on the Pt(100) electrode, enediol intermediate was formed when dehydrogenated glycerol bound through a double Pt=C bond (Garcia et al., 2016). Hence, only glyceraldehyde was formed as the stable intermediate *via* primary hydroxyl oxidation. But, on the Pt(111) electrode, dehydrogenated glycerol was bonded to the surface *via* two single Pt-C bonds resulting in enediol intermediate which is subsequently favoured by both glyceraldehyde and dihydroxyacetone formations. Plus, from the stripping experiments, it was suggested that an inactive intermediate was strongly bonded during glycerol, glyceraldehyde, and dihydroxyacetone oxidations, and it is very difficult to oxidize. The substitution of d-group and p-group elements on Pt catalyst is capable of significantly reducing electrode preparation cost and sustaining the electrochemical conversion performance in the future. Although it is obvious that further investigations are needed to determine both the reaction mechanisms of glycerol electrooxidation and electroreduction on the platinum surface, general mechanism pathways on Pt-based with d-group and p-group are suggested in Scheme 2.1 and Scheme 2.2, respectively.

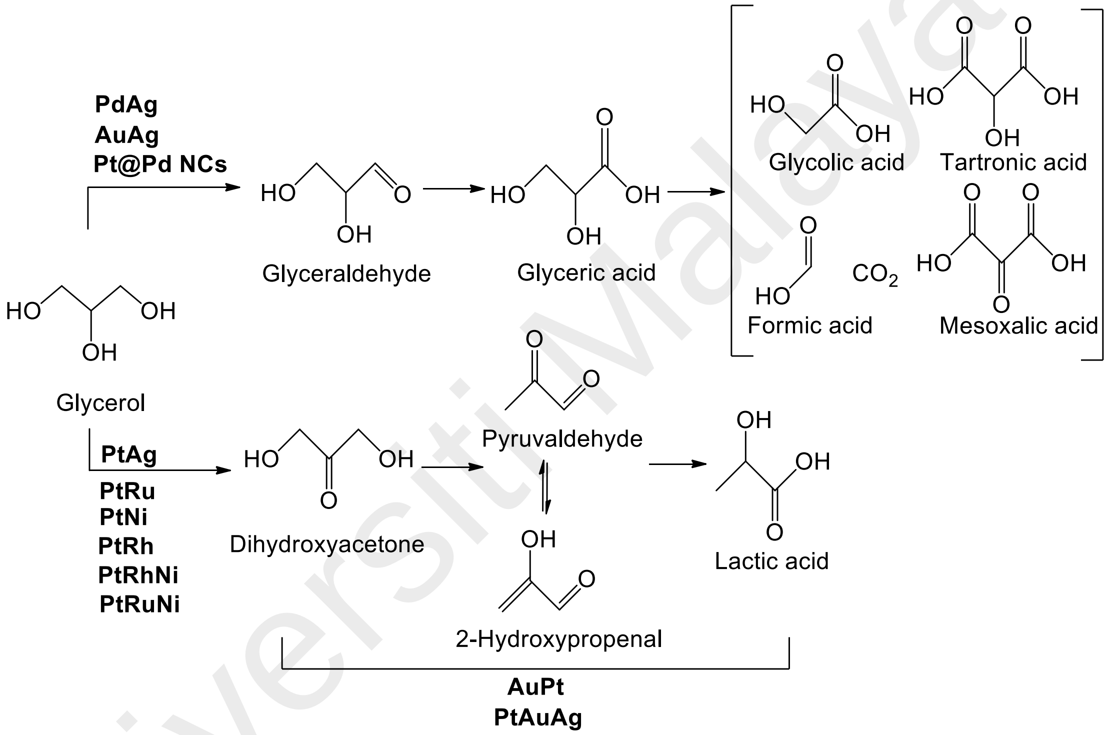

Scheme 2.1: General reaction pathway of glycerol electrooxidation on Pt-based electrodes incorporated with d-group metals in alkaline medium.

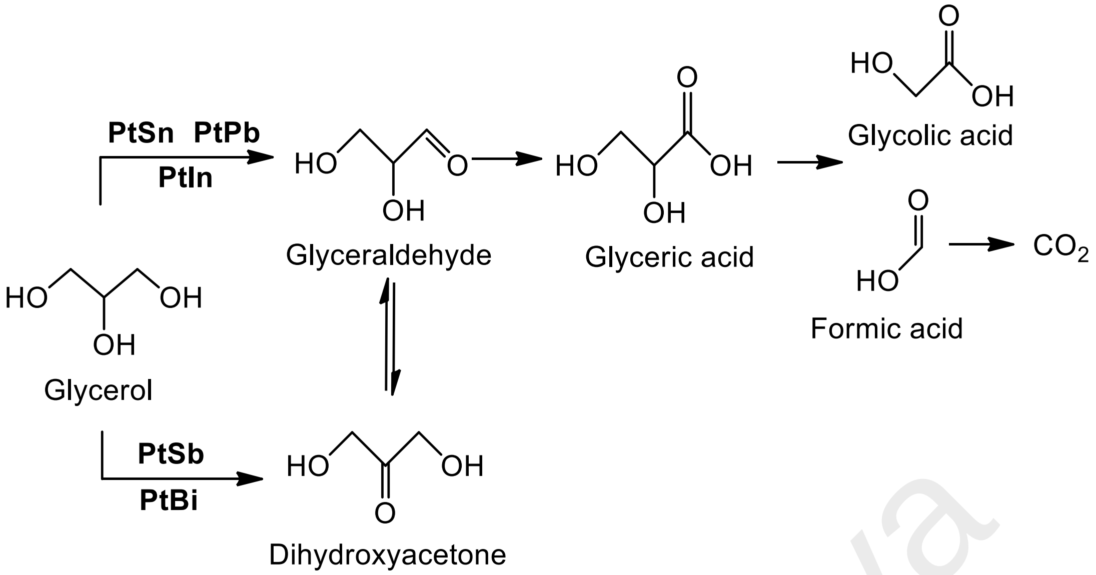

Scheme 2.2: General reaction pathway of glycerol electrooxidation on Pt-based electrodes incorporated with p-group metals in acidic medium.

2.4.2 Effect of electrolyte pH

An electrolyte in the electrochemical conversion process is usually a salt that provides ions to enhance the conductivity of the solution (Frontana-Uribe et al., 2010). The choice of electrolyte for different electrodes is important to selectively produce the desired intermediates for further reactions. Table 2.3 shows the advantages and disadvantages of various electrodes in the alkaline or acidic medium, which would be useful for future works in the selection of electrolytes based on the electrode types. With the increment of pH, the glycerol conversion rates change which is due to the different conversion mechanisms in the presence of H^+ and OH^- concentrations. In an acidic medium, Pt-based catalyst demonstrates better performance compared to an alkaline medium where in particular, glyceraldehyde and DHA are obtained as the intermediates, while, glyceric acid, tartronic acid, glycolic acid, glyoxylic acid, formic acid, and CO_2 are formed as the products from the glycerol electrooxidation (Gomes et al., 2012; Gomes & Tremiliosi-Filho, 2011; Kongjao et al., 2011; Kwon et al., 2011).

The glycerol electroreduction study was started by Kongjao et al. (2011) but the influence of pH electrolyte (1, 7, and 11) for this reaction was done by Hunsom and Saila (2013). Following 13 hours of electrolysis, Pt catalyst has shown its ability to break the C-C bond of glycerol to C_3 and C_2 species. The most elevated glycerol conversion rate was acquired at pH 1 (100%), followed by pH 11 (67.6%) and pH 7 (49.4%), indicating acidic is important for electroreduction reaction (Hunsom & Saila, 2013). As shown in Scheme 2.3, ethylene glycol was only produced at pH 1 and 11 *via* dehydrogenation of glycerol to glyceraldehyde followed by the splitting of the C-C bond. Plus, in these media, acetol was formed through dehydration of the primary hydroxyl group of glycerol. Under a strong acidic condition (pH 1), only 1,2-propanediol and 1,3-propanediol were generated by the reduction of acetol and acrolein, respectively. It was noted the mechanistic pathways of each pH reaction medium on Pt cathode catalysts have not been proved by the researchers. Hunsom and Saila (2015) carried out further investigation by utilizing enriched glycerol on Pt electrode to explore the influence of initial pH (1, 7, and 11) towards the electrochemical conversion. It was proven in polarization curves that various peaks were obtained at pH 1 which was specified as the best condition for glycerol conversion (Hunsom & Saila, 2015). Though glycerol electroreduction mechanism pathway study is very limited, this reaction preferred acidic medium to produce acetol intermediate *via* dehydration which is important for 1,2-propanediol formation (Ishiyama et al., 2013; Lee et al., 2018). From the recent catalytic studies, tungstic acid (H_2WO_4) has a potential role as the medium to reduce glycerol into propanediol compounds, which can be beneficial for 1,3-propanediol formation using the electroreduction reaction (Nakagawa et al., 2014).

Table 2.3: Advantages and disadvantages of some of the recent mono-metallic electrocatalysts/ electrodes.

Electrodes	Advantages	Disadvantages	References
Pt-based	▪ The most active catalyst in the fuel cell and electrolysis cell under acidic and alkaline conditions.	▪ Costly. ▪ Easily poisoned by carbonaceous intermediates species such as CO that are released from glyceraldehyde formation. ▪ Smaller catalytic activity in the alkaline and neutral media compared to the acidic medium.	(Araujo et al., 2019; Garcia et al., 2017; Ferreira Jr. et al., 2017; Kwon et al., 2012; Lee et al., 2019; Moraes et al., 2019)
Pd-based	▪ Less expensive and improved poison tolerance than Pt catalyst. ▪ At least 50 times more abundant than Pt catalyst.	▪ The durability and tolerance to poison are required to enhance.	(Coutanceau et al., 2014; Ferreira Jr et al., 2013; Geraldes et al., 2015; Inoue et al., 2018)
Au-based	▪ Less pricey than Pt and Pd catalysts. ▪ Enhanced oxygen resistance and high tolerance to carbonaceous intermediates species. ▪ Promotes C-C breakage to C_2 and C_1 products with higher overpotential than Pt catalyst.	▪ Highly active under basic conditions.	(Dodekatos et al., 2018; Kwon et al., 2014; Kwon et al., 2011; Qi et al., 2014)
Ag-based	▪ Less expensive than Pt and Pd catalysts. ▪ Suitable as co-catalyst in Pt, Au, and Pd catalysts since it helps facilitate C-C bond cleavage.	▪ Weak performance, the oxidation reaction is blocked at potentials >1.125 V, irrespective of glycerol concentration in the solution.	(Gomes et al., 2014; Hirasawa et al., 2013; Suzuki et al., 2016)
Ni-based	▪ Inexpensive and durable in an alkaline medium as well as well-tolerant to poisoning. ▪ Notable catalytic activity as Pt catalyst. ▪ It can provide different oxygen-containing species such as NiOOH and $Ni(OH)_2$, hence, increasing adsorption/desorption of glycerol, intermediates, and products when applied as co-catalyst.	▪ Only active in alkaline medium. ▪ Under acidic conditions, the dissolution of nickel could happen.	(Han et al., 2017; Lin et al., 2017; Moraes et al., 2019)

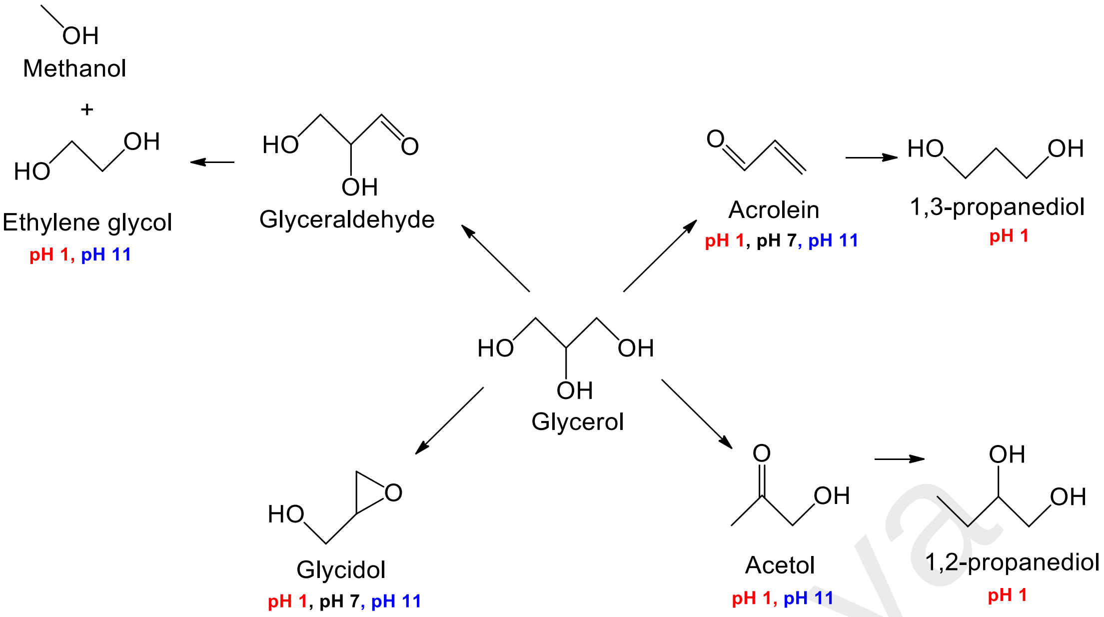

Scheme 2.3: Proposed reaction mechanism of glycerol electroreduction on Pt cathode electrode in different pH of reaction media.

The selectivity towards intermediates and final products from glycerol electrooxidation as well as the electrocatalysts (or electrodes) activity are strongly dependent on the pH of reaction media. Othman and Ahmad (2015) conducted glycerol electrooxidation on the gold plate (Au) and gold composite electrodes (Au-PVC) using potassium hydroxide (KOH) and sulfuric acid (H_2SO_4) as the media. The glycerol electrooxidation rate occurred twice as much in alkaline medium on both Au and Au-PVC electrodes compared to an acidic medium in which oxidation only happened once on Au electrode (Othman & Ahmad, 2015). However, more recently, Valter et al. (2018) proposed that Au electrodes also exhibited catalytic activity in an acidic medium. Instead of using 0.5 M H_2SO_4 (Beden et al., 1987; Kwon et al., 2011), they used 0.1 M $HClO_4$ as a supporting electrolyte. Initially, both perchlorate ions and sulfate ions will compete with the relatively weakly bound electrically neutral glycerol for free adsorption sites. The stronger adsorption of sulfate ions than perchlorate ions on Au surface could be an explanation for the inactive catalytic activity of anode surface (Au catalyst) in 0.5 M H_2SO_4 medium previously. This is because the stronger binding of sulfate ions on the Au surface has led to the blockage of its surface with the lack of observed activity.

Computationally, it was observed that partial dehydrogenation started in the potential range below 1.0 V *vs.* RHE. The formation of dihydroxyacetone, 2,3-dihydroxy-2-propenal, and glyceraldehyde was observed and proposed at 0.39, 0.39, and 0.60 V *vs.* RHE, respectively, whereas the complete dehydrogenation to carbon monoxide (CO) happened at 0.50V *vs.* RHE (Valter et al., 2018). The presence of this CO specified that the C-C bond was broken which means low selectivity in C_3 species in the process. Plus, because of the adsorbed CO and glyceraldehyde on the surface it has led to very low activity and current densities in their CV curve.

Yet, Au and Au-based electrodes still show higher activity in the alkaline medium compared to the acidic solution. It also has well-tolerance to adsorbed poisoning species such as CO where this species is the main poisoning agent for Pt and Pd catalysts. Zhang et al., (2012) evaluated the reactivity of glycerol, methanol, and ethylene glycol in an AEM-direct glycerol fuel cell (AEM-DGFC). From the CV curves, the results revealed that glycerol has higher catalyst activity on Au/C with lower on-set potential and higher electrooxidation currents compared to ethylene glycol and methanol. Since the first deprotonation of H_α in alcohol on Au/C involved base-catalyzed reaction, a lower pK_a favour the higher reactivity. To clarify, glycerol with pK_a of 14.15 is easier to deprotonate into highly reactive glyceroalate in high pH media compared to ethylene glycol (14.77) and methanol (15.50). The higher pH will boost the OH^- adsorbed coverage rate on the Au/C surface and enhance glycerol electrooxidation. However, when the concentration of KOH was too high (3.0M), the excessive $OH^-_{adsorbed}$ on the Au catalyst surface blocked the glycerol adsorption, resulting in a lower reactivity (Zhang et al., 2012). De Souza et al. (2017) further compared the glycerol electrooxidation with other 3-carbon atoms chain alcohols such as 1-propanol, 2-propanol, propane-1,2-diol, and propane-1,3-diol on Au catalyst in 1.0 M NaOH medium. Glycerol showed the highest reactivity followed by propane-1,2-diol, where both exhibited a high C-C bond cleavage rate with the presence of C_1 and C_2 species. The vicinal OH groups in glycerol and propane-1,2-diol are key components to stimulate the C-C breaking of molecules and enhance the electrooxidation reaction in an alkaline medium. In fact, the current densities were higher in the alkaline medium compared to the acidic and neutral media. It was reported that the surface was blocked with ClO_4^- and inhibited the electrooxidation in the acidic and neutral media. Additionally, the lack of alkoxide ions or active species in the alkaline medium could negatively affect the oxidation rates of the investigated 3-carbon-atom chain alcohols. Under the acidic condition, the alcohol molecule is protonated by H^+ rather than deprotonated H^+ of alcohol molecule (losing H^+) to form alkoxide. The repulsive forces between the positively charged alcohol molecule and the gold electrode will exist and thus, the adsorption process of the alcohol molecule to the surface will be difficult to achieve. However, the unprotonated alcohol adsorbed on the surface via Brownian motion occurs but the quantity of active species to the electrode surface is not sufficient to proceed with more oxidation reaction, resulting in low current densities (De Souza et al., 2017).

As mentioned in the electrodes materials section, Pt electrodes containing bismuth in acidic solution have the potential to produce dihydroxyacetone (DHA) intermediate (Kwon et al., 2012). Nonetheless, DHA could also be formed in an alkaline medium with the presence of bismuth on the Pd electrode (Zalineeva et al., 2015). Other than the presence of bismuth which inhibits the dissociative adsorption/oxidation of primary OH to glyceraldehyde, DHA formation could also be explained by the Lobry-de Bruyn-van Ekenstein transformation (Epimerization) known as rearrangement reaction of the equilibrium aldose and ketose. This rearrangement happens in the base-catalyzed reaction and thus, when the local pH increased, the reaction favoured the labile OH group adsorption and further formation of very reactive alcoholate (CH_2OH-CHO^--CH_2OH). This species was further transformed into DHA intermediate (Clavilier et al., 1988; Zalineeva et al., 2013). The Lobry-de Bruyn-van Ekenstein transformation could also be applied in an acidic medium which is well-known as aldose ketose transformation and tautomeric enediol as intermediate (Garcia et al., 2016; Nimlos et al., 2006). But these Pd-based electrocatalysts are still highly active under alkaline medium compared to the acidic medium.

For instance, Pd_3Sn/phen-C has superior durability and poisoning tolerance in 0.1 M KOH higher than Pd/C (Wang et al., 2016). Since nickel and silver are also very stable in alkaline medium, the utilization of these elements on Pd catalyst (PdNi/C and PdAg/C) in 0.1 M NaOH has exhibited good reaction kinetics at low applied potentials (Holade, et al., 2013). The CO poisoning that is owned by the Pd catalyst was successfully reduced by a bifunctional mechanism of the oxidative desorption involving the transfer of OH^- species at lower potentials from the $Ni(OH)_2$ surface toward adsorbed organic molecules close to the palladium surface where the reaction takes place (Holade et al., 2013). For the Ag element, according to the d-band theory, the d-band of Pd catalyst was shifted when Ag was added on its surface, leading to more hydroxyl groups adsorbed on PdAg/C and subsequently, enhanced the removal of CO from the PdAg/C surface (Zhang et al., 2017). In Ferreira Jr et al. (2013) work, carbonate was generated during glycolate and oxalate formation during glycerol electrooxidation in 0.1 M KOH. But, when low pH or OH concentrations (0.1 M KOH) are used, carbonate was abruptly substituted to a mechanism route that generates CO_2 at high potentials. The formation of CO_2 instead of CO is significant as demonstrated by Gomes et al. (2013). The results revealed the effect of glycerol concentrations (0.05 M, 0.1 M, 0.5 M, and 1.0 M) in an acidic medium towards the glycerol adsorption and electrooxidation pathways. At high glycerol concentration, the Pt surface was more covered glycerol adsorbed residue and thus, inhibited the water co-adsorption. The formation of adsorbed OH species on the Pt surface was delayed and further the CO_{ads} desorption into CO_2 as defined from the Langmuir-Hinshelwood mechanism cannot be happened; ($CO_{ads} + OH_{ads} \rightarrow CO_2 + H^+ + e^-$). Consequently, CO remains adsorbed on Pt up to higher potentials and led to catalyst poisoning. The formation of the CO layer was also contributed from the glycerol oxidation to glyceraldehyde in the concentrated glycerol medium at the low and medium potential. In diluted glycerol, CO_2 was successfully formed 2343 cm^{-1} from CO and carboxylic acid generation seems to be independent on the glycerol concentration for this contribution. This is because CO_2 was partially oxidized from carboxylic acids at high potential (2040 cm^{-1}) as shown in *in-situ* FTIR spectra (Figure 2.2) (Gomes et al., 2013).

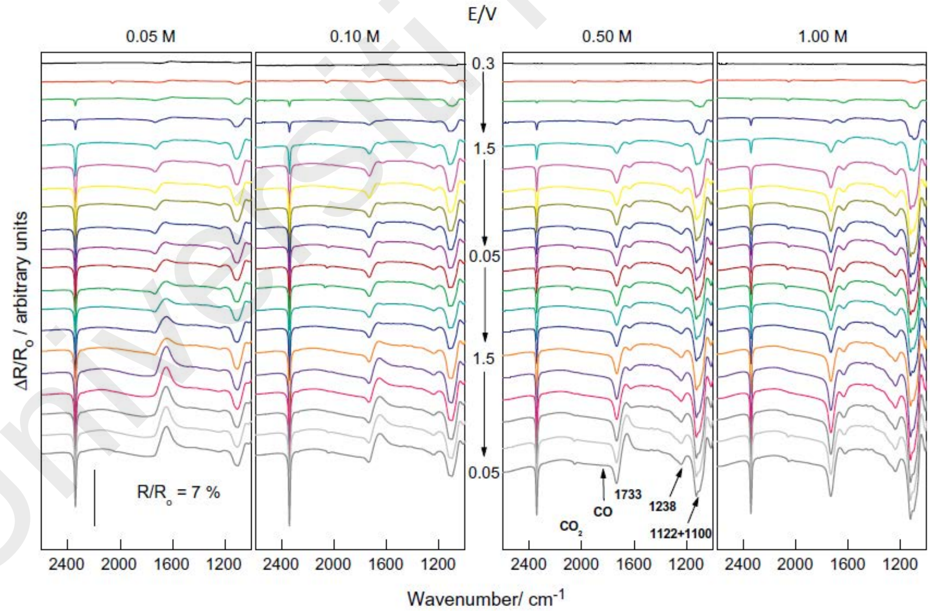

Figure 2.2: *In situ* FTIR spectra for a Pt electrode in 0.1 M $HClO_4$ and different concentrations of glycerol (Gomes et al. 2013).

Though the removal of CO species and high desired products selectivity could be achieved in several current studies, the low yield of these products remained as one of the main issues. As such, under strongly acidic conditions cleavage of glycerol is the main anodic reaction and the current yield is low, thus, the utilization of alkali hydroxides will provide a better current yield. But large excess is needed as alkali hydroxides are consumed by many competitive reactions leading to complex product mixtures. To encounter this problem, Lux et al. (2010) have used alkali metal salts under an acidic or alkaline medium because mixtures of metal ions will accelerate the rate-determining step. In their work, with 3.6% (w/w) $Al_2(SO_4)_3$ medium, lactic acid with 90% yield was successfully formed and this remarkable yield has not been achieved by other work.

Angelucci et al. (2013) studied the interaction of hydrated alkali metal cations ($M^+(H_2O)_x$, $M^+ = Li^+$, Na^+, and K^+) with $OH_{adsorbed}$ on Pt catalyst and found that the current density of glycerol electrooxidation reaction increased by increasing cations radius ($Li^+ < Na^+ < K^+$). This happened due to the formation of clusters resulting from non-covalent interactions between hydrated cations and $OH_{adsorbed}$ on Pt, which is favoured as the cation radius decreased. In Li^+ electrolyte, OH_{ad}-$Li^+(H_2O)_x$ clusters partially blocked the Pt surface and inhibited the reaction to occur, leading to low current density. The choice of suitable electrolyte is vital in achieving high catalytic activity as well as products selectivity and yield. The formation of CO species is not only hindered by using Au-based, Ag-based, or Ni-based electrocatalysts but it also could be avoided by using the right concentrations of electrolyte and glycerol. As presented in Table 2.2, 0.5 M glycerol and 0.5 M electrolyte were mostly used to achieve high selectivity of products. A high concentration of glycerol could only be used on Au-based electrodes since it can oxidize and remove adsorbed CO species from its surface efficiently. To avoid low catalytic activity, the electrolyte with high cations radii like NaOH and KOH should be used.

2.4.3 Effect of applied potential and current density

Fundamentally, the electrochemical conversion could be conducted on the current (galvanostatic) or applied potential (potentiostatic) is controlled. Both parameters have high impacts especially on the selectivity of compounds formed during the process. In a potentiostatic mode, the desired molecular transformations can be determined accurately by only adjusting the applied potential. A variation of electrode potential in the process can manipulate the size activation energy barrier and subsequently can control the products selectivity. This electrode potential adjustment is related to the Gibbs free energy ($\Delta G = nF\Delta E$), where ΔG is the Gibbs free energy of reaction or adsorption, ΔE is the electrode potential, n is the number of electrons, and F is Faraday's constant (96485 C/mol). The electrode potential influences the Gibbs chemisorption energy of the products if the electrocatalytic process contains an adsorbed product.

Hence, the electrode potential control in the electrocatalytic system may be used to manipulate and tune the relative rates of competing for electrocatalytic processes and the products selectivity. However, the rate of electrolysis is not controlled directly because the applied potential needs to be set to a particular value and the current corresponds to the electrode reaction. Hence, this mode may take a longer time to control the applied potential (Pauwels, 2018). Even though this mode is inexpensive to be operated in laboratories, it is still not practical for operation on an industrial scale. This is ascribed to the additional cost associated with a potentiostat that could operate at the current values needed in large-scale transformations. Thus, the galvanostatic mode is the alternative since the setup is much simpler for large-scale electrolysis. It only controls the electrical current that flows through the cell using a galvanostat or DC power supply and this device is cheaper than a high current potentiostat (Frontana-Uribe et al., 2010).

In the potential electrolysis, glycerol is oxidized into the value-added compounds when the applied potential was set in the so-called “oxygen region”. A study showed the selectivity of glyceraldehyde intermediate is inversely proportional to applied potential (Roquet et al., 1994). In their work, the glycerol electrooxidation mechanism on the platinum electrodes has been explored in the acidic and alkaline media at different applied potentials. It has been proposed that the electrooxidation reaction involved different steps which are the adsorption of hydroxyl (OH) group of glycerol on the electrode surface (Step 1), followed by breaking inter-atomic bonds (Step 2) and electronic charges transfer (Step 3). Subsequently, further interaction between the oxygenated species such as adsorbed OH group or oxides on the electrode surface with the fragments from glycerol molecule (Step 4) and desorption of the products (Step 5) (Gomes & Tremiliosi-Filho, 2011).

As demonstrated in Scheme 2.4, at 0.75 V *vs.* RHE, the hydroxyl (OH) group from glycerol is adsorbed and interacted with the platinum electrode, further oxidized into glyceraldehyde fragment. Meanwhile, at 1.30 V *vs.* RHE, glycerol interacted oxide formed on the Pt (PtO) electrode surface, led to the cleavage of C-C bond, and produced glycolic and formic acids. The results also exposed 97% selectivity of glyceraldehyde which was obtained at 0.75 V *vs.* RHE and was reduced to 56% selectivity at 1.30 V *vs.* RHE. The reduction in glyceraldehyde selectivity was agreed by Kim et al. (2014) as the applied potential increased, glycerol conversion was increased up to 97.3% at 1.297 V *vs.* SHE. Glyceraldehyde selectivity also changed when applied potential was tuned from 0.697 V (48.8% selectivity) to 1.097 V (2.5% selectivity) *vs.* SHE. Though glyceraldehyde selectivity was reduced at 1.097 V *vs.* SHE, glyceric acid selectivity has increased which indicates that acid was electro-oxidized from glyceraldehyde intermediate (Kim et al., 2014).

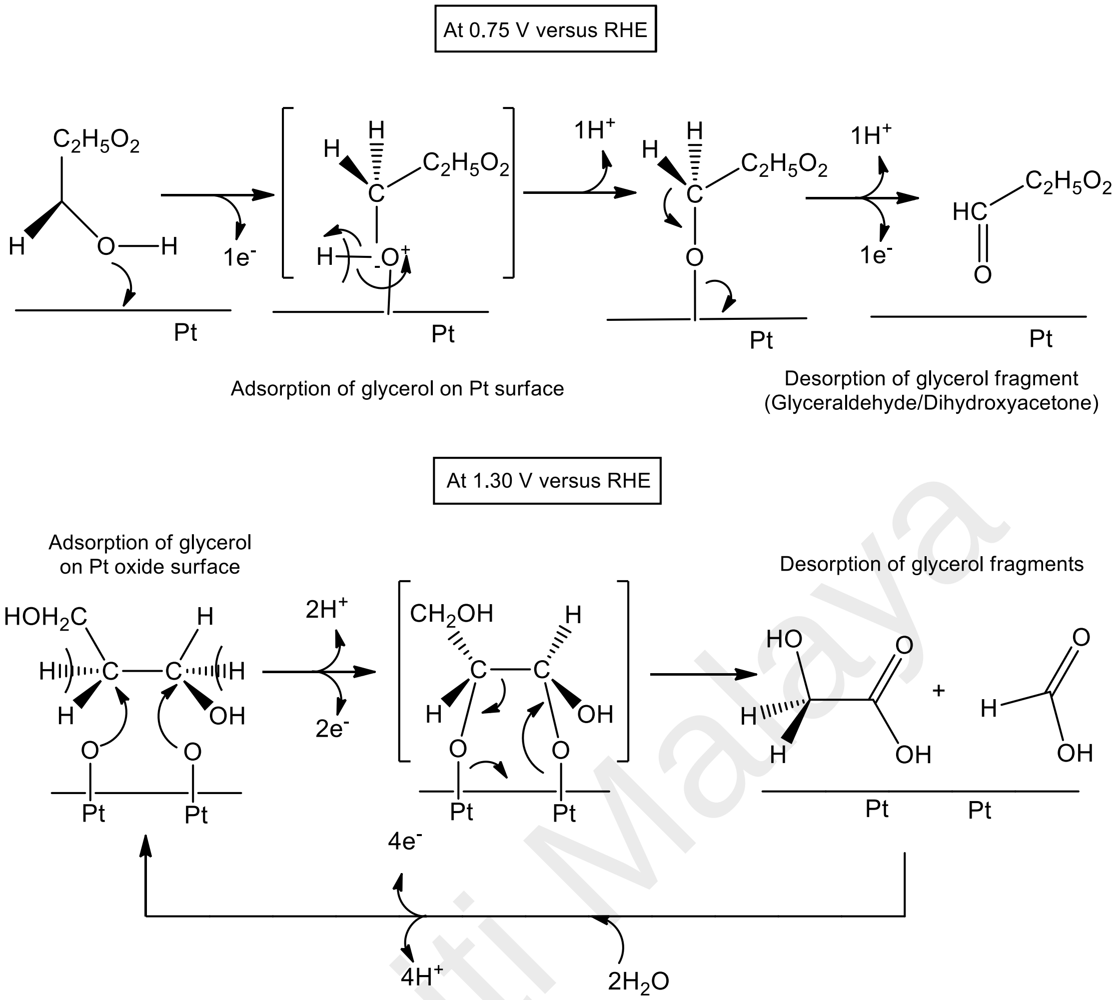

Scheme 2.4: Glycerol electrooxidation pathway on the platinum electrode in an acidic medium at 0.75 V and 1.30 V *vs.* RHE (Roquet et al., 1994).

With the increasing of applied potential, it is said that more C_3 and C_2 oxygenated compounds are generated. Zhang et al. (2012) produced high selectivity of glycolate using Au/C anode catalyst and Fe-based cathode in the anion-exchange membrane fuel cells. At 1.0 V *vs.* RHE, the glycolate selectivity was 41%, and it was improved to 85% when the applied potential was adjusted to 1.6 V *vs.* RHE (2.0 M KOH with 1.0 M glycerol). Yet, when the applied potential was further increased, the selectivity of tartronate and glycoxylate were steadily decreased. In the extension of their work, Zhang et al. (2014) studied the selectivity of tatronate and mesoxalate compounds using the same electrochemical system in order to verify their proposed mechanism. It was reported that when the anode potential was at < 0.45 V *vs.* RHE, the major product was tartronate with 79% selectivity and mesoxalate was not detected. Conversely, the selectivity of mesoxalate was gradually increased and reached the maximum selectivity of 57% with 26% selectivity of tartronate when the applied potential was increased to 0.69 V vs. RHE. The further increase of the applied potential to 0.70 V *vs.* RHE showed the selectivity of mesoxalate was decreased to 55% and the selectivity of oxalate was increased from 5% to 8% which indicates the mesoxalate oxidation to oxalate. Scheme 2.5 summarizes and proves that the reaction mechanisms of glycerol oxidation were shifted from glycolate to tartronate when the applied potential reduced from 0.9 V to 0.35 V *vs*. RHE (Zhang et al., 2014). It can be concluded that as the reaction takes place under mild conditions without any toxic or strongly oxidative reactants, it implies that the regulation of the applied potential was able to control the products distribution and the mechanism pathways.

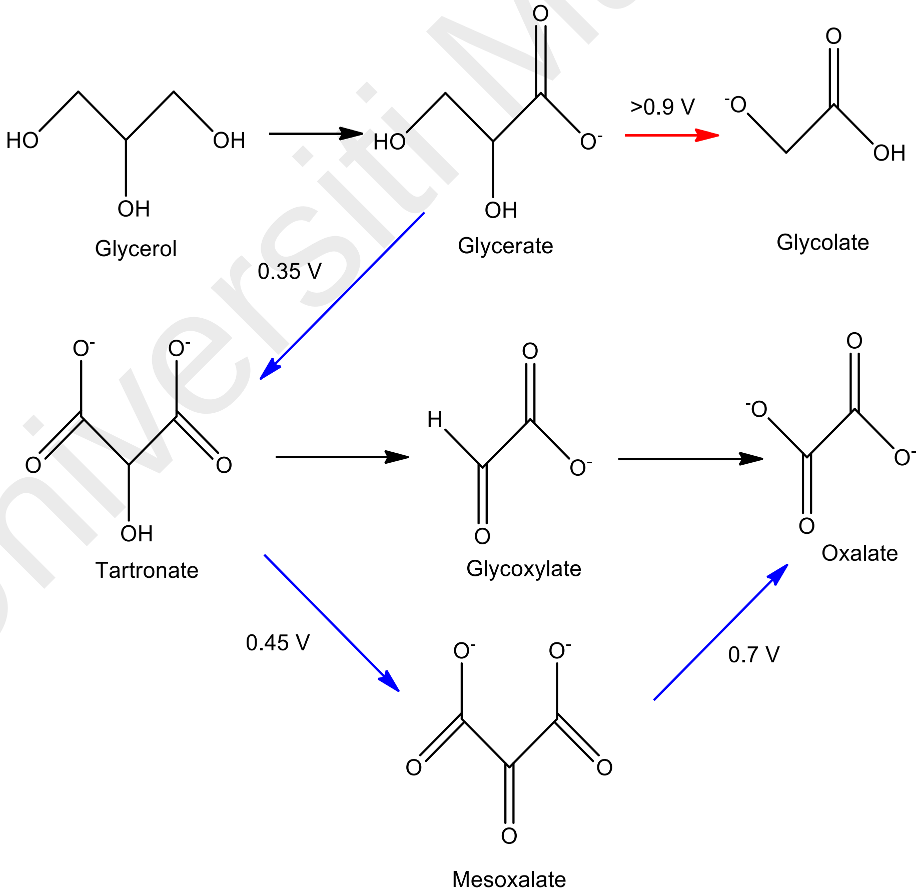

Scheme 2.5: Proposed reaction mechanisms for electrooxidation of glycerol (Zhang et al., 2012; Zhang et al., 2014)

In the galvanostatic mode, Paula et al. (2014) produced hydrogen from the electrochemical glycerol reformation in alkaline-doped polybenzimidazole proton-exchange membrane (PBI-based PEM) fuel cell. At a high current density (0.80 A/cm^2) with a temperature of 60 °C, they successfully achieved the optimal hydrogen production, and the result also demonstrated the highest selectivity of the oxidized compound was tartronate. Hunsom and Saila (2015) also proved the relationship of current densities with the selectivity of desired products using different current densities (0.08, 0.14, 0.24, and 0.27 A/cm^2) on Pt electrodes at pH 1. They found that acetol and 1,2-propanediol were produced only at medium to high current densities (0.14-0.27 A/cm^2) while acrolein and 1,3-propanediol were generated at current densities of 0.14 A/cm^2 and 0.24 A/cm^2. This result indicated the dehydration of the first hydroxyl group is not preferred at too low current density and the second hydroxyl group is not preferred at too low or too high current densities.

In addition, according to Faraday's law, the increase in the current density also led to the improvement of glycerol conversion which they have obtained the highest current density (0.27 A/cm^2) with approximately 100% glycerol conversion compared to 0.24 A/cm^2 with around 50% glycerol conversion after 8 hours (Hunsom & Saila, 2015). However, too high a current density (0.27 A/cm^2) will not improve the generation of desired products because it will facilitate the glycerol decomposition to carbon dioxide (Ishiyama et al., 2013). Although the electrochemical conversion of glycerol with the galvanostatic mode is limited, the regulation of this current would yield different products distribution, especially in the dehydration step. This step is important in glycerol electroreduction in order to selectively produce acetol or acrolein intermediate and subsequently reduced into 1,2-propanediol and 1,3-propanediol, respectively.

2.4.4 Effect of reaction temperature

Glycerol electrooxidation and -reduction are endothermic reaction that requires electricity and a moderate amount of heat to drive the reaction. This phenomenon explains why glycerol conversion was low at room temperature and C_2 compound (glycolic acid) is a dominant product with high glycerol conversion at high temperature (Lee et al., 2019). Glycerol is not completely electro-oxidized to CO_2 at room temperature either in alkaline or acidic medium due to slow electrooxidation kinetics and high energy barrier of C-C bond dissociation, but it can be obtained at around 250 °C (Ishiyama et al., 2013). When the temperature was increased, glycerol conversion rates increased and the conversion rates were 0.406 h^{-1}, 0.402 h^{-1}, and 0.774 h^{-1} at 27 °C, 50 °C, and 80 °C, respectively. The increasing of the temperature accelerated the C-C bond breakage, hence, converting glycerol into glycolic acid with the highest yield of 66.1% and 72% selectivity at 80.0 °C on Pt catalyst (Lee et al., 2019). It has promoted higher glycerol electrooxidation similar to Jr. et al. (2017) work, indicating that the glycerol electrooxidation process is thermally activated. They used two different temperatures (60 °C and 90 °C) to determine the influence of Pt loading on glycerol electrooxidation reaction and the result revealed that 90 °C of temperature favoured C_3 species formation compared to the C_2 species like glycolate and oxalate.

In a single direct alkaline fuel cell, 80 - 85 °C of temperature was identified as the optimum condition on Pd-based, Pt-based, and Au-based electrodes for this process (Geraldes et al., 2015; Geraldes et al., 2013; Zhang et al., 2013). Geraldes et al. (2015) obtained the highest power density at 85 °C on $Pd_{0.5}Au_{0.4}Sn_{0.1}/C$ (51 $mWcm^{-2}$), followed by $Pd_{0.5}Au_{0.1}Sn_{0.}/C$ electrode with (42 $mWcm^{-2}$) while in a single alkaline direct ethanol fuel cell (ADEFC), 44 $mWcm^{-2}$ was the best performance on $Pd_{0.9}Au_{0.1}$ electrocatalyst (Geraldes et al., 2013). Zhang et al. (2013) also reported the highest performances on

Pt/C, Pd/C, and Au/C electrodes were achieved (184.2, 93.9, and 50.1 mWcm^{-2}, respectively) with 6.0 M KOH and 1.0 M crude glycerol at 80.0 °C compared to lower temperature of 60 °C. Above this temperature range (80-85 °C), membrane dryness and water management started to impede electrode performance, which was most likely because of an increase in cell resistance. The unstable performance of this glycerol electrooxidation reaction in fuel cells implied that a better reacting diffusion and higher kinetics of electrodes will be favoured at higher temperatures.

The selection of the electrocatalysts or solid acid catalysts (additives) is also critical in temperature studies because heat can deactivate thermally unstable catalysts. As such, a sulfonic acid resin (Amberlyst-15) is thermally unstable when operated around 120 ˚C and result in a sharp decrease in catalytic activity (Liao et al., 2009). The influence of temperature on reaction rates and activation energies could be determined by confirming experimental runs with various temperatures (*e. g.*; 235 - 260 ˚C) using the Arrhenius equation as presented in 2.1, where E_a (kJ/mol) is the activation energy, R (J mol^{-1} K^{-1}) is the gas constant or the Boltzmann constant, K is the reaction rate constant, and A (s^{-1} for the first-order reaction) is the frequency factor, which varies with the rate order and same unit as the rate constant. This equation shows the relationship between intrinsic temperature and equilibrium constant and hence, it can be used to determine rate law parameters. Based on this equation, when the temperature increases or activation energy decreases (when the catalyst is added), it will increase the rate constant that is directly proportional to the rate of reaction.

$$K = Ae^{E_a/RT} \qquad 2.1$$

As shown in Figure 2.3, higher current densities were detected with the increased temperature, particularly at low and intermediate electrode potentials (120-500 mV). But, the current densities became almost equivalent at around 700 mV caused by high adsorbed OH coverage on Pt surface, which came from water dissociation at high applied potentials (Ishiyama et al., 2013). From the CV result (Figure 2.3a), linearity between the natural logarithm of their current densities, $ln\ i$, and the inverse of reaction temperature were observed at electrode potentials of 150-500 mV as shown in Figure 2.3b. Therefore, activation energy (E_a) for each electrode potential with different temperatures could be calculated using Butler-Volmer equations where 2.2 for anodic current (i) and 2.3 is represented for the apparent activation energy (E_a), where n is electron transfer, F is Faraday constant, A is pre-exponential factor, α is transfer coefficient and R is gas constant. As demonstrated in Figure 2.3c, the rate-determining step of glycerol electrooxidation is proven to be dependent on temperature as well as electrode potential when the activation energy decreased (from 70 to 20 kJ mol^{-1}) with increasing electrode potential from 150 to 500 mV.

$$i = nFA^{\left(\frac{E_{a,0}}{RT}\right)\left(\frac{(1-\alpha)\,nFE}{RT}\right)} \qquad 2.2$$

$$E_a = -R\left(\frac{\partial lni}{\partial\left(\frac{1}{T}\right)}\right)_E = E_{a,0} - (1-\alpha)nFE \qquad 2.3$$

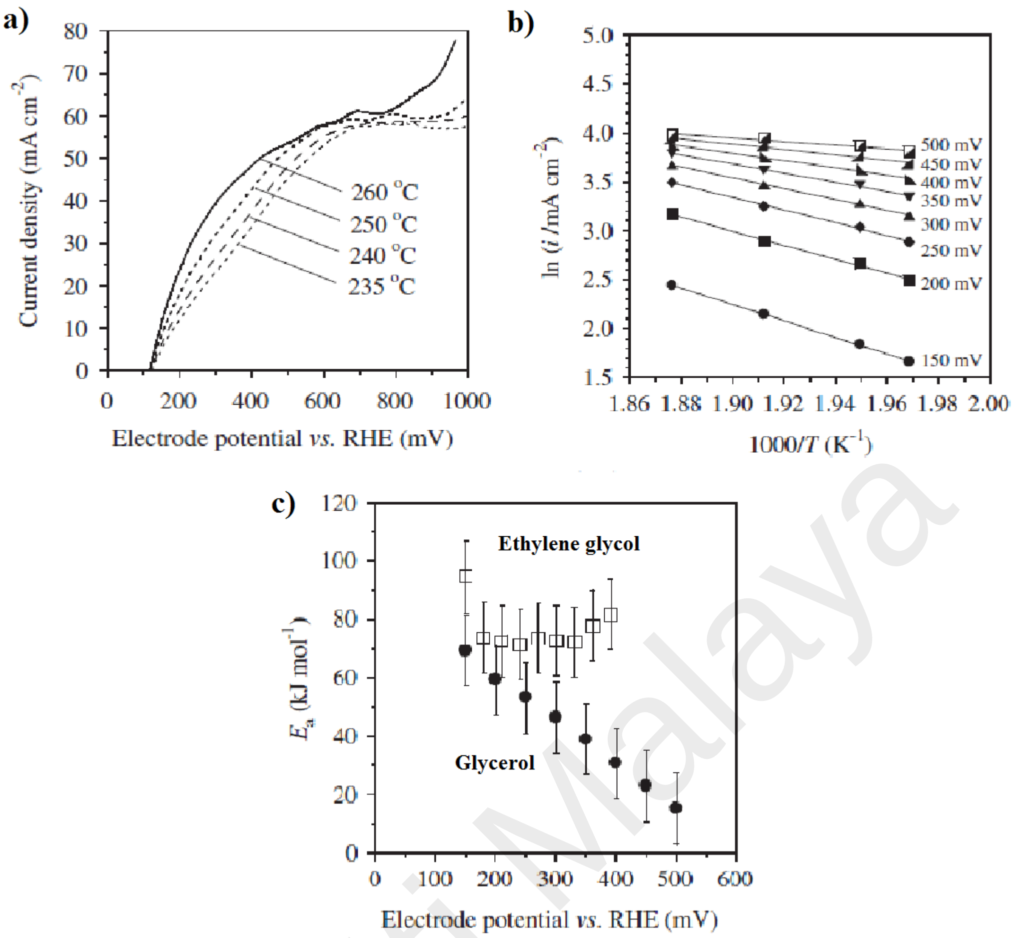

Figure 2.3: a) Cyclic voltammogram of glycerol electrooxidation at different temperatures (235-260 °C), b) Arrhenius plots for current densities of glycerol electrooxidation at different applied potentials (150-500 mV) and c) Apparent activation energies of glycerol and ethylene glycol electrooxidation *vs.* electrode potentials.

2.4.5 Effect of additives

During the electrochemical process, redox catalysis can occur through direct electrolysis or indirect electrolysis (Figure 2.4). Direct electrolysis involves the transfer of a heterogeneous electron between molecule substrate (*e. g.*, fuel) and electrode before or after chemical reaction while indirect electrolysis focuses on a mediated electron transfer due to the addition of redox mediators or catalysts (*e. g.*, oxidizing agents or solid acid catalyst) in the electrolyte (Fuchigami et al., 2015). The use of redox mediators can prevent the kinetic inhibition, electrode passivation, and the over-oxidation or –reduction of the substrate which are associated with the direct electrolysis (Francke & Little, 2014; Pauwels, 2018). The presence of different additives in the electrochemical conversion could improve the glycerol conversion and products distribution. To be noted, homogeneous mediators have been frequently used and Amberlyst-15 was the first heterogeneous catalyst that selectively dehydrated glycerol to acetol in Lee et al. (2018) work. The utilization of heterogeneous catalysts is capable to control product selectivity and has better separation from the obtained products (Nakagawa et al., 2018).

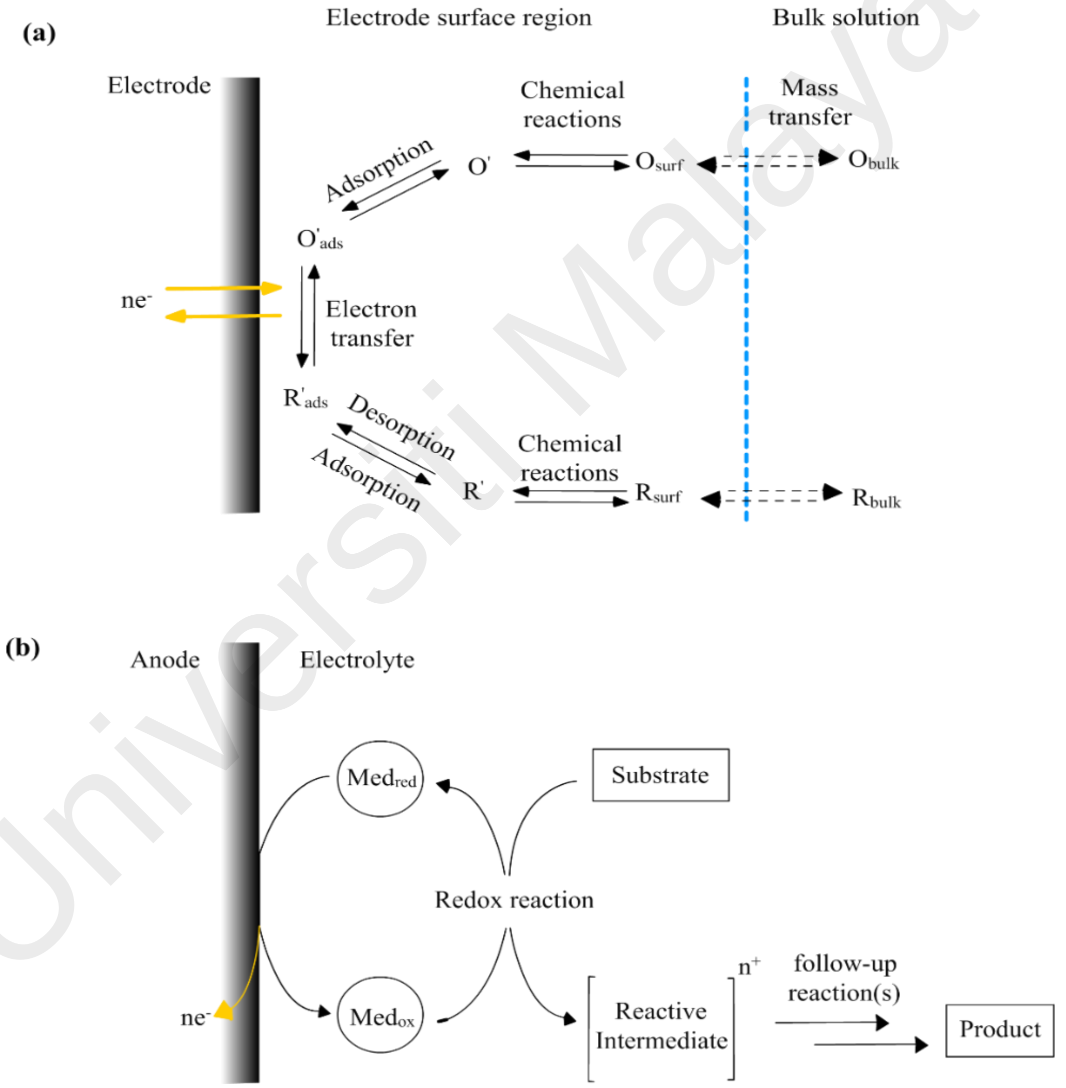

Figure 2.4: Basic principles of a) direct electrolysis and b) indirect electrolysis (Francke and Little, 2014; Pauwels, 2018).

The earlier study obtained 1,3-dihydroxyacetone by applying 1.1 V *vs.* Ag/AgCl applied potential to a glycerol solution buffered at pH 9.1 in the presence of 15 mol % TEMPO (2,2,6,6-tetramethylpiperidine-1-oxyl) (Ciriminna et al., 2006). After 20 hours, glycerol was selectively oxidized at the secondary alcohol group which was mediated by radical TEMPO to produce DHA (with 25% yield). When the time was prolonged to 200 hours, the percentage yield of DHA was increased to 30% and hydroxypyruvic acid was formed with a 35% yield (Ciriminna et al., 2006). Saila and Hunsom's co-workers also attempted glycerol conversion on Pt cathode at pH 1 with different oxidizing agents (H_2O_2, $Na_2S_2O_8$, and TEMPO) (Saila & Hunsom, 2015). In the absence of these oxidizing agents, glycidol and acrolein appeared as the primary products through dehydration and reduction. However, when these oxidants were added, each oxidizing agent successfully changed the direction of the mechanism path, principally via direct oxidation of the primary or secondary hydroxyl group. As such, ethylene glycol, glycolic acid, and 1,3-DHA were found as the main products in $Na_2S_2O_8$, H_2O_2, and TEMPO, correspondingly. Plus, the conversion rate becomes faster from 14 hours without oxidants to 10 hours with oxidants (Saila & Hunsom, 2015). In Kwon et al. (2014) work, glyceraldehyde intermediate was not also detected at the low applied potential in the presence of H_2O_2 oxidant. In an alkaline medium, it has no significant effect on the overall glycerol electrooxidation activity or selectivity. Nonetheless, low activity can be seen under neutral and acidic conditions.

Recent efforts have focused on the deployment of the multi-enzymes cascade in order to facilitate the complete electrochemical oxidation of glycerol to CO_2 (Hickey et al., 2014). With a combination of oxalate oxidase (OxO) and 4-amino-TEMPO (TEMPO-NH_2), one molecule of glycerol can be oxidized completely to CO_2 on the carbon electrode and deliberated 16 electrons. TEMPO-NH_2 has exhibited the highest current density among other TEMPO derivatives and obtained an 8-fold increase in catalytic rate over the unmodified TEMPO. The results showed TEMPO-NH_2 maintains the catalytic activity as low as pH 4 which allows OxO to function compared to the unmodified TEMPO that was only active in the alkaline condition to pH 6. When TEMPO-NH_2 was able to catalyze oxidation reaction at pH lower than its pKa, thus, it is assumed that the amine (NH_2) functional group is capable to lower the energy required for deprotonation/oxidation of the TEMPO-NH_2 hydroxylamine intermediate. Glycerol cascade was initially oxidized to glyceraldehyde and further oxidized multiple times to mesoxalic acid. A combined OxO and TEMPO-NH_2 subsequently converted mesoxalic acid to glyoxylic acid, oxalic acid, and finally to CO_2. This result differs from Saila and Hunsom (2015) that used the unmodified TEMPO and favoured secondary hydroxyl oxidation pathway. A larger amount of the nitrosonium cation from higher TEMPO concentration has increased the yield of 1,3-DHA from 57.2% to 69.2% with increasing concentration of TEMPO (from 1 to 5 mM TEMPO).

The presence of these additives either in homogeneous or heterogeneous form, in the electrochemical conversion, could selectively produce the desired intermediates and products from glycerol electrooxidation or –reduction reaction. Table 2.4 presents the additives that have been used in the glycerol electroreduction and catalytic conversions. These solid acid catalysts have the potential to be applied as the acidic electrolyte in the glycerol electroreduction reaction, especially for the dehydration step. Solid acid catalysts are much better than the mineral acids media like H_2SO_4, HCl, and $HClO_4$ because these mineral acids require neutralization in the water quenching step at the end of the process, leading to salt waste formation. With solid acid catalysts, they can be separated easily and reused several times without loss of activity in the process. The reactions are also generally clean, and products will be obtained in high purity (Gupta & Paul, 2014).

Table 2.4: Additives used in the glycerol electroreduction and catalytic conversion.

Additives	Electrolyte	Reaction conditions	Products (selectivity (%))	Products (yield (%))	Ref.
Glycerol electroreduction					
9.6% (w/v) Amberlyst-15^a	0.3 M glycerol + 24 g Amberlyst-15	A: Pt C: Pt Current: 2.0 A 80 ˚C (8 h) 67%^{c}	1,2-PDO (61), ACT (24), DEG (15)	1,2-PDO (8.6), ACT (3.4), DEG (2.1)	(Lee et al., 2018)
9.6% (w/v) Amberlyst-15^a	0.3 M glycerol + 24 g Amberlyst-15	A: Pt C: CBAC Current: 2.0 A 80 ˚C (8 h) 74%^{c}	1,2-PDO (86), ACT (3), DEG (11)	1,2-PDO (8.8), ACT (0.3), DEG (3.1)	(Lee et al., 2018)
9.6% (w/v) Amberlyst-15^a	0.3 M glycerol + 24 g Amberlyst-15	A: Pt C: CBD Current: 2.0 A 80 ˚C (8 h) 88%^{c}	1,2-PDO (68), ACT (17), DEG (15)	1,2-PDO (9.5), ACT (2.3), DEG (2.1)	(Lee et al., 2018)
Additives	Glycerol/water/catalyst + additive (g)	Reaction conditions	Products (selectivity (%))	Products (yield (%))	Ref.
Glycerol hydrogenolysis					
$H_3PW_{12}O_{40}/ZrO_2$ or TPA/ZrO_2 (15 wt %)^a	10/40/0.15 + 0.3	Ru/C^b 6 H_2/MPa 453 K (8 h) 44.0%^{c}	1,2-PDO (64.3), EG (27.0), Others (8.9)	-	(Balaraju et al., 2009)
Nb_2O_5^{a}	10/40/0.15 + 0.3	Ru/C^b 6 H_2/MPa 453 K (8 h) 44.6%^{c}	1,2-PDO (60.9), EG (21.1), Others (12.3)	-	(Balaraju et al., 2009)

Note: ^{a}solid acid catalyst, ^{b}catalyst, ^{c}glycerol conversion, A: anode, C: cathode, ACT: acetol, DEG, diethylene glycol, and 1,2-PDO: 1,2-propanediol.

Table 2.4 continued.

Nb_2O_5[a]	10/40/0.6 + 1.2	Ru/C[b] 6 H_2/MPa 453 K (8 h) 62.8%[c]	1,2-PDO (66.5), EG (21.2), Others (12.3)	-	(Balaraju et al., 2009)
Nb_2O_5[a]	10/40/0.45 + 0.9	Ru/C[b] 6 H_2/MPa 453 K (8 h) 58.7%[c]	1,2-PDO (64.7), EG (29.1), Others (14.2)	-	(Balaraju et al., 2009)
Amberlyst-15[a]	4/16/0.15 + 0.3	Ru/C[b] 8 H_2/MPa 393 K (10 h) 79.3%[c]	1,2-PDO (74.7), 1-PrOH (7.7), 2-PrOH (1.6), EG (6.8)	-	(Miyazawa et al., 2007a)
Amberlyst-70[a]	4/16/0.015 + 140 μmol H^+	Ru/C[b] 8 H_2/MPa 453 K (10 h) 48.8%[c]	1,2-PDO (70.2), 1,3-PDO (1.3), 1-PrOH (7.1), 2-PrOH (1.0), EG (8.3)	-	(Miyazawa et al., 2007b)
Amberlyst-70[a] reused as recovered (Usage times:1)	4/16/0.15 + 0.01	Ir-ReO_x/SiO_2[b] 8 H_2/MPa 393 K (24 h) 69.7%[c]	1,3-PDO (44.4), 1,2-PDO (8.0), 1-PrOH (39.4), 2-PrOH (8.0), Propane (0.2)	-	(Nakagawa et al., 2012)
Amberlyst-70[a] reused as recovered (Usage times: 2)	4/16/0.15 + 0.01	Ir-ReO_x/SiO_2[b] 8 H_2/MPa 393 K (24 h) 49.9%[c]	1,3-PDO (44.7), 1,2-PDO (9.4), 1-PrOH (36.1), 2-PrOH (8.5), Propane (1.4)	-	(Nakagawa et al., 2012)

Note: [a]solid acid catalyst, [b]catalyst, [c]glycerol conversion, 1,2-PDO: 1,2-propanediol, 1,3-PDO: 1,3-propanediol, 1-PrOH: 1-propanol, 2-PrOH: 2-propanol, and EG: ethylene glycol.

Table 2.4 continued.

Amberlyst-70[a] reused as recovered (Usage times:3)	4/16/0.15 + 0.01	Ir-ReO$_x$/SiO$_2$[b] 8 H$_2$/MPa 393 K (24 h) 37.5%[c]	1,3-PDO (48.6), 1,2-PDO (9.6), 1-PrOH (32.8), 2-PrOH (8.0), Propane (0.9)	-	(Nakagawa et al., 2012)
H-ZSM-5[a] reused as recovered (Usage times:1)	4/16/0.15 + 0.06	Ir-ReO$_x$/SiO$_2$[b] 8 H$_2$/MPa 393 K (24 h) 58.8%[c]	1,3-PDO (44.7), 1,2-PDO (9.3), 1-PrOH (35.3), 2-PrOH (9.4), Propane (1.3)	-	(Nakagawa et al., 2012)
H-ZSM-5[a] reused as recovered (Usage times:2)	4/16/0.15 + 0.06	Ir-ReO$_x$/SiO$_2$[b] 8 H$_2$/MPa 393 K (24 h) 36.1%[c]	1,3-PDO (50.3), 1,2-PDO (12.8), 1-PrOH (27.3), 2-PrOH (8.8), Propane (0.8)	-	(Nakagawa et al., 2012)
H-ZSM-5[a] reused as recovered (Usage times:3)	4/16/0.15 + 0.06	Ir-ReO$_x$/SiO$_2$[b] 8 H$_2$/MPa 393 K (24 h) 24.9%[c]	1,3-PDO (51.2), 1,2-PDO (13.9), 1-PrOH (26.1), 2-PrOH (8.8), Propane (<0.1)	-	(Nakagawa et al., 2012)

Note: [a]solid acid catalyst, [b]catalyst, [c]glycerol conversion, 1,2-PDO: 1,2-propanediol, 1,3-PDO: 1,3-propanediol, 1-PrOH: 1-propanol and 2-PrOH: 2-propanol.

Literature has shown the combination of metal catalysts with solid acid catalysts yielded 1,2-propanediol and 1,3-propanediol as the products of hydrogenolysis reaction, while propanols (1-PrOH and 2-PrOH) and propane were obtained from overhydrogenolysis reaction. However, propanols and propane have not been regarded as major targets in the glycerol conversion because they have lower market prices as well as poorer atom efficiency in their production compared to 1,2-propanediol and 1,3-propanediol. The addition of solid acids catalysts (such as Amberlyst-15 and Amberlyst-70) and inorganic solid acids (like niobia (Nb_2O_5) and zirconia-supported 12-tungstophosphoric $H_3PW_{12}O_{40}/ZrO_2$) to Ru/C catalyst have resulted in high selectivity of 1,2-propanediol. These solid acids would be useful for further investigation in the glycerol electrochemical conversion process. Amberlyst-15 was the most effective additive/co-catalyst used to enhance glycerol conversion and 1,2-propanediol selectivity in the glycerol hydrogenolysis. At 393 K, 1,2-propanediol with 74.7% selectivity was obtained mainly by dehydration of glycerol to acetol catalyzed by Amberlyst-15 and subsequent acetol hydrogenation to 1,2-propanediol on Ru/C (Miyazawa et al., 2007a). A heat-resistant ion exchange resin Amberlyst-70 showed a much higher reaction rate over Ru/C at 453 K compared to Amberlyst-15 at 393 K (Miyazawa et al., 2007b). Though, inorganic acids such as niobia (Nb_2O_5) and zirconia-supported 12-tungstophosphoric $H_3PW_{12}O_{40}/ZrO_2$ are thermally more stable than these ion-exchange resins and possess moderate acid sites which thereby, exhibited a better activity (Balaraju et al., 2009). Amberlyst would become deactivated as the sulfonic acid group decomposed when the temperature at around 120 ˚C and above (Kusunoki et al., 2005; Miyazawa et al., 2007a; Miyazawa et al., 2006). A glycerol conversion of 62.8% with 1,2-propanediol (66.5% selectivity) was achieved using Nb_2O_5 solid acid at a high temperature.

The formation of 1,2-propanediol and 1,3-propanediol was also related to the concentration of Lewis acid and Brønsted acid, respectively. Two types of mechanism routes have been proposed by many researchers as shown in Scheme 2.6. The dehydration glycerol with Lewis acid gives acetol and hydrogenation of this intermediate yields 1,2-propanediol (Scheme 2.6a). In another mechanism route (Scheme 2.6b), glycerol is dehydrogenated to glyceraldehyde AND this intermediate dehydrated to 2-hydroxyacrolein and thereby, generated 1,2-propanediol via hydrogenation (Nakagawa et al., 2014). Under Brønsted acid condition, glycerol will be dehydrated into 3-hydroxypropanal, however, acetol is thermodynamically stable than 3-hydroxypropanal, favouring acetol as the main mechanism pathway. But the cationic intermediate (secondary carbocation) for 3-hydroxypropanal is more stable compared to the acetol secondary carbocation, in other words, 3-hydroxypropanal is more kinetically favourable than acetol. Therefore, fast hydrogenation of 3-hydroxypropanal is important in 1,3-propanediol formation because further dehydration of 3-hydroxypropanal would yield acrolein (a precursor of propanols).

In Nakagawa et al. (2012) work, 1,3-propanediol was obtained from glycerol hydrogenolysis over Ir-ReOx/SiO_2 with the addition of various types of acids such as zeolites, silica-alumina, ion-exchange resin, and sulfuric acid. Among these acids, solid acid catalyst (Amberlyst-70) was the most effective additive in enhancing the activity but in terms of additive reusability, H-ZSM-5 is more suitable since it produced 1,3-propanediol with 51.2% selectivity after three times of usage. These additives could be applied in 1,3-propanediol formation during glycerol dehydration step into 3-hydroxypropanal intermediate. Although these co-catalysts, especially Amberlyst-15, have shown great results in both catalytic and electrochemical conversions of glycerol to propanediols, other operating kinetics parameters such as the expensive electrodes must be improved. Hence, the overall performance for the electrochemical conversion of glycerol could lead to high selectivity and yield of final products with the low-cost operation.

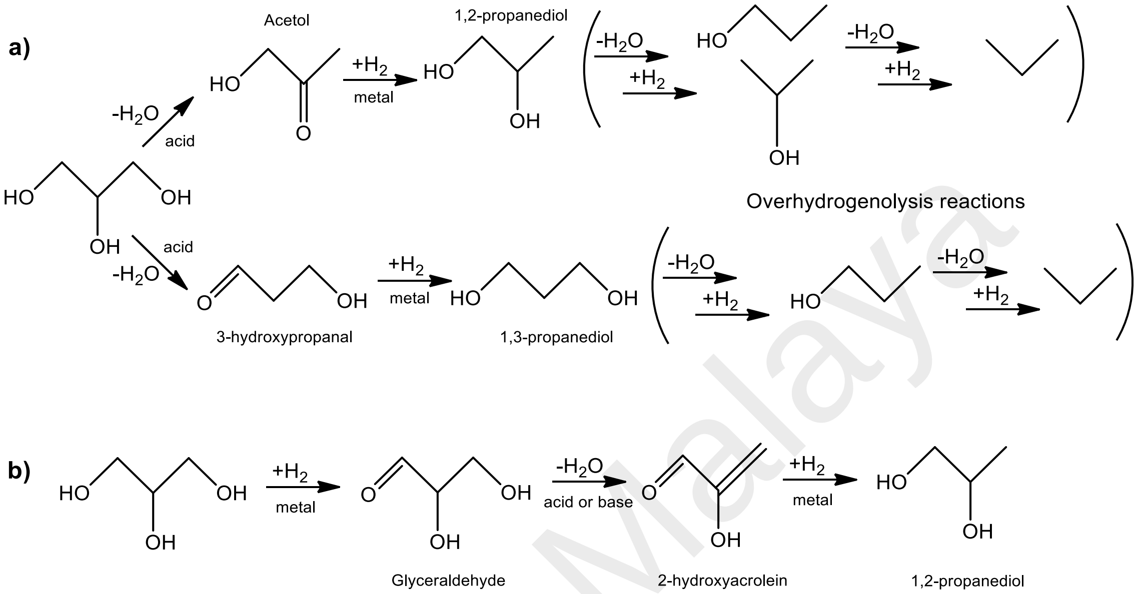

Scheme 2.6: Reaction mechanisms for 1,2-propanediol and 1,3-propanediol production from glycerol a) Two-step mechanism (Dehydration and hydrogenation) and b) Three-step mechanism (Dehydrogenation, dehydration, and hydrogenation)

2.5 Activated carbon-based electrodes and modification techniques

Activated carbon is an amorphous carbon that has been acknowledged because of its excellent properties like large specific surface area, well-developed structure, high thermo-stability, and high adsorptive effect (Dhawane et al., 2018). This material is generally produced from readily biomass feedstocks such as coal, wood, lignite, peat, petroleum residues, and polymers, where its production involved carbonization and chemical or physical activation steps (Sufiani et al., 2019; Zhu et al., 2015). Activated carbon is the cheapest among the carbon materials that are commonly used as adsorbents for pollutants removal and as catalysts or catalyst supports in various fields. In the electrochemistry area, it is employed as an electrode for supercapacitors, electrochemical fuel cells, electroreduction of carbon dioxide (CO_2RR) (Cui et al., 2018; Duan et al., 2017; Hursán et al., 2019; Zhu et al., 2019), oxygen reduction reaction (ORR) in a fuel cell

(Liang et al., 2014; Liang et al., 2012; Ma et al., 2015; Mamtani et al., 2017), water splitting (Nemiwal et al., 2021) and contaminants electro-sorption in wastewater treatment (Ajeel et al., 2015a; Ajeel et al., 2018). It is due to the high electron conductivity and relative chemical inertness properties belong to the activated carbon-based electrodes (Yan et al., 2016).

According to the literature, activated carbon catalytic efficiency is determined either by its surface morphology or surface chemistry. These criteria can be tailored based on different applications requirements (Daud & Houshamnd, 2010). By using micropores or mesopores of activated carbon structure as the electrode, the electrochemical performance can be upgraded. It acts as a support matrix to boost the active component dispersion, facilitate the accessibility of electrolyte into the electrode, and hence, increase its catalytic activity (Card et al., 1990; Tang et al., 2013). Nevertheless, activated carbon alone is not regarded as an efficient electrode, it requires functionalization with polymer and other functional groups or materials like Au, Pt, Rh, and Pd metals (Linares et al., 2014; Murayama & Yamanaka, 2011). Ajeel et al. (2015a) reported that the activated carbon composite electrode that functionalized with polytetrafluoroethylene was used as an anode electrode for phenol degradation and it successfully removed 2-chlorophenol up to 82.5% at low pH. Similar material was also employed by Lee et al. (2018) where the carbon black activated carbon (CBAC) electrode obtained high selectivity (86%) of 1,2-propanediol from glycerol electroreduction reaction. The results of both studies indicated that the mesoporous structure of activated carbon plays a vital role in the electrochemical reaction.

Furthermore, doping carbon-based material with heteroatoms has also gained researchers' attention in CO_2RR as it can increase the materials' charge density and modify the inert carbon structures to be highly active (Duan et al., 2017; Jia et al., 2019). The discrepancy in electronegativity of these heteroatom dopants (P = 2.19, B=2.04, S = 2.58, I = 2.66, Br = 2.96, N = 3.04, and Cl = 3.16) doped with carbon (C) (2.55) element will generate negative/positive charge density that can enable the electron transfer in the process (Yang et al., 2012). Most studies used various carbon materials such as graphene, diamond, carbon nanotubes, and porous carbon for this technique. Different porous size structures of these heteroatom-doped carbon-based electrodes exhibit different CO_2RR capabilities. As such, micropores improve their surface areas and active sites while mesopores would favour the diffusion of CO_2 as well as facilitate ion transfer into the pores of electrocatalysts (Wang et al., 2008). Whereas the heteroatom-doped activated carbon electrode has been widely used as the supercapacitor. Activated carbon-based electrodes with high surface area, mesopores structure, and nitrogen atoms properties are also important as excellent capacitors. Likewise, these criteria could enhance other materials particles dispersion on their composites. Lee et al. (2017) dispersed nickel oxide on activated and successfully obtained specific capacitance of nitrogen-doped activated carbon with nickel oxide was 530% than bare activated carbon electrode with good cycling (1000 cycles). Nickel hydroxide/activated carbon composite electrode also revealed a high specific capacitance (314.5 F/g) and 23.3% higher than pure activated carbon (255.1 F/g).

Even so, few authors claimed that doping electron-rich nitrogen onto activated carbon is still under debate because of its difficulty to controllably generate the target of nitrogen type. Henceforward, these researchers then initiated a defective mechanism technique to create a unique defect on activated carbon and make it highly active. Intrinsically, in Yan et al. (2016) work, the defective activated carbon (D-AC) electrode unveiled a remarkable catalytic activity for ORR under an alkaline condition with low overpotentials and higher long-term stability compared to commercial Pt/C. It showed a good performance for HER in an acidic medium, suggesting that the non-active activated carbon material can be very active for both the ORR and HER through this surface morphology modification. Attachment of functional groups or metals on activated carbon can also break the electroneutrality of its surface chemistry and improve the catalytic activity. The metals and functional groups added in the activated carbon materials have unveiled different CO_2RR and ORR activity and selectivity, where it might be good for glycerol electroreduction reaction as well.

From other perspectives, the surface structure and electronic properties could be adjusted by shifting the intermediates binding energies with different metals electrocatalysts (Roy et al., 2018). Yet, in most cases, the oxidation step is important before the modification because acidic groups will facilitate metal ion/metallic species adsorption from solution onto activated carbon structure by ion-exchange mechanism and complex formation. The introduction of these oxygen-containing groups on activated carbon can be done either *via* dry oxidation or wet oxidation. Further attachment of functional groups may be achieved through physical adsorption such as impregnation and calcination or chemically bonded by diverse grafting methods.

2.6 Optimization study

In the electrochemical conversion of glycerol, the production of final compounds is greatly affected by electrodes type, electrolytes pH, temperature, applied current and potential, and addition of additives (Md Rahim et al., 2020). The optimization of these parameters is essential to enhance the desired product yield which can be done by the conventional one-factor-at-time (OFAT) or statistical methods. OFAT is known as a time-consuming technique and it cannot describe the interaction between the factors due to many experimental works that will be required (Abdel-Rahman et al., 2020). Therefore, the statistical method is recently advocated to solve these issues and thereby, maximize the final product yield. Response surface methodology (RSM) is a combination method of statistical and mathematical techniques for model formation, evaluating the influence of various independent variables and finding optimal values of variables that were invented in 1951 (Breig & Luti, 2021). In electrolysis systems, RSM has been effectively applied for optimization with various types of computer software including Design expert, Minitab, and Satistica which made its application easier.

In RSM, the models are built up based on the data in experimental design, evaluating the relationship of independent factors and dependent factors, interactions on response, and optimization of the process. It requires many stages where in the first step, the factors and levels are decided, followed by the actual experiments, proper model design selection, verifying the model adequacy, demonstrating the model by the graph, and finally optimization to get the optimum condition. The outcomes are usually illustrated by a 3D plot or by 2D contour plot. The factors and magnitude of these factors are selected based on the literature to achieve an accurate model. Central composite design (CCD) and Box-Behnken design (BBD) are the experiment designs that have been developed in the electrolysis process (Kadier et al., 2021; Khosravanipour Mostafazadeh et al., 2021;

Kowthaman et al., 2021; Yaqub et al., 2021). Although BBD has a lower number of experiments, it does not include extreme points which makes it less expensive. However, there are no points in the cubic vertex that creates upper and lower levels of each variable and make this design less accurate. The difference between CCD and BBD is that CCD operates five levels (-α, − 1, 0, +1, +α) for the study variables but BBD has only three levels (− 1, 0, +1). CCD also consists of duplications at the central point, which offers properties, for instance, rotativity and orthogonality to the modification of quadratic polynomials. The axial points (2k) allow the curvature to be evaluated and to assess new extremes for all study factors in high and low configurations. This design is valuable because it provides complete knowledge of responses with the least quantity of experiments (Pereira et al., 2021). Hence, CCD can provide excellent prediction capability near the center of the design compared to BBD.

2.7 Outlook and conclusion

From the mentioned studies, the trend of research work is currently more emphasized to find out the alternative of replacing metal-based electrodes with carbon-based electrodes. The good feature of these materials is they have a high surface area and huge pores size that could contribute to increasing the ion transport and electrolyte accessibility (Card et al., 1990; Tang et al., 2013), which lead to enhance the enrichment of target chemicals on the catalysts' surface and facilitate their diffusion onto the structure of catalysts (Shen et al., 2015). Lee et al. (2018) were the first researchers to reveal the capability of macroporous mixed carbon-black activated carbon (CBAC) (90-170 nm pore sizes) and mesoporous mixed carbon-black diamond (CBD) (14-22 nm) electrodes to selectively produce 1,2-propanediol from glycerol, but, with the low yield. This work has been a good start to evolve cheaper carbon-based electrocatalysts for this technology. More studies on inexpensive electrodes like activated carbon-based and heteroatom-doped carbon-based materials should be conducted in the future to replace the expensive metal-based electrodes (such as Pt catalyst). Several authors have reported the successful utilization of heteroatom-doped carbon-based materials for oxygen reduction reaction (ORR), oxygen evolution reaction (OER), and carbon dioxide electroreduction reaction (CO_2RR), resulting in promising material design. As alternatives, doping carbon materials with heteroatoms elements (like nitrogen (N), fluorine (F), iodine (I), chlorine (C), bromine (Br), sulfur (S), silicon (Si), phosphorus (P), and their mixtures) could be used to increase the charge density and alter the inert carbon structures to be highly active, and make it suitable for glycerol electrooxidation and –reduction technology (Hoyt et al., 2017; Yang et al., 2015). Besides, the attachments of transition metals on activated carbon or other carbon allotropes would generate positive/negative charge density that can enable the electron transfer in the glycerol electrocatalytic oxidation and reduction processes (Gong et al., 2009; Song et al., 2016). Other than their bifunctionality characteristic, the increase of pores diameter in their structures could improve the catalytic activity with high active sites by decreasing oxygen adsorption and enhancing conductivity, thereby facilitating the reactions (Song et al., 2016; Yadav et al., 2015). The investigation of these carbon-based materials in both alkaline and acidic media ought to be done to achieve the goal of practical industrial development of glycerol electrochemical conversion with low-cost, sustainable, and high-performance electrocatalysts in the future which rival those of Pt-based and other expensive metals materials.

Despite the developments in this field making great progress, the implementation of this technology at a large scale still faces a few challenges such as the electricity consumption in the current state may affect its green attribute. Most of the studies are still on a small scale and/or only work well for pure glycerol, and the real costs of production are uncertain. Therefore, more engineering research and the investigation of crude glycerol as starting material are essential to provide solutions to the challenges related to the process commercialization. The separation and purification of products formed also must be put into researchers' priority lists since the products generated are in a mixture form with the homogeneous electrolyte. A major disadvantage of using this homogeneous electrolyte for this process is the requirement of other technology to separate the electrooxidation and -reduction products from its medium, leading to the additional cost in the operation. Thus, future efforts should firstly focus on the mechanistic and kinetics studies to achieve the precise mechanism pathways with as highest as possible selectivity (purity) and yield of products. Besides, the electrolytes used in the current studies such as mineral acids (like HCl and H_2SO_4) are hazardous in handling, damaging the plant through their corrosiveness and adding process difficulties using quenching and separation stages, which lead to a large volume of toxic and corrosive wastes. Therefore, the replacement of these media with more eco-friendly reagents like solid acids catalysts is highly needed. These co-catalysts could be easily separated and reused few times without losing their activity compared to the mineral acids that are currently used in the glycerol electrochemical conversion technology (Balaraju et al., 2009; Gupta & Paul, 2014). So that, the high purity of products could be obtained due to their selective reactions, and it improves this technology in future for the industrial scale.

CHAPTER 3: METHODOLOGY

3.1 Introduction

This study was divided into three stages, and they were aligned with the research objectives of this work as presented in Figure 3.1. Part I comprised of activated carbon composite (ACC) electrodes synthesis with different activated carbon and carbon black ratios. The physicochemical and electrochemical characteristics of ACC electrodes were firstly analyzed using field emission scanning electron microscopy with energy dispersive X-ray spectroscopy (FESEM-EDX), cyclic voltammetry (CV), and chronoamperometry (CA). To investigate the performance of electrodes, all ACC electrodes were used as the cathode electrodes for glycerol electrochemical conversion, and this work focused on the electroreduction part. In the second stage, the suggested intermediates (acetol and ethylene glycol) were used as the feedstocks to elucidate the reaction mechanisms of glycerol electroreduction on the selected ACC electrode. The effects of kinetics parameters such as reaction temperature, glycerol initial concentration, and current density on the glycerol electroreduction reaction were explored in the third section. An optimization study was done using response surface methodology (RSM) and analysis of variance (ANOVA) to maximize the response, (*e. g.*, the product yield namely, 1,2-propanediol) in RSM models.

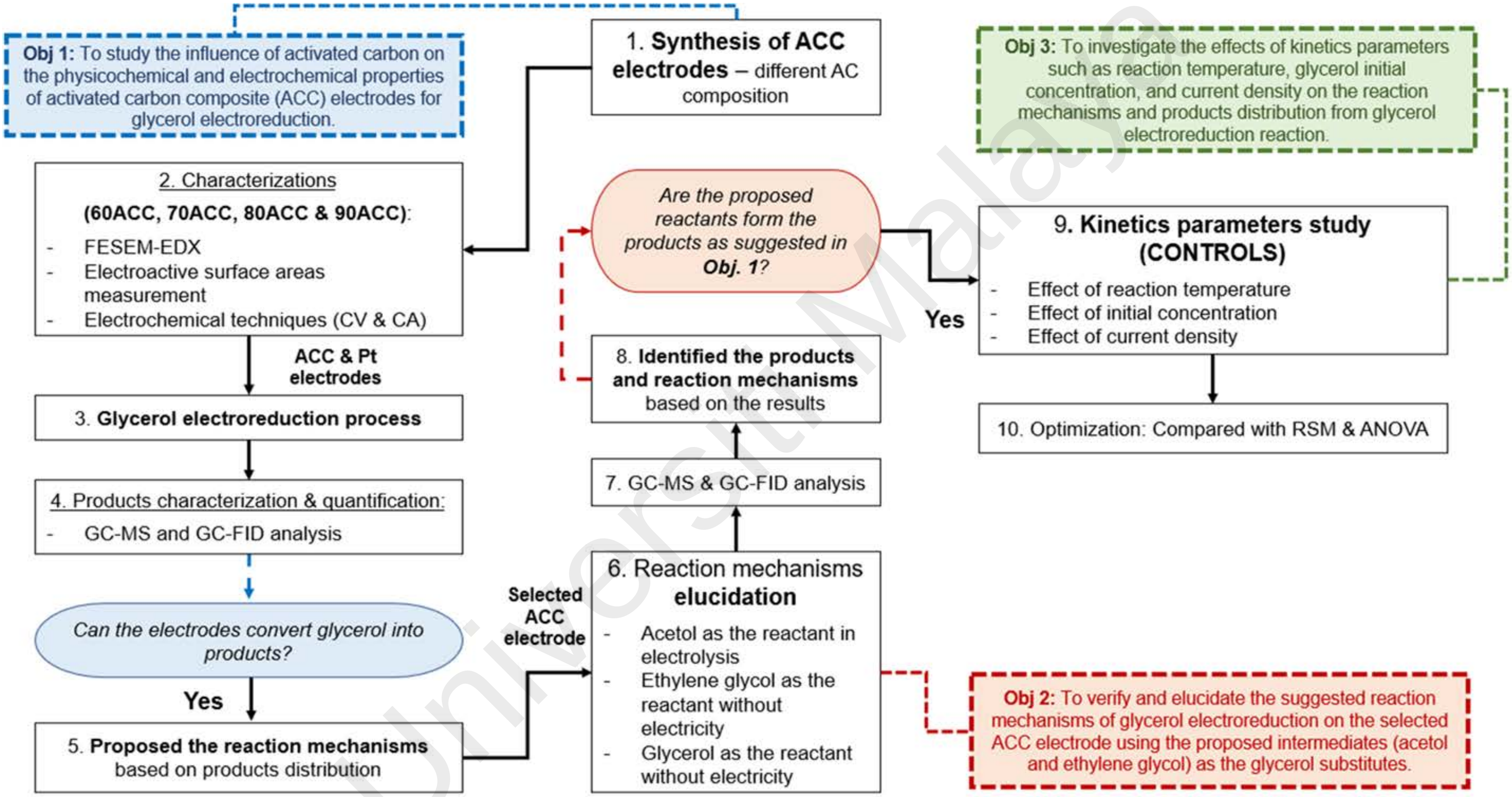

Figure 3.1: Flowchart of complete research methodology.

3.2 Chemicals and reagents list

All the chemicals and reagents used in this work are listed in Table 3.1.

Table 3.1: List of chemicals and reagents used.

Chemicals or reagents	Purity	Manufacturer
Acetol	>90%, Technical grade	Sigma Aldrich, Malaysia
Acetone	99.8%, AR grade	Fisher Scientific, Malaysia
Activated carbon powder	99.5%, AR grade	Sigma Aldrich, Malaysia
Amberlyst-15	100%, AR grade	Sigma Aldrich, Malaysia
Carbon black powder	99%, AR grade	Alfa-Chemicals, Malaysia
Diethylene glycol	≥99%, puriss p.a. (GC)	Sigma Aldrich
Ethyl alcohol	>95%, AR grade	R&M Chemicals, Malaysia
Ethylene glycol	99.5%, AR grade	R&M Chemicals, Malaysia
Glycerol	>99.8%, AR grade	R&M Chemicals, Malaysia
Potassium ferrocyanide	99%, AR grade	R&M Chemicals, Malaysia
Polytetrafluorethylene (PTFE)	60wt% dispersion in H_2O	Sigma Aldrich, Malaysia
Sodium sulfate	>99%, AR grade	Acros, Organics, Belgium
Sulfuric acid	98%, AR grade	Merck, Malaysia
Sodium hydroxide	>97%, AR grade	Fisher Scientific, Malaysia
Tetraethylene glycol, dimethyl ether	>99%, GC grade	Sigma Aldrich, Germany
1,2-Propanediol	99%, GC grade	Acros Organics, Belgium
1,3-Propanediol	99%, GC grade	Acros Organics, Belgium

3.3 Activated carbon composite (ACC) electrodes preparation

To study the effect of activated carbon: carbon black ratio on the physicochemical, and electrochemical properties of activated carbon composite (ACC) electrodes for glycerol electroreduction, ACC electrodes (with the geometrical surface area of 0.5 and 7.1 cm^2) were prepared through the blending and deep drying method. Four ACC cathode electrodes of 60ACC, 70ACC, 80ACC, and 90ACC were synthesized by mixing different compositions of activated carbon (60, 70, 80, and 90% weight) with carbon black (40, 30, 20, and 10% weight, respectively) to total weight. The pre-mixed powder was blended with a mixture solution of 20% (v/v) polytetrafluoroethylene (PTFE) and 80% (v/v) 1,3-propanediol with 1:2 ratio for 25 min. The obtained slurries were neatly pressed and dried using a drying sequence of 100 °C (2 h), 180 °C (1 h), 250 °C (1 h), and 350 °C (30 minutes) to allow a complete sintering process and increase the electrode hardness. It was respective to the heating rates of 0.8 °C/min, 1.3 °C/min, 1.2 °C/min, and 3.3 °C/min. The copper wire was used as the current collector by adhering to discs of electrodes and insulating them by the organic adhesive.

3.4 Electrochemical and physicochemical characterization

3.4.1 Field emission scanning electron microscopy with energy dispersive x-ray spectroscopy (FESEM-EDX)

To examine the surface morphology and elemental composition of the ACC electrodes, the field emission scanning electron microscopy and energy-dispersive X-ray spectroscopy (FESEM/EDX) methods were employed (FEG Quanta 450). The samples were directly tested for the FESEM-EDX characterization as the activated carbon is a conductive material. The accelerating voltages of 10 kV and 20 kV were applied to determine the surface morphology and EDX analysis, respectively. The same detector of Everhart-Thornley detector (ETD) was utilized for both methods.

3.4.2 Electroactive surface areas measurement

A redox solution, 5 mM of potassium ferrocyanide [$K_4Fe(CN)_6$] in 0.1 M of potassium dihydrogen phosphate (KH_2PO_4) was exploited to determine the electroactive surface areas (EASA) by the chronoamperometry (CA). All analyses were operated using BioLogicScience instrument with EC-Lab Software connected to a three electrodes cell (Figure 3.2). Pt and Ag/AgCl were applied as the counter and reference electrodes, correspondingly. Meanwhile, the prepared electrodes were assigned as the working electrode. The oxidation of ferrocyanide which happened on the working electrode is shown in 3.1. This reaction was controlled by the ferrocyanide ions diffusion on the ACC electrodes surface; where the current correlated with the charge transfer from its surface to the reactant can be expressed in 3.2 (Trasatti & Petrii, 1992)

$$[Fe(CN_6)]^{4-} \rightarrow [Fe(CN_6)]^{3-} + e^- \qquad 3.1$$

$$I = \frac{nFADC_0}{\delta} \qquad 3.2$$

I is the current (A), n is the stoichiometric number of electrons involved in the reaction ($n = 1$) as depicted in 3.1, F is the Faraday constant 96485 (C/mol), A is the electroactive surface area of the electrode (cm^2), D is the diffusion coefficient of $K_4Fe(CN)_6$ (6.2×10^{-6} cm^2/s), C_0 is the bulk concentration of $K_4Fe(CN)_6$ (mol/cm^3), and δ is the diffusion layer thickness. CA analysis describes the faradaic current-time response for a macroelectrode based on the growth of the Nernst diffusion layer, δ. The Nernst diffusion layer is the area near the working electrode where the electroactive species concentration grows linearly from zero at the working electrode to the bulk concentration of the electrolyte. δ at a time, t is given by 3.3:

$$\delta = (\pi Dt)^{1/2} \qquad 3.3$$

Thus, 3.3 was substituted for 3.2 and the electroactive surface areas (EASA) of the prepared electrodes were calculated using the Cottrell equation (3.4) (Bard, 1980; Brownson & Banks, 2014). EASA was evaluated in a stage from the time when the diffusion layer initially exists to the time when the Nernst diffusion layer is established.

As mentioned by Aoki and Osteryoung (1981), a short time interval ($t < 20$ s) during the analysis with the planar macroelectrode will obey the Cottrell equation.

$$I = \frac{nFAD^{1/2}C_0}{\pi^{1/2}t^{1/2}} \tag{3.4}$$

3.4.3 Electrochemical responses on ACC electrodes by cyclic voltammetry (CV) and chronoamperometry (CA) analyses

The investigation of electrochemical activity on the ACC electrodes was carried out using the same instrument connected with a three-electrodes cell (Figure 3.2). Cyclic voltammetry (CV) was conducted, and the analysis was scanned between -3.5 V and +1.0 V at a constant scan rate of 50 mVs^{-1}. Pt planar (total surface area of 0.20 cm^2) and Ag/AgCl were applied as the counter and reference electrodes, respectively. The prepared electrodes (geometrical surface area of 0.50 cm^2) were assigned as the working electrodes. The system was agitated with a magnetic stirrer at a constant rate of 350 rpm in an acidic electrolyte (pH 1) of 0.3 M Na_2SO_4 with 9.6% (w/v) Amberlyst-15. To evaluate the effectiveness of ACC electrodes, they were tested with CV analysis in the absence and presence of 0.3 M glycerol. The durability and stability of electrodes were determined using the chronoamperometry (CA) technique for 3600 s at -2.5 V *vs*. Ag/AgCl. All the obtained currents were normalized with the geometrical surface area of ACC electrodes.

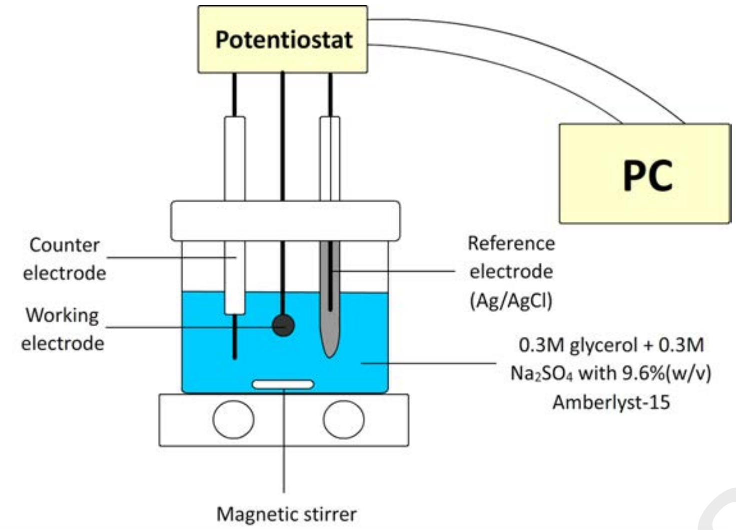

Figure 3.2: CV and CA analyses setup.

3.5 Glycerol electroreduction reaction under galvanostatic mode

The glycerol electroreduction was conducted in a two-compartment reactor separated by a cation exchange membrane (Nafion-117) at a laboratory scale. Each compartment was filled with 250 mL 0.3 M of pure glycerol with electrolyte solution (24 g of Amberlyst-15 as an additive in 0.3 M of sodium sulfate (Na_2SO_4)). Platinum (Pt) (with 22 cm^2 and 33 cm^2 geometrical surface area) was utilized as anode and cathode electrodes, correspondingly. In the first part, different ACC electrodes (60ACC, 70ACC, 80ACC, and 90ACC) with a geometrical surface area of 7.1 cm^2 were used as the cathode electrodes to evaluate their performance. The reaction temperature of 27.0 °C and current density of 0.14 A/cm^2 were utilized in the system for 8 hours at 350 rpm of stirring speed. The temperature and applied current were controlled by a laboratory chiller and a DC power supply, respectively. The liquid sample was squeezed using a dropper for every hour and further prepared for the characterization and quantification using the gas chromatography-mass spectroscopy (GC-MS) and gas chromatography connected with a flame ionization detector (GC-FID). This study was majorly focused on the electroreduction reaction.

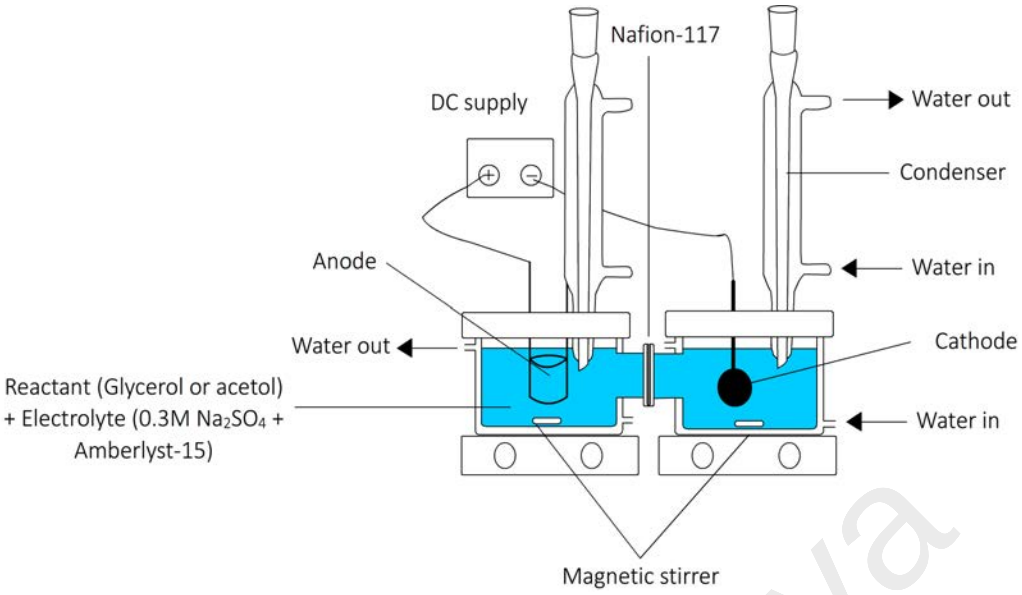

Figure 3.3: Experimental setup in a two-compartment reactor.

3.6 Reaction mechanisms elucidation for glycerol electroreduction

Two suggested intermediates, acetol and ethylene glycol were evaluated as the starting materials to verify and elucidate the reaction mechanisms of glycerol electroreduction. Since 80ACC cathode (with 7.1 cm^2 of geometrical surface area) achieved the highest selectivity and yield of 1,2-propanediol, it was then used as cathode, and Pt mesh cylinder (with 22 cm^2 of geometrical surface area) as anode for acetol electroreduction reaction in a two-compartment reactor (Figure 3.3). The alteration of kinetics parameters was carried out to assess their effects on the distribution of the products. In the first part, 250 mL of 0.3 M acetol was filled in a two-compartment reactor. At the constant stirring speed of 350 rpm and current density of 0.14 A/cm^2, the reaction temperature was changed from 27.0 °C to 53.5 °C, 80.0 °C, and 106.5 °C. The initial glycerol concentration was also modified from 0.3 M to 1.65 M, 3.0 M, and 4.35 M in the second investigation. 0.14 A/cm^2, 0.21 A/cm^2, 0.28 A/cm^2, and 0.35 A/cm^2 of current density were varied in the last part. The experiments were carried out for 8 hours and the sample was taken in each hour. Later, to prove ethylene glycol produces diethylene glycol, 100 mL of ethylene glycol was filled in a one-compartment reactor (Figure 3.4), without the application of electricity.

The optimum conditions from acetol reaction experiments were used. The experiment was conducted for 8 hours. Lastly, at the optimal conditions, glycerol was used as a starting material for dehydration without the electrical current.

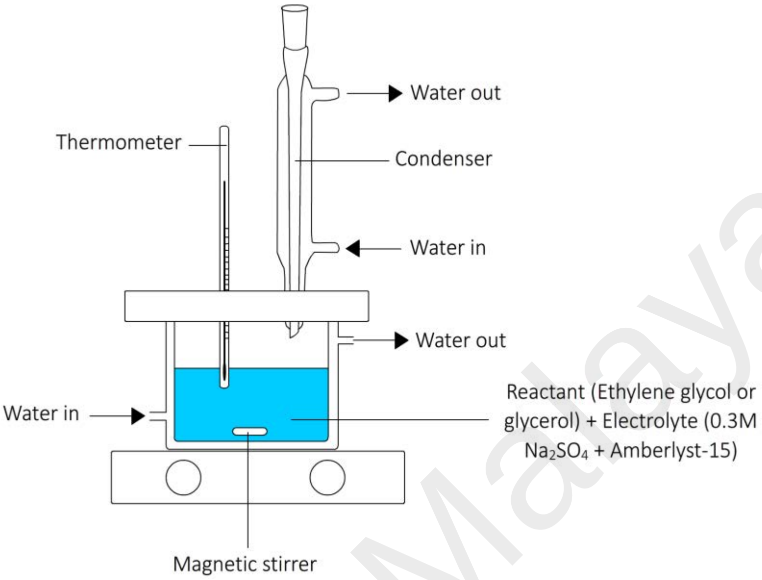

Figure 3.4: Experimental setup in a one-compartment reactor without electricity.

3.7 Preliminary experiments: Glycerol electroreduction on 80ACC

The same two-compartment reactor was used for the preliminary experiments of glycerol electroreduction. The studies were performed for 8 hours with 80ACC as cathode and Pt as anode electrodes. Both anode and cathode parts were filled with 250 mL of 0.3 M pure glycerol. An acidic medium (9.6% (w/v) of Amberlyst-15 in 0.3 M of Na_2SO_4) was applied as the electrolyte. The work was divided into a few parts to study the effects of each kinetics parameter. In the first part, with 0.3 M of glycerol as the reactant, the temperature was changed from room temperature (27 °C) to 53.5 °C, 80 °C, and 106.5 °C, and the current density was 0.14 A/cm^2 at 350 rpm of stirring rate. In every hour, the sample was manually acquired and prepared for characterization using the GC-MS. The quantification of the presented compounds was done with the GC-FID. The next batch of experiments involved the variation of glycerol initial concentration (0.3 M, 1.65 M, 3.0 M, and 4.35 M). With the optimum reaction temperature and initial concentration of glycerol, the current density was varied (0.14 A/cm^2, 0.21 A/cm^2, 0.28 A/cm^2, and 0.35 A/cm^2); applied current of 1.0 A, 1.5 A, 2.0 A, and 2.5 A. The experiments were conducted in a batch mode.

3.8 Optimization study of glycerol electroreduction

In this part, Design-Expert software Version 8.0.0 (Stat-Ease, Inc., Minneapolis, USA) was used for both response surface methodology (RSM) and the analysis of variance (ANOVA). The three points of every parameter that generated a high yield of 1,2-propanediol as the final product was selected for the optimization study. This investigation was intended to evaluate the parameters such as temperature, glycerol initial concentration and current density as the factors that have the greatest effect on the electroreduction of glycerol to 1,2-propanediol yield as the response, and further develop the variables in the polynomial model (Khosravanipour Mostafazadeh et al., 2021). In accordance with the central composite design (CCD) technique, RSM was first employed to identify the experimental design. Table 3.2 presents the independent variables and the experimental domain used in the CCD technique. The CCD matrix of changing these parameters was further tabulated in Table 3.3. The CCD consisted of the axial points (2n), the number of independent variables (2n), and replications of center points (nc), where respective to 2n = 6, 2n = 8, and nc= 8. Subsequently, it resulted in 20 experiments. These experiments were arbitrarily conducted to decrease the influence of unexplainable variance in the observed response caused by irrelevant variables.

Table 3.2: Range of independent variables with their coded experimental domains.

Independent variables		Unit	Experimental domain		
Coded	Actual		Low (-1)	Medium (0)	High (+1)
A	Reaction temperature	°C	27.0	53.5	80.0
B	Initial concentration	M	0.30	1.65	3.00
C	Current density	A/cm^2	0.14	0.21	0.28

Table 3.3: The central composite design (CCD) matrix for 20 experiments of glycerol electroreduction.

Run	Actual variables			Coded variables		
	Reaction temperature (°C)	Initial concentration (M)	Current density (A/cm^2)	A	B	C
1[a]	80.00	0.30	0.28	1	-1	1
2[b]	27.00	1.65	0.21	-1	0	0
3[c]	53.50	1.65	0.21	0	0	0
4[b]	53.50	1.65	0.14	0	0	-1
5[a]	80.00	0.30	0.14	1	-1	-1
6[b]	53.50	0.30	0.21	0	-1	0
7[c]	53.50	1.65	0.21	0	0	0
8[a]	80.00	3.00	0.28	1	1	1
9[b]	53.50	1.65	0.28	0	0	1
10[b]	53.50	3.00	0.21	0	1	0
11[c]	53.50	1.65	0.21	0	0	0
12[a]	27.00	0.30	0.28	-1	-1	1
13[a]	27.00	0.30	0.14	-1	-1	-1
14[a]	27.00	3.00	0.14	-1	1	-1
15[c]	53.50	1.65	0.21	0	0	0
16[a]	80.00	3.00	0.14	1	1	-1
17[c]	53.50	1.65	0.21	0	0	0
18[a]	27.00	3.00	0.28	-1	1	1
19[c]	53.50	1.65	0.21	0	0	0
20[b]	80.00	1.65	0.21	1	0	0

The different alphabets in run order mean (a) factorial design, (b) axial point, and (c) center point.

After the experiments were carried out, RSM with CCD method was then used to determine the influence of each parameter (X), interactions between kinetics parameters ($X_i X_j$), and optimum conditions of the process on the response (Y). The results were fitted to a quadratic equation, polynomial model in 3.5 and 3.6, to predict the system response. The equations were also used to calculate the coefficients of the polynomial model (Khosravanipour Mostafazadeh et al., 2021).

$$Y = b_0 + \sum_{i=1}^{n} b_i X_i + \sum_{i=1}^{n} b_{ii} X_i^2 + \sum_{i=1}^{n} \sum_{j>1}^{n} b_{ij} X_i X_j \qquad 3.5$$

$$Y = b_0 + b_1 X_1 + b_2 X_2 + b_3 X_3 + b_{11} X_1^2 + b_{22} X_2^2 + b_{33} X_3^2 + \qquad 3.6$$

$$b_{12} X_1 X_{12} + b_{13} X_1 X_{13} + b_{23} X_1 X_{23} +$$

Y is the experimental response (1,2-propanediol yield). b_0, b_i, b_{ii}, and b_{ij} are the regression coefficients for constant, linear, quadratic, and interaction coefficients. b_0 signifies the average value of the responses of the assays, b_i denotes the principal effect of each factor i on the response and b_{ij} is the interaction effect between factor i and factor j on the response (Y). Analysis of variance (ANOVA) was carried out to estimate the significance of the obtained models. A correlation coefficient that surpasses 0.8 suggests that the models are acceptable with a good correlation between predicted and experimental values. This is also validated by comparing Pr > F with α value ($\alpha = 0.05$). Pr > F should be lesser to α for the models to be accepted.

3.9 Standards calibration and samples preparation

The standards calibration curves are important for the quantification analysis of a specific compound in an unknown sample. The determination of this compound concentration was done by comparing its unknown concentration to the set of standards of known concentration. As such, a calibration curve for glycerol was plotted based on glycerol concentrations ranging from 0.1 mg/mL to 1.50 mg/mL. 1000 μL of 20.0 mg/mL tetraethylene glycol (TEG) as an internal standard was spiked into each concentration and the solutions were added with ethanol in a 10 mL volumetric flask. The amount of glycerol standards prepared for the calibration, area of each concentration, and area of TEG are summarized in Table 3.4 and the calibration curve is shown in Figure 3.5.

Table 3.4: Glycerol standards solutions prepared for the calibration curve.

Mother solution (mg/mL)	Volume taken from mother solution (μL)	Theoretical conc. (mg/mL)	Actual conc. (mg/mL) **	Area of glycerol (GC-FID)	Area of TEG (GC-FID)	Area glycerol/ Area TEG
10.12	100	0.10	0.0988	1.4	125.8	0.011128
10.12	100	0.10	0.0988	5.9	294.9	0.020006
10.12	100	0.10	0.0988	2.0	133.5	0.014981
10.12	500	0.50	0.4941	23.4	234.3	0.099871
10.12	500	0.50	0.4941	27.4	266.7	0.102737
10.12	500	0.50	0.4941	38.9	342.9	0.113444
10.12	1000	1.00	0.9881	43.9	226.5	0.193818
10.12	1000	1.00	0.9881	17.0	83.6	0.203349
10.12	1000	1.00	0.9881	62.3	334	0.186526
10.12	1500	1.50	1.4822	360.5	1002.1	0.359744
10.12	1500	1.50	1.4822	86.2	241.1	0.357527
10.12	1500	1.50	1.4822	83.9	228.6	0.367016

Preparation of mother solution: 253.00 mg of glycerol in 25 mL volumetric flask consisted of ethanol.

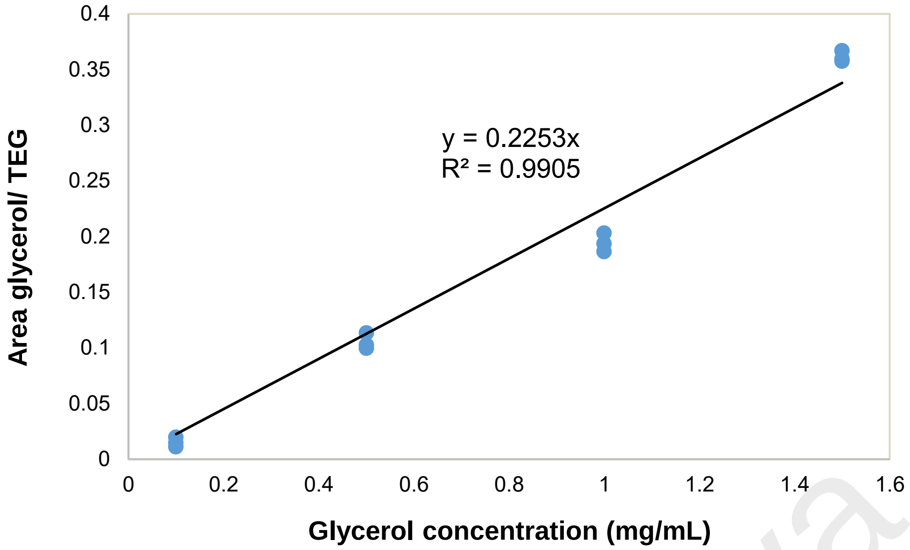

Figure 3.5: Calibration curve of glycerol.

Three-level and four-level concentrations calibration curves for other chemical standards such as acetol, acetone, ethylene glycol, diethylene glycol, 1,2-propanediol, 1,3-propanediol, 1-ethoxy-2-propanol, and methanol were prepared within 0.10-2.00 mg/mL. Dipropylene glycol and 3-methoxy-1,2-propanediol which are grouped under ether class similar to diethylene glycol was quantified using the calibration curve of diethylene glycol. Meanwhile, 3-hydroxy-2-butanone which is in the carbonyl group like acetone was quantified using an acetone calibration curve. Triplicate injections were done to increase the accuracy of calibration curves for all standards and quantification of each compound in a sample. Their calibration curves are shown in APPENDIX D and they were adopted during the yield calculation for each compound. To prepare the sample, 1000 µL of the liquid sample was mixed with 1000 µL of 20.0 mg/mL internal standard (tetraethylene glycol), and ethanol was added to make up to 10 mL of solution. Later, it was neutralized with sodium hydroxide. Both standards and samples were filtered using a 0.45 µm nylon syringe.

3.10 Products characterization and quantification (GC-MS and GC-FID)

The prepared standards and samples were characterized by gas chromatography-mass spectroscopy (GC-MS) (Agilent Model 7890, United States) equipped with DB-Wax (Phenomenex, United States) capillary column (30 m × 0.25 mm × 0.25 μm). Helium (> 99.99% purity) with a constant flow rate of 2.0 mLmin^{-1} was operated as a carrier gas and the injection volume was 1 μL. The initial oven temperature was at 45 °C and conducted for 5 min. The temperature was increased at 10 °Cmin^{-1} to a final temperature of 240 °C which was maintained for 5 mins. The results were compared with the MS Library (Agilent, ChemStation software) and chemical standards. The retention time (R_t) of each product is displayed in Table 3.5 and the MS spectra of the obtained compounds are shown in APPENDIX B.

Table 3.5: List of chemical standards, their physical properties, and retention time generated in GC-MS and GC-FID analyses.

Compound	Molecular structure	MW (g/mole)	BP (°C)	R_t, GC-MS (min)	R_t, GC-FID (min)
Acetone	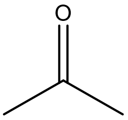	58.09	56.30	2.24	1.75
Methanol		32	65	2.90	2.43
1-ethoxy-2-propanol	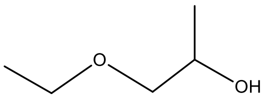	104.15	217.8	6.72	6.50
3-hydroxy-2-butanone	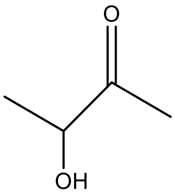	176.22	147	10.80	10.98

Table 3.5 continued.

Acetol	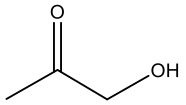	74.08	145	11.20	10.26
3-methoxy-1,2-propanediol	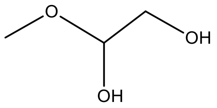	106.12	220	11.92	11.38
1,2-propanediol	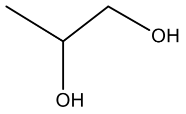	76.10	188.2	14.75	14.83
Ethylene glycol	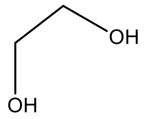	62.07	197.3	15.32	15.28
1,3-propanediol	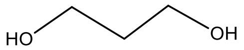	76.10	211	16.37	17.25
Diethylene glycol	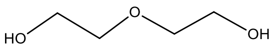	106.12	244	18.90	19.46
Dipropylene glycol	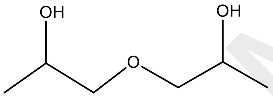	134.17	230.5	19.20	19.80
Tetraethylene glycol		194.23	313	21.20	20.97
Glycerol	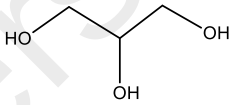	92.08	290	22.10	22.97

MW: Molecular weight, BP: boiling point, and R_t: retention time.

Quantitative analysis was performed by gas chromatography (GC) equipment (Model 6890, Agilent) connected with a flame ionization detector (FID) attached with the same capillary column. The analysis was carried out under the same condition as GC-MS analysis. The integrated peak areas calculation for samples was made based on the standards calibration curves plotted with known concentration. The standards retention time (R_t) and calibration data for each presented compound are shown in APPENDIX C and APPENDIX D, respectively. The glycerol (or intermediates) conversion, products yield, and selectivity were calculated by 3.7, 3.8 and 3.9, respectively. The examples of these calculations are shown in APPENDIX .

$$\text{Glycerol conversion } (\%) = \frac{\text{Converted glycerol}}{\text{Glycerol in feed (C mol)}} \times 100\% \qquad 3.7$$

$$\text{Product yield } (\%) = \frac{\text{Amount of product (C mol)}}{\text{Total of glycerol in feed (C mol)}} \times 100\% \qquad 3.8$$

$$\text{Product selectivity } (\%) = \frac{\text{Amount of product (C mol)}}{\text{Converted glycerol}} \times 100\% \qquad 3.9$$

*Glycerol is replaced with the intermediates: acetol and ethylene glycol, converted glycerol: Gly.in feed - Gly.in outlet (C mol).

CHAPTER 4: RESULTS AND DISCUSSION

4.1 Introduction

This chapter is separated into three parts. The physicochemical and electrochemical characterization of activated carbon composite (ACC) electrodes with different activated carbon content using field emission scanning electron microscopy and energy-dispersive X-ray spectroscopy (FESEM-EDX), cyclic voltammetry (CV), and chronoamperometry (CA) techniques are firstly reviewed. Later, the electroreduction of glycerol on the 60ACC, 70ACC, 80ACC, and 90ACC cathode electrodes in a two-compartment reactor is thoroughly discussed. The reaction mechanisms are proposed based on the products distribution results using these electrodes. In the second part, the suggested reaction mechanisms of glycerol electroreduction are validated using the recommended intermediates, namely acetol and ethylene glycol on the selected ACC electrode. The effects of reaction temperature, initial concentration, and current density towards the products distribution for glycerol electroreduction reaction are delineated in the third section. Investigation of the simultaneous influences and the significance of different operating kinetics parameters by the response surface methodology (RSM) and the analysis of variance (ANOVA) are also discussed.

4.2 Characterization and evaluation of ACC electrodes

4.2.1 Field emission scanning electron microscopy and energy-dispersive X-ray spectroscopy (FESEM-EDX) of the ACC electrodes

Figure 4.1a-c displays the highly disordered pores network and no separated carbon layer like the typical amorphous carbon composites (Ali et al., 2020; Meng et al., 2017). However, improving the activated carbon composition up to 90 wt% in the 90ACC electrode caused the least aggregation of the activated carbon and carbon black particles with the binder, which can lead to low stability (Figure 4.1d). At higher magnification (×50 000 with 2.0 μm of image resolution), all electrodes showed high porosity in the structures. The pores sizes were increased when the activated carbon composition was enhanced. The pores sizes were 110.7-177.9 nm, 119.6-253.2 nm, 145.7-258.1 nm, and 194.1-584.6 nm in the 60ACC, 70ACC, 80ACC, and 90ACC structures, respectively. When the pores sizes improved, the diffusion limit of the glycerol molecule can be minimized, eventually, it can facilitate the ions transport and glycerol conversion (McMorn et al., 1999). Besides, the macroporous structure in the ACC electrodes can also quicken the trapping of the electrons and reaction intermediates in the pores. Therefore, it can enhance the selectivity of products and conversion rate (Qi et al., 2014; Z. Zhang et al., 2014).

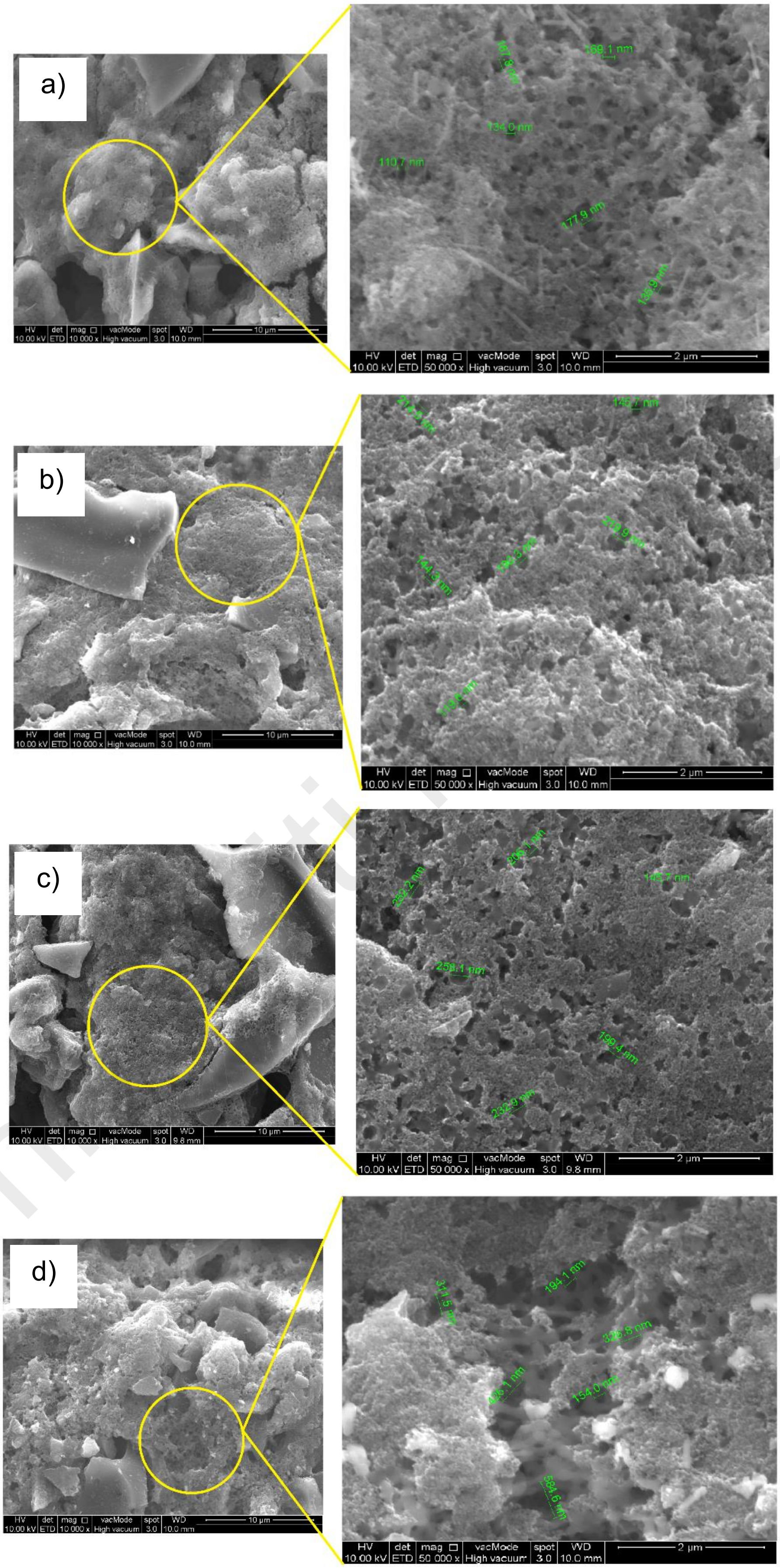

Figure 4.1: FESEM images of a) 60ACC, b) 70ACC, c) 80ACC and d) 90ACC cathode electrodes.

The elements in the ACC electrodes were discovered in Figure 4.2a-d at ×600 magnification (with 200 µm of image resolution). Except for the 90ACC electrode, the EDX maps present the well-distribution of carbon (C), fluorine (F), and oxygen (O) elements. It indicates the nanoparticles of activated carbon and carbon black were homogeneously dispersed in the binder mixture of polytetrafluoroethylene (PTFE) and 1,3-propanediol that has fluorine and oxygen compounds. The nominal value of C as the main element was vaguely increased at higher activated carbon composition; 67.8 wt%, 71.3 wt%, 72.8 wt%, and 80.4 wt% corresponding to the 60ACC, 70ACC, 80ACC, and 90ACC electrodes (Figure 4.2e-h). Contrarily, the values for F and O were reduced from 24.6 wt%, 22.4 wt%, 21.2 wt%, to 14.7 wt% for F, and from 7.7 wt%, 6.4 wt%, 6.1 wt%, to 4.9 wt% for O elements. This is because 1,3-propanediol and PTFE were eliminated faster at higher activated carbon composition and produced a structural effect that is efficient in affecting the electrocatalytic performance for the composites electrodes (Alaba et al., 2019). Ascribed to the better stability and high macroporous structure, 80ACC can provide a suitable surface area for the electrons transfer and redox reaction with glycerol.

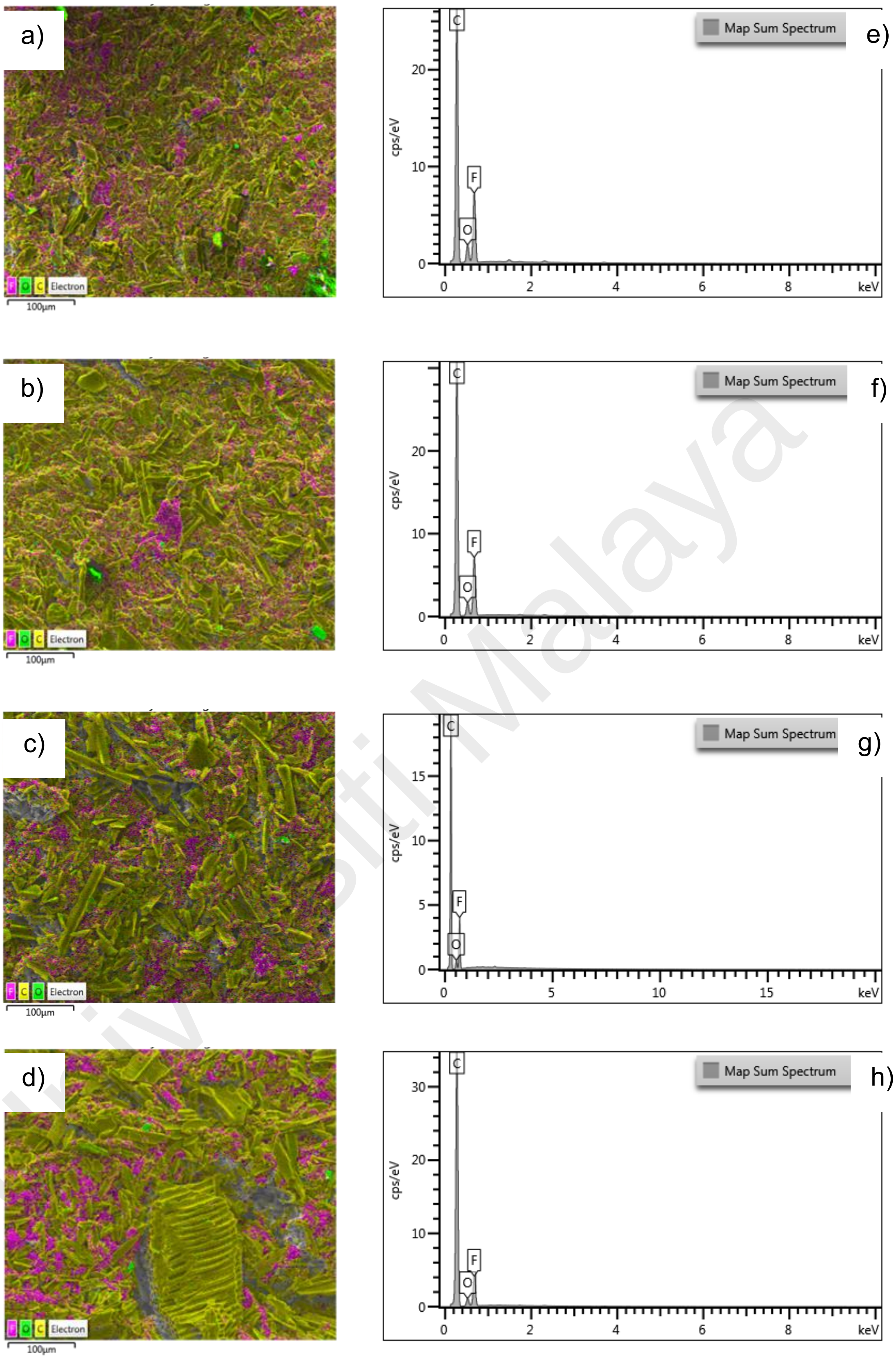

Figure 4.2: EDX maps of a) 60ACC, b) 70ACC, c) 80ACC, and d) 90ACC cathode electrodes with their EDX spectra e), f), g) and h), respectively.

4.2.2 Electroactive surface areas (EASA) of ACC electrodes

The electroactive surface areas (EASA) of the ACC electrodes were measured in a ferrocyanide solution [$Fe(CN)_6]^{4-}$] by chronoamperometry (CA) analysis. The application of $Fe(CN)_6]^{4-}$ (identified n, C_o, and D) as a redox model complex in the measurement enabled the evaluation of an accurate EASA (Brownson and Banks, 2014). From the CA results, the Cottrell plots of I *vs.* $t^{-1/2}$ give a straight line in Figure 4.3.

The EASA calculations that were made based on these plots are revealed in APPENDIX A. The EASA of 60ACC, 70ACC, 80ACC, and 90ACC electrodes (with 0.50 cm^2 geometrical surface area) were respective to 19.6 cm^2, 24.5 cm^2, 36.7 cm^2 and 30.8 cm^2. The enhancement of EASA was attributed to the higher presence of activated carbon which has a greater specific surface area (950m^2/g) than the carbon black particles (550 m^2/g) in the electrodes. It was also influenced by the combined properties of the porous structure and more accessible surface-active areas in the activated carbon particles (Xu et al., 2017). Through the largest EASA, 80ACC electrode can promptly increase the electrons transfer movement, as well as mass transport of glycerol and intermediates. Consequently, a better electrocatalytic activity can be achieved (Huang et al., 2015; Xu et al., 2017). Nevertheless, the EASA was reduced when activated carbon composition was increased up to 90 wt.% of total weight (90ACC). The minimum aggregation in the dispersion of activated carbon, carbon black particles, and the binder might have dwindled the EASA of 90ACC along with its electrocatalytic activity (Ma et al., 2015). The pattern could also suggest that 80ACC is more stable than 90ACC.

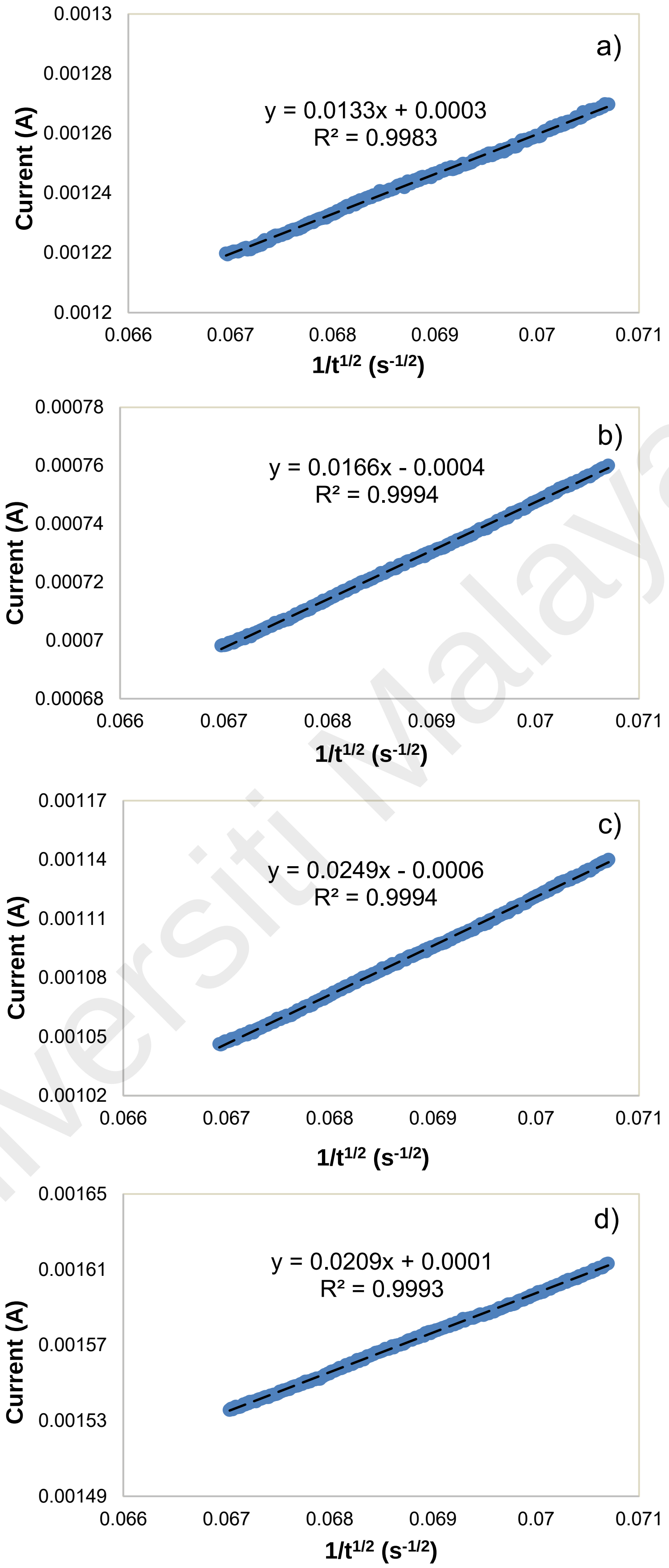

Figure 4.3: Cottrell plots of a) 60ACC, b) 70ACC, c) 80ACC, and d) 90ACC electrodes in the ferrocyanide solution.

4.2.3 Electrochemical behaviour on ACC electrodes using cyclic voltammetry (CV)

The efficacy of the ACC electrodes for glycerol electroreduction was evaluated in the absence and presence of glycerol using cyclic voltammetry (CV). Figure 4.4a shows the CV curves without glycerol that were studied from -3.5 V to 1.0 V at 50 mVs^{-1} in 0.3 M of sodium sulfate (Na_2SO_4) and 9.6% (w/v) of Amberlyst-15 electrolyte. The forward and backward current densities were improved at high ($E > +0.50$ V) and low potential ($E < -1.00$ V) as the activated carbon composition was increased. This trend was related to the oxygen evolution reaction (H_2O oxidation to O_2) in the region I and hydrogen evolution reaction (reduction of H^+ to H_2) in region II which favoured high activated carbon: carbon black ratio in the ACC electrodes. The high current density for HER was elevated because of the ACC electrodes' ability to conduct this reaction in an acidic electrolyte like platinum (Khosravanipour Mostafazadeh et al., 2021). A pair of quasi-reversible redox peaks was also detected at -0.50 V (peak (a)) and +0.25 V (peak (b)) electrode potentials. The peaks were slightly changed to more positive and negative potentials when the activated carbon loading was enhanced in the electrodes. The appearance of these peaks was assigned to the existence of Amberlyst-15, where the oxidation and reduction of this mediator happened in the system. When the applied potential achieved the potentials of redox mediator ($E_{mediator}$), the activated Amberlyst-15 (Med_{ox} or Med_{red}) was formed (Reid et al., 2018). Amberlyst-15 facilitated the heterogeneous electrons transfer between the electrode and glycerol, followed by the homogeneous redox catalysis between the electrochemically activated Amberlyst-15 (A-15•$^-$) and glycerol (Francke & Little, 2014). For 60ACC, the background current density was featureless between -0.50 V to +1.0 V, divulging the Amberlyst-15 redox reaction occurred the least. Amberlyst-15 is useful in indirect electrolysis because it can avert the electrode passivation, kinetic inhibition, and over-reduction or -oxidation reaction owned by direct electrolysis (Md Rahim et al., 2020;

Pauwels, 2018). From Figure 4.4a, it can be concluded that a fast redox reaction of Amberlyst-15 seems ideal for high activated carbon: carbon black composition of ACC electrodes.

In Figure 4.4b, the cathodic current density was greater for all ACC electrodes in the presence of 0.3 M glycerol than without it (Figure 4.4a). However, when the activated carbon content was lessened, the electrocatalytic activity was reduced where 60ACC < 70ACC < 80ACC = 90ACC. This outcome was equivalent to the effect of the carbon black presence in the carbon black diamond (CBD) composite electrode (Ajeel et al., 2015b) and graphite in the boron-doped diamond (BDD) electrode (Guinea et al., 2009). The higher ratio of carbon black and graphite impurities in the respective electrodes caused the diminishment of electrochemical performance. Even with that result, a cathodic peak (peak (c)) connected to the HER region was found at a potential of -2.5 V, and no oxidation peak appeared for all electrodes. It suggests an electroreduction reaction took place in the similar potential of HER and the reaction is irreversible. Nevertheless, an organic compound with hydroxyl groups like glycerol cannot directly undergo an electroreduction process. The system needs the carbonyl group in the molecule for the reduction (hydro-deoxygenation or hydrogenation) reaction to be initiated. An indirect redox catalytic reaction may occur on glycerol with the aid of Amberlyst-15 in the earlier potential during its redox reactions (E = -0.5 V or E = +0.25 V). The homogeneous redox reaction between the activated Amberlyst-15 and glycerol can obliquely produce the organic compound intermediates through an indirect process. The intermediates which were produced from this reaction are likely being reduced at -2.5 V *vs.* Ag/AgCl. 80ACC and 90ACC electrodes demonstrated the highest value (-0.2018 A/cm^2 and -0.2005 A/cm^2, individually) for this peak, signifying a significant electrocatalytic performance with higher EASA compared to 60ACC and 70ACC electrodes (-0.1639 A/cm^2 and -

0.1913 A/cm^2, correspondingly). Besides, the cathodic peak potential was positively shifted at 80ACC than 90ACC, showing its remarkable activity and stability. Though without the oxidation peaks, a slight increase in anodic current density was detected and preferred 80ACC. This result imputes the fact that the glycerol oxidation potential and OER peaks cannot be split or the oxidation proceeds by an indirect mechanism (Ajeel et al., 2015a).

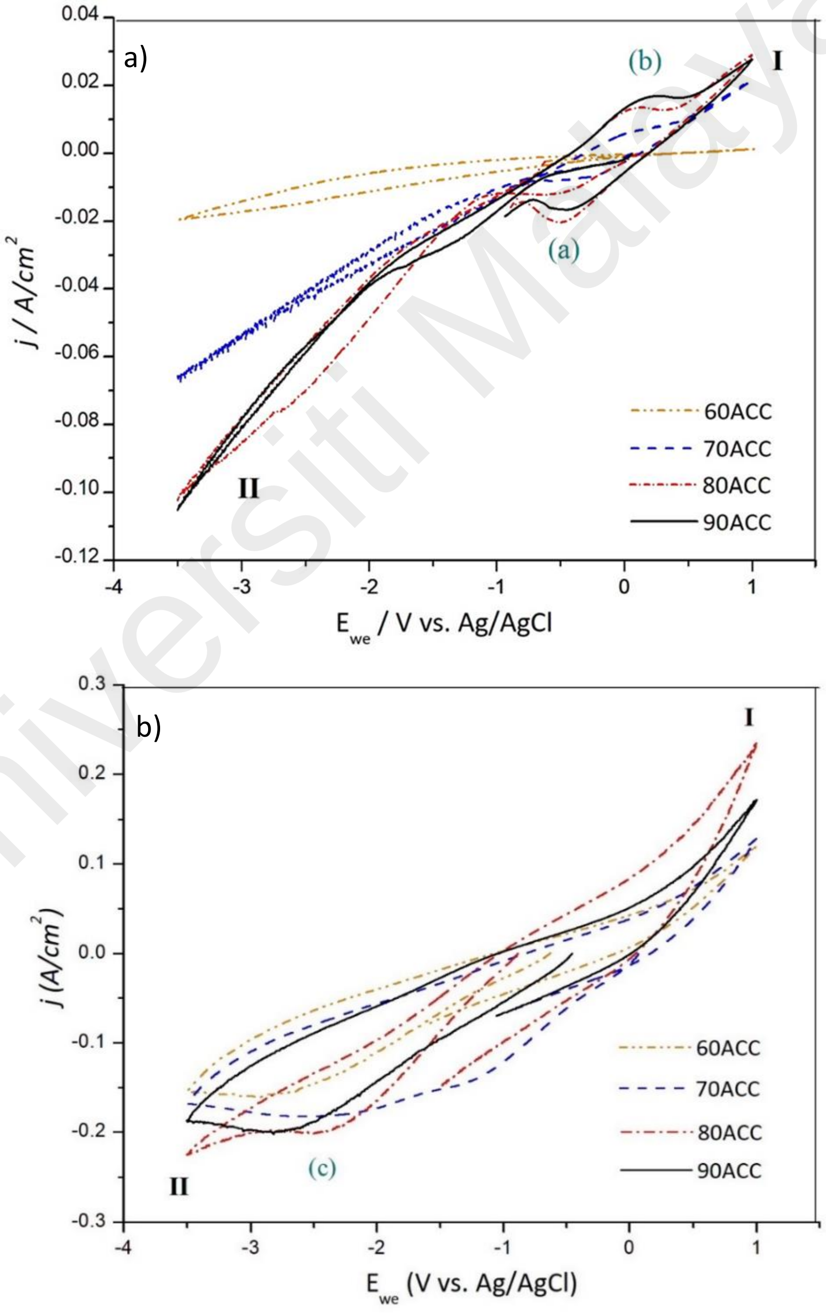

Figure 4.4: Electrochemical responses in acidic Amberlyst-15 electrolyte a) without and b) with 0.3 M of glycerol.

4.2.4 Electrochemical performance by chronoamperometry (CA)

Figure 4.5 illustrates the chronoamperometric measurements of the ACC electrodes in 0.3 M of glycerol and 0.3 M of Na_2SO_4 with 9.6% (w/v) of Amberlyst-15 for 3600 s and Table 4.1 summarizes their electrochemical characteristics. This analysis discovered the durability (Lertthahan et al., 2017; Xu et al., 2017) and electrochemical performance of ACC electrodes. Regardless of the fast decrease of current density for all ACC electrodes in the early state, the current density decay for the reaction on the 80ACC electrode was steadier than those of other electrodes. This decline was caused by glycerol accumulation on the electrodes. When an electrode adsorbed glycerol and the surface was covered by the molecule during electrolysis, the electrical resistance speedily improved due to the double-layer discharge. Consequently, it led to a fast reduction in the current density (Khosravanipour Mostafazadeh et al., 2021). With this principle, the process was proved to be diffusion-controlled and the experiments were carried out at a constant current to prevent a decline in the bulk electrolysis efficiency.

Additionally, the variation of activated carbon composition in the ACC electrodes also led to different final residual current densities. As shown in Figure 4.5, initially, the current density was rapidly decreased for all electrodes and achieved a constant current density rate around 200s for 60ACC and 1000 s for 70ACC, 80ACC, and 90ACC. After 3600 s, the highest residual (or equilibrium) current density was detected on the 80ACC (-0.1648 A/cm^2), which disclosed better electrocatalytic performance than others. The results are in great accordance with the CV results. To assess the stability of ACC electrodes, the current density at 3600 s was divided by the initial current density (j_{3600}/j_0) and the current density at 200 s after the start of measurement considering the capacitive current decay (j_{3600}/j_{200}). 80ACC exposed significant stability with the highest value of j_{3600}/j_0. It has a lower j_{3600}/j_{200} value than 60ACC because 60ACC reached the constant current density earlier than other electrodes due to its lowest EASA. Hence, with an additional result on durability and stability investigation, the overall electrochemical properties found 80ACC is a promising candidate for glycerol electroreduction in Amberlyst-15 solution.

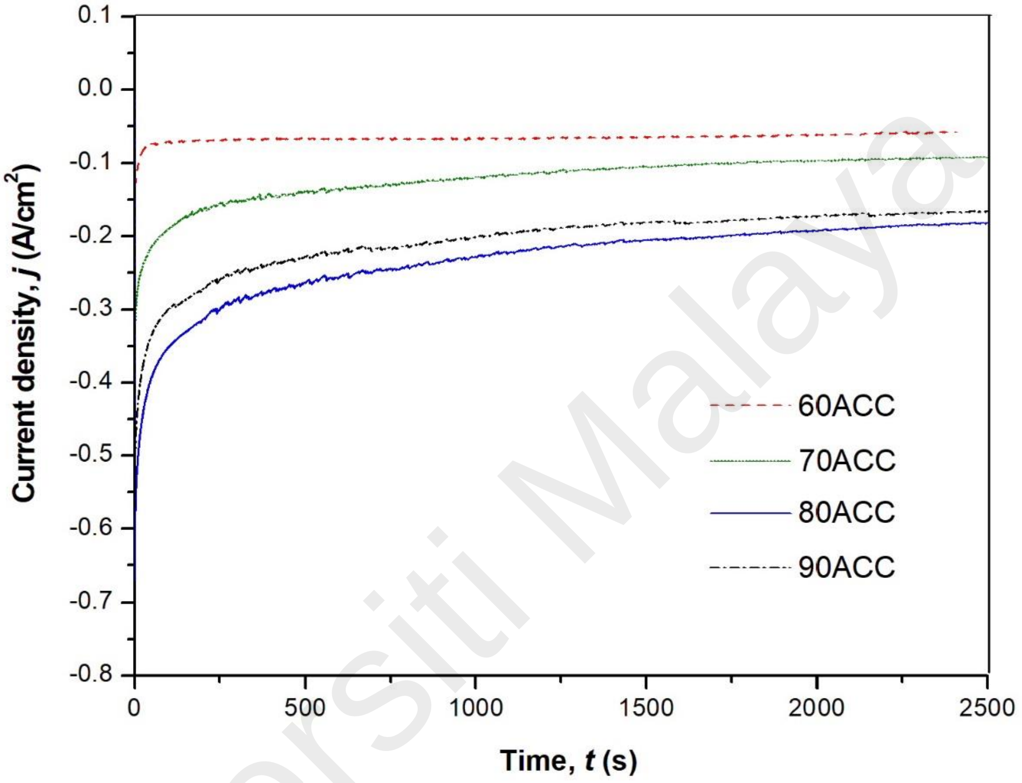

Figure 4.5: Chronoamperometric measurements of the ACC electrodes at -2.5 V versus Ag/AgCl in 0.3 M glycerol + 9.6% (w/v) Amberlyst-15 in 0.3 M Na_2SO_4 solution.

Table 4.1: Electrochemical properties from cyclic voltammetry and chronoamperometric measurements.

Electrodes	EASA (cm^2)	j_{peak} current (A/cm^2)[a]	j_{3600} (A/cm^2)	j_{3600}/j_0 (%)	j_{3600}/j_{200} (%)
60ACC	19.6	-0.1639	-0.0585	41.88	82.98
70ACC	24.5	-0.1913	-0.0855	36.99	52.17
80ACC	36.7	-0.2018	-0.1648	42.13	65.94
90ACC	30.8	-0.2005	-0.1503	38.43	55.28

[a] The peak current densities were acquired from the reverse scanning peak of CV.

4.2.5 Bulk electrolysis: Glycerol electroreduction on ACC electrodes

The effectiveness of glycerol electrochemical conversion is perceptively dependent on the interaction between the electrode surface and the glycerol molecule (Hunsom & Saila, 2013; Jr. et al., 2017; Lam et al., 2017). Therefore, the evaluation of ACC electrodes performance for glycerol electroreduction was done at the minimum conditions in the bulk electrolysis. The Pt electrode was also applied as a cathode electrode for comparison since most research reports recognized Pt for 1,2-propanediol formation (Hunsom & Saila, 2013, 2015; Kongjao et al., 2011; Saila & Hunsom, 2015). Results in Figure 4.6 display glycerol conversion increased with increasing reaction time, but the rate was differently associated with the EASA of the electrodes. After 8 hours of reaction, the maximum glycerol conversion for ACC electrodes was identified on 80ACC (83.2%), followed by 90ACC (78.2%), 70ACC (63.2%) and 60ACC (59.4%). The glycerol electrochemical conversion is a time-dependent process; hence it is crucial to understand the conversion rate in its system. The initial kinetics constants of glycerol conversion were determined by the micro-kinetics model (Roquet et al., 1994). The linear plots in the graphs of ln (C_t/C_o) *vs.* time were accurately fitted to the first-order kinetics and it can be represented in its integral expressions in equation 4.1 or 4.2. The reliability between experimental data and the model-predicted values was conveyed by the correlation coefficients (R^2, values closeness to 1). C_t is the instantaneous concentration of glycerol, C_o is the initial concentration of glycerol, t is time, and the slope delivers k is the rate constant of the reaction (4.3).

$$C_t = C_o\, e^{-kt} \qquad 4.1$$

$$\ln C_t = \ln C_o - kt \qquad 4.2$$

$$\ln(C_t/C_o) = -kt \quad 4.3$$

The slopes of straight line for 90ACC, 80ACC, 70ACC, and 60ACC respective to the rate constants (k) of 0.4200 $\times10^{-4}$ s^{-1}, 0.5722 $\times10^{-4}$ s^{-1}, 0.3081 $\times10^{-4}$ s^{-1} and 0.2189 $\times10^{-4}$ s^{-1} with a determination coefficient (R^2) higher than 0.9499. 80ACC has a conversion value nearly close to Pt electrode (83.9% with kinetic rate constant of 0.6242 $\times10^{-4}$ s^{-1}); hence, it confirmed that the indirect glycerol electroreduction happened more comprehensively on 80ACC than other ACC electrodes. As revealed earlier, the macropores structure in the electrode boosted the EASA, and electrons transfer between the activated mediator and glycerol/intermediates onto its surface. Finally, it enhanced the conversion as high as Pt electrode (Shen et al., 2015). From the GC-MS chromatogram (Figure 4.7), three compounds were observed with tetraethylene glycol (the internal standard) after 8 hours of electrolysis for all electrodes. The findings resulted in 1,2-propanediol as the main product while diethylene glycol and acetol are the by-products. The MS spectra for these products are shown in APPENDIX B.

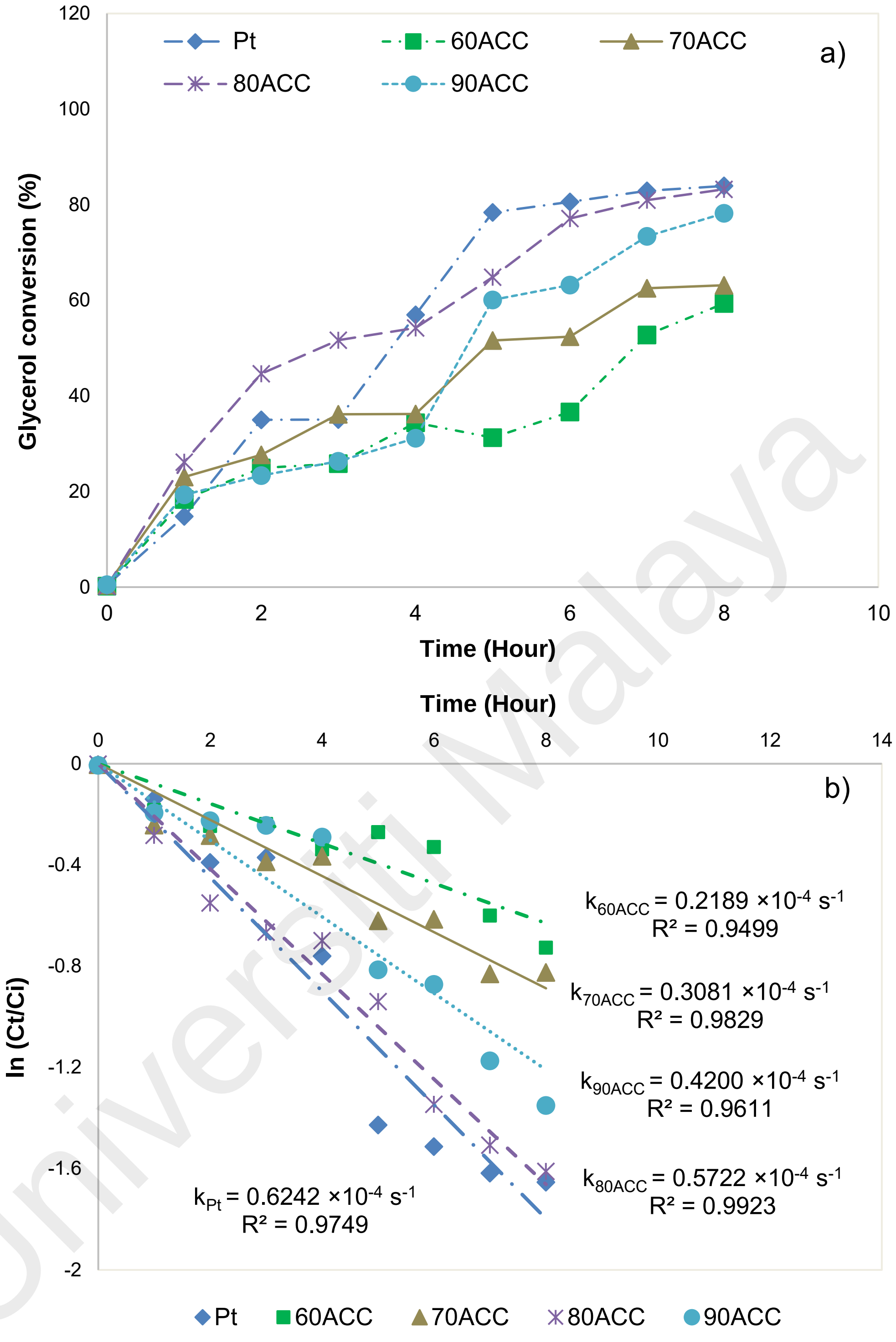

Figure 4.6: a) Glycerol conversion and b) first-order kinetics model for glycerol electroreduction on Pt, 60ACC, 70ACC, 80ACC, and 90ACC electrodes in Amberlyst-15 solution after 8 hours of electrolysis.

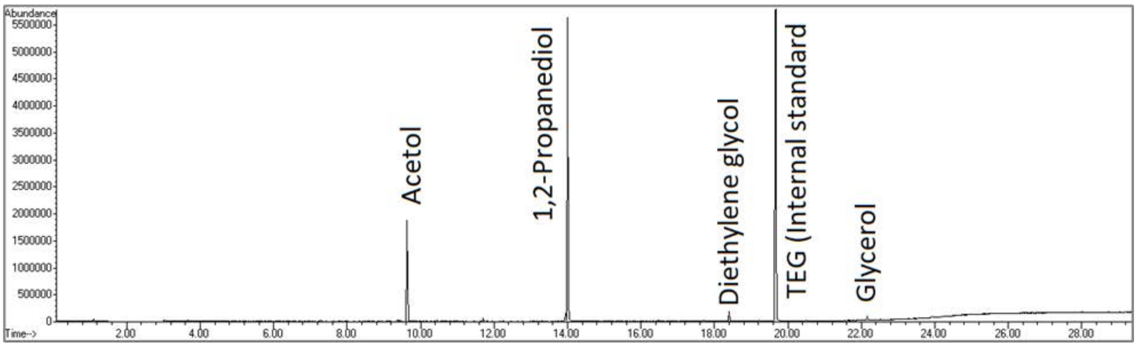

Figure 4.7: GC-MS chromatogram after 8 hours of reaction on the 80ACC electrode.

4.2.5.1 Products distribution and the proposed reaction mechanisms

The products distribution and selectivity for the glycerol electroreduction on ACC and Pt electrodes are shown in Figure 4.8 and Figure 4.9. The yield and selectivity of the main compound, *e. g*., 1,2-propanediol on the 80ACC were comparable to those acquired on Pt and greater than 60ACC, 70ACC, and 90ACC. A similar trend in the distribution of products for all electrodes is presented in Figure 4.8 and the reaction mechanisms pathway is suggested in Scheme 4.1 based on these findings. From Figure 4.8, the yield of acetol achieved the highest value at the 3rd to 6th hour and was reduced afterward, revealing that acetol was obtained from glycerol. Whereas, 1,2-propanediol yield remained increasing, justifying its successive formation from glycerol through acetol as the intermediate.

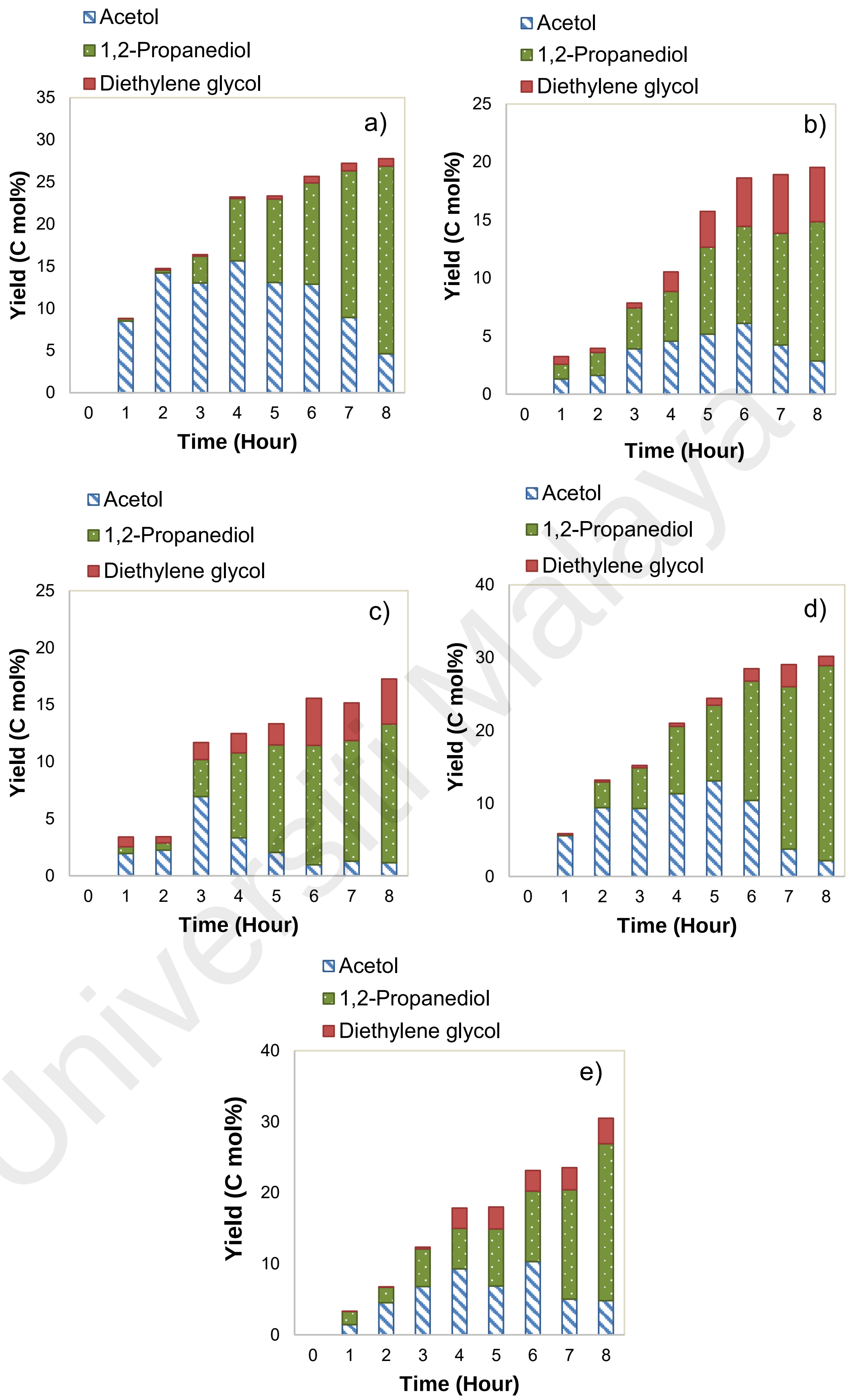

Figure 4.8: Products distribution from 8 hours of glycerol electroreduction on a) Pt, b) 60ACC, c) 70ACC, d) 80ACC and e) 90ACC cathode electrodes.

As the earlier works revealed glycerol with three hydroxyl (OH) groups prefers to break the C-OH group into a keto group rather than a direct reduction into alcohol (Ardila et al., 2017; Lee et al., 2018; Miyazawa et al., 2007b). The dispersion of Amberlyst-15 in water will generate the hydronium ions (H_3O^+) (Pal et al., 2012). As shown in Scheme 4.1, Amberlyst-15 released H^+ ions from its sulfonic group and dehydrated glycerol to acetol. This has also been reported by Kongjao et al. (2011). 1° OH group attached to the carbon atom of glycerol molecule was protonated by H^+ ions and removed. The hydrogen atom of its neighboring C atom was also removed and hence, produced 2,3-dihyroxypropene. It was further rearranged into acetol through the tautomerization route, and the maximum yield value was discovered at 4th hour on Pt (15.6 C mol%), 5th hour on 80ACC (13.1 C mol%), 3rd hour on 70ACC (7.0 C mol%) and 6th hour (6.1 C mol%) on 60ACC and 90ACC (10.3 C mol%). The higher yield of acetol on 80ACC and 90ACC electrodes than 60ACC and 70ACC proved that indirect electroreduction also happened with the aid of Amberlyst-15. It was supported by the CV outcome in Figure 4.4 where 80ACC has the highest current density value for peak (a). This route is ideal when a higher activated carbon composition in ACC electrodes was used. The high electroactive surface area and pore sizes of 80ACC and 90ACC electrodes helped to enhance the electrons diffusion between these electrodes and glycerol.

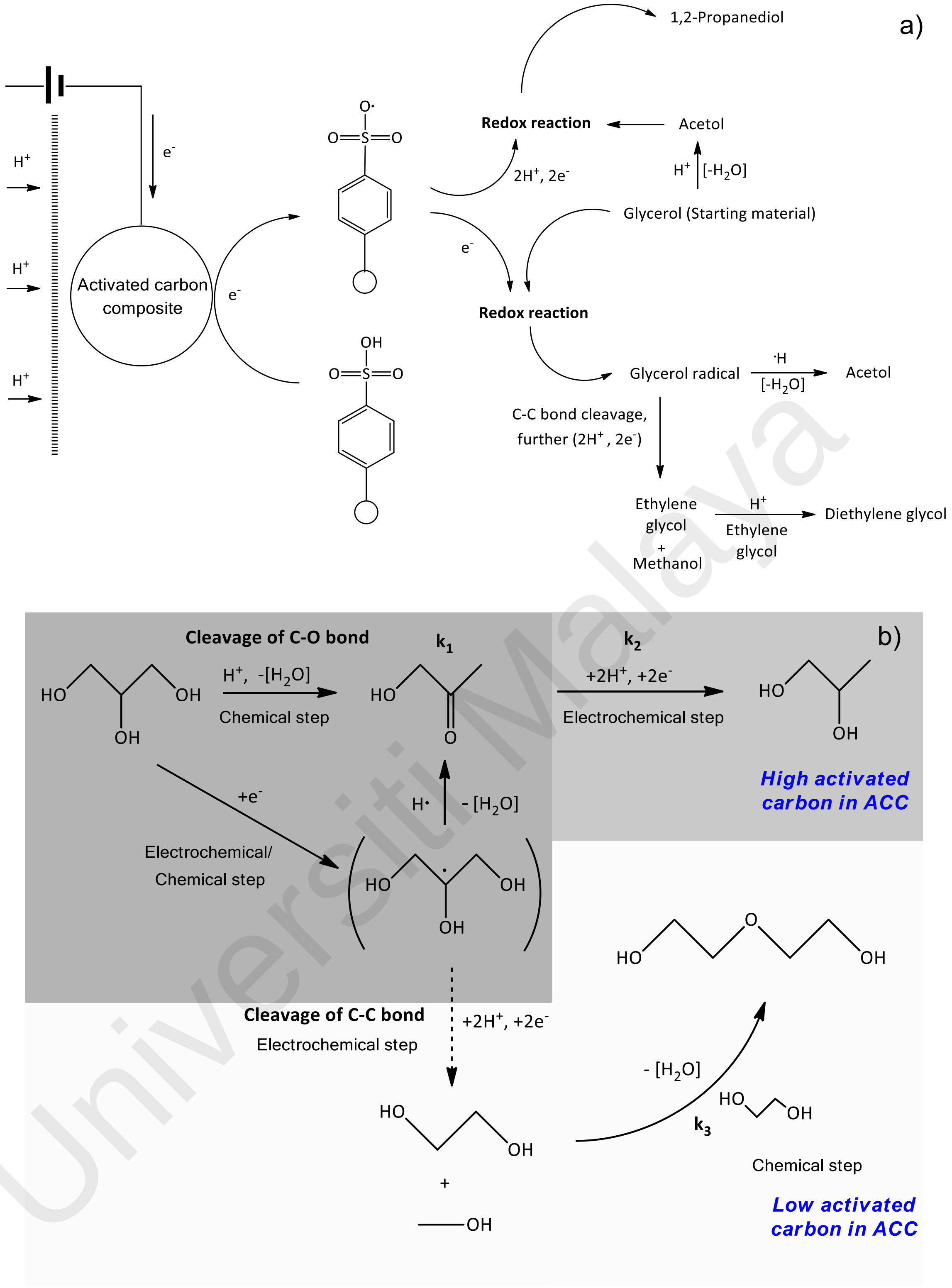

Scheme 4.1: Schematic diagrams of a) general two-steps catalytic/electroreduction mediated by Amberlyst-15 and b) the proposed reactions mechanism for glycerol electroreduction.

When the electrical current was applied, reduction of glycerol occurred with a nucleophilic attack (e^-) through the Amberlyst-15 radicals (A-15$\bullet^-$) (Scheme 4.1a). A single electron transferred to glycerol generated glycerol radical anions ($CH_3OHC\bullet^- HOHCH_3OH$) (Steckhan, 1986). In the conventional water electrolysis system, water breaks into hydrogen at the cathode and oxygen at the anode. Since hydrogen evolution reaction (HER) happened at the cathode, H• radical formed on the electrodes could abstract the H• atom from OH group at the C_1 or C_2 position in glycerol radical molecule. The extraction led to enol intermediates and further generated into acetol. This H• radical may produce through two types of mechanisms either (i) Volmer-Heyrovsky (equations 4.4 and 4.5) or (ii) Volmer-Tafel (equations 4.4 and 4.6) during HER in an acidic medium (Murthy et al., 2018; Nemiwal et al., 2021). The acetol formation mechanism which can be proposed as glycerol was reduced in the presence of electricity and Amberlyst-15 mediator as well as concurrently dehydrated in acidic electrolyte without electricity (Scheme 4.1).

$$H^+ + e^- \rightarrow ACC\text{-}H_{ads} \qquad 4.4$$

$$ACC\text{-}H_{ads} + H^+ + e^- \rightarrow H_2 + ACC \qquad 4.5$$

$$ACC\text{-}H_{ads} + ACC\text{-}H_{ads} \rightarrow H_2 + 2ACC \qquad 4.6$$

As reported in recent investigations, acetol is a reactive compound and is readily reduced to 1,2-propanediol (Chiu et al., 2006b; Hunsom & Saila, 2013). In hydrogenolysis and hydrodeoxygenation of glycerol, 1,2-propanediol was produced with the addition of hydrogen in those reactions (Ardila et al., 2017; Cai et al., 2019; Gabrysch et al., 2019; Yfanti & Lemonidou, 2018). Miyazawa et al. (2007a) used Amberlyst-15 as an additive/co-catalyst in improving 1,2-propanediol selectivity *via* hydrogenolysis of glycerol. The authors found that at 120 °C, 1,2-propanediol selectivity was 74.7%. The mechanism route meant dehydration of glycerol to acetol, which was catalyzed by Amberlyst-15 and followed by acetol hydrogenation to 1,2-propanediol which occurred on Ru/C catalyst (Miyazawa et al., 2007a; Miyazawa et al., 2006). Therefore, 1,2-propanediol was formed under a similar pathway with H^+ ions and electrons obtained through the activated Amberlyst-15 mediator. The highest 1,2-propanediol yield achieved was 26.7 C mol% on 80ACC followed by 22.3 C mol% (Pt), 22.1 C mol% (90ACC), 12.2 C mol% (70ACC), and 12.0 C mol% (60ACC).

Another minor product is diethylene glycol. Its yield was slightly increased for 80ACC, 90ACC, and Pt electrodes while a significant growth of yield was observed on 60ACC and 70ACC at 4th and 3rd hours. This pattern established that glycerol cannot be directly converted into diethylene glycol, where a fast reaction may take place before its formation. Saila and Hunsom (2015) proposed oxidative C-C bond cleavage of glycerol occurred and formed C_2 ethylene free radical with C_1 alcohol-free radical. C_2 ethylene-free radical is further dehydrated to acetaldehyde or reduced to ethylene glycol whereas aldehyde is formed from C_1 alcohol-free radical dehydration. Nonetheless, these reactions occurred in an undivided reactor where both oxidation and reduction reactions simultaneously proceeded. In this work, the electrochemically activated Amberlyst-15 mediator can cleave the C-C bond of glycerol radical into ethylene glycol radical and alcohol-free radical (Steckhan, 1986). Subsequent reduction process with the addition of protons and electrons from the anode part directed to ethylene glycol and alcohol generation. Thus, ethylene glycol could be an intermediate for diethylene glycol formation. It was assumed that diethylene glycol was generated from intermolecular dehydration of ethylene glycol under the indirect electrolysis conditions (Steckhan, 1986). The reaction mechanism route is identical to dipropylene glycol synthesis, where two propylene glycol molecules reacted to one another in an acidic medium (Chitwood & Freure, 1946; Chiu et al., 2008; Yu et al., 2009).

By comparing the results of 1,2-propanediol and diethylene glycol, they give an insight that the first step of glycerol dissociation occurred either through C-C bond or C-O bond breakage. These two breakages correspond to ethylene glycol and acetol production as a key to ascertain a selective pathway for 1,2-propanediol formation. From Figure 4.9, diethylene selectivity was higher on 60ACC (7.9%) and 70ACC (6.3%) compared to 80ACC (1.5%) and Pt (1.0%), showing lower activated carbon content in ACC electrodes favoured ethylene glycol formation and led to a higher amount of diethylene glycol. However, diethylene selectivity on 90ACC (4.6%) was higher than 80ACC because it produced higher acetol intermediate with lower 1,2-propanediol selectivity. In other words, the higher activated carbon content in ACC electrodes generated more acetol but the production of 1,2-propanediol was sluggish, which is reinforced by the EASA results. As the reaction time increased, acetol selectivity reduced because it has developed into another compound, namely, 1,2-propanediol. Following 8 hours of reaction, the selectivity of 1,2-propanediol for 60ACC, 70ACC, 80ACC, 90ACC and Pt were 20.2%, 19.2%, 32.1%, 28.3% and 26.5%, suggesting 80ACC is the most suitable for 1,2-propanediol formation. From the simplified mechanism route in Scheme 4.1b, k is the overall kinetics rate constant for glycerol electroreduction. To accomplish high 1,2-propanediol yield and selectivity, the mechanism pathway needs to be elucidated and properly understood. The validation of the proposed mechanism pathway is required for process optimization. Therefore, the mechanistic study and influences of kinetics parameters (temperature, glycerol initial concentration, and current density) for glycerol electroreduction are further studied.

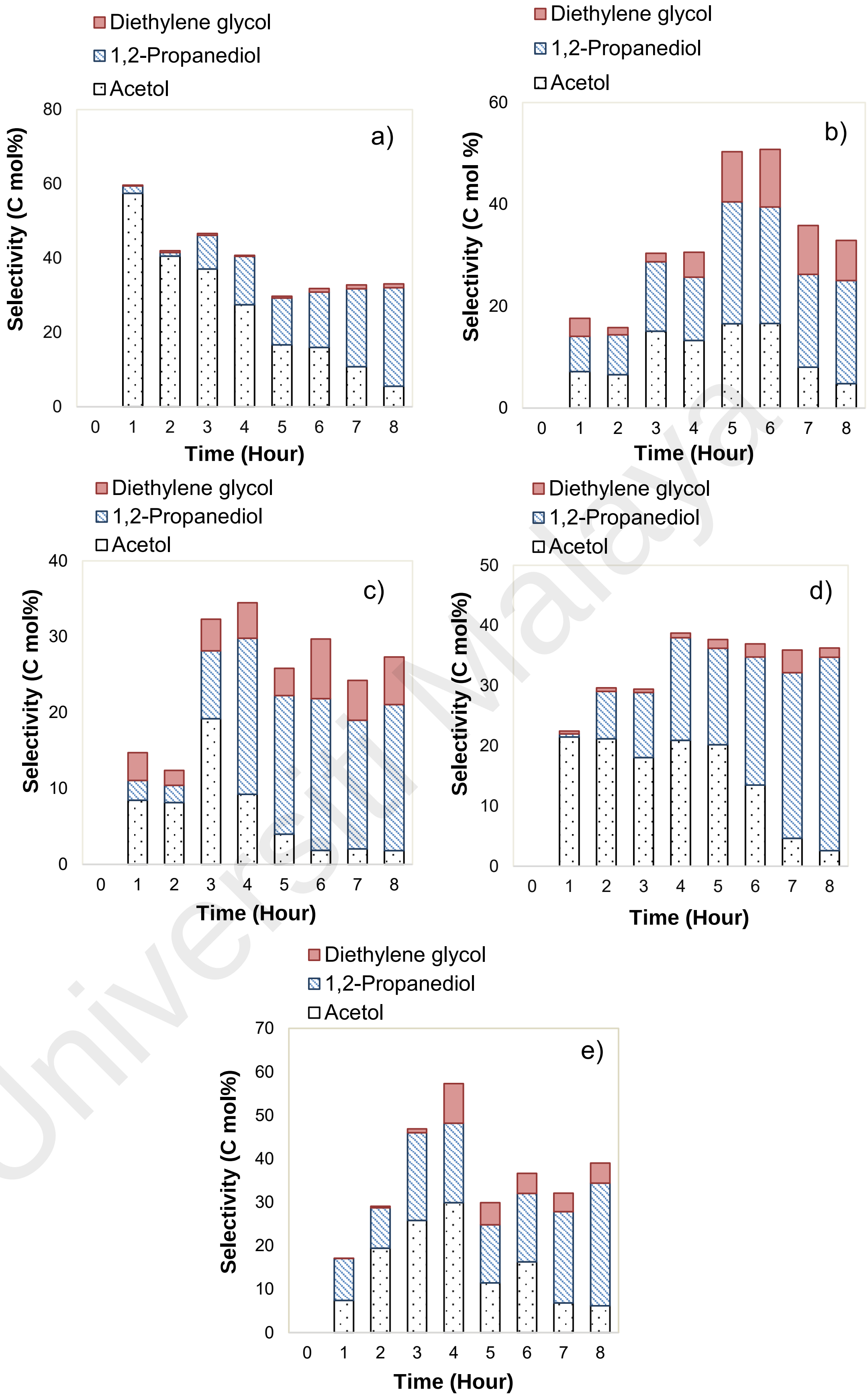

Figure 4.9: Products selectivity (%) on a) Pt, b) 60ACC, c) 70ACC, d) 80ACC and e) 90ACC cathode electrodes.

4.3 Reaction mechanisms investigation on the selected ACC electrode

4.3.1 Acetol as a reactant in the presence of electricity

In this section, the acetol electrolysis and ethylene glycol dehydration (intermediates) experiments were performed to elucidate the proposed reaction mechanisms pathway. Figure 4.10 presents the compounds that appeared when acetol was used as a glycerol substitute. The presence of 1,2-propanediol proved that acetol electro-hydrogenation reaction happened in the cathode compartment. Other minor products like acetone, 1-ethoxy-2-propanol, 3-hydroxy-2-butanone, and dipropylene glycol were also discovered. The chemical structures of these compounds were characterized using GC-MS analysis and their MS spectra are presented in APPENDIX B. Acetone was perceived only in a small amount at less than 80.0 °C of temperature because of its fast volatility at a high temperature (Sauter et al., 2017).

The proposed reaction mechanisms for these by-products are depicted in Scheme 4.2. 1,2-propanediol was attained through the hydrogenation route, validating acetol as the intermediate for 1,2-propanediol. Intermolecular and intramolecular dehydration of 1,2-propanediol occurred in an acidic medium and developed dipropylene glycol and propylene oxide, correspondingly. Propylene oxide isomerization led to other minor products formation, namely acetone and 1-ethoxy-2-propanol (Yu et al., 2009). In the presence of the basic compound, *e.g.,* ethanol, the propylene oxide ring favourably opened at the C-O bond with a less sterically hindered position and dominated secondary alcohol (1-ethoxy-2-propanol) formation (Zhang et al., 2005; Zhang et al., 2014). Zhang et al. (2016) successfully produced 1-ethoxy-2-propanol by alcoholysis of propylene oxide and ethanol in the presence of catalyst whilst Chitwood and Freure (1946) acquired it even without any catalyst. In great support from the later work, 1-ethoxy-2-propanol was indirectly generated through this reaction during the sample preparation and GC-MS characterization that incriminated ethanol as the solvent (Chitwood & Freure, 1946; Ślipko & Chlebicki, 1981). During the sample preparation, sodium hydroxide (NaOH) was used to precipitate out the sodium sulfate electrolyte from the taken sample. With this fact, under alkaline conditions, carbonyl compound like acetol with α-CH (H-Cα-C=O) bond is reactive compound; hence, it reacted with this base to form an enolate ion. Swiftly, it produced 3-hydroxy-2-butanone as a side product (Heathcock, 2014). Its formation was not only as a minor product, but also from the sample neutralization *via* the intermolecular aldol-condensation mechanism.

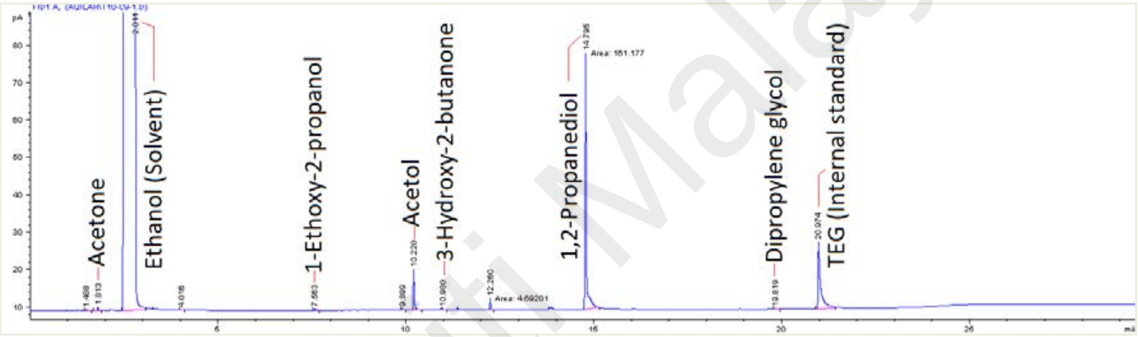

Figure 4.10: GC-MS chromatogram of acetol electrolysis.

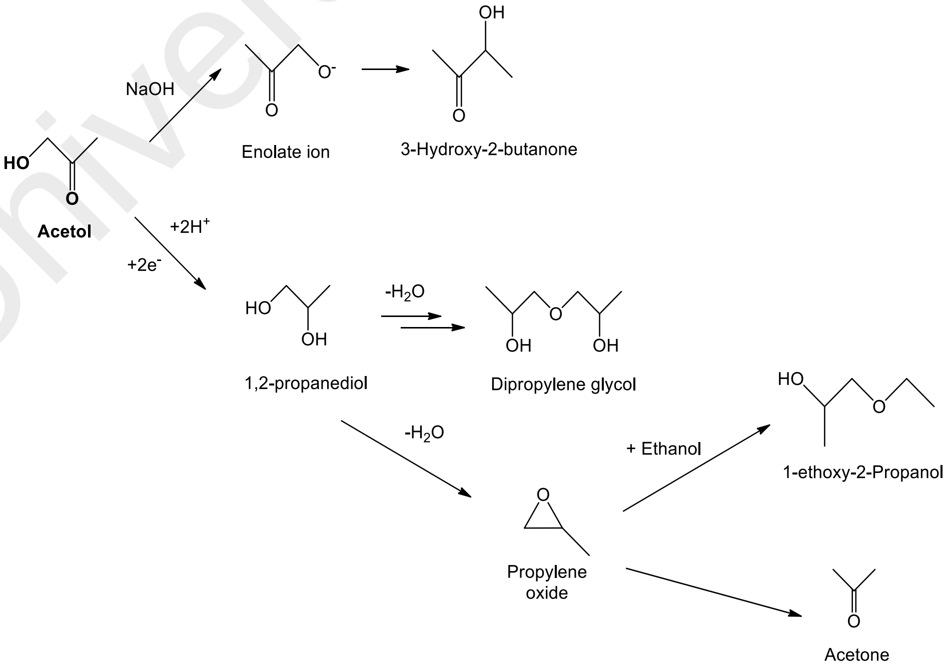

Scheme 4.2: Formation of 1,2-propanediol and by-products from acetol reaction.

Table 4.2: 1,2-propanediol and minor products selectivity and yield under different operating conditions using Pt anode and 80ACC cathode electrodes for 8 hours of electrolysis.

[Acetol] (M)	*j* (A/cm^2)	E (V)	T (°C)	Acetol conversion		1,2-Propanediol		Dipropylene glycol		1-ethoxy-2-propanol		Acetone		3-hydroxy-2-butanone	
				(%)	k (s^{-1})	Y	S	Y	S	Y	S	Y	S	Y	S
										(%, C mol)					
Effect of reaction temperature															
0.30	0.14	18.2	27.0	96.2	0.3547×10^{-4}	9.2	9.6	-	-	0.6	0.6	-	-	0.04	0.4
0.30	0.14	15.9	53.5	98.4	0.5403×10^{-4}	15.8	16.0	5.0	5.1	2.8	2.9	1.4	1.4	0.08	0.08
0.30	0.14	13.1	80.0	98.5	0.7192×10^{-4}	28.9	29.4	10.9	11.1	9.1	9.2	-	-	3.8	3.8
0.30	0.14	11.7	106.5	99.0	0.7664×10^{-4}	19.6	19.9	12.8	13.0	7.6	7.7	-	-	3.6	3.7
Effect of acetol initial concentration															
0.30	0.14	15.8	80.0	98.5	0.7192×10^{-4}	28.9	29.4	11.0	11.1	9.0	9.2	-	-	3.8	3.8
1.65	0.14	19.8	80.0	83.1	0.6075×10^{-4}	37.8	45.5	11.0	13.2	5.0	6.0	-	-	3.5	4.2
3.00	0.14	20.3	80.0	71.5	0.1600×10^{-4}	42.5	59.4	4.1	5.7	4.0	5.6	-	-	2.8	3.9
4.35	0.14	21.1	80.0	42.6	0.1492×10^{-4}	20.2	45.9	4.8	11.0	4.0	9.0	-	-	2.3	5.2
Effect of current density															
3.00	0.14	21.0	80.0	71.5	0.1600×10^{-4}	42.5	59.4	4.1	5.7	4.0	5.6	-	-	2.8	3.9
3.00	0.21	22.4	80.0	73.2	0.3844×10^{-4}	44.7	61.1	7.4	13.3	3.7	5.0	-	-	3.7	5.0
3.00	0.28	25.7	80.0	83.7	0.4892×10^{-4}	47.3	56.5	14.0	16.7	4.9	5.4	-	-	2.4	2.8
3.00	0.35	30.4	80.0	87.5	0.5804×10^{-4}	37.7	43.1	15.0	18.0	13.1	15.7	-	-	2.5	3.1

Table 4.2 shows the effects on 1,2-propanediol yield and selectivity when the kinetics parameters, *e. g.*, reaction temperature, initial concentration, and current density were altered. 1,2-propanediol appeared as the main product, although the changes in the kinetics parameters caused the high production of by-products. All the conditions were fitted to the first-order kinetics model in the linear form with the determination coefficients (R^2) that larger than 0.9426. This is corroborated with Hunsom and Saila (2013) and Roquet et al. (1994) studies.

4.3.1.1 Effect of reaction temperature

Figure 4.11 reveals the acetol conversion and kinetics model when the reaction temperature was modified in the range of 27.0 °C to 106.5 °C at a constant acetol initial concentration (0.3 M). The model was well-fitted during the first 3 to 5 hours of acetol electrolysis. The acetol conversion for all temperatures was over 90% after 8 hours of electrolysis. The kinetics rate constants of 106.5 °C (0.7664×10^{-4} s^{-1}), 80.0 °C (0.7192×10^{-4} s^{-1}), and 53.5 °C (0.5403×10^{-4} s^{-1}) temperatures were higher than the room temperature, 27.0 °C (0.3547×10^{-4} s^{-1}), showing the high external energy accelerated the conversion of acetol.

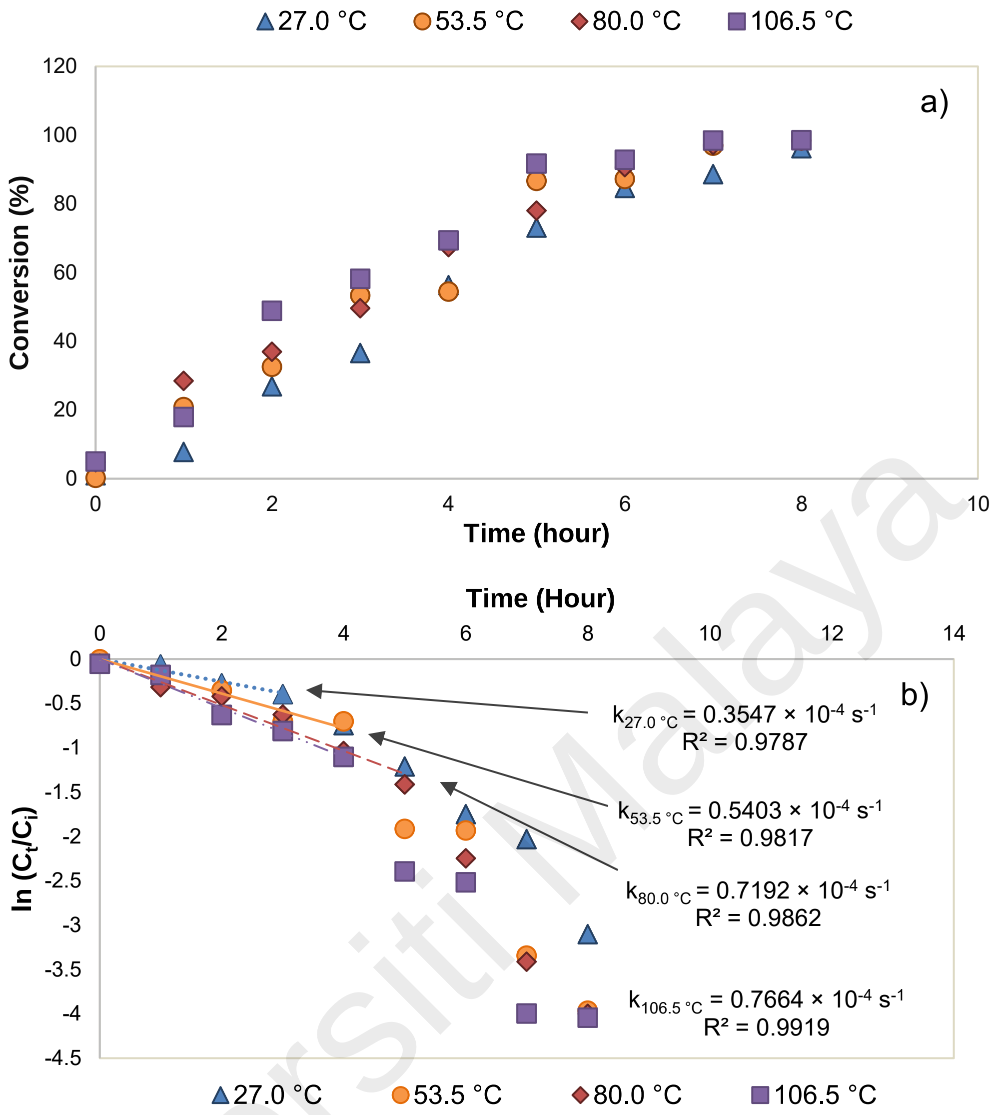

Figure 4.11: a) Conversion and b) first-order kinetics model of acetol electrolysis at different reaction temperatures.

From Table 4.2, 1,2-propanediol has a higher yield and selectivity than other minor compounds such as dipropylene glycol, acetone, 1-ethoxy-2-propanol, and 3-hydroxy-2-butanone for all temperatures. Even so, the yield of total products from the converted glycerol could not accomplish 100 C mol%. It reveals that hydrogen evolution reaction (HER) is the prominent reaction at low acetol concentration regardless of the temperature used in the system. The formed hydrogen may carry the compounds with high volatility like acetone and acetol out from the reactor. Literature surmised that low pH also slightly contributed to a dictating impact of HER (Sauter et al., 2017). H^+ ions from the anode part compete with acetol for the redox reaction and are reduced into hydrogen instead of only 1,2-propanediol. 1,2-propanediol yield increased with the temperature improvement and achieved the highest value (28.9 C mol%) at 80.0 °C. However, the by-products yield was rapidly boosted and sparked the decline in 1,2-propanediol selectivity and yield at the higher temperature (106.5 °C), displaying its significant role in controlling the formation of by-products.

4.3.1.2 Effect of acetol initial concentration

1,2-propanediol formation was preferred at 80.0 °C; hence, this temperature was used for the effect of acetol initial concentration study. The electrolysis was carried out with 0.30 M, 1.65 M, 3.00 M, and 4.35 M concentrations. The acetol conversions and their kinetics rate constants with these concentrations are summarized in Table 4.2 and Figure 4.12. After 8 hours of electrolysis, about 42.6% (4.35 M) to 98.5% (0.3 M) of acetol was converted into 1,2-propanediol and other valuable compounds. The rate was reduced from 0.7192×10^{-4} s^{-1} (0.3 M) to 0.1492×10^{-4} s^{-1} (4.35 M) due to its high viscosity in too high acetol concentration. It was influenced by the reduction of protons and conductivity in the electrolyte solution. In addition, a higher applied potential (21.1 V) at 4.35 M was needed to maintain the current density and number of electrons for acetol electro-hydrogenation to 1,2-propanediol, resulting in low-performance efficiency.

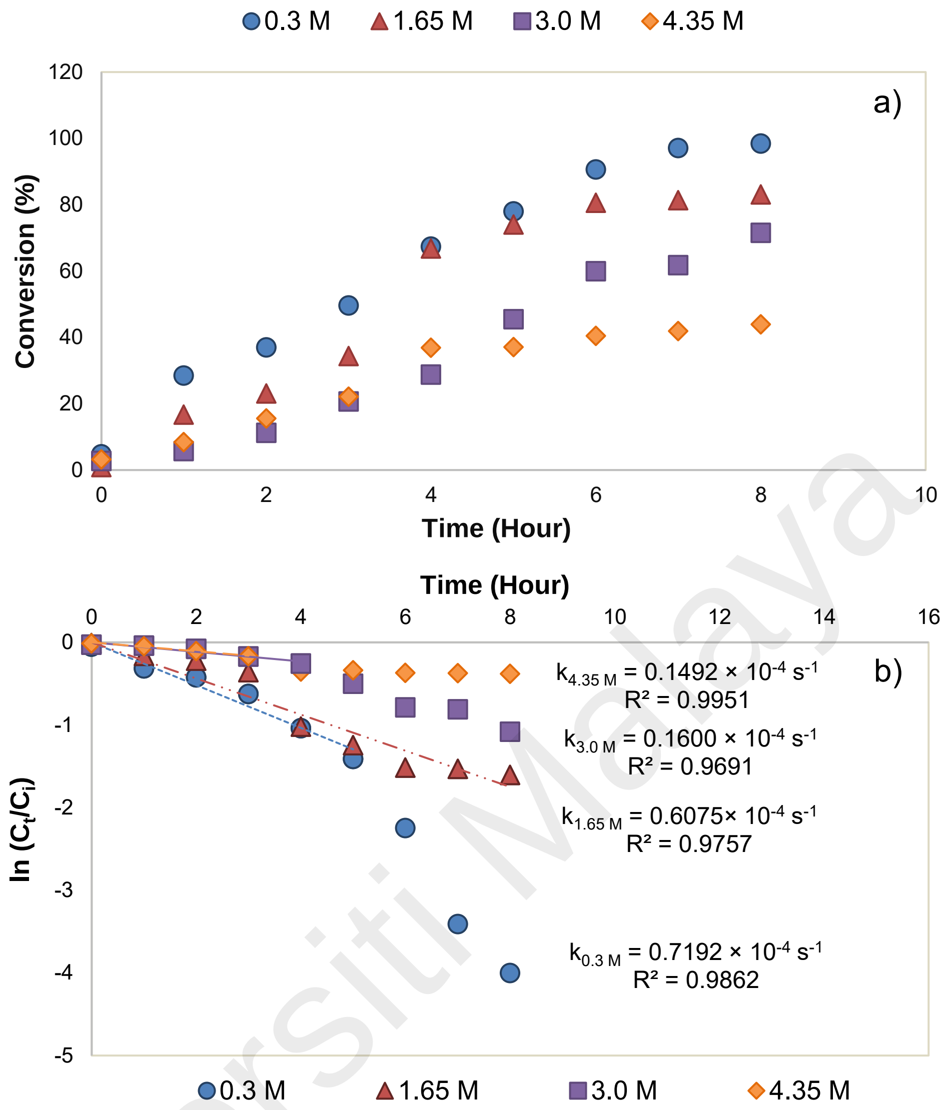

Figure 4.12: a) Conversion and first-order kinetics model of acetol electrolysis with different initial concentrations.

According to dos Santos et al. (2015), high initial concentration commonly allows to proscribe the competing HER and liquid products generation in the electrolysis; consequently, it can encourage 1,2-propanediol production. From Table 4.2, the 1,2-propanediol yield reached 42.5 C mol% (59.4% selectivity) when the concentration of acetol was changed from 0.3 M to 3.0 M. The escalating pattern illustrated the importance of acetol as an intermediate in generating 1,2-propanediol. The availability of acetol molecules to react with protons and electrons improved 1,2-propanediol yield at a higher concentration. Higher than 3.0 M, it was accompanied by side effects, in which 1,2-propanediol and minor products yields were dropped. It is because the high viscosity of the acetol solution led to the poisoning of the 80ACC cathode electrode surface (Nascimento & Linares Leon, 2014). A decline of protons in the aqueous electrolyte has also prevented the main acetol reaction, *e. g.*: electro-hydrogenation to 1,2-propanediol.

4.3.1.3 Effect of current density

In an electrochemical process, the reaction rate is an important factor that is directly determined by the current density parameter. Four different electric currents, namely 1.0 A, 1.5 A, 2.0 A, and 2.5 A correspond to 0.14 A/cm^2, 0.21 A/cm^2, 0.28 A/cm^2, and 0.35 A/cm^2 were applied. 0.14 A/cm^2 was chosen as the minimum value because 1,2-propanediol was only detected at this current density and above from the previous study (Hunsom & Saila, 2013, 2015). Table 4.2 and Figure 4.13 demonstrate the acetol conversions and the kinetics rate constants for all current densities. In arrangement with Faraday’s law, the conversion was improved from 71.5% (0.14 A/cm^2) to 87.5% (0.35 A/cm^2). Their kinetics rates were 0.1600×10^{-4} s^{-1} (0.14 A/cm^2) and 0.5806×10^{-4} s^{-1} (0.35 A/cm^2).

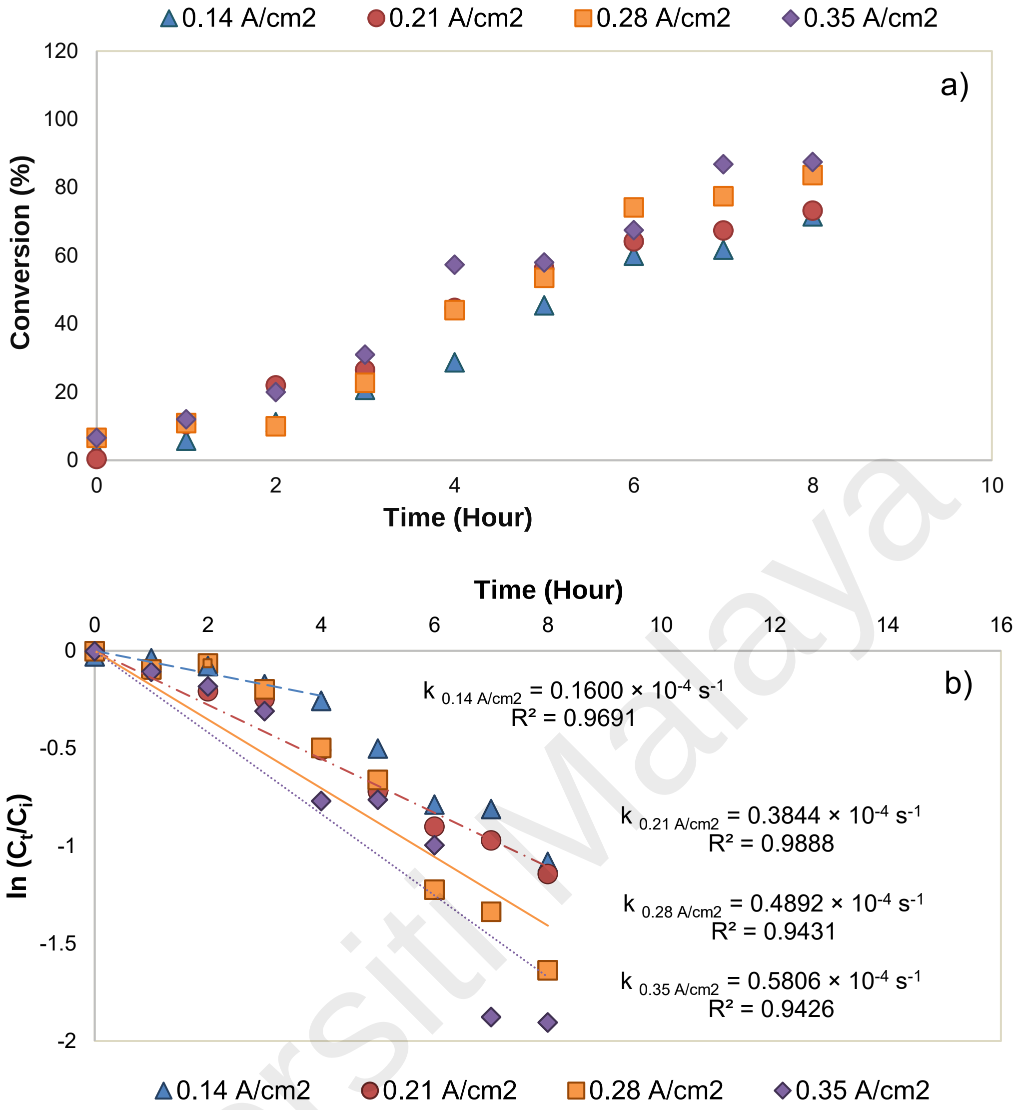

Figure 4.13: a) Conversion and b) first-order kinetics model of acetol electrolysis at different current densities.

Although acetol was not completely converted into the value-added products, the total yield of products for all current densities were above 50.0 C mol% (Table 4.2). 1,2-propanediol was gradually boosted when the current density was increased and achieved the highest yield of 47.3 C mol% (8th hour) at 0.28 A/cm^2 but decreased at 0.35 A/cm^2. Higher electricity input speeded up the hydrogen ions and electrons transportation rates, resulting in a notable 1,2-propanediol selectivity and yield. In contrast, additional growth in current density to 0.35 A/cm^2 diminished 1,2-propanediol yield and selectivity. In fact, high external energy from this electricity allowed the decomposition of 1,2-propanediol into other minor products. 0.35 A/cm^2 developed the highest yield value of 1-ethoxy-2-

propanol (13.1 C mol%) and dipropylene glycol (15.0 C mol%). Furthermore, these by-products were also formed in large amounts at longer reaction time as presented in Figure 4.14. The maximum yield (59.8 C mol%) and selectivity (77.3%) for 1,2-propanediol reached at the 7th hour (at 0.28 A/cm^2) and decreased at the 8th hour because 1,2-propanediol was converted into 1-ethoxy-2-propanol (4.9 C mol% yield) and dipropylene glycol (14.0 C mol% yield).

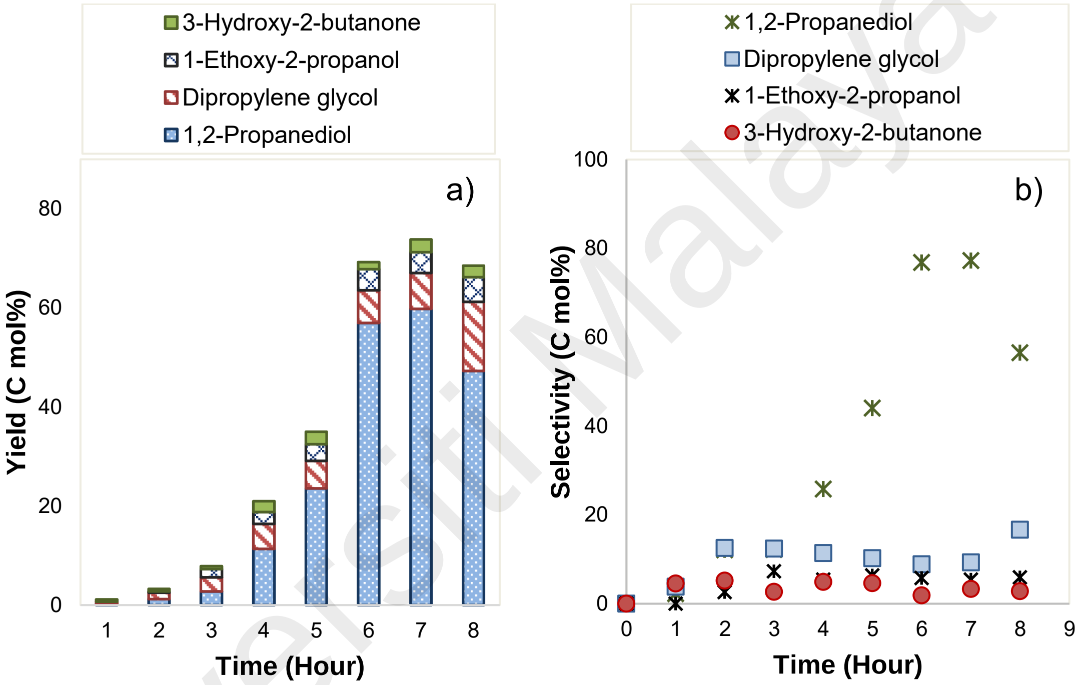

Figure 4.14: a) Products distribution (C mol%) and b) selectivity (C mol%) of acetol electrolysis at the optimum conditions.

To sum up the above discussions, acetol is an essential compound to generate 1,2-propanediol through electro-hydrogenation on the 80ACC cathode electrode. On a similar note, there is no ethylene glycol or diethylene glycol present, confirming that diethylene glycol was not from acetol intermediate. This point is affirmed during ethylene glycol dehydration in the one-compartment reactor in the next section.

4.3.2 Ethylene glycol and glycerol as the reactants without electricity

The reactions of ethylene glycol and glycerol under the optimum temperature (80.0 °C) and initial concentration (3.0 M) were conducted in the absence of electricity. Their conversion and kinetics rate constants are plotted in Figure 4.15. The conversion for glycerol (11.37%) with a kinetics rate constant of 0.0436×10^{-4} s^{-1} was lower than ethylene glycol (20.31%, 0.0867×10^{-4} s^{-1}) at 80 °C. Chimentão et al. (2021) demonstrated a small glycerol conversion (30%) in dehydration system at low temperature (190 °C) while other reports (Cecilia et al., 2015; Célerier et al., 2018; Dalla Costa et al., 2016; Ma et al., 2016) achieved high conversion (above 85%) at high temperature (above 300 °C). Thus, it is conceivable to conclude that dehydration of glycerol is not only required a good catalyst but also needs high external energy from the reaction temperature to initiate and speed up the reaction. The poorer glycerol conversion than ethylene glycol attributed to more hydrogen bond in its molecule has higher activation energy barrier for the conversion to the value-added compounds.

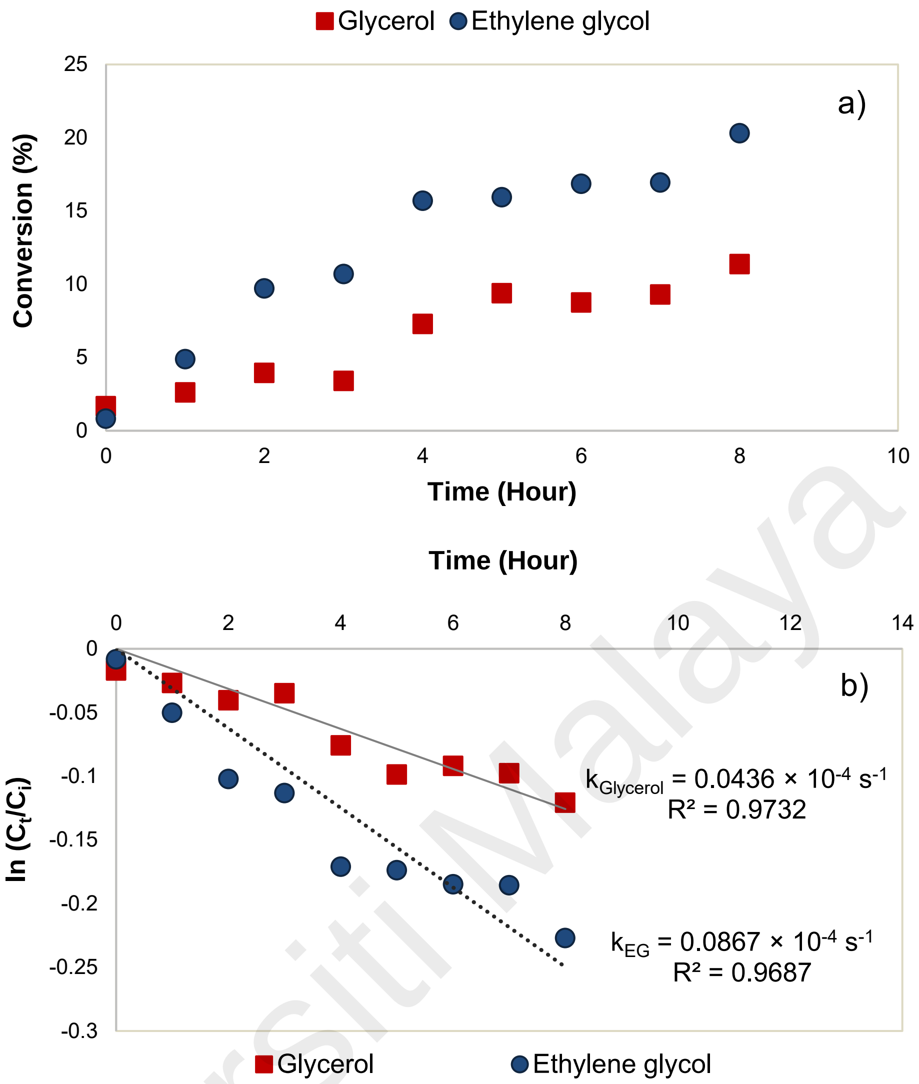

Figure 4.15: a) Glycerol and ethylene glycol conversion and b) their kinetics rate constants in the absence of electrical current.

Figure 4.16a illustrates diethylene glycol yield was enhanced with the increase of reaction time and the maximum value was 6.0 C mol%. It proves dehydration reaction occurred with the aid of Amberlyst-15 (rich in Brønsted acid sites) under high temperature similar to Lei et al. (2021) work. Lei et al. (2021) observed diethylene glycol as a minor product on Co/γ-Al_2O_3 catalyst that consisted of high Brønsted acid sites. In Figure 4.16b, acetol appeared as the only compound until the 4th hour with the maximum yield of 2.6 C mol%. This outcome surpassed Kongjao et al. (2011) report in which they obtained acetol, acrolein, and 2-propene as the final products in sulfuric acid electrolyte. With Amberlyst-15 as an acidic medium, the glycerol dehydration became more selective to acetol, and the reaction mechanism is more promising. This is because acetol is prevalent in this pathway and is an important intermediate in achieving high 1,2-propanediol selectivity. Other researchers also showed Amberlyst co-catalyst enabled the generation of 1,2-propanediol through acetol intermediate which corroborates our results (Miyazawa et al., 2007a, 2007b; Miyazawa et al., 2006). In this study, the acetol yield was relatively low and slightly dwindled at the 5th hour and 1,2-propanediol started to produce even without the presence of hydrogen since the only source of reduction agent to form 1,2-propanediol was from another acetol or glycerol molecule. Chiu et al. (2006a) assumed the scavenging of hydrogen from glycerol happened and it was used as a source to produce 1,2-propanediol. It agrees with our present study, though 1,2-propanediol yield (around 1.0 C mol%) was insignificant. Besides, with the absence of ethylene glycol and diethylene glycol in this reaction, it reinforced the formation of ethylene glycol as the intermediate which involved electrolysis mechanism route on the 80ACC electrode. Overall, the mechanistic investigation here validated that acetol produced 1,2-propanediol through the electrocatalytic hydrogenation, whereas ethylene glycol and glycerol generated diethylene glycol and acetol, respectively *via* dehydration reaction.

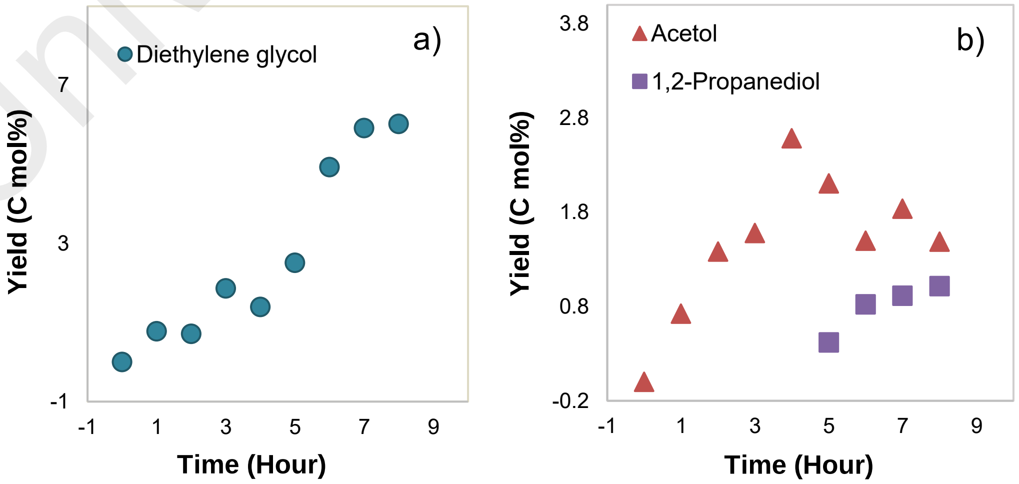

Figure 4.16: Products distributions from the reactions with a) ethylene glycol and c) glycerol as the feedstocks.

4.3.3 Identified reaction mechanisms

Generally, the direct electrochemical conversion of aqueous glycerol includes oxidation and reduction reactions at the anode and cathode electrodes, correspondingly. From the literature, glycerol electrooxidation and oxygen evolution reaction (OER) simultaneously happened at the anode (equation 4.7 to 4.11) instigating more than one intermediate adsorbed on the electrode surface (Pagliaro, 2017; Simões et al., 2012; Talebian-Kiakalaieh et al., 2018). The adsorbed glycerol species (M-$C_3H_8O_{3ads}$) on the electrode surface (M) interact with an adsorbed hydroxyl group (M-$\bullet OH_{ads}$) to oxidize glycerol into intermediates/products and CO_2 through Langmuir-Hinslewood mechanism (equation 4.10) (Gomes et al., 2013; Gonçalves et al., 1985). The intermediates/products produced depend on the essence of the electrodes and operating conditions used in the electrolysis system (Md. Rahim et al., 2020). At the cathode, in most studies, it is acknowledged that only protons from the anodic compartment are reduced into hydrogens as shown in (equation 4.12), without considering glycerol electroreduction reaction. The total reactions for a complete glycerol electrochemical conversion can be written as (equation 4.13).

Anode:

$M + C_3H_8O_3 \rightarrow M\text{-}C_3H_8O_{3ads} \rightarrow \text{Intermediates/products} + H^+ + e^-$ *(Partial electrooxidation)* 4.7

$M + C_3H_8O_3 \rightarrow 3\ M\text{-}CO_{ads} + 8H^+ + 8e^-$ *(Complete glycerol electrooxidation)* 4.8

$M + H_2O \rightarrow M\text{-}OH_{ads} + H^+$ *(Formation of hydroxyl group via oxygen evolution reaction)* 4.9

$CO_{ads} + \bullet OH_{ads} \rightarrow CO_2 + H^+ + e^-$ *(Langmuir-Hinshelwood mechanism)* 4.10

$C_3H_8O_3 + 3H_2O \rightarrow 3CO_2 + 14H^+ + 14e^-$ *(Complete glycerol electrooxidation)* 4.11

Cathode:

$14H^+ + 14e^- \rightarrow 7H_2$ *(Hydrogen evolution reaction)* 4.12

Overall:

$C_3H_8O_3 + 3H_2O \rightarrow 3CO_2 + 7H_2$ 4.13

However, this work established that glycerol can also be reduced to other valuable products such as 1,2-propanediol and diethylene glycol with acetol and ethylene glycol as the intermediates. Encapsulate to the products distribution results obtained from the mechanistic study, the overall reaction mechanisms have been identified referring to the literature reports (Freitas et al., 2018; Hunsom & Saila, 2015; Kongjao et al., 2011; Yfanti et al., 2018), and the basics of electrochemistry (Francke & Little, 2014; Kai et al., 2017; Steckhan, 1986). Partial electroreduction of glycerol involved multiple parallel and consecutive reactions, in which the reduction products were founded from three possible mechanism pathways (Figure 4.17). According to this figure, the main pathways can be categorized into four types which are (i) acid protonation and hydration, (ii) direct or indirect reduction with electricity, (iii) reduction with hydride radicals (H•) that are produced by the H^+ ions adsorption on the electrode and (iv) isomerization of intermediates. Their first intermediary step is significant to determine the production of 1,2-propanediol or diethylene glycol.

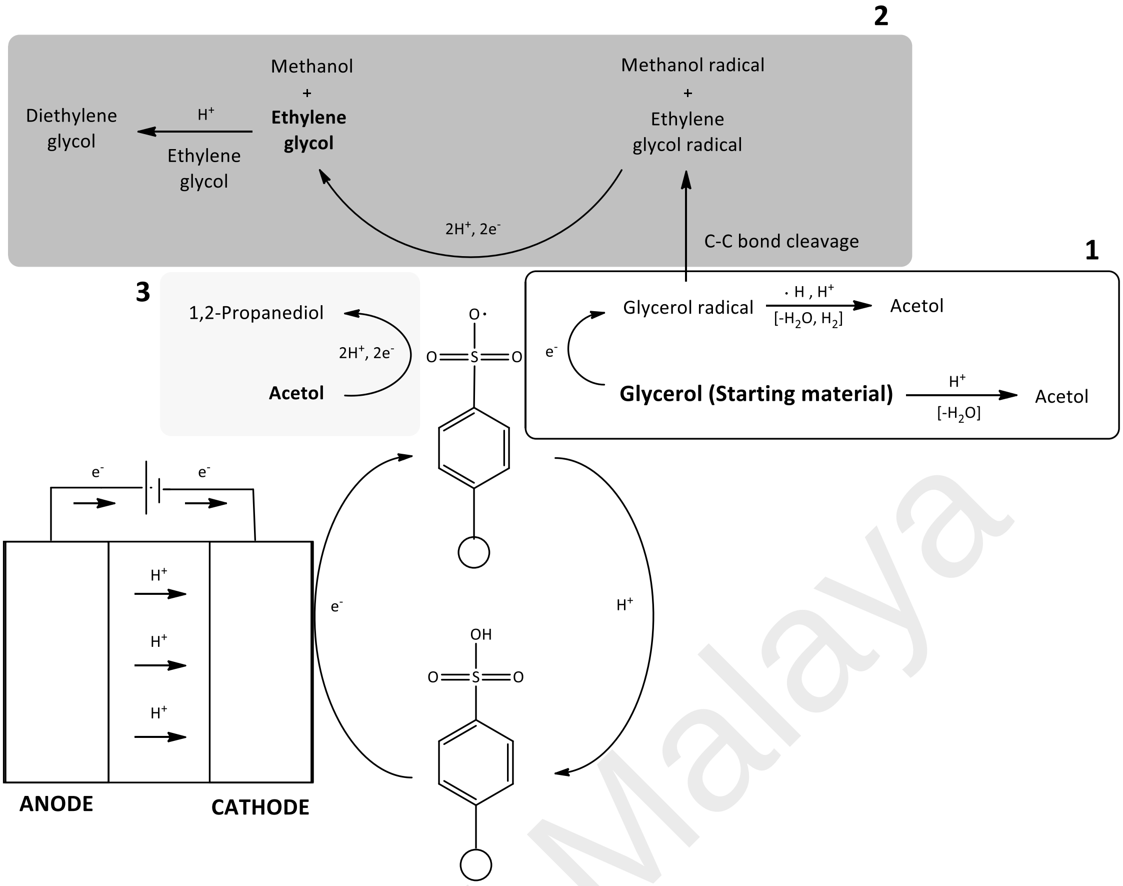

Figure 4.17: Overall identified reaction mechanisms of glycerol electroreduction

Under the highly acidic condition, acetol was obtained through dehydration by water removal from glycerol molecule and *via* the reductive C-O bond dissociation in its molecule. The detailed mechanism reaction is presented in Scheme 4.3. Glycerol dehydration into acetol assumes one of the OH groups was removed at the terminal carbons in the glycerol molecule, whereas the acrolein formation includes the abstract of OH group from the central carbon through the unstable 3-hydroxypropenal. These routes are mostly controlled by the nature of the acid sites, and it is believed that Brønsted acid sites facilitate the selectivity towards acrolein while Lewis acid sites catalyze acetol production (Célerier et al., 2018; Stošić et al., 2012). In contrast, Amberlyst-15 has Bronsted acid sites, therefore, the Lewis acid mechanism could not be applied (Cecilia et al., 2015; Pal et al., 2012).

Additionally, Nimlos et al. (2006) found that the transition state energy (E = 70.9 kcal/mol) for 1,2-dehydration in neutral glycerol through this mechanism is relatively high. This high energy barrier is more likely for reactions with high temperatures such as pyrolysis and combustion. The reaction mechanism is rather undergone a pinacol rearrangement or hydride transfer mechanism as shown in Scheme 4.3a. One of the OH groups was protonated by an H^+ ion and a stable leaving group was established. There is water loss at the protonation site, resulting in carbocation in the glycerol molecule. A carbocation is known for its lack of electrons which creates it to be an overall positive charge on the carbon atom. Attributable to the OH groups' position in glycerol, two carbocation intermediates can be produced. The first intermediate which is carbocation is positioned at the terminal carbon atom. H atom bonded to the neighboring C atom was simultaneously removed by the deprotonated Amberlyst-15, forming an enol intermediate. Acetol was obtained through the tautomerization pathway from this intermediate. In the second intermediate, the carbocation positioned at the terminal C atom rearranged (hydride shift) into carbocation in the middle chain to stabilize the carbon atom. Hydrogen atom was removed from OH group and regenerated the deprotonated Amberlyst-15. A stable double bond ketone (acetol) was finally developed.

In the presence of the redox mediator, the formation of acetol from electroreduction mediated by Amberlyst-15 can also happen and the reaction mechanism is presented in Scheme 4.3b. When the electricity was applied, the electrons transferred from the 80ACC electrode to Amberlyst-15 and further activated it into Amberlyst-15 radical anion (A-15$\bullet^-$). A single electron was then transmitted to glycerol and produced glycerol radical ($CH_3OHC\bullet HOHCH_3OH$) (Steckhan, 1986). As hydrogen evolution reaction (HER) has simultaneously occurred at the cathodic region, H• radicals formed through (i) Volmer-Heyrovsky or (ii) Volmer-Tafel mechanisms can abstract H• atom at OH group of C_1 or C_2 position in glycerol radical molecule (Murthy et al., 2018; Nemiwal et al., 2021). The H• removal in the form of H_2 happened with the excess of protons in the acidic medium which caused the protonation of the OH group. A stable leaving group was extracted as water. The hydride shift took place and subsequently, the intermediate was rapidly rearranged into acetol.

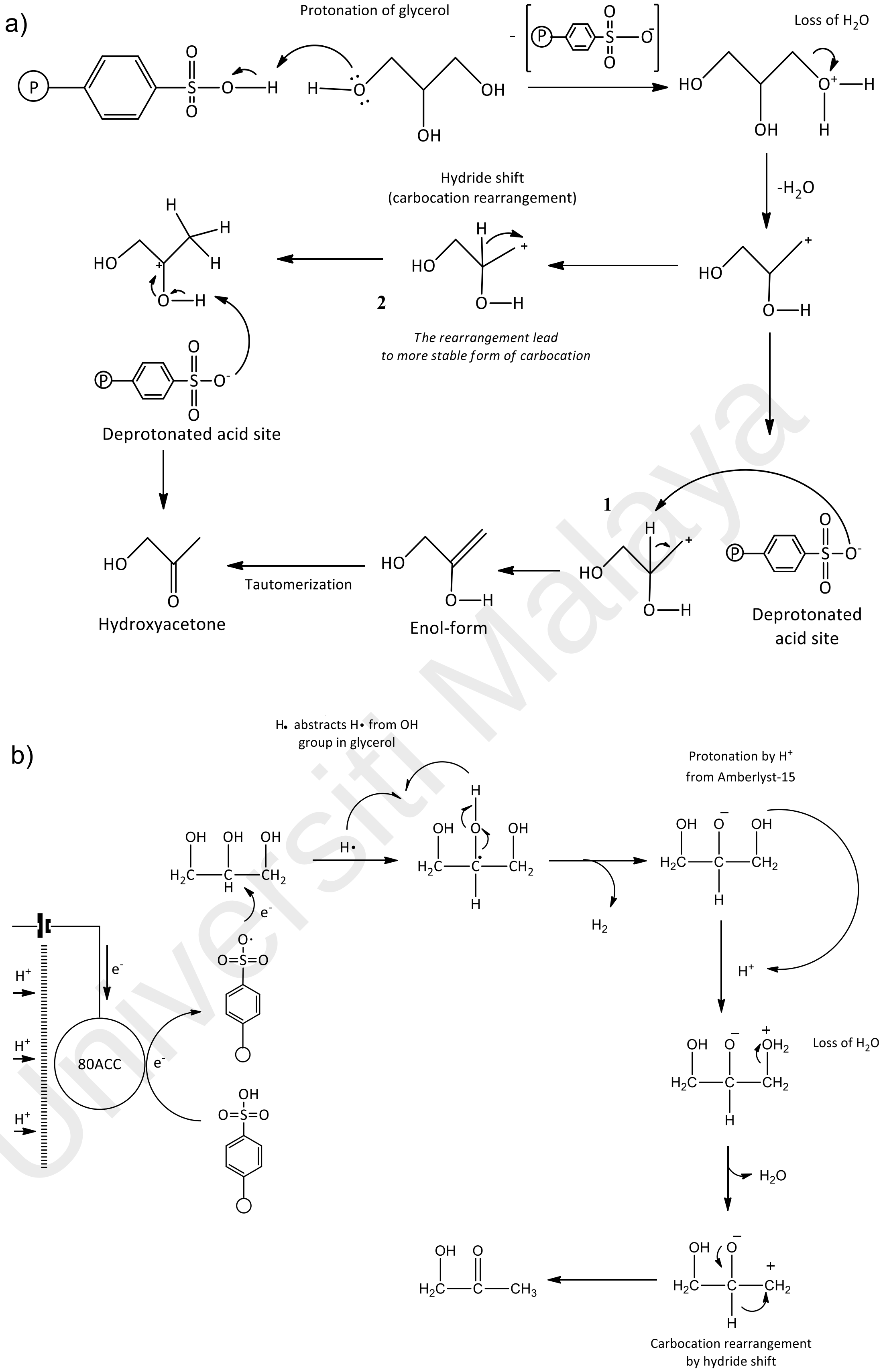

Scheme 4.3: a) Dehydration of protonated glycerol *via* pinacol rearrangement and b) reductive reaction mediated by Amberlyst-15 mechanism pathways.

Acetol with -C=O (carbonyl group) is a reactive species that was reduced into 1,2-propanediol through the electro-hydrogenation route. The simultaneous addition of protons (H^+ ions) and electrons from the anode part through the activated Amberlyst-15 radical anion (A-15•$^-$) managed to avoid over-reduction of glycerol into other minor products (Scheme 4.4).

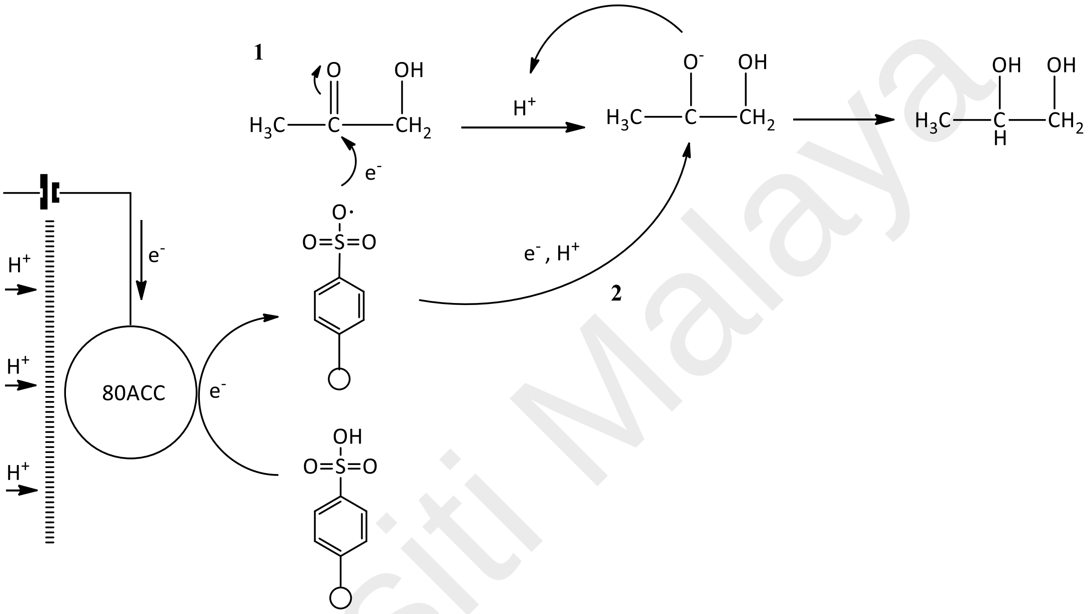

Scheme 4.4: Electro-hydrogenation of acetol.

Diethylene glycol was not obtained in acetol electrolysis and glycerol experiment without electricity, suggesting that it was directly generated from glycerol by the presence of an electrical current. From a mechanistic perspective, two free radical compounds formed through C-C bond cleavage in glycerol radical molecule is the initial step (Scheme 4.5a). Glycerol radical was dissociated into ethylene glycol radical and alcohol-free anion with the aid of Amberlyst-15 radical (A-15•$^-$) (Steckhan, 1986). Ethylene glycol radical was reduced into ethylene glycol by a parallel route (electro-hydrogenation mechanism) in agreement with the earlier reports (Dieuzeide et al., 2017; Yfanti et al., 2018). In a highly acidic medium, intermolecular dehydration of ethylene glycol occurred and generated diethylene glycol where the route is identical to dipropylene glycol synthesis (Chitwood & Freure, 1946; Chiu et al., 2008; Yu et al., 2009). As shown in Scheme 4.5b, ethylene glycol was protonated by H^+ ions and triggered the removal of water. At the same time, the OH group in the ethylene glycol with higher electrons affinity attacked the carbocation of another ethylene glycol. It was then rapidly rearranged into a stable form of diethylene glycol by the removal of H^+ using H_2O.

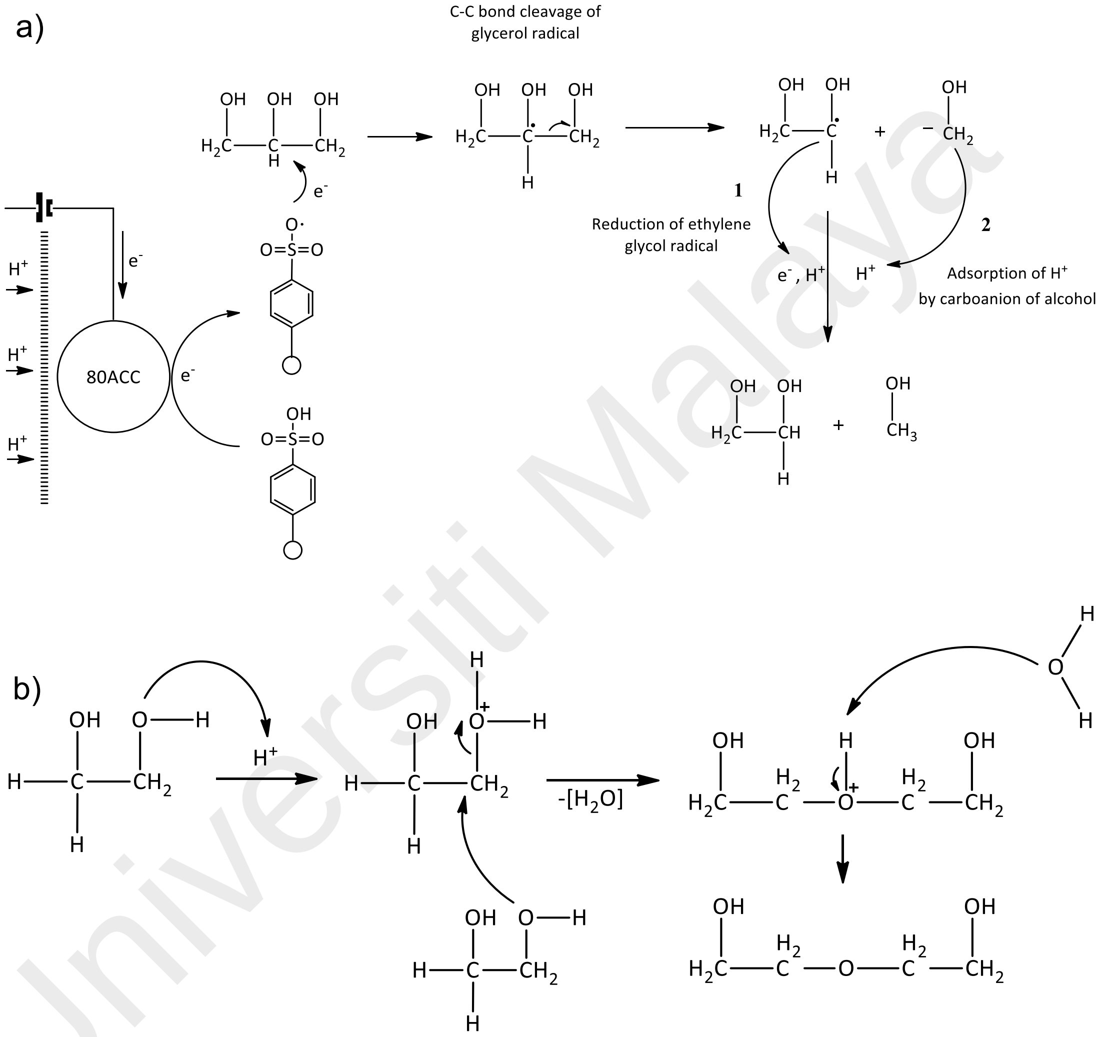

Scheme 4.5: a) Electrocatalytic cleavage of glycerol radical and b) intermolecular dehydration of ethylene glycol.

4.4 Preliminary experiments for glycerol electroreduction on 80ACC electrode

When the complete glycerol electroreduction mechanism was elucidated, the operating parameters such as reaction temperature, glycerol initial concentration, and current density (electric current) for this process were explored on the 80ACC electrode. The results demonstrated that glycerol conversion and products distribution are greatly dependent on these kinetics parameters. The GC-FID chromatogram at the optimum conditions is demonstrated in Figure 4.18. 1,2-propanediol is the primary product and a wide range of secondary compounds such as methanol, acetol, 3-methoxy-1,2-propanediol, 3-hydroxy-2-butanone, ethylene glycol, and diethylene glycol were generated in small quantities.

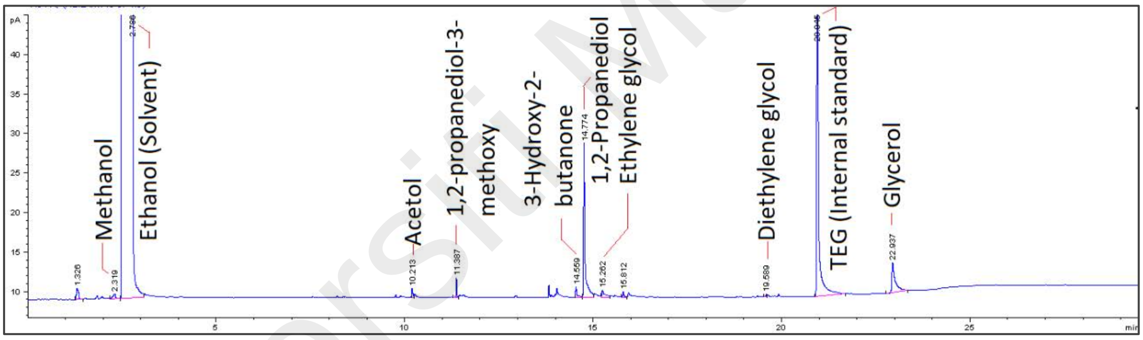

Figure 4.18: GC-FID result at the optimum conditions.

4.4.1 Effect of reaction temperature

The influence of reaction temperature was firstly investigated by utilizing 27.0 °C (room temperature), 53.5 °C, 80.0 °C, and 106.5 °C in 0.3 M of glycerol and 9.6% (w/v) of Amberlyst-15 solution at 0.14 A/cm^2 current density. The glycerol conversion and the kinetics rate constants for those temperatures are shown in Figure 4.19. The glycerol conversion was improved with the temperature improvement. At low temperatures (27.0 °C and 53.5 °C) the conversion of glycerol was similar around 84% (respective to the conversion rates of 0.5772 × 10^{-4} s^{-1} and 0.5864 × 10^{-4} s^{-1}). It completed up to around

90% at high temperatures (80.0 °C and 106.5 °C) and the kinetics rate constant reached the highest value of $0.7861 \times 10^{-4}\ s^{-1}$ (90.8%) at the highest temperature of 106.5 °C. An increase in temperature has reduced the mixture viscosity and the thickness of the diffusion layer, thus, improving the glycerol diffusion process (Gupta et al., 1984). It then enhanced the mass transfer of glycerol, promoting the interaction between its molecule or intermediates with Amberlyst-15 radical anion mediator ($A\text{-}15^{\bullet -}$) for the redox reaction with 80ACC electrode (Lee et al., 2019; Nascimento & Linares Leon, 2014). Consequently, it led to high glycerol conversion with more products.

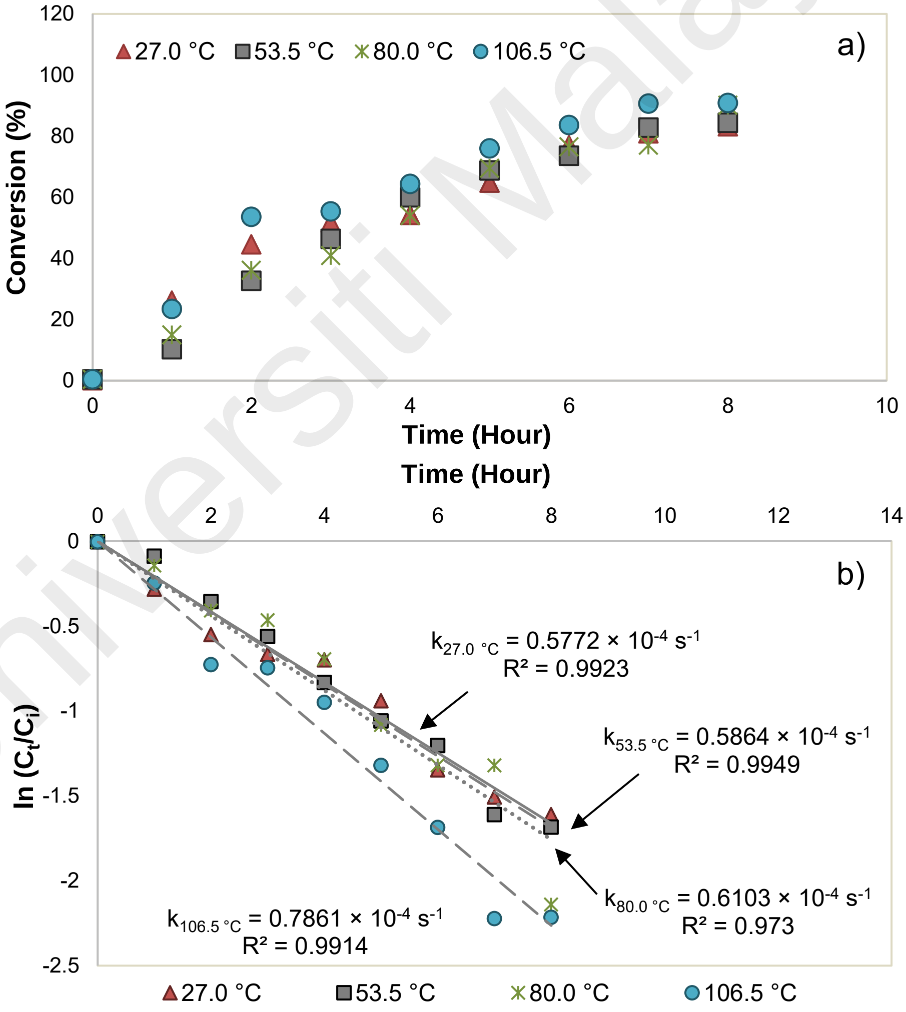

Figure 4.19: a) Glycerol conversion and b) first-order kinetics model for 0.3 M of glycerol electroreduction at different reaction temperatures.

During the electrolysis, a temperature improvement for long hours boosted both the C-O and C-C bonds breakage, transforming glycerol into acetol and diethylene glycol that came from ethylene glycol. From Figure 4.20, the maximum yields of acetol and diethylene glycol were 13.7 C mol% (4th hour) and 15.9 C mol% (8th hour) at 106.5 °C. The fast dissociation was contributed by the large energy collected from high temperature, thereby, improving the molecular collisions frequency between electrolyte ions (Licona et al., 2014). The high number of molecular collisions speeded up the electrons passage between A-15$\bullet^-$ and 80ACC electrode in producing the intermediates and 1,2-propanediol during the redox reaction with glycerol. Moreover, the highest yield of diethylene glycol accomplished at this temperature demonstrated that ethylene glycol dehydration also favoured a high temperature. Acetol and diethylene glycol yield kept increasing due to the incomplete glycerol electrocatalytic reduction reaction. Thus, shortening the electrolysis time can lessen glycerol interaction with A-15$\bullet^-$ and stop these undesirable compounds generation.

Besides, greater ionic conductivity and lower resistance at elevated temperature can also quicken the electro-hydrogenation of acetol to 1,2-propanediol. The yield was enhanced from 26.7 C mol% (27.0 °C at 8th hour) to 29.4 C mol% (80.0 °C at 7th hour) at a faster time. Albeit the high temperature is needed for 1,2-propanediol formation, it requires to mention that an additional escalation to higher temperature is not recommended. It can cause water evaporation in the solution and obstruct the reaction (Nascimento & Linares Leon, 2014). The compounds with a low boiling point like acetol might also vaporize. It can be seen in Figure 4.20d where acetol yield was spotted inconsistently at 106.5 °C. As stated in the acetol electrolysis experiments' discussion (Section 4.3.1), hydrogen evolution reaction (HER) can be the primary reaction at low substrate concentration. H^+ ions in the aqueous solution combated for hydrogen (H_2)

production and acetol electro-hydrogenation reaction into 1,2-propanediol. At too high temperature, H^+ ions and electrons that were transferred from the anode part were reduced into hydrogen quicker than acetol electro-hydrogenation. The developed H_2 gases on the cathode electrode surface can be a carrier agent for highly volatile compounds like acetone, methanol, and acetol. These minor products are expected to purge out with hydrogen in a significant yield. The losses can be abated by an appropriately sealed reactor setup and the prevention of excessive HER. From Figure 4.20, a suitable temperature range for a selective C-O bond cleavage into acetol and successive electro-hydrogenation to 1,2-propanediol reaction are low to moderate temperature (27.0 - 53.5 °C). Yet, 80.0 °C produced the highest yield of 1,2-propanediol.

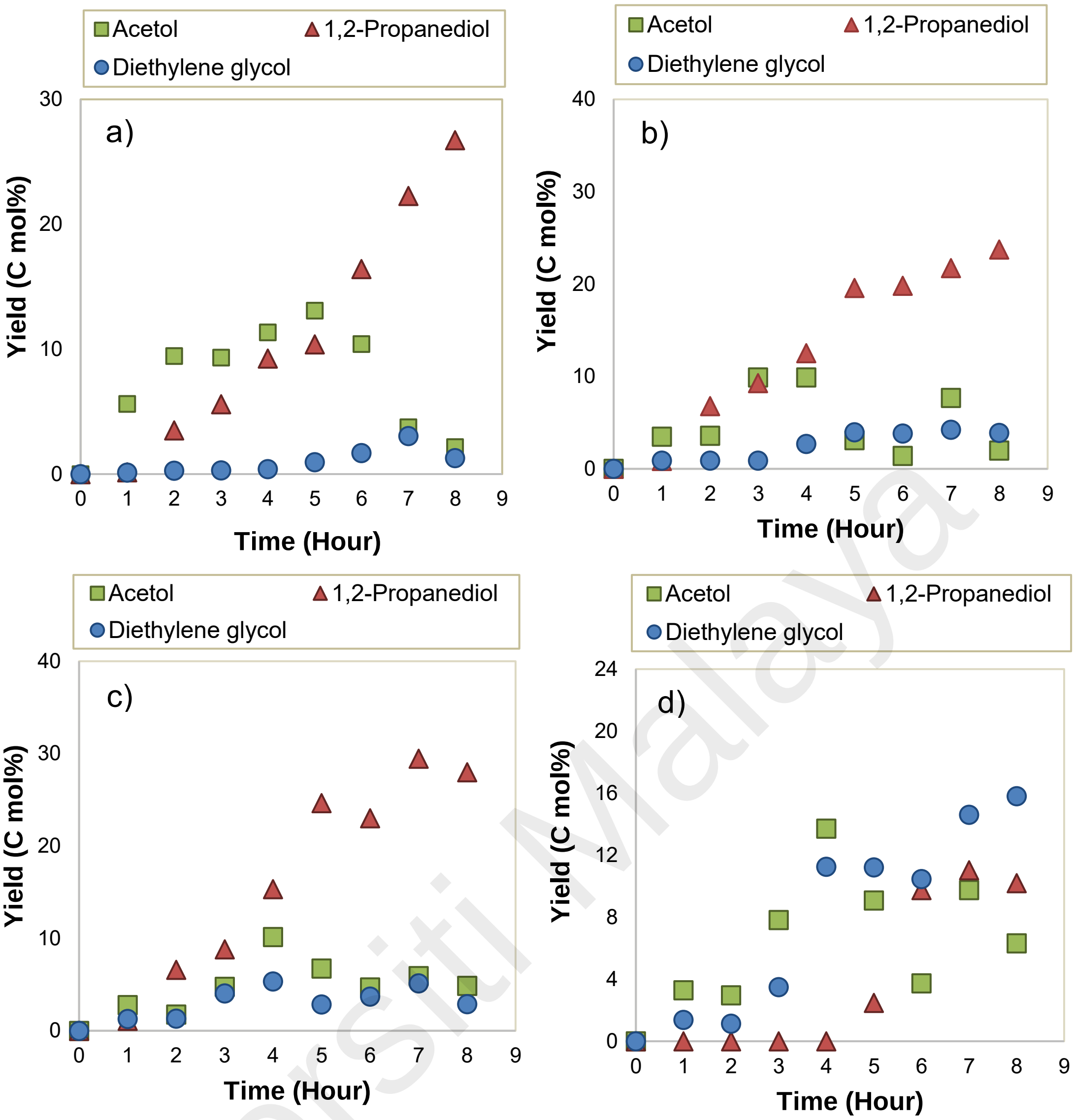

Figure 4.20: Products distribution for 0.3 M of glycerol electroreduction at a) 27.0 °C, b) 53.5 °C, c) 80.0 °C and d) 106.5 °C with 0.14 A/cm^2 of current density.

4.4.2 Effect of glycerol initial concentration

80.0 °C of reaction temperature was utilized as constant for the glycerol initial concentration study because it produced the greatest yield of 1,2-propanediol. 0.3 M, 1.65 M, 3.0 M, and 4.35 M of pure glycerol were explored at this reaction temperature and 0.14 A/cm^2 current density to ascertain its effect on the reaction mechanisms and products distribution. From Figure 4.21a, after 8 hours of electrolysis, the glycerol conversion was reduced from 90.1% (0.3 M) to 29.5% (4.35 M) when the initial concentration was raised. The decline was because of the higher viscosity in the concentrated glycerol. Supported by Nascimento and Linares Leon (2014) effort, at high glycerol concentration, it was found that too high viscosity of glycerol limited the molecule transport to the electrocatalytic layer, causing the anode surface poisoning. The phenomenon occurred because of the large amounts of glycerol competing with the hydroxyl radicals for the electrooxidation reaction. In this work, the cathode electrode efficiency was inhibited due to a similar reason. Too high glycerol concentration reduced the mass transport of glycerol molecule for the reaction with 80ACC electrode through A1-5$\bullet^-$, leading to a slow conversion. Based on first-order kinetics plots (Figure 4.21b), the kinetics rate constant of 0.3 M glycerol was the fastest (0.6103 × 10^{-4} s^{-1}), followed by 1.65 M, 3.0 M, and 4.35 M concentrations (0.3561 × 10^{-4} s^{-1}, 0.2753 × 10^{-4} s^{-1} and 0.0664 × 10^{-4} s^{-1} respectively).

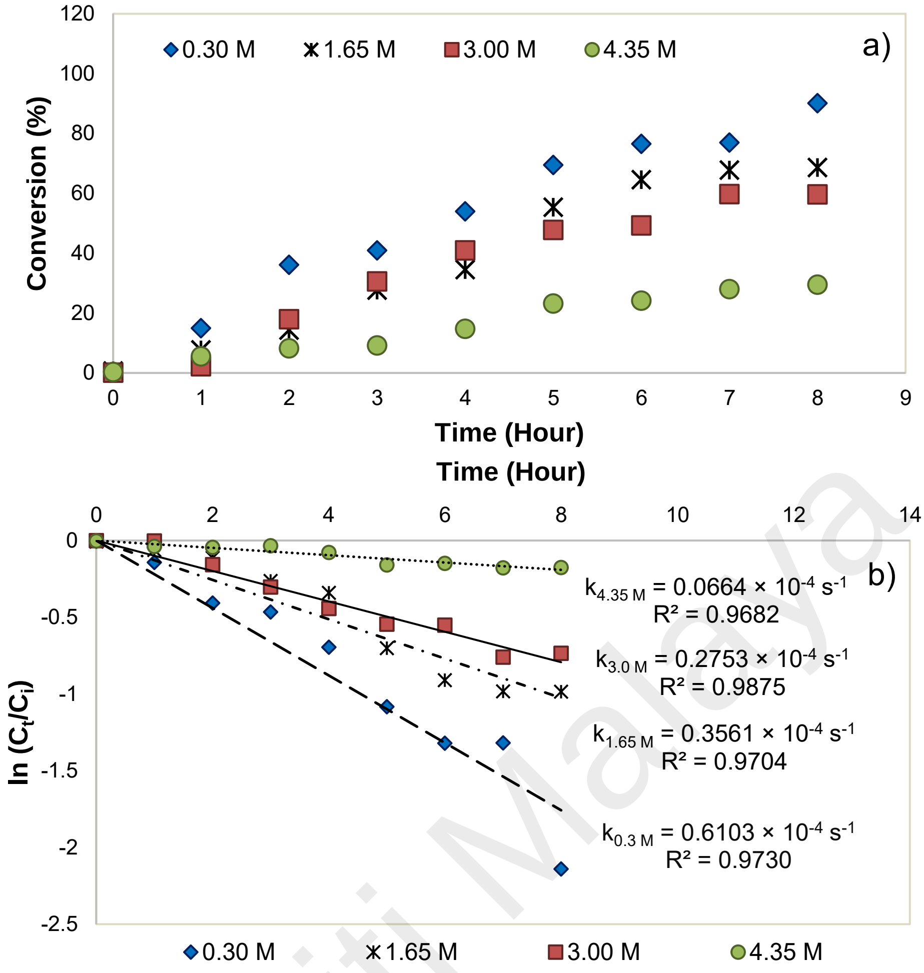

Figure 4.21: a) Glycerol conversion and b) first-order kinetics model for electroreduction of glycerol with different initial concentrations.

The products distribution for different glycerol initial concentrations is represented in Figure 4.22. 1,2-propanediol was the major compound for 0.3 M, 1.65 M, and 3.0 M concentrations. The greatest yield was attained at the 7th hour for 0.3 M (29.4 C mol%) and 1.65 M (31.9 C mol%), 6th hour for 3.0 M (35.02 C mol%). There is no direct time-dependence for 1,2-propanediol yield because it may produce other by-products with high volatility such as acetone. It was previously discussed that acetone was only observed below 80.0 °C temperature. Substantial to other new products such as methanol, ethylene glycol, 3-methoxy-1,2-propanediol, and 3-hydroxy-2-butanone which appeared at 1.65 M and 3.0 M, the reaction mechanisms were confirmed where glycerol can undergo the C-C bond dissociation to methanol and ethylene glycol in the presence of electricity. Methanol obtained from the C-C bond cleavage of glycerol reacted with the unconverted glycerol and produced 3-methoxy-1,2-propanediol through an etherification process (Bruniaux et al., 2019). The hydroxide ion (OH^-) was abstracted from methanol whereas one proton was removed from glycerol, which was catalyzed by Amberlyst-15 catalyst (Pico et al., 2012). This mechanism developed 3-methoxy-1,2-propanediol and water as a by-product. 3-hydroxy-2-butanone was formed from acetol where its formation was favoured at higher concentration.

Nonetheless, at 4.35 M of glycerol, the products combated with glycerol reactant for the redox reaction with $A\text{-}15^{\bullet -}$, consequently triggering a self-inhibition towards the total yield of products (Farma et al., 2013). This implies that glycerol conversion to 1,2-propanediol and intermediates was not favourable at the highest concentration. In contrast, at the minimum and medium concentrations, more 1,2-propanediol with C_5 to C_2 products were produced. Additionally, acetol has been identified as the main intermediate product with a yield slightly higher than ethylene glycol and diethylene glycol. The yield remained approximately 10.0 C mol% for each concentration, demonstrating that the reduction of acetol to 1,2-propanediol is a fast-consecutive reaction. In general, although glycerol was not completely converted, 3.0 M was sufficient to improve the yield of 1,2-propanediol. Hence, this concentration was applied in the following study.

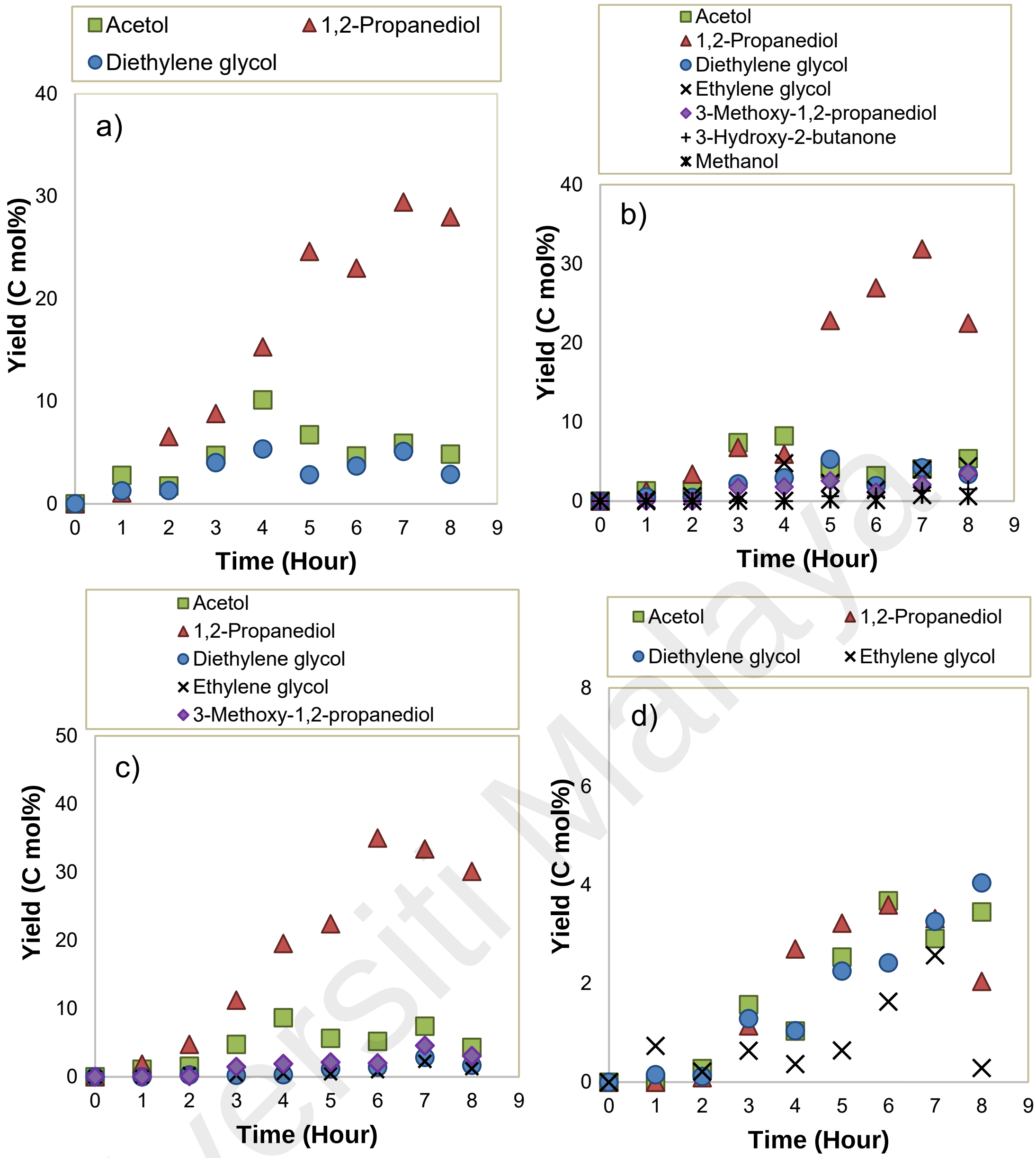

Figure 4.22: Products distribution with glycerol initial concentration of a) 0.30 M, b) 1.65 M, c) 3.00 M and d) 4.35 M during the electroreduction reaction at 80.0 °C and 0.14 A/cm^2.

4.4.3 Effect of current density

After the optimum temperature (80.0 °C) and glycerol initial concentration (3.0 M) were achieved, the electrical current was varied from 0.05 A to 1.0 A, 1.5 A, and 2.0A (equivalent to 0.07, 0.14, 0.21, and 0.28 A/cm^2 of current densities). As shown in Figure 4.23a, glycerol conversion was increased with the current density enhancement from 0.07 A/cm^2 (55.9%) to 0.28 A/cm^2 (76.0%) after 8 hours of electrolysis. A complete conversion may take a prolonged time for a lower current density. Compatible with Faraday's law, the conversion rate was improved from 0.2267 × 10^{-4} s^{-1} (0.07 A/cm^2) to 0.4847 × 10^{-4} s^{-1} (0.28 A/cm^2) (Figure 4.23b).

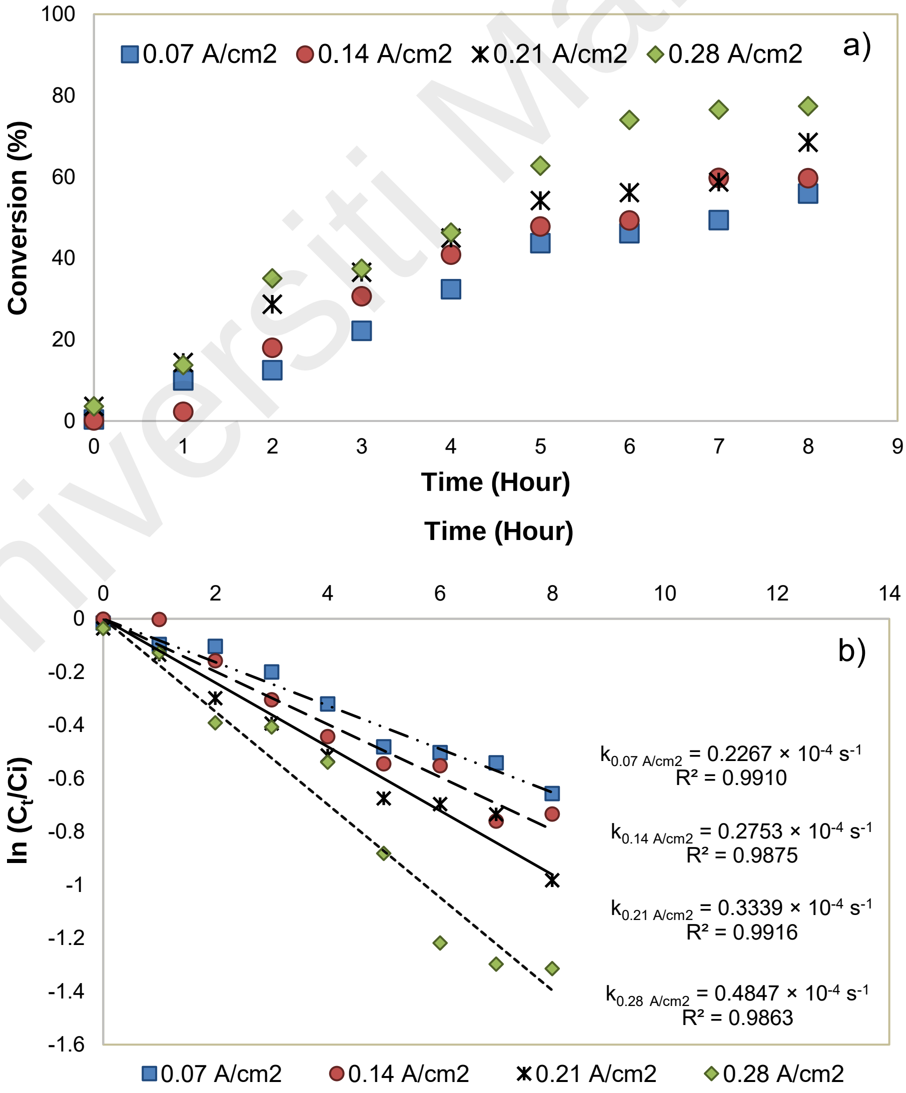

Figure 4.23: a) Glycerol conversion (%) and b) first-order kinetics model for glycerol electroreduction at different current densities.

Related to the impact on the distribution of products, the yield was affected by the change in current density given (Figure 4.24). Acetol is the major product (with 15.8 C mol%, 7th hour) generated at 0.07 A/cm^2 in Figure 4.24a. It suggests the C-O bond breakage of glycerol preferred a low current density and its development is the earliest step in glycerol electroreduction reaction. The small amount of 1,2-propanediol suggested the sluggishness of acetol electro-hydrogenation at this current density. For high 1,2-propanediol yield, medium to high current density showed the best result with the maximum yield of 42.3 C mol% at 0.21 A/cm^2. The greater the current density, the faster acetol electro-hydrogenation to 1,2-propanediol. This is because more electrons and protons were provided from the anodic compartment for this reaction. However, the yield of 1,2-propanediol was reduced to 15.1 C mol% at the 6th hour with the largest current density in Figure 4.24d. Higher electrical current can trigger the fragmentation of glycerol or 1,2-propanediol to gases products, which cannot be detected in the liquid phase analysis. HER may as well prefer a high electrical current since more electrons were accessible in the process. Therefore, medium to high current density is excellent for a selective and high yield for 1,2-propanediol.

Meanwhile, ethylene glycol was only detected at medium to high current density. In conformity to higher electrode potential enhanced the C-C bond cleavage by Colmati et al. (2009) and Gomes and Tremiliosi-Filho (2011), higher current density also led to higher production of ethylene glycol through C-C bond breakage of glycerol. The rapid rate of ethylene glycol dehydration was facilitated by a high current, the same as the etherification of glycerol with methanol. Diethylene glycol and 3-methoxy-1,2-propanediol accomplished 9.3 C mol% and 5.8 C mol% yields, respectively at 0.28 A/cm^2. A high current density can promote the conversion of glycerol into various valuable compounds especially, 1,2-propanediol. Yet, too high current density does not develop the yield of the targeted compound. Indeed, it initiated the formation of unwanted gases products and removed the minor products with high volatility.

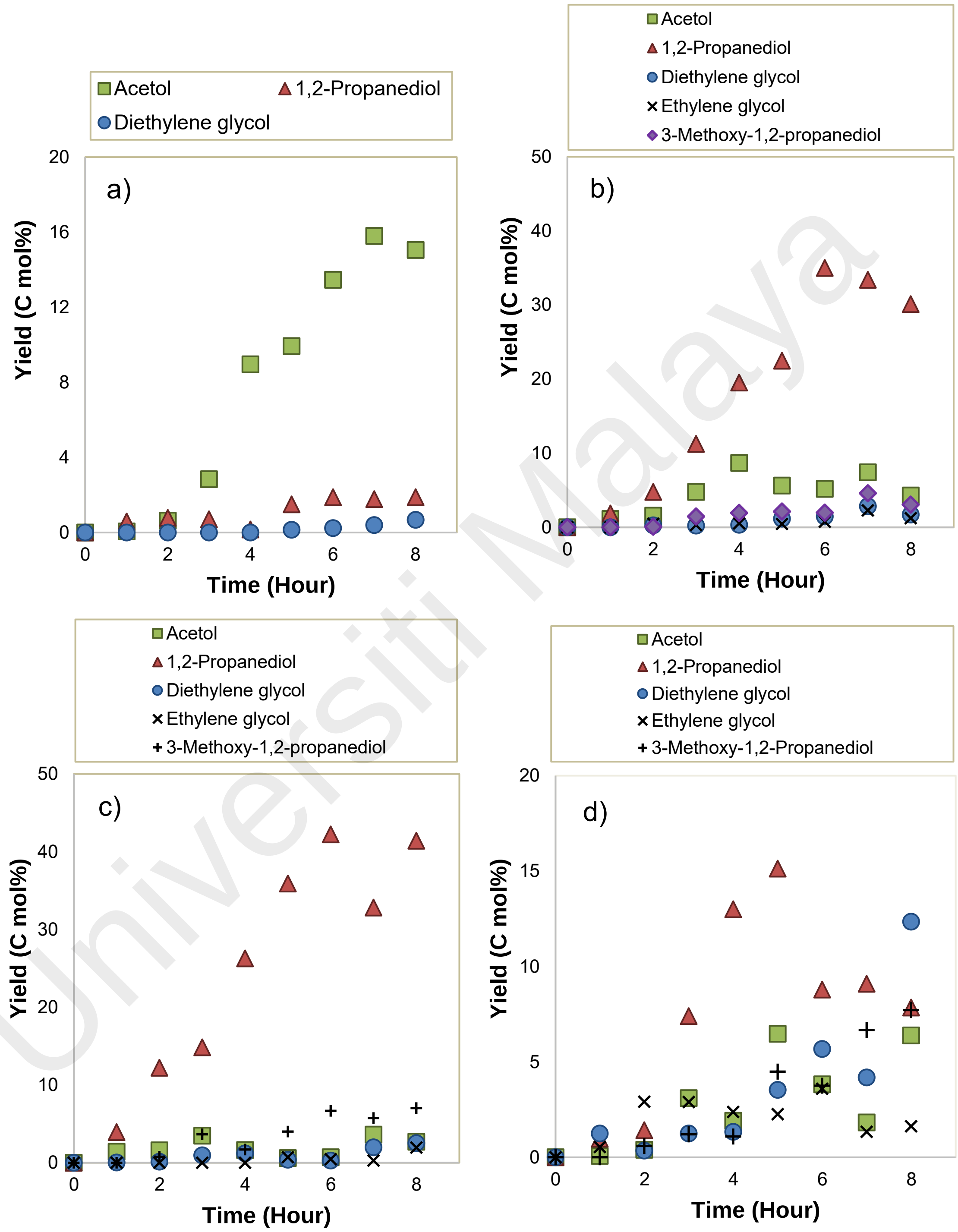

Figure 4.24: Products distribution at a) 0.07 A/cm^2, b) 0.14 A/cm^2, c) 0.21 A/cm^2, and d) 0.28 A/cm^2 of current densities with 3.0 M of glycerol at 80.0 °C.

To conclude, the initial step which involved the C-O and C-C bonds cleavage in glycerol plays a crucial role in producing either acetol or ethylene glycol intermediate. This was controlled by the temperature, where low to medium value is needed to maintain a selective acetol-1,2-propanediol route. In addition, moderate concentration reduced the hydrogen formation and indirectly improved the 1,2-propanediol yield. A mild current density raised the conversion rate and minimized the increase of intermediates. Although the greatest conversion of glycerol (76.0%) was achieved at 0.28 A/cm^2; however, the operating condition of 80.0 °C reaction temperature, 3.0 M glycerol initial concentration at 0.21 A/cm^2 was found to be optimum for 1,2-propanediol production. This is because this condition reached the maximum yield (42.3 C mol%) and selectivity (75.3%) at a quicker time (at the 6th hour) compared to other conditions.

4.4.4 Optimization of glycerol electroreduction using RSM method

The findings from the effects of kinetics parameters studies showed that high 1,2-propanediol yield was acquired with the reaction temperature of 27.0-80.0 °C, glycerol initial concentration of 0.30-3.00 M, and current density of 0.14-0.28 A/cm^2. All the data from these experiments were filled into the Design-Expert software to create the 20-experiments design matrix for the optimization study. From these experiments, 1,2-propanediol yield ranged from 4.7 C mol% to 38.1 C mol% after 6 hours of glycerol electroreduction (Table 4.3). This analysis helped to investigate on how the parameters affect the major product, 1,2-propanediol formation. The coded factor model developed from the results was fitted to a polynomial model (quadratic equation) and is represented in equation 4.14. Y is the yield of 1,2-propanediol (C mol%), A is reaction temperature (°C), B is glycerol initial concentration (M), and C is current density (A/cm^2).

$$Y = 33.46 + 3.85\,A + 1.65\,B - 6.53\,C + 3.79\,AB - 4.29\,AC - 0.44\,BC + 0.22\,A^2 - 1.18\,B^2 - 17.58\,C^2 \quad 4.14$$

Table 4.3: The central composite design (CCD) matrix for 20 experiments of glycerol electroreduction with the response (Y).

Run	Actual variables			Coded variables			Response (Y)
	Reaction temperature (°C)	Initial concentration (M)	Current density (A/cm^2)	A	B	C	1,2-propanediol yield (C mol%)
1[a]	80.00	0.30	0.28	1	-1	1	4.7
2[b]	27.00	1.65	0.21	-1	0	0	28.3
3[c]	53.50	1.65	0.21	0	0	0	33.5
4[b]	53.50	1.65	0.14	0	0	-1	23.7
5[a]	80.00	0.30	0.14	1	-1	-1	23.0
6[b]	53.50	0.30	0.21	0	-1	0	27.5
7[c]	53.50	1.65	0.21	0	0	0	34.2
8[a]	80.00	3.00	0.28	1	1	1	11.8
9[b]	53.50	1.65	0.28	0	0	1	7.1
10[b]	53.50	3.00	0.21	0	1	0	36.1
11[c]	53.50	1.65	0.21	0	0	0	34.3
12[a]	27.00	0.30	0.28	-1	-1	1	12.1
13[a]	27.00	0.30	0.14	-1	-1	-1	16.4
14[a]	27.00	3.00	0.14	-1	1	-1	10.1
15[c]	53.50	1.65	0.21	0	0	0	33.7
16[a]	80.00	3.00	0.14	1	1	-1	35.0
17[c]	53.50	1.65	0.21	0	0	0	33.5
18[a]	27.00	3.00	0.28	-1	1	1	7.2
19[c]	53.50	1.65	0.21	0	0	0	33.5
20[b]	80.00	1.65	0.21	1	0	0	38.1

The different alphabets in run order mean (a) factorial design, (b) axial point, and (c) center point.

The analysis of variance (ANOVA) outcomes is subsequently summarized in Table 4.4. The Model F-value was 77.91 which means the model is significant. Besides, the p-values were less than 0.05 for A, B, C, AB, AC, and C^2 indicating these model terms are significant. The reaction temperature and current density parameters showed the greatest impact on 1,2-propanediol yield because of their smallest p-value Prob < F. The model displayed a large determination coefficient (R^2) of 0.9859, signifying a close fit of the predicted model to the actual data. Whereas Q^2 describes how good the response can be predicted in the obtained model. If Q^2 is larger than 0.5, it is regarded as good and if greater than 0.9, the model is excellent. In this work, Q^2 was 0.8652, demonstrating a good model.

Table 4.4: ANOVA for response surface quadratic model.

Source	Sum of squares (SS)	*df*	Mean square	F value	p-value Prob > F
Model	2518.14	9	279.79	77.91	< 0.0001 (Significant)
A – Reaction temperature	148.22	1	148.22	41.27	< 0.0001
B – Glycerol initial concentration	27.22	1	27.22	7.58	0.0204
C – Current density	426.41	1	426.41	118.73	< 0.0001
AB	114.76	1	114.76	31.95	0.0002
AC	147.06	1	147.06	40.95	< 0.0001
BC	1.53	1	1.53	0.43	0.5285
A^2	0.13	1	0.13	0.036	0.8524
B^2	3.84	1	3.84	1.07	0.3254
C^2	850.08	1	850.08	236.70	< 0.0001
Residual	35.91	10	3.59		
Lack of fit	35.23	5	7.05	51.18	0.0003
Pure error	0.69	5	0.14		
Corrected total	2554.06	19			

df: Degree of freedom; R squared (R^2) = 0.9859; Adjusted R^2 = 0.9733; Q^2 = 0.8652; Adequate precision = 25.806; Prediction residual sum of squares (PRESS) = 344.20

Based on the ANOVA, the three-dimensional (3D) response surface graphs for the combined parameters of reaction temperature, glycerol initial concentration, and current density are provided in Figure 4.25. The graphs revealed optimized conditions exist within the observed design space to the highest yield of 1,2-propanediol. In Figure 4.25a, an increase in both reaction temperature and glycerol initial concentration enhanced 1,2-propanediol yield. The largest yield was obtained at the maximum points of 80.0 °C and 3.0 M. From Figure 4.25b, the medium current density of 0.21 A/cm^2 and highest temperature (80 °C) are required to reach the highest yield of 41.8 C mol%. Furthermore, Figure 4.25c showed that the highest current density resulted in a low yield of 1,2-propanediol regardless of any initial concentration used in the process. The optimum condition was found with 3.0 M glycerol initial concentration at 0.21 A/cm^2 current density and 80°C reaction temperature. The experimental value of 1,2-propanediol yield (42.3 C mol%) from the previous section was close to the predicted value (41.8 C mol%) from this model. It also proved that reaction temperature and current density are the important parameters to study in order to get high yield of 1,2-propanediol as the major product.

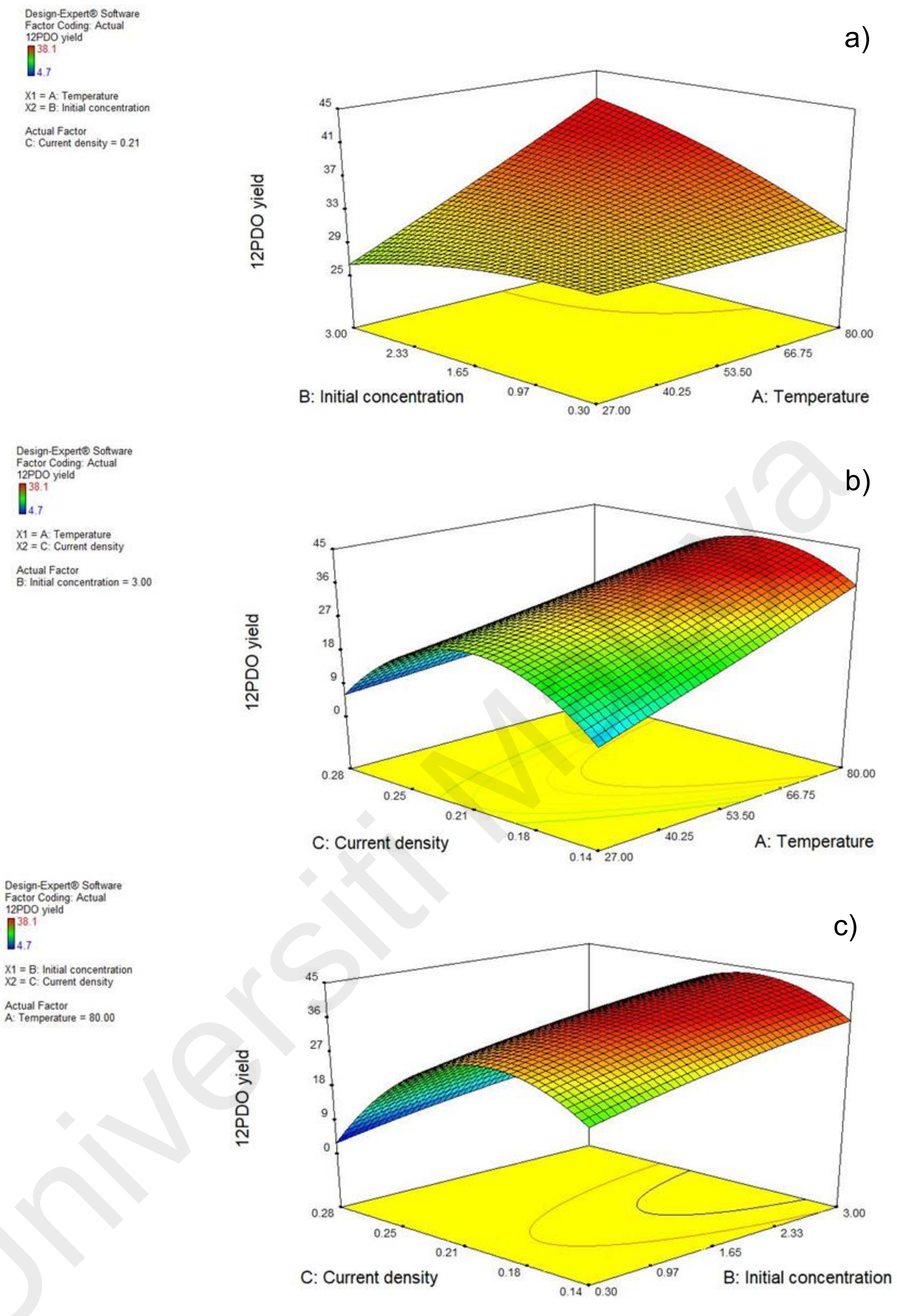

Figure 4.25: Optimization of 1,2-propanediol (12PDO) yield as a function of operating conditions: The combined of a) temperature and initial concentration, b) temperature and current density, and c) current density and initial concentration.

4.5 Energy consumptions for acetol and glycerol electrochemical conversion

The elementary steps for each reaction that were discussed in the reaction mechanisms section are described in Table 4.5. Normally, taken from stoichiometry equation (6), 14 electrons and 14 protons are needed to yield 7 moles of hydrogen in HER. However, to transform each mole of glycerol into valuable products like acetol, 1 proton or 1 H• atom, 1 proton and 1 electron for acetol dehydration and electrocatalytic reductive reactions (Step 1 and 2, respectively). 2 electrons and 2 protons for 1,2-propanediol from acetol (Step 3), 2 electrons and 2 protons for ethylene glycol from glycerol through the indirect reaction (Step 4). Meanwhile, each 1 H^+ is involved in every diethylene glycol (Step 5) and 3-methoxy-1,2-propanediol (Step 6) during the intermolecular dehydration and etherification reactions. The first-order kinetics model was found to be the best for all separated reactions' experiments (Step 1, Step 3, and Step 5). The kinetics rate constants (*k*) from the model and energy consumptions are tabulated in Table 4.5. Energy consumptions in the processes were calculated using equation 4.15 relied on the kinetics parameters used during the reactions. W is energy consumed in glycerol (or acetol) conversion (kWh/kg), I is the current (A), E is the applied potential or voltage (V) and C_0 is the initial concentration (g/L), C_t is the final concentration (mol/L), V is the volume (L), and M is the molecular weight of a compound.

$$W_{Gly\ (or\ acetol)\ conversion} = \frac{IE\Delta t}{(C_0 - C_t)VM} \qquad 4.15$$

Although the conversion rate for acetol electro-hydrogenation was better than glycerol electroreduction, the consumed energy was doubly higher (10.17 kWh/kg) than the latter reaction (5.23 kWh/kg). This is due to the required voltage to generate 1,2-propanediol using acetol being larger than for glycerol reaction. In addition to this point, compared with the catalytic conversion, a similar or higher yield of 1,2-propanediol was accomplished in our report under moderate operating conditions, which benefits in saving energy and operating cost. The data obtained by this research will also empower the possibility of 1,2-propanediol production from biomass-derivative glycerol to be done using the inexpensive and simple electrolysis technique. Certainly, it will open more research opportunities towards applying the activated carbon-based electrode for the electrochemical reactions in electro-organic synthesis.

Table 4.5: Elementary steps for the overall glycerol electroreduction reaction.

Steps	Operating conditions*	Elementary steps for reaction mechanisms	k* (s^{-1})	W (kWh/ kg)
1st step (Glycerol dehydration)	[Gly] = 3.0 mol/L T = 353 K	$C_3H_8O_3 + H^+ \rightarrow (C_3H_9O_3)^+ \rightarrow C_3H_6O_2 + H^+ + H_2O$	(k_{C3H6O2}) $k_1 = 0.0436 \times 10^{-4}$	-
2nd step (Electroreduction of glycerol)		$C_3H_8O_3 + e^- \rightarrow (C_3H_9O_3)^{\bullet -}$ $(C_3H_9O_3)^{\bullet -} + H^\bullet + H^+ + e^- \rightarrow C_3H_6O_2 + H_2O + H_2$ $H^+ + e^- \rightarrow ACC\text{-}H_{ads}$ $ACC\text{-}H_{ads} + H^+ + e^- \rightarrow H_2 + ACC$ $ACC\text{-}H_{ads} + ACC\text{-}H_{ads} \rightarrow H_2 + 2ACC$	$(k_{(C3H9O3)^{\bullet -}})$ (k_{C3H6O2}) $(k_{H\bullet})$ Volmer (k_{H2}) Heyrovsky (k_{H2}) Tafel	-
3rd step (Electro-hydrogenation of acetol)	[ACTL] = 3.0 mol/L T = 353 K *j* = 0.28 A/cm^2 E = 25.7 V	$C_3H_6O_2 + 2H^+ + 2e^- \rightarrow C_3H_8O_2$	(k_{C3H8O2}) $k_2 = 0.4892 \times 10^{-4}$	10.17
4th step (Electro-reduction and hydrogenation of glycerol)		$C_3H_8O_3 + e^- \rightarrow (C_3H_9O_3)^{\bullet -}$ $(C_3H_9O_3)^{\bullet -} \rightarrow C_2H_5O_2^\bullet + CH_2O^-$ $C_2H_5O_2^\bullet + H^+ + e^- \rightarrow C_2H_6O_2$ $CH_2O^- + H^+ \rightarrow CH_3O$	$(k_{(C3H9O3)^{\bullet -}})$ $(k_{C2H5O2\bullet})$ (k_{C2H6O2}) (k_{CH3O})	-
5th step (Dehydration of ethylene glycol to diethylene glycol)	[EG] = 3.0 mol/L T = 353 K	$C_2H_6O_2 + H^+ \rightarrow (C_2H_7O_2)^+ + C_2H_6O_2 \rightarrow C_4H_{10}O_3 + H^+ + H_2O$	$(k_{C4H10O3})$ $k_3 = 0.0867 \times 10^{-4}$	-
6th step (Etherification of glycerol with methanol)		$C_3H_8O_3 + CH_3OH \rightarrow C_4H_{10}O_3 + H_2O$	$(k_{C4H10O3})$	-
Overall (Glycerol electroreduction reaction)	[Gly] = 3.0 mol/L T = 353 K *j* = 0.21 A/cm^2 E = 21.9 V	$C_3H_8O_3 + H^+ + e^- \rightarrow C_3H_6O_2 + C_3H_8O_2 + C_4H_{10}O_3$	$k = 0.3339 \times 10^{-4}$	5.24

*: At the optimal conditions for targeted compound formation; ACC: active site of 80ACC electrode; k = kinetics rate constant; W = electrical energy or energy consumption.

CHAPTER 5: CONCLUSION

5.1 Conclusion

In summary, the synthesis of ACC electrodes with different activated carbon loading has been performed and characterized for the electroreduction of glycerol. By increasing the activated carbon content in the ACC electrodes, it improved their electroactive surface area (EASA) and electrocatalytic activity. Except for 60ACC, other electrodes have a good ability to transfer electrons between electrode and Amberlyst-15 anionic radical, followed by the catalyzation of homogenous redox reaction with glycerol. From the electrochemical measurements, 80ACC electrode is advisable for the indirect electroreduction of glycerol due to its largest reduction peak value in the CV and highest equilibrium current density in the CA plots. In the glycerol electrochemical conversion studies, these ACC electrodes were compared with platinum (Pt). 80ACC showed the highest 1,2-propanediol yield (26.7 C mol%) and selectivity (32.1%) which were higher than Pt (22.3 C mol% yield and 26.5% selectivity) and other ACC electrodes. Two main intermediates were produced from the dissociation of glycerol either through C-C bond or C-O bond cleavage, respective to ethylene glycol and acetol intermediates. These intermediates are crucial to determine a selective mechanism pathway and its final product, where it is governed by the composition of activated carbon in the electrodes. High activated carbon content favoured 1,2-propanediol formation while low percentage triggered the generation of diethylene glycol through ethylene glycol intermediate.

For the second objective, acetol and ethylene glycol were used as the glycerol substitutes to elucidate the overall glycerol electroreduction reaction mechanisms. The mechanistic experiments validated acetol as an important intermediate to produce selective 1,2-propanediol. while the intermediate for diethylene glycol was ethylene glycol. Additionally, glycerol was tested for the dehydration reaction and acetol was found as the main product, proving the necessity of H^+ ions for a selective acetol-1,2-propanediol formation in the Amberlyst-15 solution. Optimal conditions reported in this work changed depending on the types of feedstocks and types of reactors. The optimum condition for acetol electrolysis in a two-compartment reactor was a 3.0 M initial concentration, 80.0 °C reaction temperature, 0.28 A/cm^2 current density, and 7 hours of electrolysis time to generate the highest yield (59.8 C mol%) and selectivity (77.3%) of 1,2-propanediol.

In the third objective, when the overall reaction mechanisms of glycerol electroreduction were identified, the study on the effects of kinetics parameters towards 1,2-propanediol formation was carried out. The reaction temperature and initial glycerol concentration must be increased to improve both yield and purity of 1,2-propanediol and a moderate current density value is needed to avoid over-electroreduction. A high reaction temperature can promote a faster conversion rate of glycerol to the valuable products especially 1,2-propanediol, but too high temperature led to the gases products. H_2 gases can be reduced and 1,2-propanediol was improved by a mild glycerol initial concentration. The medium current density was capable to improve 1,2-propanediol selectivity and yield by limiting the formation of minor products. The optimized condition of 3.0 M glycerol initial concentration, 80.0 °C reaction temperature, and 0.21 A/cm^2 current density for glycerol electroreduction into 1,2-propanediol able to decrease the energy consumption and obtain the yield value of 42.3 C mol% (75.3 % selectivity) at the 6th hour. This finding showed excellent results among the published reports on the electrochemical conversion of glycerol into 1,2-propanediol

5.2 Recommendations

Based on the outcomes, experimental data analysis, and discussion made in this work, the subsequent suggestions can be taken into attention in the potential studies on the glycerol electrochemical conversion performance.

a) Investigation using the crude glycerol as the reactant should be carried out, hence, this work could be applied in the real application.

b) Studies on the modification of activated carbon composite (ACC) electrodes with inexpensive metals, *e. g.,* copper and nickel, could be done to improve the yield and selectivity of 1,2-propanediol.

c) This practice still demands more investigation and improvement on the separation techniques to reliably deliver a greater purity (selectivity) of any product which are operational and economical for industrial needs.

REFERENCES

Abdel-Rahman, M. A., Hassan, S. E. D., El-Din, M. N., Azab, M. S., El-Belely, E. F., Alrefaey, H. M. A., & Elsakhawy, T. (2020). One-factor-at-a-time and response surface statistical designs for improved lactic acid production from beet molasses by *Enterococcus hirae* ds10. *SN Applied Sciences*, *2*(4), 573.

Ajeel, M. A., Aroua, M. K., & Daud, W. M. A. W. (2015a). Anodic degradation of 2-chlorophenol by carbon Black diamond and activated carbon composite electrodes. *Electrochimica Acta*, *180*, 22-28.

Ajeel, M. A., Aroua, M. K., & Daud, W. M. A. W. (2015b). Preparation and characterization of carbon black diamond composite electrodes for anodic degradation of phenol. *Electrochimica Acta*, *153*, 379-384.

Ajeel, M. A., Hassan, T. A. A., Naje, A. S., & Aroua, M. K. T. (2018). Development of diamond composite electrode for anodic oxidation of organic pollutants. *Journal of Environmental Chemical Engineering*, *6*(4), 3884-3888.

Alaba, P. A., Lee, C. S., Abnisa, F., Aroua, M. K., Abakr, Y. A., Ibrahim, M. D., Cognet, P., Pérès, Y., Daud, W. M. W. (2019). Investigating the electrocatalytic oxidation of glycerol on simultaneous nitrogen- and fluorine-doped on activated carbon black composite. *Diamond and Related Materials*, 107626.

Ali, I., Afshinb, S., Poureshgh, Y., Azari, A., Rashtbari, Y., Feizizadeh, A., Hamzezadeh, A., Fazlzadeh, M. (2020). Green preparation of activated carbon from pomegranate peel coated with zero-valent iron nanoparticles (nZVI) and isotherm and kinetic studies of amoxicillin removal in water. *Environmental Science and Pollution Research*, *27*(29), 36732-36743.

Angelucci, C. A., Varela, H., Tremiliosi-Filho, G., & Gomes, J. F. (2013). The significance of non-covalent interactions on the electrooxidation of alcohols on Pt and Au in alkaline media. *Electrochemistry Communications*, *33*, 10-13.

Anitha, M., Kamarudin, S. K., & Kofli, N. T. (2016). The potential of glycerol as a value-added commodity. *Chemical Engineering Journal*, *295*, 119-130.

Aoki, K., & Osteryoung, J. (1981). Diffusion-controlled current at the stationary finite disk electrode: Theory. *Journal of Electroanalytical Chemistry and Interfacial Electrochemistry*, *122*, 19-35.

Araujo, H. R., Zanata, C. R., Teixeira-Neto, E., de Lima, R. B., Batista, B. C., Giz, M. J., & Camara, G. A. (2019). How the adsorption of Sn on Pt (100) preferentially oriented nanoparticles affects the pathways of glycerol electrooxidation. *Electrochimica Acta*, *297*, 61-69.

Arcanjo, M. R. A., Silva, I. J., Rodríguez-Castellón, E., Infantes-Molina, A., & Vieira, R. S. (2017). Conversion of glycerol into lactic acid using Pd or Pt supported on carbon as catalyst. *Catalysis Today*, *279*, 317-326.

Ardila, A. N., Sánchez-Castillo, M. A., Zepeda, T. A., Villa, A. L., & Fuentes, G. A. (2017). Glycerol hydrodeoxygenation to 1,2-propanediol catalyzed by CuPd/TiO_2-Na. *Applied Catalysis B: Environmental*, *219*, 658-671.

Ashok, A., Kumar, A., Ponraj, J., Mansour, S., & F, T. (2018). Single step synthesis of porous $NiCoO_2$ for effective electrooxidation of glycerol in alkaline medium. *Journal of The Electrochemical Society*, *165*, 3301-3309.

Bagheri, S., Julkapli, N. M., & Yehye, W. A. (2015). Catalytic conversion of biodiesel derived raw glycerol to value added products. *Renewable and Sustainable Energy Reviews*, *41*, 113-127.

Balaraju, M., Rekha, V., Prasad, P. S. S., Devi, B. L. A. P., Prasad, R. B. N., & Lingaiah, N. (2009). Influence of solid acids as co-catalysts on glycerol hydrogenolysis to propylene glycol over Ru/C catalysts. *Applied Catalysis A: General*, *354*, 82-87.

Bard, A. J. (1980). *Electrochemical methods : Fundamentals and Applications* Wiley.

Beden, B., Çetin, I., Kahyaoglu, A., Takky, D., & Lamy, C. (1987). Electrocatalytic oxidation of saturated oxygenated compounds on gold electrodes. *Journal of Catalysis*, *104*(1), 37-46.

Beltrán-Prieto, J. C., Slavík, R., & Kolomazník., K. (2013). Optimization of electrochemical oxidation of glycerol for glyceric acid production. *International Journal Of Energy And Environment*, *7*(5), 229-234.

Benipal, N., Qi, J., Liu, Q., & Li, W. (2017). Carbon nanotube supported PdAg nanoparticles for electrocatalytic oxidation of glycerol in anion exchange membrane fuel cells. *Applied Catalysis B: Environmental*, *210*, 121-130.

Biddy, M. J., Scarlata, C., & Kinchin, C. (2016). *Chemicals from Biomass: A Market Assessment of Bioproducts with Near-Term Potential* (NREL/TP-5100-65509 United States 10.2172/1244312 NREL English).

Bijvoet, J. M., Peerdeman, A. F., & van Bommel, A. J. (1951). Determination of the absolute configuration of optically active compounds by means of X-rays. *Nature*, *168*(4268), 271-272.

Breig, S. J. M., & Luti, K. J. K. (2021). Response surface methodology: A review on its applications and challenges in microbial cultures. *Materials Today: Proceedings*, *42*, 2277-2284.

Brownson, D., & Banks, C. (2014). *The handbook of graphene electrochemistry*.

Brownson, D. A. C., & Banks, C. E. (2014). Interpreting electrochemistry. In D. A. C. Brownson & C. E. Banks (Eds.), *The Handbook of Graphene Electrochemistry* (pp. 23-77). Springer London.

Bruniaux, S., Varma, R. S., & Len, C. (2019). A novel strategy for selective O-methylation of glycerol in subcritical methanol. *Frontiers in Chemistry*, *7*(357).

Bruno, A. M., Chagas, C. A., Souza, M. M. V. M., & Manfro, R. L. (2018). Lactic acid production from glycerol in alkaline medium using Pt-based catalysts in continuous flow reaction system. *Renewable Energy*, *118*, 160-171.

Cai, F., Jin, F., Hao, J., & Xiao, G. (2019). Selective hydrogenolysis of glycerol to 1,2-propanediol on Nb-modified Pd−Zr−Al catalysts. *Catalysis Communications*, *131*, 105801.

Caldeira, L. R., Madureira, F. D., Maia, T. D. F., Muller, C. V., & Fernandes, C. (2021). Simultaneous quantification of ethylene glycol and diethylene glycol in beer by gas chromatography coupled to mass spectrometry. *Food Chemistry*, *346*, 128871.

Card, J. C., Valentin, G., & Storck, A. (1990). The activated carbon electrode: A new, experimentally verified mathematical model for the potential distribution. *Journal of Electrochemical Society*, *137*(9), 2736-2745.

Carrettin, S., McMorn, P., Johnston, P., Griffin, K., & Hutchings, G. J. (2002). Selective oxidation of glycerol to glyceric acid using a gold catalyst in aqueous sodium hydroxide. *The Royal Society of Chemistry* 696-697.

Carrettin, S., McMorn, P., Johnston, P., Griffin, K., Kiely, C. J., & Hutchings, G. J. (2003). Oxidation of glycerol using supported Pt, Pd and Au catalysts. *5*, 1329-1336.

Caselli, G., Mantovanini, M., Gandolfi, C. A., Allegretti, M., Fiorentino, S., Pellegrini, L., Melillo, G., Riccardo, B., Wilma, S., Roberto, A.,Gaetano, C., Giancarlo, S., Teti, A. (1997). Tartronates: A new generation of drugs affecting bone metabolism. *Journal of Bone And Mineral Research*, *12*(6), 971-981.

Cecilia, J. A., García-Sancho, C., Mérida-Robles, J. M., Santamaría-González, J., Moreno-Tost, R., & Maireles-Torres, P. (2015). V and V–P containing Zr-SBA-15 catalysts for dehydration of glycerol to acrolein. *Catalysis Today*, *254*, 43-52.

Célerier, S., Morisset, S., Batonneau-Gener, I., Belin, T., Younes, K., & Batiot-Dupeyrat, C. (2018). Glycerol dehydration to hydroxyacetone in gas phase over copper supported on magnesium oxide (hydroxide) fluoride catalysts. *Applied Catalysis A: General*, *557*, 135-144.

Chimentão, R. J., Hirunsit, P., Torres, C. S., Ordoño, M. B., Urakawa, A., Fierro, J. L. G., & Ruiz, D. (2021). Selective dehydration of glycerol on copper based catalysts. *Catalysis Today*, *367*, 58-70.

Chitwood, H., & Freure, B. (1946). The reaction of propylene oxide with alcohols. *Journal of the American Chemical Society*, *68*.

Chiu, C.-W., Dasari, M., Suppes, G., & Sutterlin, W. (2006a). Dehydration of glycerol to acetol via catalytic Reactive distillation. *AIChE Journal*, *52*, 3543-3548.

Chiu, C.-W., Dasari, M. A., Suppes, G. J., & Sutterlin, W. R. (2006b). Dehydration of glycerol to acetol via catalytic reactive distillation. *AIChE Journal*, *52*(10), 3543-3548.

Chiu, C.-W., Tekeei, A., Ronco, J. M., Banks, M.-L., & Suppes, G. J. (2008). Reducing byproduct formation during conversion of glycerol to propylene glycol. *Industrial & Engineering Chemistry Research*, *47*(18), 6878-6884.

Ciriminna, R., & Pagliaro, M. (2004). Oxidation of tartronic acid and dihydroxyacetone to sodium mesoxalate mediated by TEMPO. *Tetrahedron Letters*, *45*(34), 6381-6383.

Ciriminna, R., Palmisano, G., Pina, C. D., Rossi, M., & Pagliaro, M. (2006). One-pot electrocatalytic oxidation of glycerol to DHA. *Tetrahedron Letters*, *47*(39), 6993-6995.

Clavilier, J., Feliu, J. M., & Aldaz, A. (1988). An irreversible structure sensitive adsorption step in bismuth underpotential deposition at platinum electrodes. *Journal of Electroanalytical Chemistry and Interfacial Electrochemistry*, *243*(2), 419-433.

Clough, S. R. (2014). Glyceraldehyde. In P. Wexler (Ed.), *Encyclopedia of Toxicology (Third Edition)* (pp. 752-753). Academic Press.

Coelho, L. C. D., Filho, N. M. L., Faria, R. P. V., Ferreira, A. F. P., Ribeiro, A. M., & Rodrigues, A. E. (2018). Separation of tartronic and glyceric acids by simulated moving bed chromatography. *Journal of Chromatography A*, *1563*, 62-70.

Colmati, F., Tremiliosi-Filho, G., Gonzalez, E. R., Berná, A., Herrero, E., & Feliu, J. M. (2009). The role of the steps in the cleavage of the C-C bond during ethanol oxidation on platinum electrodes. *Phys Chem Chem Phys*, *11*(40), 9114-9123.

Coutanceau, C., Zalineeva, A., Baranton, S., & Simoes, M. (2014). Modification of palladium surfaces by bismuth adatoms or clusters: Effect on electrochemical activity and selectivity towards polyol electrooxidation. *International Journal of Hydrogen Energy*, *39*(28), 15877-15886.

Cui, H., Guo, Y., Guo, L., Wang, L., Zhou, Z., & Peng, Z. (2018). Heteroatom-doped carbon materials and their composites as electrocatalysts for CO_2 reduction. *Journal of Materials Chemistry A*, *6*(39), 18782-18793.

Dai, C., Sun, L., Liao, H., Khezri, B., Webster, R. D., Fisher, A. C., & Xu, Z. J. (2017). Electrochemical production of lactic acid from glycerol oxidation catalyzed by AuPt nanoparticles. *Journal of Catalysis*, *356*, 14-21.

Dalla Costa, B. O., Legnoverde, M. S., Lago, C., Decolatti, H. P., & Querini, C. A. (2016). Sulfonic functionalized SBA-15 catalysts in the gas phase glycerol dehydration. Thermal stability and catalyst deactivation. *Microporous and Mesoporous Materials*, *230*, 66-75.

Daud, W. M. A. W., & Houshamnd, A. H. (2010). Textural characteristics, surface chemistry and oxidation of activated carbon. *Journal of Natural Gas Chemistry*, *19*(3), 267-279.

Davis, W. R., Tomsho, J., Nikam, S., Cook, E. M., Somand, D., & Peliska, J. A. (2000). Inhibition of HIV-1 reverse transcriptase-catalyzed DNA strand transfer reactions by 4-chlorophenylhydrazone of mesoxalic acid. *American Chemical Society*, *39*(46), 14279-14291.

De Souza, N. E., Gomes, J. F., & Tremiliosi-Filho, G. (2017). Reactivity of 3-carbon-atom chain alcohols on gold electrode: A comparison to understand the glycerol electrooxidation. *Journal of Electroanalytical Chemistry*, *800*, 106-113.

Dhawane, S. H., Kumar, T., & Halder, G. (2018). Recent advancement and prospective of heterogeneous carbonaceous catalysts in chemical and enzymatic transformation of biodiesel. *Energy Conversion and Management*, *167*, 176-202.

Dieuzeide, M. L., de Urtiaga, R., Jobbagy, M., & Amadeo, N. (2017). Vapor phase hydrogenolysis of glycerol to 1,2-propanediol at atmospheric pressure over copper catalysts supported on mesoporous alumina. *Catalysis Today*, *296*, 19-25.

Dodekatos, G., Schünemann, S., & Tüysüz, H. (2018). Recent advances in thermo-, photo-, and electro-catalytic glycerol oxidation. *ACS Catalysis*, *8*.

dos Santos, T. R., Nilges, P., Sauter, W., Harnisch, F., & Schröder, U. (2015). Electrochemistry for the generation of renewable chemicals: electrochemical conversion of levulinic acid. *RSC Advances*, *5*(34), 26634-26643.

Duan, X., Xu, J., Wei, Z., Ma, J., Guo, S., Wang, S., Liu, H., Dou, S. (2017). Metal-free carbon materials for CO_2 electrochemical reduction. *Advanced Materials*, *29*(41),

Fan, L., Liu, B., Liu, X., Senthilkumar, N., Wang, G., & Wen, Z. (2021). Recent progress in electrocatalytic glycerol oxidation. *Energy Technology*, *9*(2), 2000804.

Farma, R., Deraman, M., Awitdrus, A., Talib, I. A., Taer, E., Basri, N. H., Manjunatha, J. G., Ishak, M. M., Dollah, B. N. M., Hashmi, S. A. (2013). Preparation of highly porous binderless activated carbon electrodes from fibres of oil palm empty fruit bunches for application in supercapacitors. *Bioresource Technology*, *132*, 254-261.

Fernández, P. S., Fernandes Gomes, J., Angelucci, C. A., Tereshchuk, P., Martins, C. A., Camara, G. A., Martins, M. E., Da Silva, J. L. F., Tremiliosi-Filho, G. (2015). Establishing a link between well-ordered Pt(100) surfaces and real systems: How do random superficial defects influence the electrooxidation of glycerol? *ACS Catalysis*, *5*(7), 4227-4236.

Ferreira Jr, R. S., Janete Giz, M., & Camara, G. A. (2013). Influence of the local pH on the electrooxidation of glycerol on Palladium–Rhodium electrodeposits. *Journal of Electroanalytical Chemistry*, *697*, 15-20.

Francke, R., & Little, R. D. (2014). Redox catalysis in organic electrosynthesis: basic principles and recent developments. *The Royal Society of Chemistry*, *43*, 2492-2521.

Freitas, I. C., Manfro, R. L., & Souza, M. M. V. M. (2018). Hydrogenolysis of glycerol to propylene glycol in continuous system without hydrogen addition over Cu-Ni catalysts. *Applied Catalysis B: Environmental*, *220*, 31-41.

Frontana-Uribe, B. A., Little, R. D., Ibanez, J. G., Palma, A. ý., & Vasquez-Medranoc, R. (2010). Organic electrosynthesis: a promising green methodology in organic chemistry. *The Royal Society of Chemistry*, *12*, 2099–2119.

Fu, S., Zhu, C., Song, J., Engelhard, M. H., He, Y., Du, D., Wang, C., Lin, Y. (2016). Three-dimensional PtNi hollow nanochains as an enhanced electrocatalyst for the oxygen reduction reaction. *Journal of Materials Chemistry A*, *4*(22), 8755-8761.

Fuchigami, T., Atobe, M., & Inagi, S. (2015). *Fundamentals and Applications of Organic Electrochemistry - Synthesis, Materials, Devices* (1st Edition ed.). Wiley.

Gabrysch, T., Muhler, M., & Peng, B. (2019). The kinetics of glycerol hydrodeoxygenation to 1,2-propanediol over Cu/ZrO_2 in the aqueous phase. *Applied Catalysis A: General*, *576*, 47-53.

Garcia, A. C., Birdja, Y. Y., Tremiliosi-Filho, G., & Koper, M. T. M. (2017). Glycerol electrooxidation on bismuth-modified platinum single crystals. *Journal of Catalysis*, *346*, 117-124.

Garcia, A. C., Ferreira, E. B., Silva de Barros, V. V., Linares, J. J., & Tremiliosi-Filho, G. (2017). PtAg/MnO_x/C as a promising electrocatalyst for glycerol electrooxidation in alkaline medium. *Journal of Electroanalytical Chemistry*, *793*, 188-196.

Garcia, A. C., Kolb, M. J., Sanchez, C. v. N. y., Vos, J., Birdja, Y. Y., Kwon, Y., Tremiliosi-Filho, G., Koper, M. T. M. (2016). Strong impact of platinum surface structure on primary and secondary alcohol oxidation during electrooxidation of glycerol. *American Chemical Society*.

Geraldes, A. N., da Silva, D. F., e Silva, L. G. d. A., Spinacé, E. V., Neto, A. O., & dos Santos, M. C. (2015). Binary and ternary palladium based electrocatalysts for alkaline direct glycerol fuel cell. *Journal of Power Sources*, *293*, 823-830.

Geraldes, A. N., da Silva, D. F., Pino, E. S., da Silva, J. C. M., de Souza, R. F. B., Hammer, P., Spinacé, E. V., Neto, A. O., Linardi, M., dos Santos, M. C. (2013). Ethanol electrooxidation in an alkaline medium using Pd/C, Au/C and PdAu/C electrocatalysts prepared by electron beam irradiation. *Electrochimica Acta*, *111*, 455-465.

Gomes, J. F., de Paula, F. B. C., Gasparotto, L. H. S., & Tremiliosi-Filho, G. (2012). The influence of the Pt crystalline surface orientation on the glycerol electrooxidation in acidic media. *Electrochimica Acta*, *76*, 88-93.

Gomes, J. F., Garcia, A. C., Gasparotto, L. H. S., de Souza, N. E., Ferreira, E. B., Pires, C., & Tremiliosi-Filho, G. (2014). Influence of silver on the glycerol electrooxidation over AuAg/C catalysts in alkaline medium: a cyclic voltammetry and in situ FTIR spectroscopy study. *Electrochimica Acta*, *144*, 361-368.

Gomes, J. F., Martins, C. A., Giz, M. J., Tremiliosi-Filho, G., & Camara, G. A. (2013). Insights into the adsorption and electrooxidation of glycerol: Self-inhibition and concentration effects. *Journal of Catalysis*, *301*, 154-161.

Gomes, J. F., & Tremiliosi-Filho, G. (2011). Spectroscopic studies of the glycerol electrooxidation on polycrystalline Au and Pt surfaces in acidic and alkaline media. *Springer Science*, *2*, 96-105.

Gonçalves, R. S., Triaca, W. E., & Rabockai, T. (1985). The potentiodynamic electrooxidation of glycerol on platinized platinum electrodes. *Analytical Letters*, *18*(8), 957-973.

Gong, K., Du, F., Xia, Z., Durstock, M., & Dai, L. (2009). Nitrogen-doped carbon nanotube arrays with high electrocatalytic activity for oxygen reduction. *Science*, *323*(5915), 760.

Guinea, E., Centellas, F., Brillas, E., Cañizares, P., Sáez, C., & Rodrigo, M. A. (2009). Electrocatalytic properties of diamond in the oxidation of a persistant pollutant. *Applied Catalysis B: Environmental*, *89*(3), 645-650.

Gupta, O. P., Chauhan, M., & Loomba, R. (1984). Study of the variation in the cathode potential with temperature in Ni-Cd alloy plating from a sulphate bath. *Surface Technology*, *21*(2), 155-160.

Gupta, P., & Paul, S. (2014). Solid acids: Green alternatives for acid catalysis. *Catalysis Today*, *236*, 153-170.

Habibi, B., & Delnavaz, N. (2016). Electrooxidation of glycerol on nickel and nickel alloy (Ni–Cu and Ni–Co) nanoparticles in alkaline media. *RSC Advances*, *6*(38), 31797-31806.

Han, J., Kim, Y., Kim, H. W., Jackson, D. H. K., Lee, D., Chang, H., Chae, H-, J., Lee, K-.Y, Kim, H. J. (2017). Effect of atomic-layer-deposited TiO_2 on carbon-supported Ni catalysts for electrocatalytic glycerol oxidation in alkaline media. *Electrochemistry Communications*, *83*, 46-50.

Heathcock, C. H. (2014). 2.08 The Aldol Reaction: Group I and Group II Enolates. In P. Knochel (Ed.), *Comprehensive Organic Synthesis II (Second Edition)* (pp. 340-395). Elsevier.

Hickey, D. P., McCammant, M. S., Giroud, F., Sigman, M. S., & Minteer, S. D. (2014). Hybrid Enzymatic and Organic Electrocatalytic Cascade for the Complete Oxidation of Glycerol. *Journal of The American Society*, *136*(45), 15917–15920.

Hirasawa, S., Watanabe, H., Kizuka, T., Nakagawa, Y., & Tomishige, K. (2013). Performance, structure and mechanism of Pd–Ag alloy catalyst for selective oxidation of glycerol to dihydroxyacetone. *Journal of Catalysis*, *300*, 205-216.

Holade, Y., Morais, C., Arrii-Clacens, S., Servat, K., Napporn, T. W., & Kokoh, K. B. (2013). New preparation of PdNi/C and PdAg/C nanocatalysts for glycerol electrooxidation in alkaline medium. *Electrocatalysis*, *4*(3), 167-178.

Holade, Y., Morais, C., Servat, K., Napporn, T. W., & Kokoh, K. B. (2013). Toward the electrochemical valorization of glycerol: Fourier transform infrared spectroscopic and chromatographic studies. *ACS Catalysis*, *3*(10), 2403-2411.

Hoyt, R. A., Remillard, E. M., Cubuk, E. D., Vecitis, C. D., & Kaxiras, E. (2017). Polyiodide-doped graphene. *The Journal of Physical Chemistry C*, *121*(1), 609-615.

Hua, X., Cao, R., Zhou, X., & Xu, Y. (2018). Integrated process for scalable bioproduction of glycolic acid from cell catalysis of ethylene glycol. *Bioresource Technology*, *268*, 402-407.

Huang, S., Li, Y., Feng, Y., An, H., Long, P., Qin, C., & Feng, W. (2015). Nitrogen and fluorine co-doped graphene as a high-performance anode material for lithium-ion batteries. *Journal of Materials Chemistry A*, *3*(46), 23095-23105.

Hunsom, M., & Saila, P. (2013). Product distribution of electrochemical conversion of glycerol via Pt electrode: Effect of initial pH. *International Journal of Electrochemical Science*, *8*, 11288 - 11300.

Hunsom, M., & Saila, P. (2015). Electrochemical conversion of enriched crude glycerol: Effect of operating parameters. *Renewable Energy*, *74*, 227-236.

Hursán, D., Samu, A. A., Janovák, L., Artyushkova, K., Asset, T., Atanassov, P., & Janáky, C. (2019). Morphological attributes govern carbon dioxide reduction on N-doped carbon electrodes. *Joule*, *3*(7), 1719-1733.

Inoue, H., Kimura, S., Teraoka, Y., Chiku, M., Higuchi, E., & Lam, B. T. X. (2018). Mechanism of glycerol oxidation reaction on silver-modified palladium electrode in alkaline medium. *International Journal of Hydrogen Energy*, *43*(40), 18664-18671.

Ishiyama, K., Kosaka, F., Shimada, I., Oshima, Y., & Otomo, J. (2013). Glycerol electrooxidation on a carbon-supported platinum catalyst at intermediate temperatures. *Journal of Power Sources*, *225*, 141-149.

Iwasita, T. (2002). Fuel cells: Spectroscopic studies in the electrocatalysis of alcohol oxidation. *Journal of the Brazilian Chemical Society*, *13*.

James, O. O., Sautera, W., & Schroder, U. (2018). Towards selective electrochemical conversion of glycerol to 1,3-propanediol. *Royal Society of Chemistry*, *8*, 10818–10827.

Jia, C., Dastafkan, K., Ren, W., Yang, W., & Zhao, C. (2019). Carbon-based catalysts for electrochemical CO_2 reduction. *Sustainable Energy & Fuels*, *3*(11), 2890-2906.

Jr., E. F. F., Barros, V. V. S. d., Araújo, B. R. S. d., Purgatto, Â. G., & J.Linares, J. (2017). Pt/C containing different platinum loadings for use as electrocatalysts in alkaline PBI-based direct glycerol fuel cells. *International Journal of Hydrogen Energy*, *42*(36), 23095-23106.

Kadier, A., Wang, J., Chandrasekhar, K., Abdeshahian, P., Islam, M. A., Ghanbari, F., Bajpai, M., Katoch, S. S., Bhagawati, P. B., Li, H., Kalil, M. S., Hamid, A. A., Abu Hasan, H., Ma, P.-C. (2021). Performance optimization of microbial electrolysis cell (MEC) for palm oil mill effluent (POME) wastewater treatment and sustainable Bio-H2 production using response surface methodology (RSM). *International Journal of Hydrogen Energy*.

Kai, T., Zhou, M., Duan, Z., Henkelman, G. A., & Bard, A. J. (2017). Detection of $CO_2^{\bullet-}$ in the electrochemical reduction of carbon dioxide in *N,N*-dimethylformamide by scanning electrochemical microscopy. *Journal of the American Chemical Society*, *139*(51), 18552-18557.

Katryniok, B., Kimura, H., Skrzynska, E. z., Girardon, J.-S., Fongarland, P., Capron, M., Ducoulombier, R., Mimura, N., Paula, S., Dumeignil, F. (2011). Selective catalytic oxidation of glycerol: Perspectives for high value chemicals. *The Royal Society of Chemistry*, *13*, 1960–1979.

Khosravanipour Mostafazadeh, A., De La Torre, M. S., Padilla, Y., Drogui, P., Brar, S. K., Tyagi, R. D., Le Bihan, Y., Buelna, G., Moroyoqui, P. G. (2021). An insight into an electro-catalytic reactor concept for high value-added production from crude glycerol: Optimization, electrode passivation, product distribution, and reaction pathway identification. *Renewable Energy*, *172*, 130-144.

Kim, H. J., Kim, Y., Lee, D., Kim, J.-R., Chae, H.-J., Jeong, S.-Y., Kim, B-. S., Lee, J., Huber, G. W., Byun, J., Kim, S., Han, J. (2017). Coproducing value-added chemicals and hydrogen with electrocatalytic glycerol oxidation technology: Experimental and techno-economic investigations. *ACS Sustainable Chemistry & Engineering*, *5*(8), 6626-6634.

Kim, H. J., Lee, J., Green, S. K., Huber, G. W., & Kim, W. B. (2014). Selective glycerol oxidation by electrocatalytic dehydrogenation. *ChemSusChem*, *7*(4), 1051-1056.

Kim, Y., WooKim, H., RangKim, Kim, T.-W., Lee, S., Chul-UngKim, Kim, J. (2017). The Role of Ruthenium on Carbon-Supported PtRu Catalysts for Electrocatalytic Glycerol Oxidation under Acidic Conditions. *ChemCatChem*, *9*, 1683 –1690.

Kongjao, S., Hunsom, M., & Damronglerd, S. (2011). Electrochemical reforming of an acidic aqueous glycerol solution on Pt electrodes. *Journal of Applied Electrochemistry*, *41*, 215–222.

Kowthaman, C. N., Senthil Kumar, P., & Arul Mozhi Selvan, V. (2021). Micro-patterned graphite electrodes: An analysis and optimization of process parameters on hydrogen evolution in water electrolysis. *Fuel*, *305*, 121542.

Kusunoki, Y., Miyazawa, T., Kunimori, K., & Tomishige, K. (2005). Highly active metal–acid bifunctional catalyst system for hydrogenolysis of glycerol under mild reaction conditions. *Catalysis Communications*, *6*(10), 645-649.

Kwon, Y., Birdja, Y., Spanos, I., Rodriguez, P., & Koper, M. T. M. (2012). Highly selective electrooxidation of glycerol to dihydroxyacetone on platinum in the oresence of bismuth. *American Chemical Society*, *2*, 759−764.

Kwon, Y., Koper, M. T. M., & Hersbach, T. J. P. (2014). Electrooxidation of glycerol on platinum modified by adatoms: Activity and selectivity effects. *Springer Science*, *57*, 1272-1276.

Kwon, Y., Lai, S. C. S., Rodriguez, P., & Koper, M. T. M. (2011). Electrocatalytic oxidation of alcohols on gold in alkaline media: Base or gold catalysis? . *Journal of the American Chemical Society*, *133*, 6914–6917.

Kwon, Y., Raaijman, S. J., & Koper, M. T. M. (2014). Role of peroxide in the catalytic activity of gold for oxidation reactions in aqueous media: An electrochemical study. *ChemCatChem*, *6*(1), 79-81.

Kwon, Y., Schouten, K. J. P., & Koper, M. T. M. (2011). Mechanism of the catalytic oxidation of glycerol on polycrystalline gold and platinum electrodes. *ChemCatChem*, *3* 1176 – 1185.

Lam, C. H., Bloomfield, A. J., & Anastas, P. T. (2017). A switchable route to valuable commodity chemicals from glycerol via electrocatalytic oxidation with an earth abundant metal oxidation catalyst. *The Royal Society of Chemistry*.

Lee, C. S., Aroua, M. K., Daud, W. A. W., Cognet, P., Pérès-Lucchese, Y., & Ajeel, M. A. (2018). Selective electroreduction of glycerol to 1,2-propanediol on a mixed carbon-black activated carbon electrode and a mixed carbon black-diamond electrode. *BioResources 13*(1), 115-130.

Lee, C. S., Aroua, M. K., Daud, W. A. W., Cognet, P., Pérès-Lucchese, Y., & Ajeel, M. A. (2019). Selective electrochemical conversion of glycerol to glycolic acid and lactic acid on a mixed carbon-black activated carbon electrode in a single compartment electrochemical cell. *Frontiers in Chemistry*, *7*(110).

Lee, D., Kim, Y., Kwon, Y., Lee, J., Kim, T.-W., Noh, Y., Kim, W. B., Seo, M. H., Kim, Kyoungsoo Kim, H. J. (2019). Boosting the electrocatalytic glycerol oxidation performance with highly-dispersed Pt nanoclusters loaded on 3D graphene-like microporous carbon. *Applied Catalysis B: Environmental*, *245*, 555-568.

Lee, K. S., Park, M. S., & Kim, J.-D. (2017). Nitrogen doped activated carbon with nickel oxide for high specific capacitance as supercapacitor electrodes. *Colloids and Surfaces A: Physicochemical and Engineering Aspects*, *533*, 323-329.

Lee, S., Kim, H. J., Lim, E. J., Kim, Y., Noh, Y., Huber, G. W., & Kim, W. B. (2016). Highly selective transformation of glycerol to dihydroxyacetone without using oxidants by a PtSb/C-catalyzed electrooxidation process. *Green Chemistry*, *18*(9), 2877-2887.

Lei, X., Gu, G., Hu, Y., Wang, H., Zhang, Z., & Wang, S. (2021). Structural requirements for chemoselective ammonolysis of ethylene glycol to ethanolamine over supported cobalt catalysts. *Catalysts*, *11*(6), 736.

Lertthahan, P., Yongprapat, S., Therdthianwong, A., & Therdthianwong, S. (2017). Pt-modified Au/C catalysts for direct glycerol electrooxidation in an alkaline medium. *International Journal of Hydrogen Energy*, *42*(14), 9202-9209.

Liang, H.-W., Zhuang, X., Brüller, S., Feng, X., & Müllen, K. (2014). Hierarchically porous carbons with optimized nitrogen doping as highly active electrocatalysts for oxygen reduction. *Nature Communications*, *5*, 4973.

Liang, J., Zheng, Y., Chen, J., Liu, J., Hulicova-Jurcakova, D., Jaroniec, M., & Qiao, S. Z. (2012). Facile oxygen reduction on a three-dimensionally ordered macroporous graphitic C_3N_4/carbon composite electrocatalyst. *Angewandte Chemie International Edition*, *51*(16), 3892-3896.

Liao, X., Zhu, Y., Wang, S.-G., & Li, Y. (2009). Producing triacetylglycerol with glycerol by two steps: Esterification and acetylation. *Fuel Processing Technology*, *90*(7), 988-993.

Licona, W., Ávila, K., & Jiménez, Á. (2014). Temperature as a factor determining on water electrolysis. *International Journal of Engineering Trends and Technology*, *7*, 5-9.

Lin, Q., Wei, Y., Liu, W., Yu, Y., & Hu, J. (2017). Electrocatalytic oxidation of ethylene glycol and glycerol on nickel ion implanted-modified indium tin oxide electrode. *International Journal of Hydrogen Energy*, *42*(2), 1403-1411.

Linares, N., Silvestre-Albero, A. M., Serrano, E., Silvestre-Albero, J., & García-Martínez, J. (2014). Mesoporous materials for clean energy technologies. *Chemical Society Reviews*, *43*(22), 7681-7717.

Lux, S., Stehring, P., & Siebenhofer, M. (2010). Lactic acid production as a new approach for exploitation of glycerol. *Separation Science and Technology*, *45*(12-13), 1921-1927.

Ma, J., Wang, L., Mu, X., & Cao, Y. (2015). Enhanced electrocatalytic activity of Pt nanoparticles supported on functionalized graphene for methanol oxidation and oxygen reduction. *Journal of Colloid and Interface Science*, *457*, 102-107.

Ma, T., Yun, Z., Xu, W., Chen, L., Li, L., Ding, J., & Shao, R. (2016). Pd-$H_3PW_{12}O_{40}$/Zr-MCM^{-41}: An efficient catalyst for the sustainable dehydration of glycerol to acrolein. *Chemical Engineering Journal*, *294*, 343-352.

Mamtani, K., Jain, D., Dogu, D., Gustin, V., Gunduz, S., Co, A., & Ozkan, U. (2017). Insights into oxygen reduction reaction (ORR) and oxygen evolution reaction (OER) active sites for nitrogen-doped carbon nanostructures (CN $_x$) in acidic Media. *Applied Catalysis B: Environmental*, *220*.

Marshall, A. T., & Haverkamp, R. G. (2008). Production of hydrogen by the electrochemical reforming of glycerolâ€"water solutions in a PEM electrolysis cell. *International Journal of Hydrogen Energy*, *33*(17), 4649-4654.

McMorn, P., Roberts, G., & Hutchings, G. J. (1999). Oxidation of glycerol with hydrogen peroxide using silicalite and aluminophosphate catalysts. *Catalysis Letters*, *63*(3), 193-197.

Md Rahim, S. A. N., Lee, C. S., Abnisa, F., Aroua, M. K., Daud, W. A. W., Cognet, P., & Pérès, Y. (2020). A review of recent developments on kinetics parameters for glycerol electrochemical conversion – A by-product of biodiesel. *Science of The Total Environment*, *705*, 135137.

Meng, X., Cao, Q., Jin, L. e., Zhang, X., Gong, S., & Li, P. (2017). Carbon electrode materials for supercapacitors obtained by co-carbonization of coal-tar pitch and sawdust. *Journal of Materials Science*, *52*(2), 760-769.

Miyazawa, T., Koso, S., Kunimori, K., & Tomishige, K. (2007a). Development of a Ru/C catalyst for glycerol hydrogenolysis in combination With an ion-exchange resin. *Applied Catalysis A-general 318*, 244-251.

Miyazawa, T., Koso, S., Kunimori, K., & Tomishige, K. (2007b). Glycerol hydrogenolysis to 1,2-propanediol catalyzed by a heat-resistant Ion-exchange resin combined with Ru/C. *Applied Catalysis A-general - APPL CATAL A-GEN*, *329*, 30-35.

Miyazawa, T., Kusunoki, Y., Kunimori, K., & Tomishige, K. (2006). Glycerol conversion in the aqueous solution under hydrogen over Ru/C$^+$ an ion-exchange resin and its reaction mechanism. *Journal of Catalysis*, *240*(2), 213-221.

Mohd Hanif, M., Roila, A., & Wan Md Zin Wan, Y. (2011). A review of acetol: Application and production. *American Journal of Applied Sciences*, *8*(11).

Monteiro, M. R., Kugelmeier, C. L., Pinheiro, R. S., Batalha, M. O., & da Silva César, A. (2018). Glycerol from biodiesel production: Technological paths for sustainability. *Renewable and Sustainable Energy Reviews*, *88*, 109-122.

Moraes, M. C., Junco, G. G., Moreira, T. F. M., Pinheiro, C. J. G., Olivi, P., Profeti, D., & Profeti, L. P. R. (2019). NiO-promoted Pt electrocatalysts prepared by thermal decomposition of polymeric precursors for oxidation of glycerol in alkaline medium. *Journal of Environmental Chemical Engineering*, *7*(1), 102922.

Murayama, T., & Yamanaka, I. (2011). Electrosynthesis of neutral H_2O_2 solution from O_2 and water at a mixed carbon cathode using an exposed solid-polymer-electrolyte electrolysis Cell. *The Journal of Physical Chemistry C*, *115*(13), 5792-5799.

Murthy, A. P., Madhavan, J., & Murugan, K. (2018). Recent advances in hydrogen evolution reaction catalysts on carbon/carbon-based supports in acid media. *Journal of Power Sources*, *398*, 9-26.

Nakagawa, Y., Ning, X., Amada, Y., & Tomishige, K. (2012). Solid acid co-catalyst for the hydrogenolysis of glycerol to 1,3-propanediol over Ir-ReO_x/SiO_2. *Applied Catalysis A: General*, *433-434*, 128-134.

Nakagawa, Y., Tamura, M., & Tomishige, K. (2014). Catalytic materials for the hydrogenolysis of glycerol to 1,3-propanediol. *Journal of Materials Chemistry A*, *2*(19), 6688-6702.

Nakagawa, Y., Tamura, M., & Tomishige, K. (2018). Perspective on catalyst development for glycerol reduction to C_3 chemicals with molecular hydrogen. *Research on Chemical Intermediates*, *44*(7), 3879-3903.

Nascimento, A., & Linares Leon, J. (2014). Performance of a direct glycerol fuel cell using KOH doped polybenzimidazole as electrolyte. *Journal of the Brazilian Chemical Society*, *25*.

Nemiwal, M., Zhang, T. C., & Kumar, D. (2021). Graphene-based electrocatalysts: Hydrogen evolution reactions and overall water splitting. *International Journal of Hydrogen Energy*, *46*(41), 21401-21418.

Nimlos, M. R., Blanksby, S. J., Qian, X., Himmel, M. E., & Johnson, D. K. (2006). Mechanisms of glycerol dehydration. *American Chemical Society*, *110*(18), 6145-6156.

Oberhauser, W., Evangelisti, C., Liscio, A., Kovtun, A., Cao, Y., & Vizza, F. (2018). Glycerol to lactic acid conversion by NHC-stabilized iridium nanoparticles. *Journal of Catalysis*, *368*, 298-305.

Okoye, P. U., Abdullah, A. Z., & Hameed, B. H. (2017). A review on recent developments and progress in the kinetics and deactivation of catalytic acetylation of glycerol—A byproduct of biodiesel. *Renewable and Sustainable Energy Reviews*, *74*, 387-401.

Orella, M. J., Román-Leshkov, Y., & Brushett, F. R. (2018). Emerging opportunities for electrochemical processing to enable sustainable chemical manufacturing. *Current Opinion in Chemical Engineering*, *20*, 159-167.

Othman, M. R., & Ahmad, A. (2015). Electrochemical oxidation of glycerol using gold electrode. *Malaysian Journal of Analytical Sciences*, *19*(2), 291 - 299.

Padayachee, D., Golovko, V., Ingham, B., & Marshall, A. T. (2014). Influence of particle size on the electrocatalytic oxidation of glycerol over carbon-supported gold nanoparticles. *Electrochimica Acta*, *120*, 398-407.

Pagliaro, M. (2017). Chapter 5 - glycerol: A key platform chemical of the forthcoming bioeconomy. In M. Pagliaro (Ed.), *Glycerol* (pp. 109-132). Elsevier.

Pagliaro, M., Ciriminna, R., Kimura, H., Rossi, M., & Della Pina, C. (2007). From glycerol to value-added products. *46*(24), 4434-4440.

Pal, R., Sarkar, T., & Khasnobis, S. (2012). Amberlyst-15 in oganic snthesis. *ARKIVOC: archive for organic chemistry*, *2012*, 570-609.

Pan, Z. F., Chen, R., An, L., & Li, Y. S. (2017). Alkaline anion exchange membrane fuel cells for cogeneration of electricity and valuable chemicals. *Journal of Power Sources*, *365*, 430-445.

Paula, J. d., Nascimentoa, D., & Linaresa, J. J. (2014). Electrochemical reforming of glycerol in alkaline PBI-based PEM reactor for hydrogen production. *Chemical Engineering Transaction 41*, 205-210.

Pauwels, D. (2018). *Electrosynthesis as an environmentally friendly production method: A screening methodology towards upscaling* Universiteit Antwerpen].

Pereira, L. M. S., Milan, T. M., & Tapia-Blácido, D. R. (2021). Using response surface methodology (RSM) to optimize 2G bioethanol production: A review. *Biomass and Bioenergy*.

Petersen, A. B., Na, R., & Wulf, H. C. (2003). Sunless skin tanning with dihydroxyacetone delays broad-spectrum ultraviolet photocarcinogenesis in hairless mice. *Mutation Research/Genetic Toxicology and Environmental Mutagenesis*, *542*(1), 129-138.

Petukhov, A. V., Akemann, W., Friedrich, K. A., & Stimming, U. (1998). Kinetics of electrooxidation of a CO monolayer at the platinum/electrolyte interface. *Surface Science*, *402-404*, 182-186.

Pico, M. P., Romero, A., Rodríguez, S., & Santos, A. (2012). Etherification of glycerol by tert-butyl alcohol: Kinetic model. *Industrial & Engineering Chemistry Research*, *51*(28), 9500-9509.

Pinter, J. K., Hayashi, J. A., & Watson, J. A. (1967). Enzymic assay of glycerol, dihydroxyacetone, and glyceraldehyde. *Archives of Biochemistry and Biophysics*, *121*(2), 404-414.

Pitt, F. D., Domingos, A. M., & Barros, A. A. C. (2019). Purification of residual glycerol recovered from biodiesel production. *South African Journal of Chemical Engineering*, *29*, 42-51.

Qadariyah, L., Mahfud, Sumarno, Machmudah, S., Wahyudiono, Sasaki, M., & Goto, M. (2011). Degradation of glycerol using hydrothermal process. *Bioresource Technology*, *102*(19), 9267-9271.

Qi, J., Xin, L., Chadderdon, D. J., Qiu, Y., Jiang, Y., Benipal, N., Li, W. (2014). Electrocatalytic selective oxidation of glycerol to tartronate on Au/C anode catalysts in anion exchange membrane fuel cells with electricity cogeneration. *Applied Catalysis B: Environmental*, *154-155*, 360-368.

Rahim, S. A. N. M., Lee, C. S., Abnisa, F., Aroua, M. K., Daud, W. A. W., Cognet, P., & Pérès, Y. (2020). A review of recent developments on kinetics parameters for glycerol electrochemical conversion – A by-product of biodiesel. *Science of The Total Environment*, *705*, 135137.

Reid, Lacey M., Li, T., Cao, Y., & Berlinguette, C. P. (2018). Organic chemistry at anodes and photoanodes. *Sustainable Energy & Fuels*, *2*(9), 1905-1927.

Roquet, L., Belgsir, E. M., Léger, J. M., & Lamy, C. (1994). Kinetics and mechanisms of the electrocatalytic oxidation of glycerol as investigated by chromatographic analysis of the reaction products: Potential and pH effects. *Electrochimica Acta*, *39*(16), 2387-2394.

Rousseau, S., Coutanceau, C., Lamy, C., & Léger, J. M. (2006). Direct ethanol fuel cell (DEFC): Electrical performances and reaction products distribution under operating conditions with different platinum-based anodes. *Journal of Power Sources*, *158*(1), 18-24.

Roy, A., Hursán, D., Artyushkova, K., Atanassov, P., Janáky, C., & Serov, A. (2018). Nanostructured metal-N-C electrocatalysts for CO_2 reduction and hydrogen evolution reactions. *Applied Catalysis B: Environmental*, *232*, 512-520.

Rukowicz, B., & Alejski, K. (2018). A biologically-derived 1,3-propanediol recovery from fermentation broth using preparative liquid chromatography. *Separation and Purification Technology*, *205*, 196-202.

Saila, P., & Hunsom, M. (2015). Effect of additives on one-pot electrochemical conversion of enriched crude glycerol. *The Korean Institute of Chemical Engineers*, *32*, 2412–2417

Sankar, M., Dimitratos, N., Knight, D. W., Carley, A. F., Tiruvalam, R., Kiely, C. J., Hutchings, G. J. (2009). Oxidation of Glycerol to Glycolate by using Supported Gold and Palladium Nanoparticles. *2*, 1149-1151.

Sarno, M., & Iuliano, M. (2018). Active biocatalyst for biodiesel production from spent coffee ground. *Bioresource Technology*, *266*, 431-438.

Sauter, W., Bergmann, O. L., & Schröder, U. (2017). Hydroxyacetone: A glycerol-based platform for electrocatalytic hydrogenation and hydrodeoxygenation processes. *ChemSusChem*, *10*(15), 3105-3110.

Sharma, R. V., Kumar, P., & Dalai, A. K. (2014). Selective hydrogenolysis of glycerol to propylene glycol by using Cu:Zn:Cr:Zr mixed metal oxides catalyst. *Applied Catalysis A: General*, *477*, 147-156.

Shen, Y., Fang, Q., & Chen, B. (2015). Environmental applications of three-dimensional graphene-based macrostructures: Adsorption, transformation, and detection. *Environmental Science & Technology*, *49*(1), 67-84.

Simões, M., Baranton, S., & Coutanceau, C. (2011). Enhancement of catalytic properties for glycerol electrooxidation on Pt and Pd nanoparticles induced by Bi surface modification. *Applied Catalysis B: Environmental*, *110*, 40-49.

Simões, M., Baranton, S., & Coutanceau, C. (2012). Electrochemical valorisation of glycerol. *ChemSusChem*, *5*, 2106 – 2124.

Ślipko, K., & Chlebicki, J. (1981). The kinetics of propylene oxide reaction with certain alkylamino alcohols in the presence of basic catalysts. *International Journal of Chemical Kinetics*, *13*(12), 1243-1249.

Song, M. Y., Yang, D.-S., Singh, K. P., Yuan, J., & Yu, J.-S. (2016). Nitrogen-doped hollow carbon spheres with highly graphitized mesoporous shell: Role of Fe for oxygen evolution reaction. *Applied Catalysis B: Environmental*, *191*, 202-208.

Steckhan, E. (1986). Indirect electroorganic syntheses - A modern chapter of organic electrochemistry [New Synthetic Methods (59)]. *Angewandte Chemie International Edition*, *25*(8), 683-701.

Stošić, D., Bennici, S., Sirotin, S., Calais, C., Couturier, J.-L., Dubois, J.-L., Auroux, A. (2012). Glycerol dehydration over calcium phosphate catalysts: Effect of acidic–basic features on catalytic performance. *Applied Catalysis A: General*, *447-448*, 124-134.

Sufiani, O., Elisadiki, J., Machunda, R. L., & Jande, Y. A. C. (2019). Modification strategies to enhance electrosorption performance of activated carbon electrodes for capacitive deionization applications. *Journal of Electroanalytical Chemistry*, *848*, 113328.

Sutter, M., Silva, E. D., Duguet, N., Raoul, Y., Métay, E., & Lemaire, M. (2015). Glycerol ether synthesis: A bench test for green chemistry concepts and technologies. *Chemical Reviews*, *115*(16), 8609-8651.

Suzuki, N. Y., Santiago, P. V. B., Galhardo, T. S., Carvalho, W. A., Souza-Garcia, J., & Angelucci, C. A. (2016). Insights of glycerol electrooxidation on polycrystalline silver electrode. *Journal of Electroanalytical Chemistry*, *780*, 391-395.

Talebian-Kiakalaieh, A., Amin, N. A. S., Rajaei, K., & Tarighi, S. (2018). Oxidation of bio-renewable glycerol to value-added chemicals through catalytic and electro-chemical processes. *Applied Energy*, *230*, 1347-1379.

Tan, H. W., Abdul Aziz, A. R., & Aroua, M. K. (2013). Glycerol production and its applications as a raw material: A review. *Renewable and Sustainable Energy Reviews*, *27*, 118-127.

Tang, J., Wang, T., Sun, X., Hu, Y., Xie, Q., Guo, Y., He, J. (2013). Novel synthesis of reduced graphene oxide-ordered mesoporous carbon composites and their application in electrocatalysis. *Electrochimica Acta*, *90*, 53-62.

Tavakol, H., Ranjbari, M. A., & Mahmoudi, A. (2019). DFT study on the mechanistic details of the hydrolysis of dicyan using acetaldehyde as the first organocatalyst. *Computational and Theoretical Chemistry*, *1154*, 37-43.

Thia, L., Xie, M., Fong, W. E., Liu, Z., Ge, X., Lu, Y., & Wang, X. (2016). Copper-modified gold nanoparticles as highly selective catalysts for glycerol electrooxidation in alkaline solution. *ChemCatChem*, *8*, 1-8.

Tian, X., Wang, Z., Yang, P., Hao, R., Jia, S., Li, N., Zhu, Z. (2016). Green oxidation of bio-lactic acid with H_2O_2 into tartronic acid under UV irradiation. *The Royal Society of Chemistry*, *6*, 41007–41010.

Torres, A., Roy, D., Subramaniam, B., & Chaudhari, R. V. (2010). Kinetic modeling of aqueous-phase glycerol hydrogenolysis in a batch slurry reactor. *Industrial & Engineering Chemistry Research*, *49*(21), 10826-10835.

Trasatti, S., & Petrii, O. A. (1992). Real surface area measurements in electrochemistry. *Journal of Electroanalytical Chemistry*, *327*(1), 353-376.

Vale, A. (2007). Ethylene and diethylene glycol. *Medicine*, *35*(11), 617-618.

Valter, M., Busch, M., Wickman, B., Grönbeck, H., Baltrusaitis, J., & Hellman, A. (2018). Electrooxidation of glycerol on gold in acidic medium: A combined experimental and DFT study. *The Journal of Physical Chemistry*.

Vivek, N., Christopher, M., Kumar, M. K., Castro, E., Binod, P., & Pandey, A. (2018). Pentose rich acid pretreated liquor as co-substrate for 1,3-propanediol production. *Renewable Energy*, *129*, 794-799.

Wang, D.-W., Li, F., Liu, M., Lu, G. Q., & Cheng, H.-M. (2008). 3D aperiodic hierarchical porous graphitic carbon material for high-rate electrochemical capacitive energy storage. *Angewandte Chemie International Edition*, *47*(2), 373-376.

Wang, H., Thia, L., Li, N., Ge, X., Liu, Z., & Wang, X. (2015). Selective electrooxidation of glycerol over Au supported on extended poly(4-vinylpyridine) functionalized graphene. *Applied Catalysis B: Environmental*, *166-167*, 25-31.

Wang, J., Chen, B., & Xing, B. (2016). Wrinkles and folds of activated graphene nanosheets as fast and efficient adsorptive sites for hydrophobic organic contaminants. *Environmental Science & Technology*, *50*(7), 3798-3808.

Wang, W., Kang, Y., Yang, Y., Liu, Y., Chai, D., & Lei, Z. (2016). PdSn alloy supported on phenanthroline-functionalized carbon as highly active electrocatalysts for glycerol oxidation. *International Journal of Hydrogen Energy*, *41*(2), 1272-1280.

Waszak, M., Markowska-Szczupak, A., & Gryta, M. (2016). Application of nanofiltration for production of 1,3-propanediol in membrane bioreactor. *Catalysis Today*, *268*, 164-170.

Xu, H., Yan, B., Zhang, K., Wang, J., Li, S., Wang, C., Yang, P. (2017). Ultrasonic-assisted synthesis of N-doped graphene-supported binary PdAu nanoflowers for enhanced electrooxidation of ethylene glycol and glycerol. *Electrochimica Acta*, *245*, 227-236.

Yadav, R. M., Wu, J., Kochandra, R., Ma, L., Tiwary, C. S., Ge, L., Ajayan, P. M. (2015). Carbon nitrogen nanotubes as efficient bifunctional electrocatalysts for oxygen reduction and evolution reactions. *ACS Applied Materials & Interfaces*, *7*(22), 11991-12000.

Yahya, N., Kamarudin, S. K., Karim, N. A., Basri, S., & Zanoodin, A. M. (2019). Nanostructured Pd-based electrocatalyst and membrane electrode assembly behaviour in a passive direct glycerol fuel cell. *Nanoscale Research Letters*, *14*(1), 52.

Yan, X., Jia, Y., Odedairo, T., Zhao, X., Jin, Z., Zhu, Z., & Yao, X. (2016). Activated carbon becomes active for oxygen reduction and hydrogen evolution reactions. *Chemical Communications*, *52*(52), 8156-8159.

Yang, S., Zhi, L., Tang, K., Feng, X., Maier, J., & Müllen, K. (2012). Efficient synthesis of heteroatom (N or S)-doped graphene based on ultrathin graphene oxide-porous silica sheets for oxygen reduction reactions. *Advanced Functional Materials*, *22*(17), 3634-3640.

Yang, W., Yue, X., Liu, X., Zhai, J., & Jia, J. (2015). ILs-derived N, S Co-doped ordered mesoporous carbon for high-performance oxygen reduction. *Nanoscale*, *7*.

Yaqub, M., Woo, C., & Lee, W. (2021). Optimization of hypochlorous acid generation by HCl electrolysis through response surface methodology and artificial neural networks. *Journal of Environmental Chemical Engineering*, *9*(5), 105826.

Yfanti, V. L., Ipsakis, D., & Lemonidou, A. A. (2018). Kinetic study of liquid phase glycerol hydrodeoxygenation under inert conditions over a Cu-based catalyst. *Reaction Chemistry & Engineering*, *3*(4), 559-571.

Yfanti, V. L., & Lemonidou, A. A. (2018). Mechanistic study of liquid phase glycerol hydrodeoxygenation with in-situ generated hydrogen. *Journal of Catalysis*, *368*, 98-111.

Yu, Z., Xu, L., Wei, Y., Wang, Y., He, Y., Xia, Q., Liu, Z. (2009). A new route for the synthesis of propylene oxide from bio-glycerol derivated propylene glycol. *Chemical Communications*(26), 3934-3936.

Yue, H., Zhao, Y., Ma, X., & Gong, J. (2012). Ethylene glycol: Properties, synthesis, and applications. *Chemical Society Reviews*, *41*(11), 4218-4244.

Zalineeva, A., Baranton, S., & Coutanceau, C. (2015). How do Bi-modified palladium nanoparticles work towards glycerol electrooxidation? An in situ FTIR study. *Electrochimica Acta*, *176*, 705-717.

Zalineeva, A., Baranton, S. v., & Coutanceau, C. (2013). Bi-modified palladium nanocubes for glycerol electrooxidation. *Electrochemistry Communications*, *34*, 335-338.

Zhang, C., Wang, T., Liu, X., & Ding, Y. (2016). Cu-promoted Pt/activated carbon catalyst for glycerol oxidation to lactic acid. *Journal of Molecular Catalysis A: Chemical*, *424*, 91-97.

Zhang, W., Wang, H., Li, Q., Dong, Q., Zhao, N., Wei, W., & Sun, Y. (2005). The mechanism for the synthesis of 1-methoxy-2-propanol from methanol and propylene oxide over magnesium oxide. *Applied Catalysis A: General*, *294*(2), 188-196.

Zhang, X., Guan, P., Malic, L., Trudeau, M., Rosei, F., & Veres, T. (2015). Nanoporous twinned PtPd with highly catalytic activity and stability. *Journal of Materials Chemistry A*, *3*(5), 2050-2056.

Zhang, X., Wang, M., Zhang, C., Lu, J., Wang, Y., & Wang, F. (2016). Epoxide hydrolysis and alcoholysis reactions over crystalline Mo–V–O oxide. *RSC Advances*, *6*(75), 70842-70847.

Zhang, Y.-y., Yi, Q.-f., Chu, H., & Nie, H.-d. (2017). Catalytic activity of Pd-Ag nanoparticles supported on carbon nanotubes for the electrooxidation of ethanol and propanol. *Journal of Fuel Chemistry and Technology*, *45*(4), 475-483.

Zhang, Z.-Q., Liao, M.-C., Zeng, H.-Y., Xu, S., Xu, L.-H., Liu, X.-J., & Du, J.-Z. (2014). Mg–Al hydrotalcites as solid base catalysts for alcoholysis of propylene oxide. *Fuel Processing Technology*, *128*, 519-524.

Zhang, Z., Xin, L., & Li, W. (2012). Supported gold nanoparticles as anode catalyst for anion-exchange membrane-direct glycerol fuel cell (AEM-DGFC). *International Journal of Hydrogen Energy*, *37*(11), 9393-9401.

Zhang, Z., Xin, L., Qi, J., Chadderdon, D. J., & Li, W. (2013). Supported Pt, Pd and Au nanoparticle anode catalysts for anion-exchange membrane fuel cells with glycerol and crude glycerol fuels. *Applied Catalysis B: Environmental*, *136-137*, 29-39.

Zhang, Z., Xin, L., Qi, J., Chadderdon, D. J., Sun, K., Warsko, K. M., & Li, W. (2014). Selective electrooxidation of glycerol to tartronate or mesoxalate on Au nanoparticle catalyst via electrode potential tuning in anion-exchange membrane electro-catalytic flow reactor. *Applied Catalysis B: Environmental*, *147*, 871-878.

Zhang, Z., Xin, L., Qi, J., Wang, Z., & Li, W. (2012). Selective electro-conversion of glycerol to glycolate on carbon nanotube supported gold catalyst. *Green Chemistry*, *14*, 2150–2152.

Zhou, Y., & Shen, Y. (2018). Selective electrooxidation of glycerol over Pd and Pt@Pd nanocubes. *Electrochemistry Communications*, *90*, 106-110.

Zhou, Y., Shen, Y., & Piao, J. (2018). Sustainable conversion of glycerol into value-added chemicals by selective electrooxidation on Pt-based catalysts. *ChemElectroChem*, *5*(13), 1636-1643.

Zhou, Y., Shen, Y., & Xi, J. (2019). Seed-mediated synthesis of Pt_xAu_y@Ag electrocatalysts for the selective oxidation of glycerol. *Applied Catalysis B: Environmental*, *245*, 604-612.

Zhou, Y., Shen, Y., Xi, J., & Luo, X. (2019). Selective electrooxidation of glycerol to dihydroxyacetone by PtAg skeletons. *ACS Applied Materials & Interfaces*, *11*(32), 28953-28959.

Zhou, Z., Li, X., Zeng, T., Hong, W., Cheng, Z., & Yuan, W. (2010). Kinetics of hydrogenolysis of glycerol to propylene glycol over Cu-ZnO-Al_2O_3 catalysts. *Chinese Journal of Chemical Engineering*, *18*(3), 384-390.

Zhu, L., Gao, Q., Tan, Y., Tian, W., Xu, J., Yang, K., & Yang, C. (2015). Nitrogen and oxygen co-doped microporous carbons derived from the leaves of *Euonymus japonicas* as high performance supercapacitor electrode material. *Microporous and Mesoporous Materials*, *210*, 1-9.

Zhu, Y., Lv, K., Wang, X., Yang, H., Xiao, G., & Zhu, Y. (2019). 1D/2D nitrogen-doped carbon nanorod arrays/ultrathin carbon nanosheets: Outstanding catalysts for the highly efficient electroreduction of CO_2 to CO. *Journal of Materials Chemistry A*, *7*(24), 14895-14903.

Zope, B. N., Hibbitts, D. D., Neurock, M., & Davis, R. J. (2010). Reactivity of the gold/water interface during selective oxidation catalysis. *Science*, *330*, 74-78.

LIST OF PUBLICATIONS AND PAPERS PRESENTED

I. Publications

No	Manuscript title	Status
1.	Md. Rahim, S. A. N., Lee, C. S., Abnisa, F., Aroua, M. K., Daud, W. M. A. W., Cognet, P., Pérès, Y. A review of recent developments on kinetics parameters for glycerol electrochemical conversion – A by-product of biodiesel, Science of The Total Environment, 705 (2020) (ISI Q1 ranking journal, impact factor: 7.963)	Published
2.	Md. Rahim, S. A. N., Lee, C. S., Abnisa, F., Aroua, M. K., Daud, W. M. A. W., Cognet, P., Pérès, Y. Activated carbon-based electrodes for two-steps catalytic/ electrocatalytic reduction of glycerol in Amberlyst-15 mediator, Chemosphere (2022) (ISI Q1 ranking journal, impact factor: 7.086)	Published
3.	Md. Rahim, S. A. N., Lee, C. S., Aroua, M. K., Daud, W. M. A. W., Abnisa, F., Cognet, P., Pérès, Y. Glycerol Electrocatalytic Reduction Using an Activated Carbon Composite Electrode: Understanding the Reaction Mechanisms and an Optimization Study, Frontiers in Chemistry (2022) (ISI Q2 ranking journal, impact factor: 5.221)	Published

II. Conference or proceeding paper

1. Md. Rahim, S. A. N., Lee, C. S., Aroua, M. K., Daud, W. M. A. W., Cognet, P., Pérès, Y. Alaba, P. A. Electrochemical Reduction of CO_2 to Fuels and Chemicals: Recent Development, Challenges, and Future Opportunities. 1st Euro-Asia Conference on CO_2 Capture and Utilisation (EACCO$_2$CU 2019). 6-7 August 2019. Selangor, Malaysia. (Poster presentation).